

Copyright

by

Wei Sun

2014

**The Dissertation Committee for Wei Sun Certifies that this is the approved version
of the following dissertation:**

**Behavior of Carbon Fiber Reinforced Polymer (CFRP) Anchors
Strengthening Reinforced Concrete Structures**

Committee:

James O. Jirsa, Supervisor

Wassim Ghannoum, Co-Supervisor

Eric B. Williamson

Oguzhan Bayrak

Kenneth Liechti

**Behavior of Carbon Fiber Reinforced Polymer (CFRP) Anchors
Strengthening Reinforced Concrete Structures**

by

Wei Sun, B.E.; M.E.

Dissertation

Presented to the Faculty of the Graduate School of

The University of Texas at Austin

in Partial Fulfillment

of the Requirements

for the Degree of

Doctor of Philosophy

The University of Texas at Austin

December, 2014

Dedication

To my family, who has unconditionally supported my desire for higher education.

Acknowledgements

I am deeply grateful to the love, encouragement and support from my beloved mother and father.

I would like to express the deepest appreciation to my advising professor, Dr. James O. Jirsa and Dr. Wassim Ghannoum, for the perceptive criticism, kind encouragement, patient guidance and mentorship they provided to me. It was a great opportunity to work with them and learn from their invaluable advice. I would like to extend my gratitude to Dr. Eric B Williamson, Dr. Oguzhan Bayrak, and Dr. Kenneth Leichti, for serving in the doctoral committee and their continuous help with my dissertation.

I owe huge thank to Huaco, Changhyuk Kim, William Shekarchi and Helen Wang who worked on the same project and always willing to provide their helping hands. The technical assistance provided by the staff at Ferguson Structural Engineering Laboratory (FSEL) including Blake Stasney, Dennis Phillip, Eric Schell, David Braley and Mike Wason is also greatly appreciated.

Lastly and certainly not least, I gratefully acknowledge the Texas Department of Transportation (TxDOT) for the financial support aiding in the completion of this research and writing of this dissertation.

July 26, 2014

Behavior of Carbon Fiber Reinforced Polymer (CFRP) Anchors Strengthening Reinforced Concrete Structures

Publication No. _____

Wei Sun, Ph.D.

The University of Texas at Austin, 2014

Supervisor: James O. Jirsa

Co-supervisor: Wassim Ghannoum

Carbon Fiber Reinforcement Polymer (CFRP) materials are widely used to strengthen reinforced concrete structures because they are light weight, have high strength, and are relatively easy to install. In strengthening applications, CFRP strips are typically attached to the concrete surface using epoxy resin with fibers oriented in the direction needing additional tensile strength. However, if CFRP strips rely exclusively on bond strength with concrete, only 40% to 50% of the CFRP tensile strength can be developed before debonding occurs. In order to fully develop the tensile strength of CFRP strips, some form of anchorage is needed. CFRP anchors can be applied with relative ease and have recently been shown to provide effective anchorage of CFRP strips to concrete members. In many cases, however, current anchorage details may result in fracture or failure of CFRP anchors prior to developing the full strength of CFRP

strips. Many design parameters, the effects of which are not well understood, can affect the behavior and strength of CFRP anchors. Moreover, previous studies have demonstrated that the quality of installation can influence anchor strength substantially. The objectives of the study presented are to: 1) provide engineers with design guidelines for CFRP anchors, and 2) deliver a reliable test for controlling the quality of installation and materials of CFRP anchorage systems.

In all, 39 tests on 6"×6"×24" rectangular concrete beams were conducted to study the influence of five parameters on CFRP anchor strength and effectiveness: 1) the width of the CFRP strip being developed, 2) the material ratio of CFRP anchor to CFRP strip, 3) the concrete strength, 4) the length/angle of anchor fan, and 5) the bond between CFRP strip and concrete (bonded/unbonded). The same tests also served to develop the test methodology for quality control of the CFRP anchorage system. Based on experimental results, guidelines for designing CFRP anchors are proposed. A test specimen and methodology are also proposed for qualifying CFRP materials and anchorage-system installations.

A Finite Element (FE) formulation was selected to provide a computational tool that is suited for simulating the behavior of CFRP strips and CFRP anchors. The ability of the selected FE formulation to reproduce the effects on behavior of varying the anchor-material ratio, concrete strength, length of anchor fan, and bond conditions was investigated. Six FE simulations were built by adjusting simulation parameters and comparing results with six experimental tests. Comparisons between experimental and numerical results indicate that the proposed FE formulation and parameter selections reproduced load-deflection and local strain behaviors with high fidelity.

Table of Contents

CHAPTER 1	1
INTRODUCTION	1
1.1 OVERVIEW	1
1.2 NECESSITY OF INTRODUCING CFRP ANCHORS	1
1.3 PROJECT OBJECTIVE AND SCOPE	3
CHAPTER 2	5
BACKGROUND STUDY	5
2.1 HISTORY OF CFRP MATERIAL IN REHABILITATION	5
2.1.1 <i>Development and Properties of Carbon Fiber Material</i>	6
2.1.2 <i>Strengthening and Repairing Structures</i>	10
2.1.3 <i>Typical Failure Modes of CFRP Installations</i>	11
2.1.4 <i>Bond Strength</i>	12
2.1.5 <i>Design Philosophy</i>	16
2.2 BACKGROUND ON CFRP ANCHORS AND ANCHORAGE SYSTEMS	19
2.2.1 <i>Anchor Details</i>	20
2.2.2 <i>Confinement</i>	26
2.2.3 <i>Flexure</i>	28
2.2.4 <i>Shear</i>	29
2.3 NUMERICAL MODELING	33
2.3.1 <i>No Slip Models</i>	34
2.3.2 <i>Micro-level Analysis of Concrete Cracking</i>	34
2.3.3 <i>Interfacial Material</i>	35
2.3.4 <i>Anchor Simulation</i>	37
CHAPTER 3	40
TEST PROGRAM	40
3.1 TEST PROGRAM	40
3.2 TEST SPECIMENS.....	40
3.3 TEST MATRIX	44
3.3.1 <i>Variables</i>	44

3.3.2 Nomenclature.....	49
3.4 INSTALLATION	53
3.4.1 Preparation of Specimens.....	53
3.4.2 Installation of CFRP strips and anchors	56
3.5 TEST APPARATUS AND LOADING PROTOCOL.....	61
3.6 INSTRUMENTATION.....	62
3.6.1 Load and Deformation Measurement	62
3.6.2 Strain Gauges	64
3.6.3 UT Vision System.....	65
3.7 MATERIAL PROPERTIES OF CFRP.....	75
3.7 CONCRETE.....	76
CHAPTER 4	77
TEST RESULTS	77
4.1 OVERVIEW.....	77
4.2 SUMMARY OF TEST RESULTS.....	77
4.2.1 Typical Test and Results	77
4.2.2 Failure Modes and Strength Evaluation	88
4.2.3 Summary of test results	91
4.3 EFFECT OF CONCRETE STRENGTH	95
4.3.1 Bond Strength	95
4.3.2 Strip Fracture	98
4.3.3 Anchor Rupture.....	100
4.3.4 Summary	102
4.4 EFFECT OF ANCHOR FAN LENGTH/ANCHOR FAN ANGLE.....	102
4.4.1 Strip Fracture	103
4.4.2 Anchor Rupture.....	104
4.4.3 Summary	104
4.5 EFFECT OF WIDTH OF CFRP STRIP	105
4.5.1 Strip Fracture	105
4.5.2 Anchor Rupture.....	110
4.5.3 Summary	110
4.6 EFFECT OF MATERIAL RATIO OF CFRP ANCHOR TO CFRP STRIP	111
4.6.1 Strip Fracture	113
4.6.2 Anchor Rupture.....	119

4.6.3 Summary	121
4.7 BONDED VERSUS UNBONDED APPLICATIONS	121
4.7.1 Strip Strength & Anchor Strength.....	121
4.7.2 Summary	124
4.8 VARIABILITY STUDY	124
4.9 SUMMARY	126
CHAPTER 5	127
FINITE ELEMENT ANALYSIS	127
5.1 INTRODUCTION	127
5.2 MATERIAL MODELING.....	127
5.2.1 Element Types.....	127
5.2.2 Geometric Model	130
5.2.3 Material Properties.....	134
5.4 NUMERICAL RESULTS	140
5.4.1 Series 1 Simulations: Parametric Study Based on Beams Tested in this Study	140
5.4.2 Series 2 Simulations: Sensitivity Study	160
5.5 VALIDATION OF THE PROPOSED MODEL WITH AVAILABLE EXPERIMENTAL RESULTS	165
5.5 SUMMARY	172
CHAPTER 6	175
ANCHOR DESIGN AND QUALITY CONTROL TESTS	175
6.1 OVERVIEW.....	175
6.2 ANCHOR DESIGN FOR A GIVEN CFRP STRIP	175
6.2.1 Strength ratio of CFRP anchor to CFRP strip.....	176
6.2.2 Other Considerations for Anchor Geometry.....	179
6.2.3 Design Example for Single Anchor.....	183
6.2.4 Design Example for Multiple Anchors.....	184
6.2.5 Limits of Existing Data	186
6.2.6 Summary	187
6.3 QUALITY CONTROL TEST	187
6.3.1 Criteria for Quality of Anchor Installation.....	187
6.3.2 Criteria for Evaluation of the Anchor Design Geometry.....	188
6.4 SUMMARY	188
CHAPTER 7	190

SUMMARY AND CONCLUSIONS.....	190
7.1 SUMMARY	190
7.1.1 <i>Experimental Program</i>	190
7.1.2 <i>Simulation of Test Specimen Behavior using FE Model</i>	191
7.1.3 <i>Design Guidelines and Quality Control</i>	192
7.2 CONCLUSIONS	193
7.2.1 <i>Effects of Width of CFRP Strip</i>	193
7.2.2 <i>Anchor-Material Ratio</i>	193
7.2.3 <i>Concrete Strength</i>	194
7.2.4 <i>Anchor fan length / Anchor fan angle</i>	194
7.2.5 <i>Bonded versus Unbonded Applications</i>	194
7.2.6 <i>Finite Element Analysis</i>	194
7.2.7 <i>Quality Control Test</i>	195
7.3 DESIGN RECOMMENDATIONS	196
7.4 FUTURE WORK.....	196
APPENDIX A	197
CFRP MATERIAL PROPERTIES	197
APPENDIX B.....	198
EPOXY RESIN MATERIAL PROPERTIES.....	198
APPENDIX C	199
EXPERIMENTAL SPECIMENS DETAILS	199
APPENDIX D	202
CONTOUR PLOTS.....	203
REFERENCES	224
VITA	230

List of Tables

Table 2-1 Material properties of fibers (Juenger, 2011).....	8
Table 3-1 Details for anchor fan.....	51
Table 3-2 Test details.....	52
Table 3-3 Camera properties.....	66
Table 3-4 Comparisons of CFRP material properties between material tests and manufacturer specified values.....	76
Table 3-5 Typical concrete mixture proportions.....	76
Table 4-1 Summary of experimental results.....	93
Table 4-2 Peak bond stress, slip at peak bond stress, and ultimate slip for tests with 5 in. strips	97
Table 4-3 Peak bond stress, slip at peak bond stress, and ultimate slip for tests with 3 in. strips	97
Table 4-4 Experimental results for effect of concrete strength on strip fracture.....	99
Table 4-5 Experimental results for effect of concrete strength on anchor rupture.....	100
Table 4-6 Experimental results for effect of fan geometry on strip fracture.....	103
Table 4-7 Experimental results for effect of strip width on strip fracture.....	105
Table 4-8 Results for tests sustained strip fracture and with an anchor material ratio of 1.41 for different strip widths.....	109
Table 4-9 Experimental results for effect of anchor-material ratio on strip fracture.....	113
Table 4-10 Results for strip fracture tests with 5 in. strips.....	116
Table 4-11 Experimental results for directly comparable tests with 3 in. strips of Series III	117
Table 4-12 Results for strip fracture tests with 3 in. strips of Series IV.....	119
Table 4-13 Results for anchor rupture tests with 5 in. strips and different anchor-material ratio.....	120
Table 4-14 Experimental results for tests with different bond condition.....	122
Table 5-1 Element types.....	130
Table 5-2 Peak bond stress and slip at peak bond stress from the input in the nonlinear spring elements (Fx direction, Figure 5-10).....	139
Table 5-3 Parameters of Series 1 simulations.....	141
Table 5-4 Comparison of failure loads of FE simulations and test (kips).....	143
Table 5-5 Parameters of Series 2 simulations.....	160

Table 5-6 Spring force (F/ A_{eff}) versus elongation (Δ) input and resultant bond stress (τ) versus slip (s) values at key points of Figure 5-34.....	161
Table 5-7 Properties of concrete and CFRP material used in simulations	166
Table 5-8 Spring force (F/ A_{eff}) versus elongation (Δ) input and resultant bond (τ) versus slip (s) values at key points of Figure 5-40.....	167
Table 6- 1 Ultimate load and failure mode	177
Table 6-2 Summary of test results	178
Table 6-3 Test results.....	182
Table A-1 CFRP strips properties provided by the manufacturer	197
Table B-1 Epoxy resin Properties provided by the manufacturer.....	198

List of Figures

Figure 1-1 Complete wrapping application (ACI 440.2R-08, 2008).....	2
Figure 1-2 Anchored U-wrapping application for a I-girder	2
Figure 2-1 Installing a CFRP strip on the tensile substrate of a concrete member.....	5
Figure 2-2 Hexagonal close packed structure (M. Juenger, 2011)	7
Figure 2-3 Body center cubic structure (M. Juenger, 2011).....	7
Figure 2-4 Unidirectional CFRP strip.....	9
Figure 2-5 CFRP strengthening application	10
Figure 2-6 Application of CFRP material to repair IH 20 Bridge (D.Y. Yang, 2003).....	11
Figure 2-7 Failure mode of a test without application of CFRP anchor	12
Figure 2-8 Bond-slip model (Chen et al., 2001)	13
Figure 2-9 Pull test from Lu et al. (2005a)	14
Figure 2-10 Bond stress versus slip model (Lu et al., 2005b)	15
Figure 2-11 Test setup (Orton 2008)	20
Figure 2-12 The diameter of CFRP anchor (Niemitz, 2008).....	21
Figure 2-13 A simple test setup for quality control of CFRP anchors (Pham, 2009).....	22
Figure 2-14 Typical test setup and two-block specimen for tension test (Pham, 2009).....	23
Figure 2-15 CFRP anchor pull-test (Smith et al., 2009).....	23
Figure 2-16 Typical anchor failure modes of anchor pull-test (Smith et al., 2009)	24
Figure 2-17 CFRP anchor dowel angle (Zhang et al. 2012a).....	25
Figure 2-18 Load-slip response for anchored and unanchored pull-test (Zhang et al., 2011).....	26
Figure 2-19 Using anchored strip to wrap a column with wing walls.....	27
Figure 2-20 Recommendations on anchor details (Kobayashi et al., 2001)	27
Figure 2-21 Test setup (Kim, 2008).....	28
Figure 2-22 CFRP application with anchorage systems (Kim, 2008)	29
Figure 2-23 Using anchored CFRP strip to u-wrapping a T-beam (Kim, 2014)	30
Figure 2-24 Loading setup (Kim, 2014)	30
Figure 2-25 Comparisons between anchored and unanchored application (Kim, 2011).....	31
Figure 2-26 LVDTs configuration for shear strain.....	31
Figure 2-27 Description of the variables for calculating CFRP shear strengthening	33

Figure 2-28 Interfacial element for shear strengthening (Lu et al., 2005b).....	35
Figure 2-29 Interfacial element (Neale, K.W. et al, 2005)	36
Figure 2-30 Interfacial element (Lu et al., 2007).....	36
Figure 2-31 Interfacial element proposed by Wong et al. (2003).....	37
Figure 2-32 A eight-node quadrilateral orthotropic shell element.....	38
Figure 2-33 A nonlinear spring element	39
Figure 2-34 Force-deformation response for FRP anchor	39
Figure 3-1 Standard specimen before CFRP installation.....	41
Figure 3-2 CFRP anchors and CFRP strips (Huaco, 2010)	45
Figure 3-3 Test details	45
Figure 3-4 CFRP anchor	46
Figure 3-5 Debonding observed between CFRP strip and concrete substrate.....	47
Figure 3-6 Layout of unbonded specimens.....	48
Figure 3-7 Details of CFRP anchors (Pham, 2009)	49
Figure 3-8 Specimen nomenclature	50
Figure 3-9 Preparations before CFRP installation.....	54
Figure 3-10 Prepared specimens.....	55
Figure 3-11 U-wrapping specimens with CFRP strips	56
Figure 3-12 Preparing epoxy (Huaco, 2010)	56
Figure 3-13 Saturating epoxy on concrete (left) and CFRP strip (right)	57
Figure 3-14 U-wrapping CFRP strip.....	57
Figure 3-15 Saturating holes (left) and flexural surface (right) (Hauco, 2010).....	58
Figure 3-16 Applying CFRP strips	58
Figure 3-17 Applying the first patch.....	59
Figure 3-18 Inserting CFRP anchor.....	59
Figure 3-19 Fanning the anchor	59
Figure 3-20 Applying the second patch	60
Figure 3-21 Specimens with CFRP installed.....	60
Figure 3-22 Load setup I.....	61
Figure 3-23 Load setup II	61
Figure 3-24 Rocker assemble.....	62

Figure 3-25 Measurements for load and displacement	63
Figure 3-26 Load versus deformation plots with data collected by load cell and LVDT	63
Figure 3-27 Strain gauges on CFRP strip	64
Figure 3-28 Strain versus frame number plot with data collected by strain gauges	64
Figure 3-29 Targets affixed on tension surface of a beam specimen	65
Figure 3-30 Cameras used by the UTVS	67
Figure 3-31 UTVS computers.....	67
Figure 3-32 Setup of vision system	68
Figure 3-33 Calibration.....	69
Figure 3-34 Comparisons between UTVS strains and the strain gauges in Figure 3-27	71
Figure 3-35 Mid-span deflection comparison for two tests between LVDT and UTVS	72
Figure 3-36 Comparison between raw and smoothed deflection data for test B5H1.4S2	74
Figure 3-37 Comparison between raw and smoothed strain data for test B5H1.4S2	74
Figure 3-38 Tests for the CFRP material properties (courtesy of Changhyuk Kim).....	75
Figure 4-1 Anchor rupture of beam B5H1.4Sb	77
<i>Figure 4-2</i> Beam-section equilibrium illustration	78
Figure 4-3 Beam equilibrium.....	79
Figure 4-4 Load vs deflection at mid-span for B5H1.4Sb.....	79
Figure 4-5 Beam targets on the tensile surface of beam used for deflection measurement.....	80
Figure 4-6 Contour plot of ϵ_x for B5H1.4Sb.....	82
Figure 4-7 Critical sections on CFRP strip.....	82
Figure 4-8 X-direction CFRP strip strain distribution across the mid-span section for test B5H1.4Sb.....	84
Figure 4-9 X-direction CFRP strip strain distribution nearby CFRP anchors for test B5H1.4Sb	84
Figure 4-10 Centerline strains in the longitudinal direction for test B5H1.4Sb	85
Figure 4-11 Tensile force transfer from CFRP strip to concrete substrate	87
Figure 4-12 Bond stress vs slip reaction for test B5H1.4Sb	88
Figure 4-13 Debonding failure.....	89
Figure 4-14 CFRP strip fracture	89
Figure 4-15 CFRP anchor rupture.....	89
Figure 4-16 Concrete beam shear failure (Huaco, 2010).....	90

Figure 4-17 Delamination between CFRP strip and anchor	90
Figure 4-18 Area and targets selected for strain measurements	92
Figure 4-19 P_{ult} / P_{exp} vs failure modes.....	94
Figure 4-20 The distribution on the values of the strain ratio $\epsilon_{sx\ 98\% \text{ ult}} / \epsilon_{sx\ \text{mid}\ 98\% \text{ ult}}$ among tests	95
Figure 4-21 Concrete-CFRP bond stress versus slip relations extracted from UTVS strain data	96
Figure 4-22 Concrete and CFRP surfaces after debonding	98
Figure 4-23 Load vs deflection for effect of concrete strength on strip fracture.....	99
Figure 4-24 Load transferring from CFRP strip to CFRP anchor	101
Figure 4-25 Load vs deflection for effect of concrete strength on anchor rupture.....	102
Figure 4-26 Load vs deflection for effect of fan geometry on strip fracture	104
Figure 4-27 Strain comparison between $\epsilon_{fx\ \text{mid}\ \text{ult}}$ and the mean of $\epsilon_{sx\ \text{mid}\ 98\% \text{ ult}}$ for different strip widths.....	106
Figure 4-28 Comparison of mean and maximum values of $\epsilon_{sx\ 98\% \text{ ult}}$ for different strip widths .	107
Figure 4-29 Load vs deflection for effect of strip width on strip fracture	108
Figure 4-30 Strain comparison between mean and maximum $\epsilon_{sx\ 98\% \text{ ult}}$ for different strip widths tests sustaining strip fracture and with an anchor material ratio of 1.41	110
Figure 4-31 Failure modes for tests with 5 in. strips	112
Figure 4-32 Failure modes for tests with 3 in. strips	112
Figure 4-33 Strain comparison between Mean and Maximum $\epsilon_{sx\ 98\% \text{ ult}}$ for directly comparable tests with 5 in. strips and different anchor-material ratio	114
Figure 4-34 Strain comparison between Mean and Maximum $\epsilon_{sx\ 95\% \text{ exp}}$ for directly comparable tests with 5 in. strips and different anchor-material ratio	115
Figure 4-35 Load vs deflection for effect of anchor-material ratio on strip fracture.....	115
Figure 4-36 Strain comparison between Mean $\epsilon_{sx\ 98\% \text{ ult}}$ and Max $\epsilon_{sx\ 98\% \text{ ult}}$ for directly comparable tests with 3 in. strips and different anchor material ratio.....	118
Figure 4-37 Load vs deflection response of tests with varying anchor-material ratios for 3 in. strips.....	118
Figure 4-38 Typical load vs deflection responses for tests with different bond condition and a 2.0 anchor-material ratio.....	123
Figure 4-39 Typical load vs deflection responses for tests with different bond condition and a 1.41 anchor-material ratio.....	123

Figure 4-40 Load vs deflection of nominally identical test specimens	125
Figure 4-41 Bond stress vs slip of nominally identical test specimens	125
Figure 5-1 Element Types.....	129
Figure 5-2 Complete beam showing planes of symmetry for the quarter model simulated	130
Figure 5-3 1/4 beam model and its boundary conditions.....	131
Figure 5-4 CFRP strip and CFRP anchor	132
Figure 5-5 Connections between CFRP strip and CFRP anchor	133
Figure 5-6 CFRP-concrete interface modeling	134
Figure 5-7 Spatial failure surface for concrete (SAS, 2009);	135
Figure 5-8 Compressive stress-strain curve for concrete.....	137
Figure 5-9 Comparison between the selected bond stress-slip relations and the average relations extracted from tests	138
Figure 5-10 Input behavior of F/A_{eff} vs. Elongation and resultant behavior of bond stress vs. slip for 5.4 ksi and 11.5 ksi concrete (A_{eff} = the effective surface area represented by a nonlinear spring element)	140
Figure 5-11 Comparison between the computationally derived bond stress versus slip relations and the relations extracted from sample tests	142
Figure 5-12 Load-deflection comparison for Simulation 1 and comparable tests.....	145
Figure 5-13 Load-deflection comparison for Simulation 2 and comparable tests.....	146
Figure 5-14 Load-deflection comparison for Simulation 3 and comparable tests.....	146
Figure 5-15 Load-deflection comparison for Simulation 4 and comparable tests.....	147
Figure 5-16 Load-deflection comparison for Simulation 5 and comparable tests.....	147
Figure 5-17 Load-deflection comparison for Simulation 6 and comparable tests.....	148
Figure 5-18 Selected sections on specimens used to perform average strain comparisons.....	149
Figure 5-19 Comparison of load-strain response between Simulation 1 and comparable tests .	150
Figure 5-20 Comparison of load-strain response between Simulation 1 and comparable tests .	150
Figure 5-21 Comparison of load-strain response between Simulation 3 and comparable tests .	151
Figure 5-22 Comparison of load-strain response between Simulation 4 and comparable tests .	151
Figure 5-23 Comparison of load-strain response between Simulation 5 and comparable test...	152
Figure 5-24 Comparison of load-strain response between Simulation 6 and comparable tests .	153
Figure 5-25 Comparison of load-strain response between Simulation 1 and comparable tests .	154

Figure 5-26 Comparison of load-strain response between Simulation 2 and comparable tests .	154
Figure 5-27 Comparison of load-strain response between Simulation 3 and comparable tests .	155
Figure 5-28 Comparison of load-strain response between Simulation 4 and comparable tests .	155
Figure 5-29 Comparison of load-strain response between Simulation 5 and comparable test (anchor fan end is not available due to lack of experimental data in that region in test B5H1.4Sb)	156
Figure 5-30 Comparison of load-strain response between Simulation 6 and its comparable tests	156
Figure 5-31 Locations of selected targets along width of the CFRP strip	157
Figure 5-32 Strain comparisons across CFRP strip width between Simulation 2 and B5H1Mc and d.....	158
Figure 5-33 Strain comparisons across CFRP strip width between Simulation 4 and B5L1.4Mc	159
Figure 5-34 Input F/A_{eff} -Elongation relations used in the nonlinear spring bond elements with varying shape	161
Figure 5-35 Load-deflection comparisons for sensitivity study	163
Figure 5-36 Comparison of load-strain response at mid-span for Series 2.....	163
Figure 5-37 Comparison of load-strain responses across strip width for Series 2 simulations ..	164
Figure 5-38 The anchorage tests of Huaco (2009).....	166
Figure 5-39 Anchored strip attached on the tensile surface of specimens (Huaco, 2009).....	166
Figure 5-40 Input F/A_{eff} -Elongation relations used to simulate tests with 4 in. strip or 3 in. strip	167
Figure 5-41 1/4 beam models for the simulations of Huaco's tests (2009).....	168
Figure 5-42 Comparison of load-strain response between simulations and comparable tests of Huaco (2009)	169
Figure 5-43 Comparison of load-strain response between Simulation 11 and gauges at mid-span from Huaco 1	170
Figure 5-44 Comparison of load-strain response between Simulation 12 and gauge at centerline at mid-span from Huaco 2.....	171
Figure 6-1 Radius gauge and bend radius (Pham, 2009).....	182
Figure 6-2 Layout of CFRP strip with one CFRP anchor.....	184

Figure 6-3 Layout of CFRP strip with two CFRP anchors	186
Figure C-1 Side view without CFRP	199
Figure C-2 Bottom view without CFRP	199
Figure C-3 Side view with CFRP	200
Figure C-4 Bottom view with 5 in. CFRP strip	200
Figure C-5 Bottom view with 3 in. CFRP strip	201
Figure D-1 Contour plots for B5H2Ma	203
Figure D-2 Contour plots for B5H1.4Mc	204
Figure D-3 Contour plots for B5H1.4Sa.....	205
Figure D-4 Contour plots for B5H1.4La.....	206
Figure D-5 Contour plots for B5H1.4Lb	207
Figure D-6 Contour plots for B5L1.4Mc.....	208
Figure D-7 Contour plots for B5L1.4Md.....	209
Figure D-8 Contour plots for B5H1Mc	210
Figure D-9 Contour plots for B5H1Md	211
Figure D-10 Contour plots for B5L1Me.....	212
Figure D-11 Contour plots for B5L1Mg.....	213
Figure D-12 Contour plots for U5H1.4Mb.....	214
Figure D-13 Contour plots for B3H1.4Sa.....	215
Figure D-14 Contour plots for B3H1.4Sb.....	216
Figure D-15 Contour plots for B3H1.4Ma	217
Figure D-16 Contour plots for B3H1.4Mb	218
Figure D-17 Contour plots for B3H1.4Lb	219
Figure D-18 Contour plots for B3H1.4XLa.....	220
Figure D-19 Contour plots for B3H1.4XLb	221
Figure D-20 Contour plots for B311XLa	222
Figure D-21 Contour plots for B311XLb	223

CHAPTER 1

Introduction

1.1 OVERVIEW

The application of Carbon Fiber Reinforced Polymers (CFRP) in rehabilitation of concrete structures has progressively increased since the 1980's because of its high strength, light-weight, and flexibility, which provides an easy and efficient way to repair and strengthen concrete structures. Normally, epoxy resin has been used as an interface material to attach CFRP material to concrete surfaces to transfer load from the concrete substrate to the CFRP. The substrate material is much weaker than the CFRP strips and epoxy resin and fails before the capacity of the CFRP strips is reached. Recent research suggests that the introduction of CFRP anchors provides an alternate force transfer mechanism so that more of the strength of the CFRP material can be developed after debonding occurs. This research is focused on the behavior of CFRP anchors and their ability to fully develop the strength of CFRP materials used in strengthening of concrete structures.

1.2 NECESSITY OF INTRODUCING CFRP ANCHORS

In the state of Texas, CFRP materials have been used primarily for durability or for repair of members with impact damage. CFRP anchors, however, are rarely used in these projects. CFRP materials may be used for repair or strengthening bridges if there is a loss of capacity due to corrosion, construction error, damage by impact load, or the need to increase load capacity. In unanchored applications, tensile force is transferred from CFRP strips to the concrete substrate

through interface bond only. As a result, less than 40% of the tensile strength of CFRP strips can be realized before the strips debond from the concrete substrate (Orton, 2007). Available solutions to prevent a premature debonding failure are complete wrapping (Figure 1-1) and using CFRP anchors on U-wrapping (Figure 1-2). Both complete wrapping applications and anchored U-wrapping applications have been tested with an anchored CFRP strip reaching rupture strain (Kim, 2011). Without anchors, however, U-wrapping applications are less efficient than complete wrapping application (ACI 440.2R-08, 2008). While complete wrapping produces excellent behavior, it is less practical than U-wrapping applications if 1) there is a deck in place on the girder so that complete wrapping is impossible and 2) re-entrant corners in some girders results in the CFRP strip pulling away at the corners.

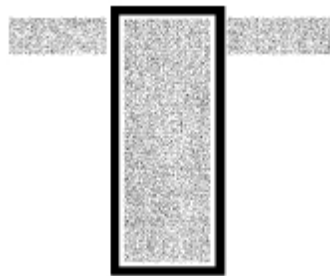


Figure 1-1 Complete wrapping application (ACI 440.2R-08, 2008)

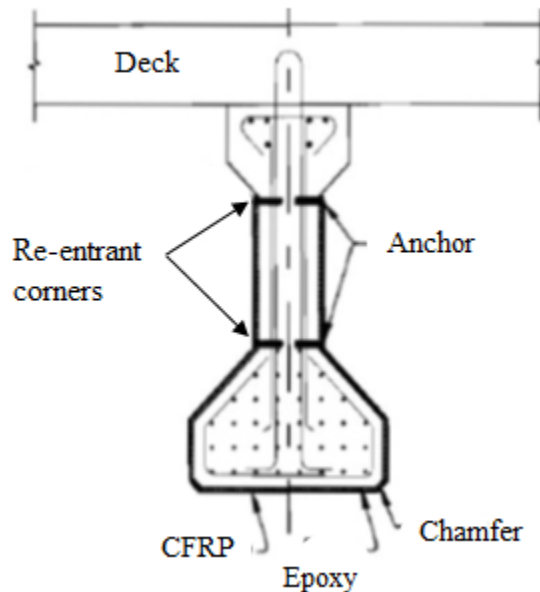


Figure 1-2 Anchored U-wrapping application for a I-girder

1.3 PROJECT OBJECTIVE AND SCOPE

The goal of this research is to provide guidelines for a reliable anchorage system to utilize the high tensile strength of CFRP materials. The study reported here consists of the following topics:

1. Literature review in which the history and current applications of CFRP materials in rehabilitation are presented in Chapter 2. Additional information about design philosophy, quality control of installation, numerical investigations of the behavior of CFRP strengthening systems are also presented in Chapter 2.
2. The test program is discussed in Chapter 3 in which 39 tests were conducted to improve anchor design and quality control procedures. A key feature of the test program was the use of a non-contact deformation measurement system to record displacements in CFRP strips and deformations of test specimens.
3. Based on that data, load versus deformation relations, strain distributions along and across CFRP strips, and strain contours were plotted to determine the influence of the following parameters on the performance of anchorage systems (Chapter 4).
 - I. Width of CFRP strips
 - II. Material ratio of CFRP anchors to CFRP strips
 - III. Concrete strength
 - IV. Geometry of anchor fan
 - V. Bonded vs. unbonded installations
4. A 3-D Finite Element (FE) model is described in Chapter 5 that was used to simulate the behavior of anchored CFRP strips on concrete members. In order to ensure that the proposed FE model properly represents the parameters investigated in the experimental portion of the study, six simulations were conducted using the model by adjusting parameters to match those of six tests

having various anchor-material ratios, concrete strengths, length of anchor fans, and bond conditions. Comparisons between computed and experimental results are presented in Chapter 5.

5. Design guidelines for CFRP anchorage systems are proposed in Chapter 6 with consideration of the influence of CFRP strip width, anchor-material ratio, anchor fan length, embedment length, bending radius, and anchor hole. Two criteria, one is based on ultimate test load and another based on failure mode, are presented in Chapter 6 to evaluate the quality control test for 1) the validation of the quality of anchor installation, and 2) the evaluation of the design parameters for different geometry and material characteristics. The limits of this testing methodology for quality control are also listed in Chapter 6
6. Summary and conclusions are presented in Chapter 7.

CHAPTER 2

Background Study

2.1 HISTORY OF CFRP MATERIAL IN REHABILITATION

In reinforced concrete members, the concrete generally resists compressive forces and steel reinforcing bars embedded in the concrete carry tensile forces. Such an arrangement produces an efficient concrete member utilizing the most desirable characteristics of each material. As concrete structures age, they may face numerous challenges from increasing load demands, deterioration due to environmental conditions, and damage due to the result of impact loading or the action of natural phenomena such as flooding, wind or hurricanes, and earthquakes. Efforts to rapidly and effectively upgrade and rehabilitate structures have resulted in increased interest in the use of CFRP material in rehabilitation. In typical applications, CFRP materials are attached to the tensile surface of a concrete member as shown in Figure 2-1.



Figure 2-1 Installing a CFRP strip on the tensile substrate of a concrete member

(Orton et al., 2007)

2.1.1 Development and Properties of Carbon Fiber Material

2.1.1.1 Development

In 1880, Thomas Edison first suggested and patented the production and application of carbon fibers for his light bulbs. In the middle of the 20th century, the increasing demands on light weight, high strength, good heat insulation, and corrosion resistant material for aerospace, marine, electrical and transportation systems resulted in renewed interest in carbon fibers. In 1958, high-performance carbon fiber material was made from Rayon at the Union Carbide Parma Technical Center (Artem, 2010). In the 1960s, commercial uses of carbon fiber by the US Air Force and NASA resulted in lighter and faster aircraft. The production of fiber at that time, however, required production under high temperature and high pressure conditions (Artem, 2010). Applications of carbon fiber in civil engineering structures were not considered due to cost. During the 1970s, the manufacturing cost was reduced by using polyacrylonitrile (PNA) instead of mono-crystal graphitic fiber as a raw material for creating carbon fiber. The application of the pultrusion process in the 1980s reduced manufacturing costs and enabled carbon fiber to be used as a material for civil engineering structures.

2.1.1.2 Introduction

Fiber Reinforced Polymers (FRP) are manufactured materials consisting of fiber polymers and additives.

2.1.1.3 Fiber

Fibers comprise the largest volume in a composite laminate. Different materials such as glass (GFRP), aramid (AFRP), and carbon (CFRP) are used to make fiber to suit different industrial and commercial purposes.

In material science, a slip system describes the set of symmetrically identical slip planes allowing dislocation motion to easily occur in certain slip directions which eventually produces plastic deformation. Generally, a material with fewer slip systems is stronger and more brittle

than another material with more slip systems. The hexagonal close packed structure (Figure 2-2) of fibers has fewer slip systems (3-6) than a body center cubic structure (12 slip systems) (Figure 2-3) such as iron, molybdenum, potassium, and tungsten. Since deformation is a matter of the number of slip systems, fiber materials are brittle and normally undergo very little deformation before the bond between atoms fracture under tension. In addition, more energy is required to break the bond between atoms than between slip surfaces making fiber materials stronger than body centered materials such as iron and steel.

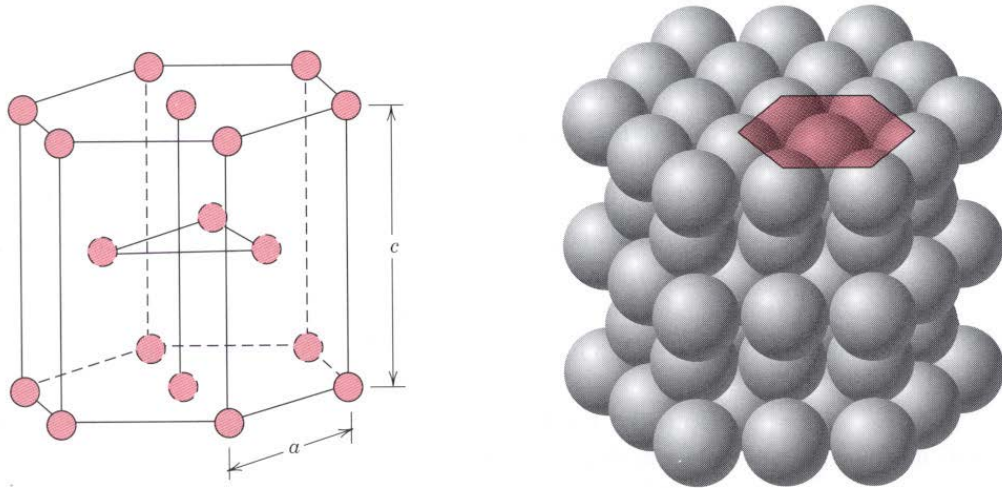


Figure 2-2 Hexagonal close packed structure (Juenger, 2011)

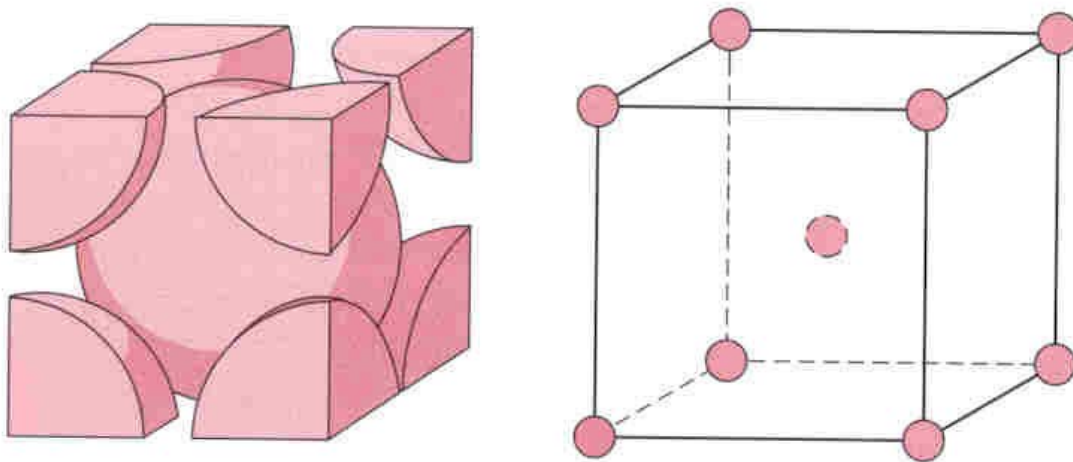


Figure 2-3 Body center cubic structure (Juenger, 2011)

A summary of fiber properties is listed in Table 2-1. Characteristics of fiber materials can be summarized as follows:

1. High tensile strength and high tensile modulus
2. Limited influence of fatigue
3. Limited influence of the environment
4. Four to six times lower density than steel
5. High cost per unit weight
6. High brittleness

Table 2-1 Material properties of fibers (Juenger, 2011)

Types of Fibers	Carbon	Aramid	E-Glass
Strength (ksi)	550 to 700	500 to 600	270 to 390
Tensile Modulus (1000 ksi)	32 to 34	16 to 18	10 to 10.5
Creep-Rupture % of Ultimate strength	91%	47%	30%
Moisture and Chemistry resistance	Excellent	Good	Low
Cost	High	Highest	Low
Density Ratio of Steel to Fiber	8:1.59	8:1.38	8:1.99

2.1.1.4 Polymers and Additives

Manufactured epoxy resins are commonly used as additives to attach FRP on the surface of specimens. It is a long-chain polymer material with multiple repeating poly units of molecules connected through covalent bonds.

Normally, the liquid state of epoxy resin is used for FRP installations. After epoxy resin cured, the resulting product is a solid state epoxy resin performing like a matrix to bind fibers together. Since covalent bonds are much weaker than atomic bonds, the strength contributed by the matrix is much less than that contributed by the fibers. The matrix allows load to be transferred between fibers, thereby preventing premature failure caused by uneven load

distribution between fibers. The matrix increases resistance to environmental effects and to mechanical abrasion.

2.1.1.5 Application of Unidirectional CFRP Strips to Strengthen Structural Members

Unidirectional CFRP strips are most commonly produced by manufacturers for strengthening applications of structural members. All fibers are arranged in a longitudinal direction and glued together by epoxy resin as shown in Figure 2-4. The tensile strength of this strip is largest in the longitudinal direction which is also known as the fiber direction, and lowest along transverse direction determined mostly by epoxy resin. In general, the strip is oriented to augment the tensile strength of the structure as shown in Figure 2-5. Unfortunately, CFRP strips are prone to delaminate from concrete surfaces under stresses 40% to 50% of the fiber strength due to lack of an effective load transfer path or to poor substrate surface failure before epoxy failure. The introduction of CFRP anchors provides an effective approach to transfer the tensile load from the CFRP strip to the underlying substrate after debonding occurs.

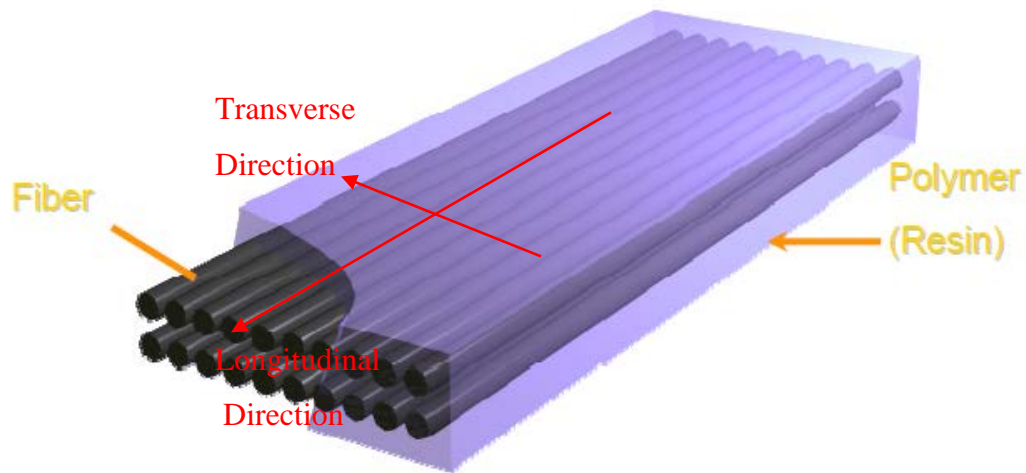


Figure 2-4 Unidirectional CFRP strip



Figure 2-5 CFRP strengthening application

2.1.2 Strengthening and Repairing Structures

CFRP reinforcing bars were used to internally reinforce concrete members and to replace steel reinforcement when high tensile strength, nonmagnetic properties, or high corrosion resistance were required (Kim, 2011). CFRP reinforcing bars, however, cannot replace steel reinforcement where ductility is needed. CFRP materials may be used where rapid rehabilitation is needed and can be externally bonded to a concrete member. A CFRP strip may reach high strains but remains linear up to fracture. As a rehabilitation material, the installation of the CFRP leads to improved durability, short installation time, and visually no change in the geometry of the structure. Figure 2-6 shows a prestressed concrete bridge in Texas damaged due to an over-height load and repaired using CFRP strips.



Figure 2-6 Application of CFRP material to repair IH 20 Bridge (D.Y. Yang, 2003)

2.1.3 Typical Failure Modes of CFRP Installations

Typically, failures result when the CFRP strip debonds from a concrete substrate. Experimental data indicate debonding failure occurs when a CFRP strip develops about 40%-50% of its tensile strength (Bonacci et al., 2001; Orton, 2008). Figure 2-7 (a) shows specimens that failed prematurely because of debonding. The tensile strength of CFRP is realized only if fracture occurs. Although this type of failure is typically identified as a debonding failure, the failure actually occurred in the concrete substrate with the epoxy pulling off the concrete surface of the substrate as shown in Figure 2-7 (b).



(a) Debonding failure

(b) Concrete adhering to epoxy

Figure 2-7 Failure mode of a test without application of CFRP anchor

2.1.4 Bond Strength

Bond strength is the shear strength at the interface between the CFRP material and the concrete substrate. Bond strength determines the maximum tensile force that can be developed in a CFRP strip when a debonding failure occurs. Bond and slip between FRP and concrete are simulated using bond-slip models of varying complexity in the literature. The simplest relation used for bond strength and slip is linear, while more complex bond-slip models assume bi-linear relations or even non-linear relations. Nakaba et al., 2002 proposed a bond-slip relation defined by an ascending branch and a maximum bond stress values.

The proposed bond stress (τ) versus slip (s) relations are given as:

$$\tau = \tau_{max} \left(\frac{s}{s_0} \right) \left[3 / \left(2 + \left(\frac{s}{s_0} \right)^3 \right) \right] \quad \text{Equation 2-1}$$

$$\tau_{max} = 3.5 f'_c{}^{0.19} \quad \text{Equation 2-2}$$

Where,

s = bond slip, mm.

s_o = bond slip at maximum bond stress, mm. Here $s_o = 0.065$ mm based on the average value of experimental results,

Chen et al. (2001) used pull tests to determine the bond mechanism between CFRP strips and the concrete substrate. The tests consisted of adhering CFRP strips with epoxy to a concrete block and then pulling them until complete detachment from the concrete. The bond-slip model of Chen et al has linear ascending and descending branches as shown in Figure 2-8. The slip (σ_l) at peak bond stress (τ_f) was taken as 0.02 mm (0.0008 in.) and the maximum slip (σ_f) was taken as 0.2 mm (0.008 in.) based on experimental results. The calculation of peak bond stress considered the influence of concrete strength (f_c), FRP strip modulus (E_f), effective bond length ($l_e = \sqrt{\frac{E_f t_f}{\sqrt{f_c}}}$, mm) and width ratio as shown in Equation 2-3. The predictions of Equation 2-3 are found to be in close agreement with single-shear pull tests performed by Yao et al (2005).

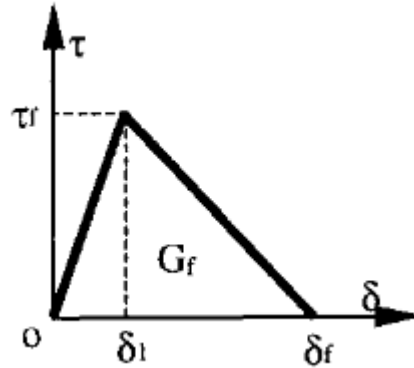


Figure 2-8 Bond-slip model (Chen et al., 2001)

Teng, et al (2003) calibrated Equation 2-3 with experimental data from pull-off test and proposed a better-fit coefficient α ($\alpha=0.48$) to account for both flexural crack induced debonding and flexural-shear crack induced debonding.

$$\tau_f = \alpha \beta_w \beta_l \sqrt{\frac{E_f \sqrt{f'_c}}{t_f}}, MPa \quad \text{Equation 2-3}$$

in which

$$\beta_w = \sqrt{\frac{2-b_f/b_c}{1+b_f/b_c}} \quad \text{Equation 2-4}$$

$$\beta_l = \begin{cases} 1 & \text{if } l \geq l_e \\ \sin \frac{\pi l}{2l_e} & \text{if } l < l_e \end{cases} \quad \text{Equation 2-5}$$

Where

- α = coefficient ($\alpha=0.427$)
- b_c = width of concrete block, mm.
- b_f = width of CFRP strip, mm
- t_f = thickness of CFRP strip, mm
- l = the bond length, mm
- l_e = the effective bond length, mm

Based on the assessment of numerical models using experimental results of 253 pull tests as shown in Figure 2-9, Lu et al. (2005a) found that 1) available bond-slip models cannot accurately predict both shape and interfacial fracture energy, and 2) the most accurate models are the bond-slip model proposed by Lu et al. (2005 a).

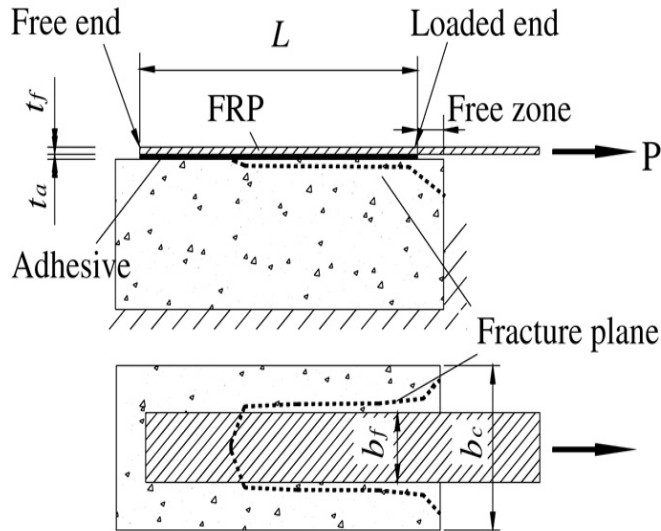


Figure 2-9 Pull test from Lu et al. (2005a)

The nonlinear bond-model included the influence of CFRP width, concrete strength and CFRP modulus. The bond behavior was defined by empirical stress-slip curves that consist of an ascending branch and a descending branch until the bond stress reaches zero as shown in following equations and Figure 2-10.

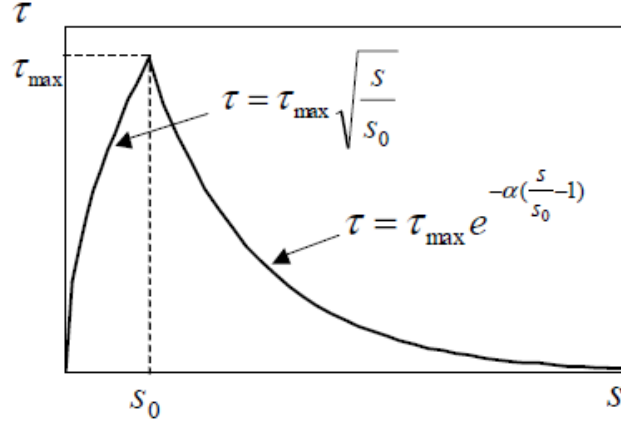


Figure 2-10 Bond stress versus slip model (Lu et al., 2005b)

$$\tau = \begin{cases} \tau_{max} \sqrt{\frac{s}{s_0}}, & \text{if } s \leq s_0 \\ \tau_{max} e^{-\alpha(\frac{s}{s_0}-1)}, & \text{if } s \geq s_0 \end{cases} \quad \text{Equation 2-6}$$

in which

$$\tau_{max} = 1.5\beta_w f_t \quad \text{Equation 2-7}$$

$$s_0 = 0.0195\beta_w f_t \quad \text{Equation 2-8}$$

$$\beta_w = \sqrt{\frac{2-b_f/b_c}{1+b_f/b_c}} \quad \text{Equation 2-9}$$

$$\alpha = \sqrt{\frac{1}{\frac{G_f}{\tau_{max} s_0} - \frac{2}{3}}} \quad \text{Equation 2-10}$$

$$G_f = 0.308\beta_w^2 \sqrt{f_t} \quad \text{Equation 2-11}$$

where

b_c = width of concrete block, mm.

b_f = width of CFRP strip, mm

f_t = tensile strength of concrete, Mpa

G_f = interfacial fracture energy, Mpa mm

τ = bond stress, Mpa

τ_{max} = Maximum bond stress, Mpa

While bond models provide some understanding of the force transfer between CFRP and the concrete substrate and are valuable for use in FEM analysis, they cannot be easily integrated into design equations as will be discussed in the next section.

2.1.5 Design Philosophy

The most recent and widely accepted guidelines for CFRP flexural and shear strengthening have been reported by ACI 440.2R (2008). Based on limit-state-design principles, the acceptable level of design for this approach considers both serviceability and ultimate limit states.

2.1.5.1 Flexural Design

An environmental reduction factor C_E is recommended to account for the strength loss due to long-term exposure to environmental conditions. The design tensile strain is therefore determined by

$$\varepsilon_{fu} = C_E \times \varepsilon_{fu}^* \quad \text{Equation 2-12}$$

where

ε_{fu} = design rupture strain of CFRP with consideration of reduction for service environment.

C_E = environmental reduction factor which is either 1 for CFRP on a concrete unexposed to earth and weather or 0.9 on exposed concrete.

ε_{fu}^* = guaranteed rupture strain of CFRP reinforcement defined as the mean tensile strain at failure of sample test specimens minus three times the standard deviation.

To account for other unknowns, a strength reduction factor Φ is used to reduce the calculated nominal moment capacity to a design moment that must equal or exceed moments due to the applied factored loads. The moment at section M_u is therefore determined by the following equations

$$\Phi M_n \geq M_u \quad \text{Equation 2-13}$$

$$M_n = A_f f_{fu} \left(d_s - \frac{\beta_1 c_b}{2} \right) \quad \text{Equation 2-14}$$

$$c_b = \left(\frac{\varepsilon_{cu}}{\varepsilon_{cu} + \varepsilon_{fu}} \right) d_s \quad \text{Equation 2-15}$$

where

M_n = nominal moment capacity, kips-in

M_u = factored moment at a section, kips-in

A_f = area of CFRP, in.²

f_{fu} = design tensile strength of CFRP, ksi.

d_s = distance from extreme compression fiber to centroid of tension reinforcement, in.

c_b = distance from extreme compression fiber to neutral axis at balance strain condition, in.

ε_{cu} = ultimate strain in concrete.

β_1 = factor relating depth of equivalent rectangular compressive stress block to neutral axis depth.

The ultimate strain for a member governed by debonding failure should be limited to the strain level at which debonding may occur, ε_{fd} , as defined by ACI 440.2R in the following equations.

$$\varepsilon_{fd} = 0.083 \sqrt{\frac{f'_c}{n E_f t_f}} \leq 0.9 \quad \text{Equation 2-16}$$

in which

n = number of plies of FRP reinforcement

ε_{fu} = design rupture strain of FRP reinforcement provided by the manufacturer.

E_f = tensile modulus of elasticity of FRP provided by manufacturer, psi

t_f = the specified thickness of the CFRP strip, in.

where

$$E_f = f_{fu} / \varepsilon_{fu} \quad \text{Equation 2-17}$$

2.1.5.2 Shear Design

According to ACI 440.2R (2008), the nominal shear strength of a CFRP-strengthened concrete member can be determined by summarizing the shear contribution of steel, concrete and CFRP strip as shown in the equation below:

$$\phi V_n = \phi(V_c + V_s + \psi_f V_f) \quad \text{Equation 2-18}$$

Where

- ϕ = the strength reduction factor
- ψ_f = CFRP strength reduction factor
(0.95 for completely wrapped member; 0.85 for unanchored U-wrapped member)
- V_c = concrete shear contribution, kips
- V_f = CFRP shear contribution, kips
- V_n = the nominal shear strength, kips
- V_s = steel shear contribution, kips

The shear contribution of the CFRP strip is determined by the following equations

$$V_f = \frac{A_{fv} f_{fe} (\sin \alpha + \cos \alpha) d_{fv}}{s_f} \quad \text{Equation 2-19}$$

where $A_{fv} = 2nt_f w_f$ and $f_{fe} = \varepsilon_{fe} E_f$

- A_{fv} = area of CFRP shear strip on two sides of beam, in²
- d_{fv} = effective depth of FRP strip, in²
- f_{fe} = effective stress in the CFRP strip, ksi
- n = number of plies of FRP reinforcement
- s_f = center to center spacing of CFRP strips, in.
- w_f = width of CFRP reinforcing plies, in.
- ε_{fe} = effective strain level in FRP reinforcement attained at failure
(The average strain in the CFRP strips crossing the critical shear crack when the peak shear capacity is reached)
- t_f = thickness of CFRP strip, in.

Kim (2011) suggested several changes. Complete wrapping is the most efficient method for shear strengthening concrete members. The effective strain is determined by the equation below

$$\varepsilon_{fe} = 0.004 \leq 0.75\varepsilon_{fu} \quad \text{Equation 2-20}$$

which limits the maximum effective strain to 0.004

For unanchored U-wrapping applications, Kim suggested that the effective strain be determined by

$$\varepsilon_{fe} = \kappa_v \varepsilon_{fu} \leq 0.004 \quad \text{Equation 2-21}$$

where

κ_v = bond-dependent coefficient for shear applications (1.0 for complete wrapping and 0.75 for U-wrapping).

Therefore, the effective strain of an unanchored U-wrapping application should be limited to 0.003

2.2 BACKGROUND ON CFRP ANCHORS AND ANCHORAGE SYSTEMS

In order to prevent CFRP prematurely debonding from the concrete substrate, anchorage systems have been developed. Mechanically fastened joints involving steel plates and bolts were used to anchor CFRP strips (Lamanna, 2002). The application of mechanically fastened joints, however, unavoidably introduced practical issues such as stress concentration and corrosion. The application of CFRP anchorage systems provides an efficient approach to increase the capacity of CFRP strips without corrosion issues and minimum stress concentrations (Orton, 2008).

A brief review of previous research on the study of CFRP anchors is presented in this section.

2.2.1 Anchor Details

2.2.1.1 Orton (2008)

In Orton's tests, CFRP strips were used to connect two concrete blocks of the same or different heights. As shown in Figure 2-11, the tension force on the CFRP sheet was developed by the mid-span ram so that the two-block specimens were loaded as a 3 point flexural test.

Orton found that by using CFRP anchors having twice the area of the cross-section of the CFRP sheet being anchored, it was possible to fracture the CFRP strip. Several small anchors were more efficient than a large anchor with the same amount of CFRP material. The anchors were placed to prevent debonding of the sheet at the reentrant corner (bottom of the transition slope). In order to prevent anchor failure, a 13 cm - 15 cm (5.1 inch - 5.9 inch) embedment length was recommended to ensure a 5 cm (2 inch) depth into the core concrete and the edge of anchor hole needed to be rounded.

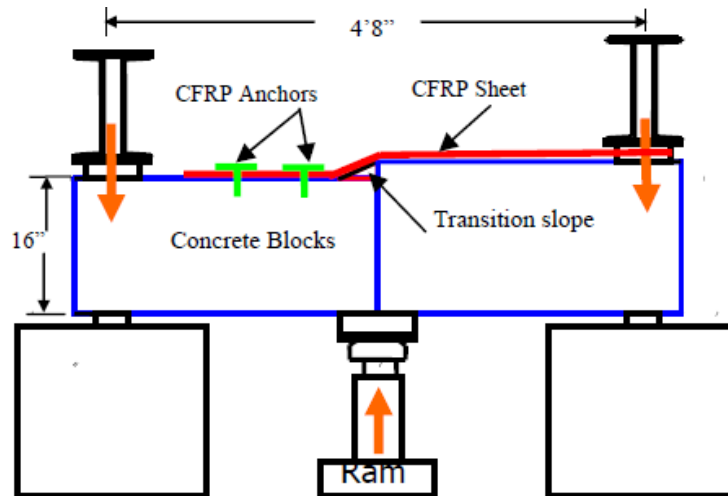


Figure 2-11 Test setup (Orton 2008)

2.2.1.2 Niemitz (2008)

Niemitz (2008) found that the diameter of CFRP anchors (Figure 2-12) is an important parameter in determining the force being transferred at the anchor from the CFRP strip into the concrete substrate. An insufficient amount of CFRP material in the anchors leads to rupture of

the anchors before fracture of CFRP strips. This premature failure due to anchor rupture reduces the effective tensile capacity of the CFRP strips.



Figure 2-12 The diameter of CFRP anchor (Niemitz, 2008)

2.2.1.3 Pham (2009) and Huaco (2009)

Installation of CFRP strips for strengthening members using anchors requires that installers follow manufacturer's recommendations and procedures in order to achieve the desired or design capacity of the CFRP. Therefore, quality control is needed to minimize the effects of improper installation of the CFRP anchors and CFRP strips (Huaco, 2009; Pham, 2009).

Unfortunately, only a limited amount of pertinent literature regarding quality control of CFRP anchors was found. The standard Test Method for Flexural Strength of Concrete Using Simple Beam with Center-Point Loading was applied by Huaco (2009) and Pham (2009) to test the quality of CFRP material. A 6 in. by 8 in. by 20 in. plain concrete block was simply supported with a CFRP strip attached on the tensile surface as shown in Figure 2-13. However, the concrete beam often failed before the CFRP ruptured and did not provide reliable results. High strength ($f'_c=11.5$ ksi) concrete was used by Pham (2009) to prevent concrete shear failure. However, 2 out of 3 tests cast with high strength concrete still failed because of concrete shear. In order to prevent concrete failure in shear, the plain concrete blocks used in this research were strengthened by two U-wrapped CFRP strips which will be discussed in Section 3.3.1.



Figure 2-13 A simple test setup for quality control of CFRP anchors (Pham, 2009)

Based on the results of 18 tests and experimental experience, Pham (2009) and Huaco (2009) listed the following parameters that influence the performance of CFRP anchors: 1) quality of CFRP installation, including the quality of CFRP material and epoxy resin; 2) CFRP anchor size; 3) details of anchor holes which includes bending radius and hole size; 4) Curing of the CFRP system. In addition, Pham recommended a 0.5 inch bend radius which increased the anchor capacity up to 30% compared with zero radius application (no rounding). The area ratio of anchor hole to the cross section of anchor was recommended no less than 1.4 by Pham (2009).

A tension test developed by Pham (2009) was unaffected by concrete failure modes. The tension test consists of two concrete blocks of the same size as shown in Figure 2-14. Anchored CFRP strips were attached on opposite sides of a two-block specimen. The tensile force was developed by a hydraulic jack placed between the blocks to push them apart. Since the discontinuous blocks are vulnerable to eccentricities, loading on the strips was not equal. The tension test was not recommended because of alignment problems and the complexity of the specimen fabrication and test procedure.

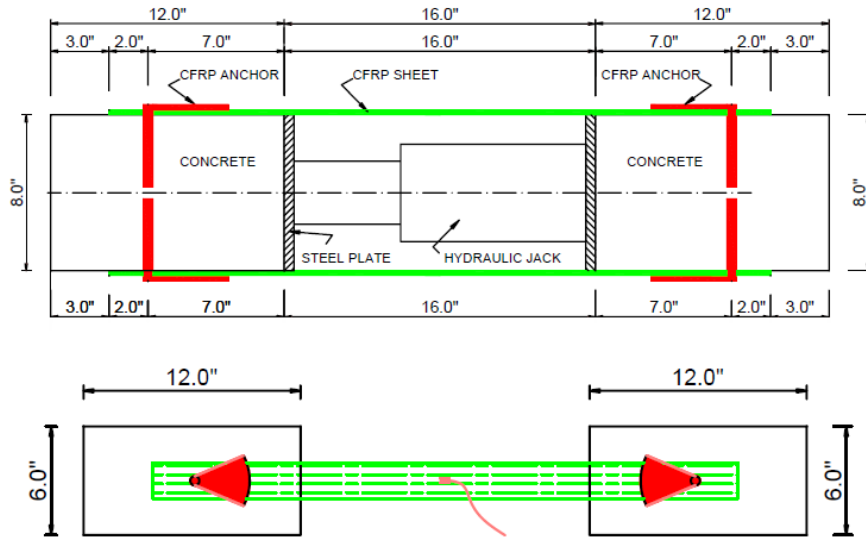


Figure 2-14 Typical test setup and two-block specimen for tension test (Pham, 2009)

2.2.1.4 Smith et al (2009, 2013)

In order to isolate anchor behavior, a pull-test shown in Figure 2-15 was used by Smith (2009) to determine the load-transfer mechanism (bond-slip response) from CFRP strip to CFRP anchor. Typical failure modes of CFRP anchors were anchor shear failure, anchor fan failure (delamination of anchor fan from strip) and anchor pullout failures shown in Figure 2-16. It indicated an inadequate anchor failed before the tensile strength of CFRP strip fully developed. A simplified best-fit and a design equation for the strength of anchors were derived by Smith (2009) based on the anchor pull-test as shown in Figure 2-15. The tensile strength P_u of CFRP anchor is a function of the bond-slip model for the interface material.

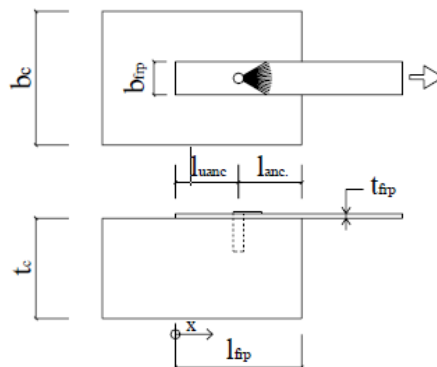


Figure 2-15 CFRP anchor pull-test (Smith et al., 2009)



(a) Anchor shear failure (b) Anchor fan failure (c) Anchor pullout failure

Figure 2-16 Typical anchor failure modes of anchor pull-test (Smith et al., 2009)

$$P_u = k\beta_w b_f \sqrt{0.616 E_f t_f \sqrt{f_{ct,com}}} \quad \text{Equation 2-22}$$

where

$$k = 0.69 + 2.0e^{-1.75(l_{anc}/l_{frp})} \text{ (best-fit model)} \quad \text{Equation 2-23}$$

$$k = 0.51 + 2.0e^{-1.75(l_{anc}/l_{frp})} \text{ (design model)} \quad \text{Equation 2-24}$$

And

l_{anc} and l_{uanc} are shown in Figure 2-15.

$$f_{ct,com} = 0.395(1.32f'_c)^{0.55} \quad \text{Equation 2-25}$$

$$\beta_w = \sqrt{\frac{2-b_{frp}/b_c}{1+b_{frp}/b_c}} \quad \text{Equation 2-26}$$

where

- E_f = tensile modulus of elasticity of FRP
- t_f = the specified thickness of the CFRP strip
- b_f = width of CFRP strip
- f'_c = concrete strength at time of test.

More recent experimental reported by Smith et al. (2013) from 4-point bending tests indicated large anchors increased the strip strain and lead to anchor failure before strip fracture. A more efficient application is breaking large anchors into multiple smaller anchors with the same amount CFRP material. The application of multiple smaller anchors were more efficient in preventing anchor failure by reducing the release of debonding energy that resulted in more even strain distribution and higher ultimate loads.

2.2.1.5 Brena et al. (2013)

A pull-test was also used by Brena et al. (2013) to improve the understanding of the load transfer mechanism between CFRP strip and CFRP anchor. Based on both experimental and analytical studies, Brena et al found that 1) strains were developed unevenly along the width of CFRP strips which suggested the strain distribution obtained along the CFRP strip centerline are not the same as the strain distributions near the edges of a strip, 2) the CFRP anchor fans are recommended to cover the entire width of CFRP strip to fully develop the tensile strength of CFRP strip, and 3) the size of anchor diameter should be designed to reach the force demands of the CFRP strip and required further research.

2.2.1.6 Zhang et al (2012)

The influence of anchor dowel angle on anchor performance was investigated by Zhang et al. (2012a). The angles of anchor dowel and anchor fan are shown in Figure 2-17. The experimental results of 26 tests using angle of anchor dowel from 45° to 157.5° indicates the anchor strength was increased as the angle of anchor dowel (β_{anc}) relative to the direction of load increased.

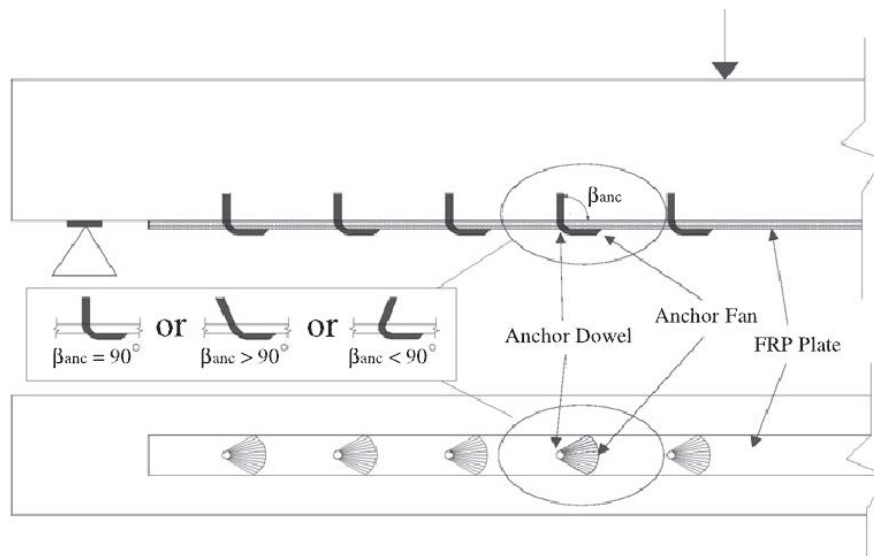


Figure 2-17 CFRP anchor dowel angle (Zhang et al. 2012a)

Later, a force-slip model was proposed by Zhang et al. (2012) based on 3 unanchored and 24 anchored pull-tests. As shown in Figure 2-18, the load-slip response has four regions represented by 1) A-B pre-debonding stage, 2) B-C debonding stage, 3) C-D post debonding stage, and 4) E-F anchor failure. In region A-B, the tensile force on CFRP strips is transferred through interfacial bond material to concrete. Unanchored tests fail in region B-C when CFRP strips start debonding from the CFRP substrate and the tensile load is gradually transferred to the CFRP anchor. In the region C-D-E-F, rigid body movement due to the complete debonding suddenly releases the tensile force in CFRP strip. Then, the rigid body movement is halted and anchor force increases up to anchor failure.

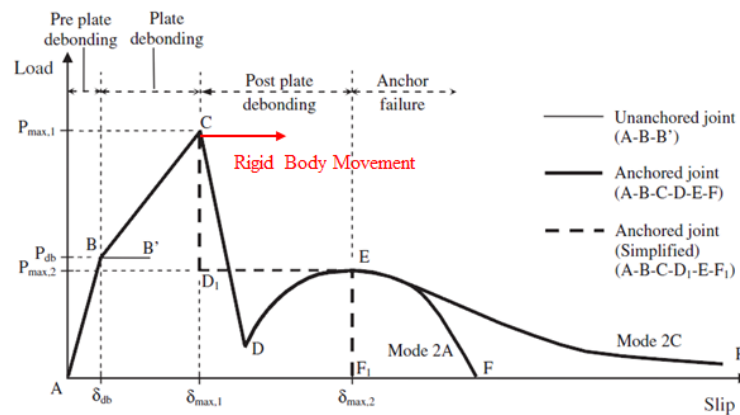


Figure 2-18 Load-slip response for anchored and unanchored pull-test (Zhang et al., 2011)

2.2.1.7 Kalfat et al. (2013)

More recent report from Kalfat et al. (2013) indicates the use of bidirectional fiber patch anchorages was found to improve the performance of a single anchor in terms of larger elongation and strength.

2.2.2 Confinement

2.2.2.1 Kobayashi et al. (2001)

In order to effectively wrap a column at the end of a wall, CFRP anchors were used to achieve a continuous wrapping application as shown in Figure 2-19. The stress transfer mechanism of a CFRP anchor was studied by Kobayashi et al. (2001).

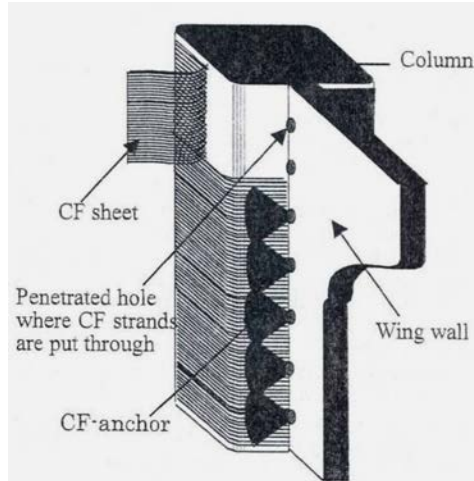
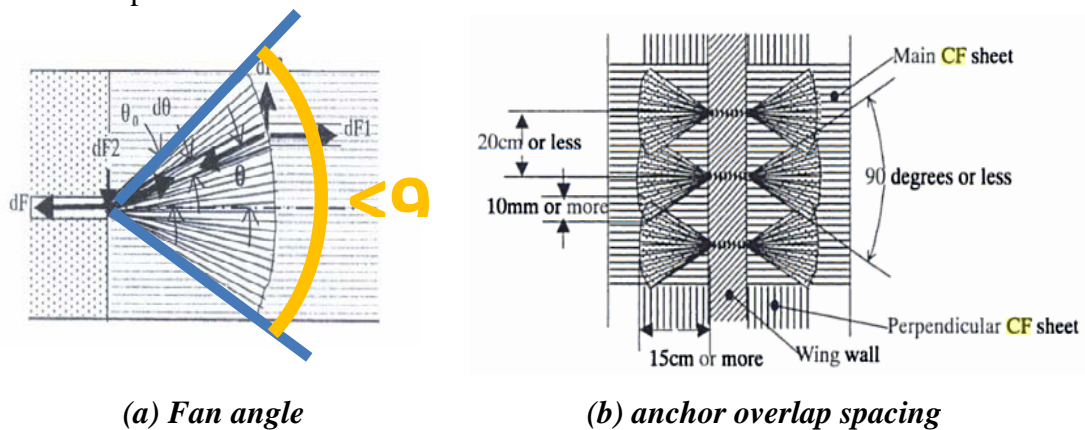


Figure 2-19 Using anchored strip to wrap a column with wing walls

Based on the experimental results, Kobayashi et al found that:

- Fan angle should be less than 90° as shown in Figure 2-20 (a).
- A 10 mm (0.39 inch) or more overlap is recommended for anchor fans as shown in Figure 2-20 (b).
- The length of angle fan should be 150 mm (5.9 inch) or more as shown in Figure 2-20 (b).
- The interval of CFRP anchors should be less than 200 mm (7.9 inch) as shown in Figure 2-20 (b).
- The amount of CFRP material used for anchors should be more than those used for main strips



(a) Fan angle

(b) anchor overlap spacing

Figure 2-20 Recommendations on anchor details (Kobayashi et al., 2001)

2.2.3 Flexure

2.2.3.1 Kim (2008)

Beam tests were used by Kim (2008) to explore the behavior of different anchorage systems under dynamic load. As shown in Figure 2-21, the dynamic load was produced by a pendulum mass. The anchorage systems included U-wrapping and CFRP anchors as shown in Figure 2-22.

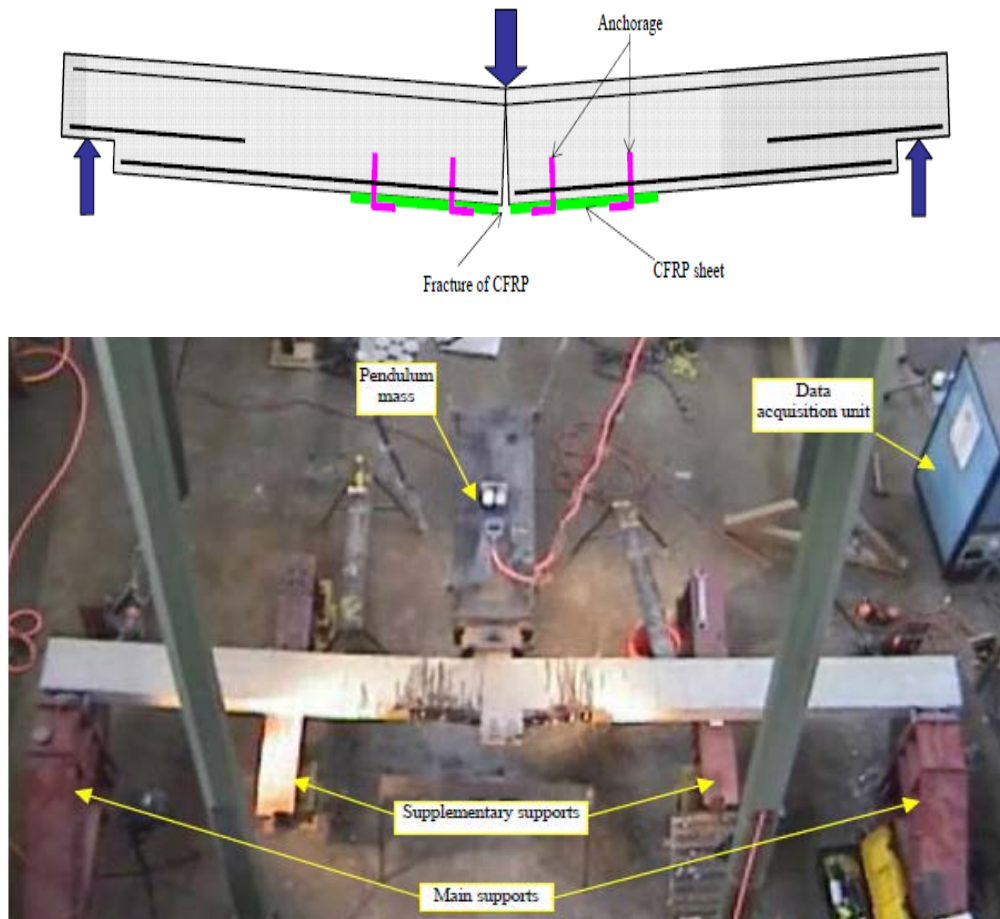


Figure 2-21 Test setup (Kim, 2008)

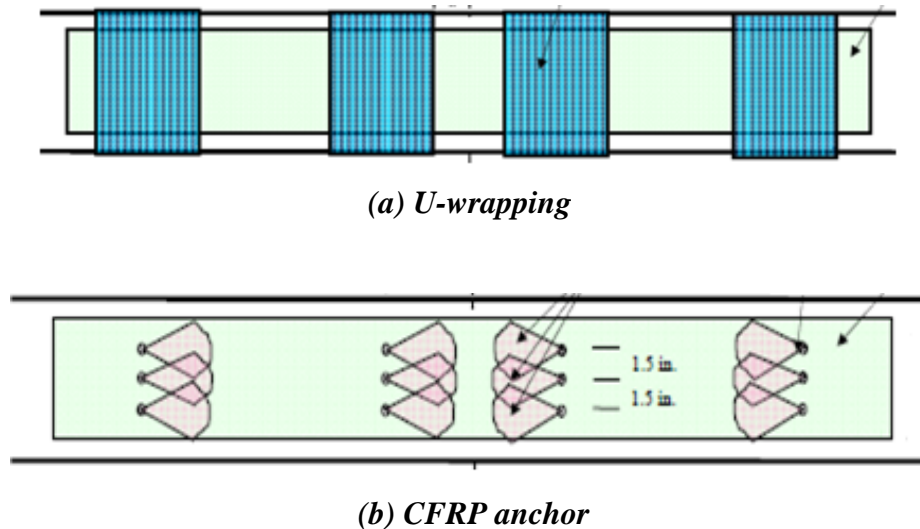


Figure 2-22 CFRP application with anchorage systems (Kim, 2008)

The experimental results indicated both applications produced fracture of the CFRP strip under dynamic load. The CFRP anchors distributed the stress across the CFRP strip more evenly than the U-wrapping application. More stress was transferred to steel reinforcement from CFRP anchored strip than from the U-wrapping application.

In addition, the study of Kim (2008) also reveals the importance of developing a reliable test methodology for isolating the anchor behavior, validating CFRP material properties and inspecting CFRP installations.

2.2.4 Shear

2.2.4.1 Kim (2014)

Kim (2014) used anchored CFRP strips to shear strengthen T-beams as shown in Figure 2-23. An elevation of loading setup is shown in Figure 2-24. In order to prevent anchor failure, two patches with fiber direction either perpendicular or parallel to the fiber direction of the CFRP strip were used.

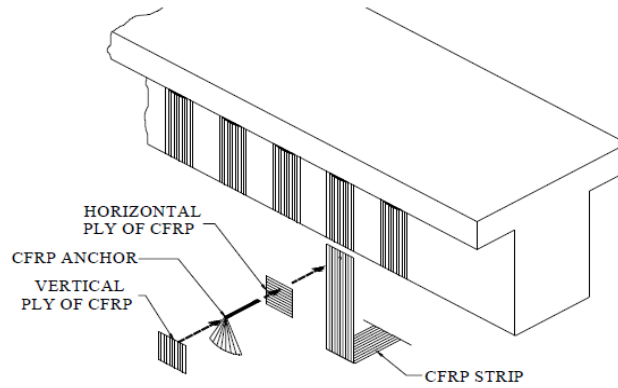


Figure 2-23 Using anchored CFRP strip to u-wrapping a T-beam (Kim, 2014)

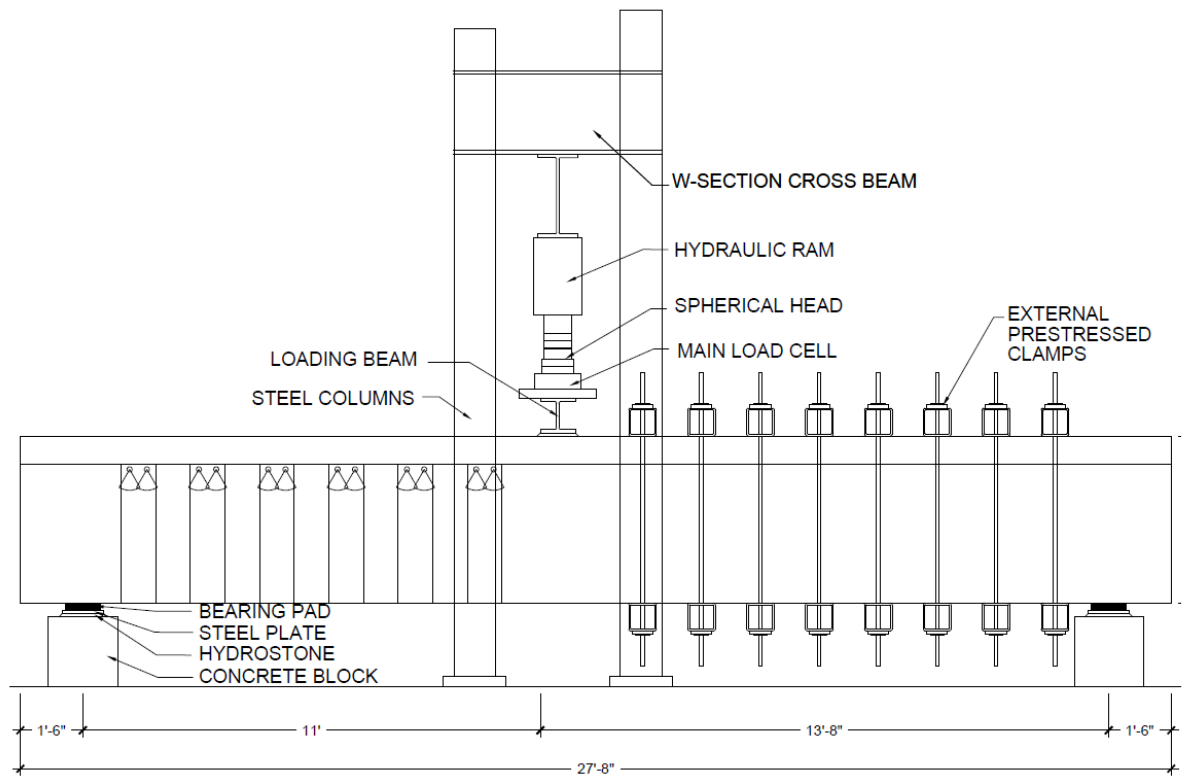


Figure 2-24 Loading setup (Kim, 2014)

As shown in Figure 2-25, Kim (2014) found that unanchored applications did not increase the shear capacity due to the CFRP strip prematurely debonding from concrete surface. For anchored U-wrapping CFRP application, the tensile strength of CFRP strips could be fully developed (Kim, 2014). The average strain on the strip along a critical crack at failure, however, was less than 0.005 because as a brittle material, CFRP material has no plastic behavior and the

strain distribution on strips at failure therefore is not uniform. An effective strain of 0.004 was recommended to represent the average strain on strips at failure for design purposes. The shear strain was obtained from six LVDTs arranged in a rectangle shape as shown in Figure 2-26.

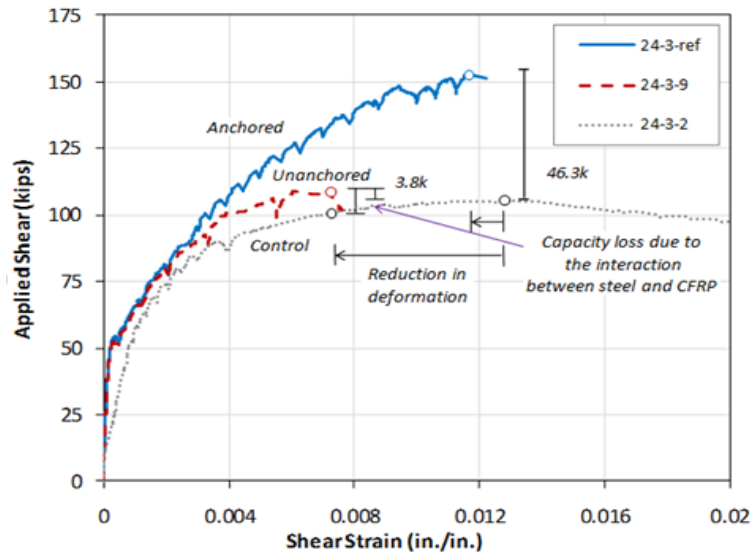


Figure 2-25 Comparisons between anchored and unanchored application (Kim, 2011)



Figure 2-26 LVDTs configuration for shear strain

The two modifications to the ACI 440.2R-08 procedures were proposed by Kim (2011). The modified design equation for FRP shear strengthening is given below with the proposed changes in bold print:

$$V_n = \phi(V_c + V_s + \psi_f V_f) \quad \text{Equation 2-27}$$

Where V_c , V_s , V_f = concrete, steel, and CFRP shear contribution

ϕ =strength reduction factor=0.75

ψ_f =additional reduction factors for FRP shear reinforcement

0.95: completely wrapped member

0.9: U-wraps with anchorage (Kim, 2011)

0.85: U-wraps and 2 sided schemes

$$V_c = 2\sqrt{f'_c}b_wd \quad \text{Equation 2-28}$$

$$V_s = \frac{A_{sv}f_{sy}(\sin \alpha s + \cos \alpha s)d}{s} \quad \text{Equation 2-29}$$

$$V_f = \frac{A_{vf}f_{fe}(\sin \alpha s + \cos \alpha s)d_{fv}}{s_f} \quad \text{Equation 2-30}$$

$$A_{vf} = 2t_f w_f \quad \text{Equation 2-31}$$

$$f_{fe} = \varepsilon_{fe} E_f \quad \text{Equation 2-32}$$

where d_{fv} , s_f , w_f and α are illustrated in Figure 2-27

f'_c = concrete specified compressive strength (psi)

b_w = section web width

d = section effective depth

A_{sv} = area of transverse reinforcement spaced at s

f_{sy} = yield strength of transverse reinforcements

s_f = center to center spacing of CFRP strips

d_{fv} =distance from another to section extreme tension fiber

t_f = nominal thickness of one ply of CFRP reinforcement

w_f = width of CFRP reinforcement plies

E_f = tensile modulus of elasticity of CFRP

ε_{fe} = effective strain level in CFRP reinforcement attained at failure

$\varepsilon_{fe} = 0.004 \leq 0.75\varepsilon_{fu}$ (U-wraps with anchorage proposed by Kim (2011))

ε_{fu} = ultimate strain capacity of CFRP reinforcement

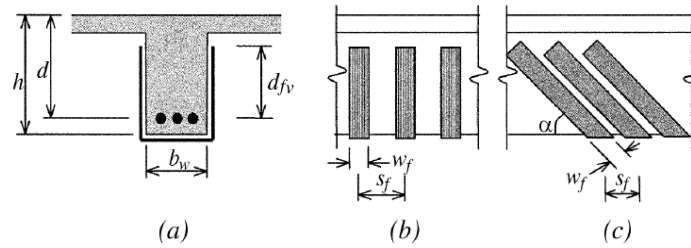


**Figure 2-27 Description of the variables for calculating CFRP shear strengthening
(ACI 440.2)**

Although anchored U-wrapping applications performed like complete wrapping and allowed CFRP strips to reach fracture, the strength of anchored U-wrapping applications were found more variable than complete wrapping applications having a factor $\psi_f=0.95$ and less variable than unanchored U-wrapping applications having a factor $\psi_f=0.85$. A value of $\psi_f=0.9$ was therefore recommended for design of anchored U-wrapping applications. In the study by Kim et al. (2012), all CFRP strips crossing a critical inclined crack did not rupture simultaneously. The measured average CFRP strip strain across the critical crack at failure was found to be around 0.005. For design purposes, an effective strain of 0.004 was recommended.

2.3 NUMERICAL MODELING

Numerous Finite Element (FE) models have been proposed to simulate the behavior of CFRP-strengthened concrete members numerically

Computational models for simulating the behavior of CFRP strengthening systems consist of elements representing the CFRP laminates, the CFRP anchors where applicable, the concrete material, and in some cases the interfacial elements that simulate the debonding behavior between concrete and FRP. The CFRP elements are typically given linear elastic material properties due to the linear/brittle behavior of CFRP. Concrete is typically simulated using continuum finite elements. To account for failure of the concrete at the interface with CFRP during debonding, either a coarse concrete element mesh is used in conjunction with

interfacial elements, or a fine concrete mesh is used at the interface with elements possessing constitutive relations capable of simulating bond failure directly. In the simplest case, “perfect” bond and no slip are assumed between FRP and concrete.

2.3.1 No Slip Models

Modeling the complex interfacial contact mechanism between CFRP material and concrete is a difficult challenge in the numerical analysis of CFRP-strengthened structures. In many numerical investigations for CFRP-strengthened structures (Vecchio et al., 1999; Inbrahim et al., 2009; Chansawat et al., 2009; Kachlakev et al., 2001; Mahjoub et al., 2010; Santhakumar et al., 2004), a layered solid element is used to model the CFRP composite that allows no slip between the CFRP material and the concrete substrates. In such analyses, numerical results show promise for predicting the overall behavior of CFRP-strengthened structures. However, a larger ultimate load is typically obtained because the “perfect” bond assumption precludes the softening effect of CFRP debonding.

2.3.2 Micro-level Analysis of Concrete Cracking

Since the debonding of CFRP from the concrete substrate occurs within a 2 to 5 mm (0.08-0.2 in.) layer of concrete under the epoxy layer, several crack models of continuum-type elements were proposed to simulate CFRP-concrete bond. The rotating angle crack model, with the capability of simulating the shapes and paths of the crack, was proposed to simulate the entire debonding process (Lu et al, 2005c). Unfortunately, the rotating angle crack model is not available in commonly used FE software. Very small elements (0.2-0.5 mm in size) are another hindrance to the use of the rotating angle crack models. Alternatively, an interfacial crack model, using a smeared crack approach can be used to describe the bond mechanisms in CFRP-strengthened structures (Al-Mahaidi, 2001; Pham et al., 2006; Camata et al., 2006). Good agreements between computational and experimental results proved that the interfacial crack model could be used to represent the bond behavior between CFRP and the concrete substrate.

However, the accuracy of the interfacial crack model depends on the prediction of a crack propagation path, which may limit its capability to predict the performance of structural elements with complex crack patterns. Furthermore, the continuum-type models are complex to implement for use by practicing engineers in design or assessment applications.

2.3.3 Interfacial Material

Recently, researchers have attempted to use interfacial elements to simulate the debonding mechanism between CFRP material and the concrete substrate. Lu et al, 2005b used nonlinear spring elements with well-defined bond stress-slip properties (Figure 2-10) as interfacial elements to connect CFRP elements to a coarse mesh of concrete elements (Figure 2-28). Similarly, a two-node nonlinear translational interfacial element incorporating a bond stress-slip relation was used to model the CFRP-concrete bond by Neale, K.W. et al, 2005 and Kotynia, R. et al, 2008 (Figure 2-29). The uni-directional interfacial-element approach was shown to result in satisfactory behavioral representations in cases where bond forces are aligned with the CFRP fibers. This analytical approach, however, cannot simulate the bond behavior when the debonding occurs in an unknown direction (such as in shear strengthening applications where concrete cracks occur at variables angles to the CFRP fibers direction).

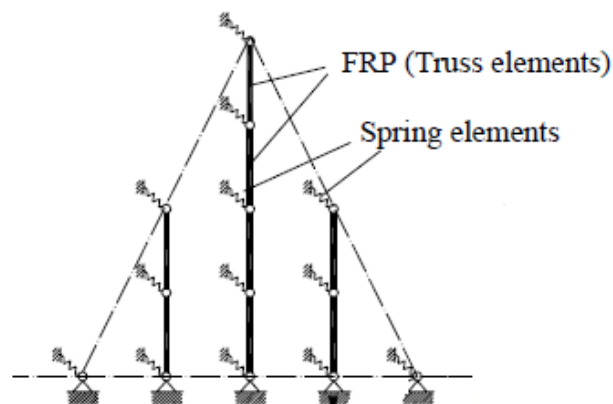


Figure 2-28 Interfacial element for shear strengthening (Lu et al., 2005b)

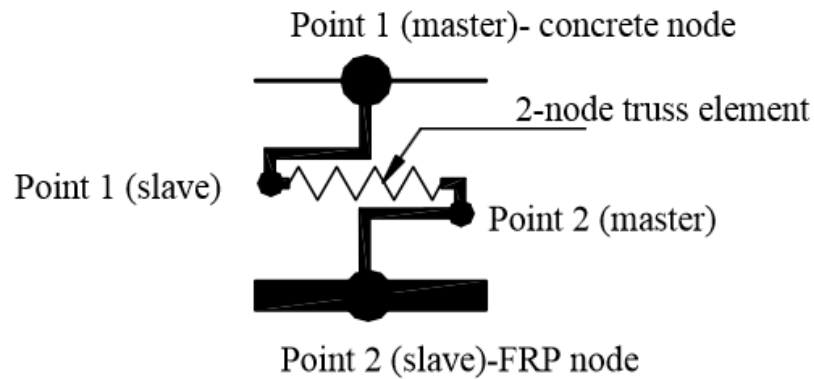


Figure 2-29 Interfacial element (Neale, K.W. et al, 2005)

When simulating the behavior of structures strengthened in shear or the load transfer mechanisms between concrete and CFRP anchors, loads must be transferred in both directions of the interfacial plane. Such planar load transfer mechanisms cannot be simulated using only unidirectional spring elements. A four-node element shown in Figure 2-30 was introduced by Lu et al. (2007) to represent the bond-slip behavior at the interface between CFRP and concrete. The shear interface is defined using bond-slip behavior at the CFRP-concrete interface with a spring in the fiber direction having a stiffness K_u and a spring in the normal direction having a stiffness K_v . K_v is infinite prior to debonding but goes to zero after debonding is determined in the K_u direction.

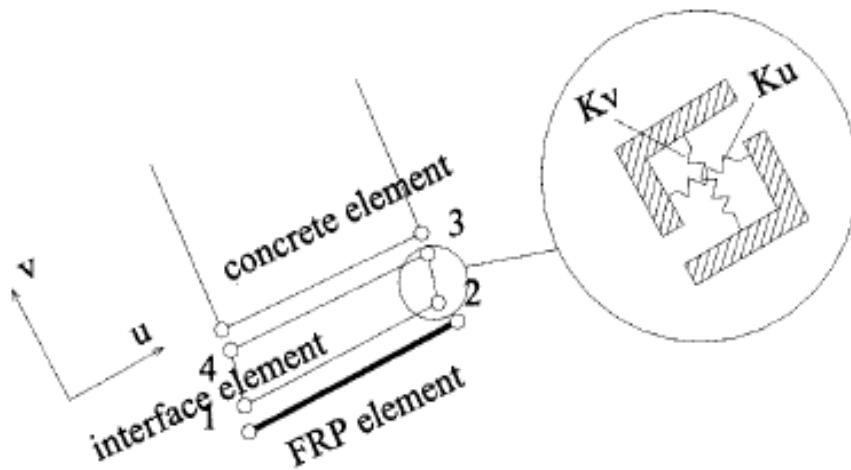


Figure 2-30 Interfacial element (Lu et al., 2007)

Comparisons between numerical and experimental results indicate the application of this bidirectional interfacial elements can accurately predict local debonding in cracked regions (Lu et al., 2007).

As shown in Figure 2-31 (a), the interfacial element proposed by Wong et al. (2003) consists of two independent springs parallel to the orthogonal axes h and v representing the shear and normal stiffness of the interfacial material. This interfacial element has capability to account for bond slip at any arbitrary angle θ . However, the behavior of each orthogonal direction is independent. Therefore loss of bond from slip in one direction does not translate into loss of bond strength in the other direction in the element.



Figure 2-31 Interfacial element proposed by Wong et al. (2003)

Bidirectional interfacial elements such as those proposed by either Lu et al. (2007) and Wong et al. (2003), while an improvement on unidirectional elements, require some form of coupling between the two interfacial planar degrees of freedom to account for loss of bond in one direction due to bond loss in the other. Such coupling is often complex to implement and use in most commercial software.

2.3.4 Anchor Simulation

As shown in Figure 2-32, an eight-node quadrilateral orthotropic shell element incorporating a bilinear bond stress-slip relationship (Sato et al., 2003) was used by You et al. (2011) to take into account the debonding mechanism between each concrete nodes and FRP strip nodes. Element responses were independent in each direction. This shell element was also

used to simulate the anchorage behavior by calibrating the bond condition of interfacial elements located within the anchorage region. The comparisons between experimental and computational results validate the capability of this shell element in predicating interfacial bond behavior for both anchored and unanchored strips.

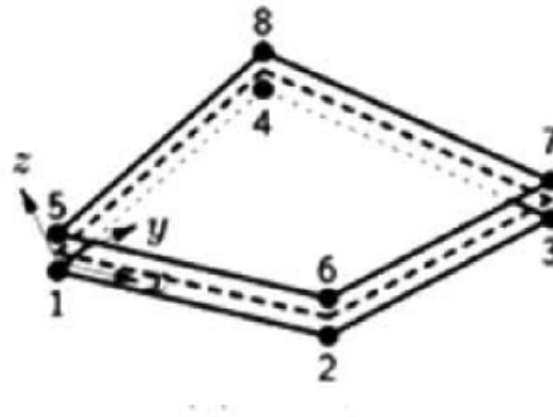


Figure 2-32 A eight-node quadrilateral orthotropic shell element

Limited analytical work has been conducted to simulate the behavior of CFRP strips anchored to concrete using CFRP anchors. As shown in Figure 2-33, nonlinear spring elements were used by Brena et al. (2013) to simulate the load-deformation response of anchored CFRP strips. Two nonlinear elements incorporate the calibrated load-deformation response of interfacial bond-slip away from anchors. At the anchorage region, the nonlinear springs restrict movements of FRP nodes in both transverse and longitudinal directions using elastic-plastic material relations (Figure 2-34).

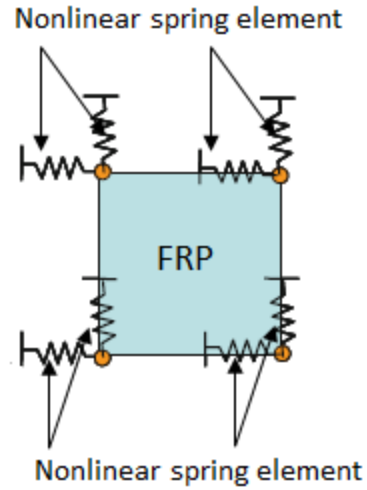


Figure 2-33 A nonlinear spring element

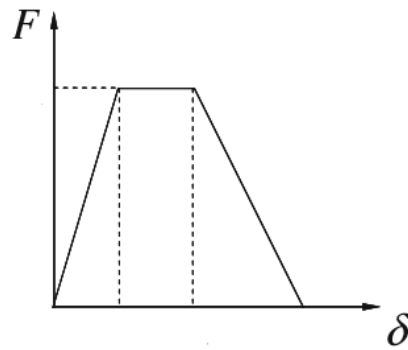


Figure 2-34 Force-deformation response for FRP anchor

The anchorage FE model Brena et al. (2013), however, fails to isolate the details of anchor configurations such as the spread of the load along the fan. In addition, the bond-slip elements are defined independently in either direction, thus de-coupling a coupled response.

CHAPTER 3

Test Program

3.1 TEST PROGRAM

A test methodology based on ASTM C293 (2007) for the modulus of rupture of concrete was designed to study the behavior of CFRP strips attached to a concrete surface.

To find out the influence of CFRP anchor properties on the development of tensile strength of CFRP strips, 39 tests were conducted varying the following parameters; material ratio of CFRP anchor to CFRP strip, length/ angle of anchor fan, width of CFRP strip, concrete strength, and bonded or unbonded CFRP strips.

The results were evaluated to assess the test for determining the force-transfer mechanism between the CFRP and concrete and for quality control of such installations.

3.2 TEST SPECIMENS

A concrete beam from the standard test for flexural strength of concrete (ASTM C293, 2007) with dimension of 6 in. by 6 in. by 24 in. (Figure 3-1) was used as the standard for test specimens in this program because its size and weight will permit it to be moved by a researcher. Previous research (Huaco, 2010; Kim, 2011) on CFRP strips and CFRP anchors have been conducted with the same size specimens providing very valuable and useful information for this study. A notch was cut to initiate the cracking at mid-span, and two holes were drilled for installing CFRP anchors.



Figure 3-1 Standard specimen before CFRP installation

In previous tests (Huaco, 2010; Pham, 2009), a large number of specimens failed in shear as shown in Figure 3-2, such specimens were unable to fully develop the tensile strength of CFRP strip.



Figure 3-2 Pure concrete specimen failed in shear (Huaco, 2010)

In order to prevent the undesirable shear failure, CFRP strips were used to U-wrap the side of specimens. A gap as shown in Figure 3-3 was made between the two U-wrap CFRP strips to limit the effects of side CFRP strip on flexural contribution. The use of the side CFRP strip provided the specimen with a reasonable path for the load transfer from the loading plate to the reaction as shown in Figure 3-4, and prevented a flexural crack that formed at the anchor hole

from developing into a shear crack that would trigger a shear failure of the beam. The shear capacity of specimens is therefore increased by introduction of side CFRP strip to prevent reaching either anchor rupture or strip fracture at failure. After the CFRP strip debonded from the concrete substrate, the tensile force in the CFRP strip was transferred to the CFRP anchor. The use of side CFRP strip therefore had a very limited effect on the anchor or strip strength at failure.

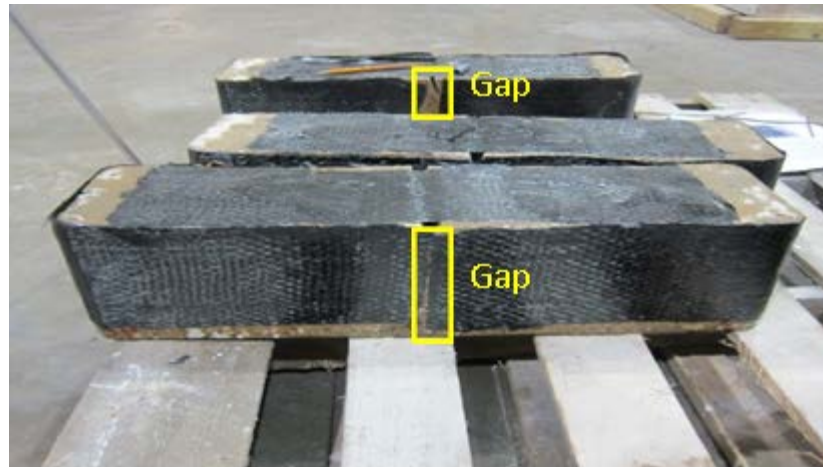


Figure 3-3 U-wrap side CFRP strip

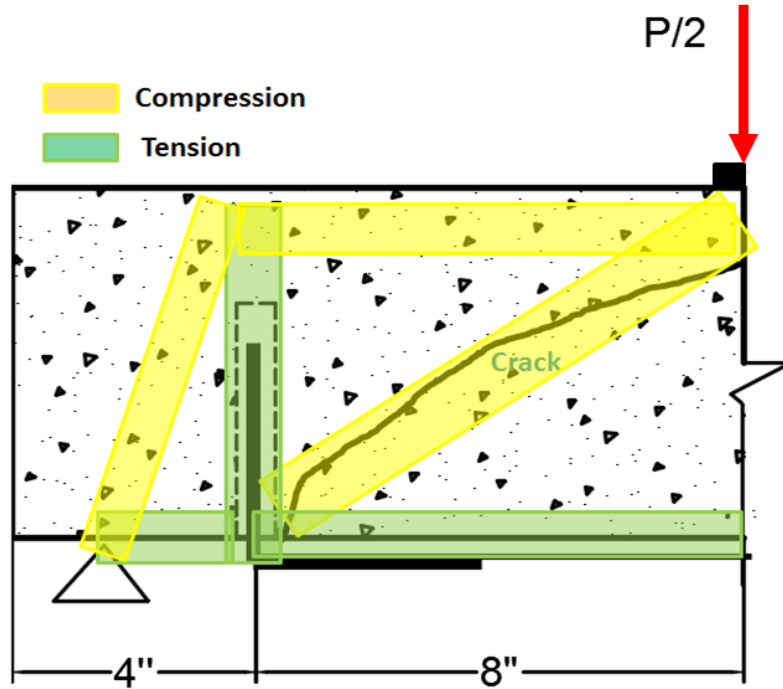


Figure 3-4 Truss model

Other options for preventing concrete failure in shear include using higher-strength concrete, wider specimens or a different test setup (e.g. pull-off test). High strength ($f'_c=11.5$ ksi) concrete was used by Pham (2009) to prevent concrete shear failure. However, 2 out of 3 tests cast with high strength concrete still failed because of concrete shear. Wider specimens will increase the size of specimens which requires more concrete material, more manpower and longer test period. The pull off test is also not recommended because of alignment problems and the complexity of specimen fabrication and test procedure.

All in all, the use of side CFRP provided an efficient and easy way to strengthen the concrete beam.

3.3 TEST MATRIX

3.3.1 Variables

In order to develop anchor design guidelines, tests were conducted with focus on the following parameters:

1. Material ratio of CFRP anchors to CFRP strip
2. Anchor fan length/angle
3. CFRP strip width
4. Concrete strength
5. Contribution of epoxy bonding on load transfer mechanism (Bonded vs. Unbonded).

In order to fracture the CFRFP strip, the tensile strength of CFRP anchor should be larger than the tensile strength of CFRP strip. That is $f_{anchor} \times A_{anchor} \geq f_{strip} \times A_{strip}$ in which f_{anchor} and f_{strip} are the tensile strength of anchor and strip material, respectively. The A_{anchor} and A_{strip} are the section area of CFRP anchor and CFRP strip. In this study, the same CFRP laminate as shown in Figure 3-5 was used to fabricate CFRP strips and CFRP anchors which result in the f_{anchor} equal to f_{strip} . The same amount of CFRP material was used over the entire length of the anchor. The CFRP material was concentrated at the anchor hole area and gradually fanned out to cover the entire width of CFRP strip. The material ratio of CFRP anchors to CFRP strips mentioned in this research actually is simplified as an area ratio of CFRP anchors to CFRP strips in any section for anchor hole to anchor fan end. For example, the anchor material ratio can be determined by the area ratio of CFRP anchors represented by the blue line to the CFRP strip represented by the red line in Section A of Figure 3-6 in which Section A could be any section from anchor hole to anchor fan end.

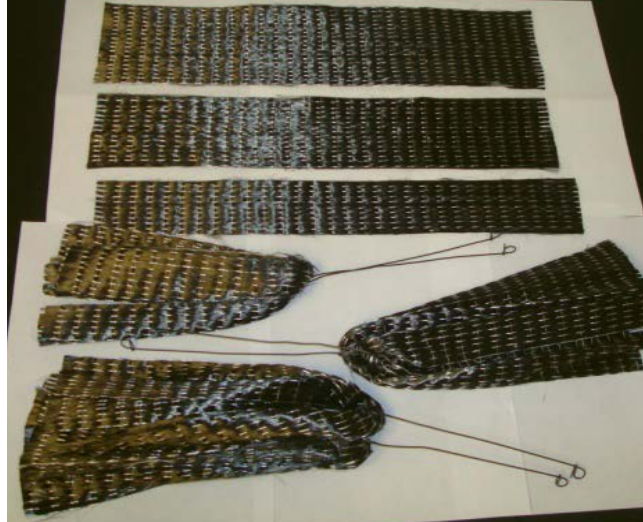


Figure 3-5 CFRP anchors and CFRP strips (Huaco, 2010)

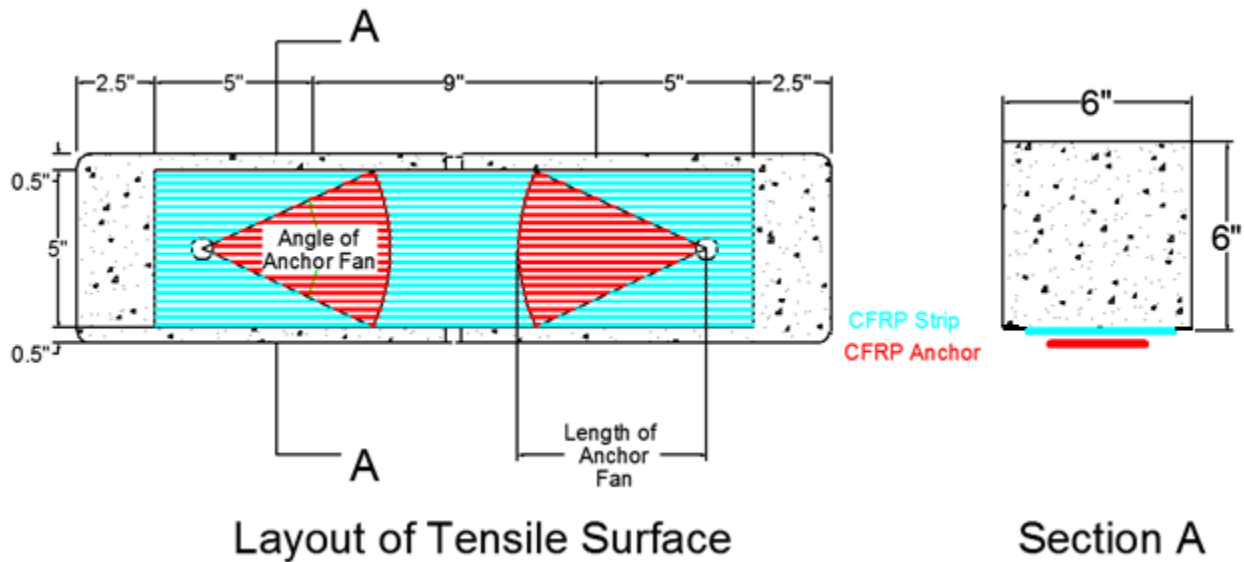


Figure 3-6 Test details

Anchor fan length is the length between the anchor hole and the end of the anchor fan. The angle between the edges of the anchor fan defines the angle as shown in Figure 3-6.

CFRP strip width is the width of CFRP strip attached to the tensile surface as shown in Figure 3-6. Different concrete strengths were used to study the influence of the concrete strength on debonding. Unbonded strips were also tested to investigate the contribution of interface bond to the load transfer mechanism. A plastic film was inserted between the CFRP strip and the

concrete surface to produce the unbonded specimens. It is also labeled as bonded and unbonded in this study.

3.3.1.1 Material ratio of CFRP anchor to CFRP strip

Niemitz found that the diameter of CFRP anchors is an important parameter in determining the force being transferred at the anchor from the CFRP strip into the concrete substrate (Niemitz, 2008). An insufficient amount of CFRP material in the anchors leads to rupture of the anchors before fracture of CFRP strips. This premature failure due to anchor rupture reduces the effective tensile capacity of the CFRP strips.

The amount of CFRP material in anchors was suggested by Kim and Orton to be 1.5 to 2 times the amount of CFRP material in the strips. To install CFRP anchors, the area of holes was suggested to be 1.4 times larger than the area of FRP material in the anchor (Kim, 2008). A large CFRP anchor may be hard to install and may reduce the quality of the installation. Figure 3-7 shows the CFRP anchor used in this study. Anchor-material ratios from 1.06 to 2 were studied.



Figure 3-7 CFRP anchor

3.3.1.2 CFRP Strip Width and Concrete Strength

Increasing the width of a CFRP strip led to an increase in bond strength as reported by Lu et al., 2007; Lu et al., 2005b; Niemitz, 2008; Smith et al., 2007; Thamrin & Kaku, 2007.

The tensile capacity of concrete is generally less than that of epoxy resin. Thus, debonding is mostly observed by separation of the epoxy layer from the concrete substrate as shown in Figure 3-8.



Figure 3-8 Debonding observed between CFRP strip and concrete substrate

CFRP strip widths of 3 in. and 5 in. were selected to investigate the influence of width on the load transfer mechanism. Normal (5.4 ksi) and high (11.5 ksi) strength concrete were selected to study the influence of concrete strength on the bonding mechanism between CFRP strips and the concrete substrate.

3.3.1.3 Anchor Fan Length/ Anchor Fan Angle

The length of anchor fan is directly related to the width covered by anchors on the CFRP strip. The covered width determines the effective width of CFRP strips that a CFRP anchor can engage (Niemitz, 2008). The required material ratio of CFRP anchors should be a function of the width of the CFRP strip and should be large enough to prevent premature failure by anchor rupture (Niemitz, 2008).

The angle of anchor fan is determined by anchor fan length and the effective width. Considering that the tensile capacity of CFRP composite is mostly determined by the fiber, load

transfer in the outer fibers of a fan with a large angle is less effective than the center fibers in the same direction. A reduction of anchor capacity should be expected when a large angle is used. Therefore, a fan anchor angle less than 60° was suggested by Kim (2011).

The parameter of anchor fan length and anchor fan angle were selected in this study to investigate the influence of the anchor on the load transfer mechanism. Anchor fan lengths of 4 in. to 7.5 in. with angles from 64° to 37° were used on 5 in. CFRP strips. Fan lengths from 2.4 in. to 4.5 in. with angles from 64° to 37° were used with 3 in. CFRP strips.

3.3.1.4 Bonded and Unbonded

In order to investigate the load transfer mechanism with and without epoxy resin, a plastic film was attached on the concrete surface to prevent any bond between the concrete surface and the CFRP strip as shown in Figure 3-9. Unbonded tests were compared with bonded tests to determine the contribution of epoxy resin on the load transfer mechanism of anchorage system.

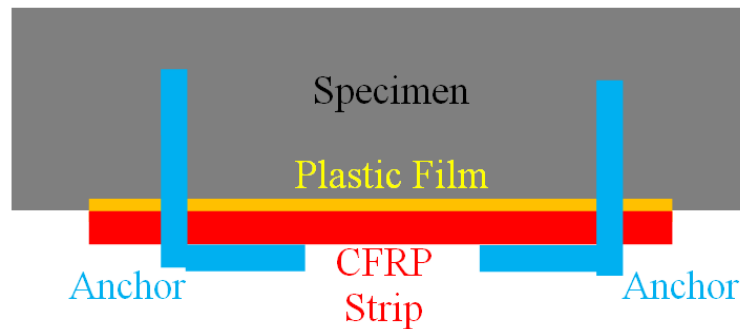


Figure 3-9 Layout of unbonded specimens

3.3.1.5 Other Variables

Other variables that need to be considered for CFRP anchor design and installation are embedment depth (h), hole diameter (d) and bend radius of the anchor (R_a) as shown in Figure 3-10 (Pham, 2009).

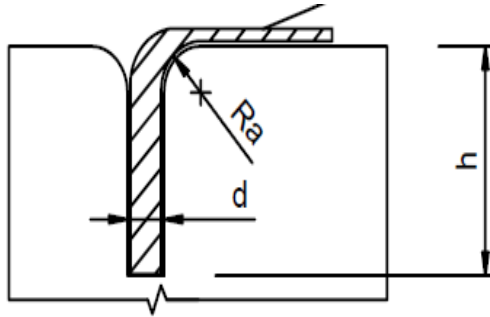


Figure 3-10 Details of CFRP anchors (Pham, 2009)

An insufficient embedment depth provides less contact area between CFRP anchor and its surrounding concrete element. It will reduce the capacity of anchorage systems, and the anchor may pull out before the CFRP strip fractures. A 4 in. embedment depth suggested by Huaco (2010) was used throughout in this research.

The edge of the anchor hole needs to be ground to prevent anchor fracture. A ½ in. or greater bend radius was used as recommended by Pham 2009.

Too large or too small a hole diameter is prone to make installation more difficult and lower the installation quality as well as the capacity of anchors. Therefore, the diameter of anchor hole should be selected carefully. The area of hole was suggested to be at least 1.4 times larger than the area of the CFRP anchor (Pham, 2009).

3.3.2 Nomenclature

The labeling system used to identify specimens is shown in Figure 3-11.

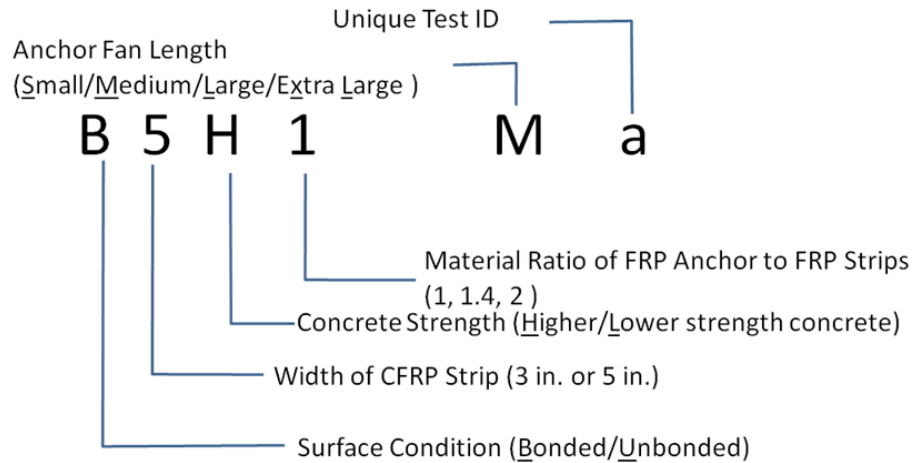


Figure 3-11 Specimen nomenclature

The first character B or U refers to the bonded or unbonded specimens. For unbonded specimens, a plastic film was placed between concrete substrate and CFRP strip to simulate the initially debonded scenario.

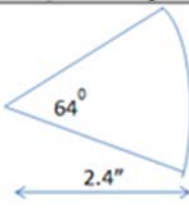
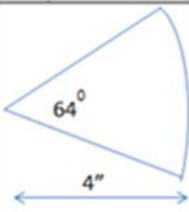
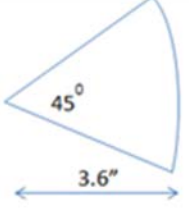
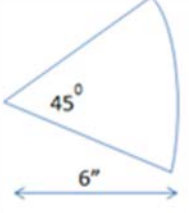
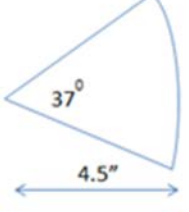
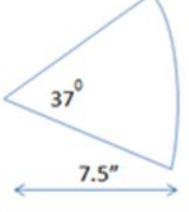
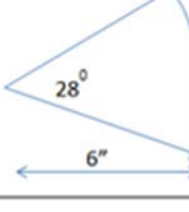
The second number refers to the width of the CFRP strip. Considering the width of specimens is 6 in., two widths (3 in. and 5 in.) of CFRP strip were investigated in this research.

The third character refers to concrete strength. Two concrete strength were used and will be referred to as H (higher, 11.5 ksi) and L (lower, 5.4 ksi).

The fourth number refers to the anchor material ratio of CFRP anchor to CFRP strip. This research focuses on the investigation of ratios from 1.06 which is represented by 1 in the nomenclature to 2.0 (See section 3.3.1 for calculation of anchor material ratio).

The fifth character refers to anchor fan length. Details are shown in Table 3-1.

Table 3-1 Details for anchor fan

Anchor fan length	3 in. strip	5 in. strip
S		
M		
L		
XL		

The last character refers the unique test number. To obtain a more reasonable and stable result, at least two identical specimens were tested. The unique test number was applied to distinguish those tests. The details of 39 tests are presented in Table 3-2.

Table 3-2 Test details

Number	Specimen	fc' (ksi)	Strip width (in.)	Anchor material ratio	Anchor hole (in.)
1	B5H2Ma	11.5	5	2.0	3/4
2	B5H2Mb	11.5	5	2.0	3/4
3	B5H1.4Ma	11.5	5	1.41	5/8
4	B5H1.4Mb	11.5	5	1.41	5/8
5	B5H1.4Mc	11.5	5	1.41	5/8
6	B5H1.4Md	11.5	5	1.41	5/8
7	B5H1.4Sa	11.5	5	1.41	5/8
8	B5H1.4Sb	11.5	5	1.41	5/8
9	B5H1.4La	11.5	5	1.41	5/8
10	B5H1.4Lb	11.5	5	1.41	5/8
11	B5L1.4Ma	5.4	5	1.41	5/8
12	B5L1.4Mb	5.4	5	1.41	5/8
13	B5L1.4Mc	5.4	5	1.41	5/8
14	B5L1.4Md	5.4	5	1.41	5/8
15	B5H1Ma	11.5	5	1.06	5/8
16	B5H1Mb	11.5	5	1.06	5/8
17	B5H1Mc	11.5	5	1.06	5/8
18	B5H1Md	11.5	5	1.06	5/8
19	B5L1Ma	5.4	5	1.06	7/16
20	B5L1Mb	5.4	5	1.06	7/16
21	B5L1Mc	5.4	5	1.06	7/16
22	B5L1Md	5.4	5	1.06	7/16
23	B5L1Me	5.4	5	1.06	5/8
24	B5L1Mf	5.4	5	1.06	5/8
25	B5L1Mg	5.4	5	1.06	5/8
26	B5L1Mh	5.4	5	1.06	5/8
27	U5H2Ma	11.5	5	2.0	3/4
28	U5H1.4Ma	11.5	5	1.41	5/8
29	U5H1.4Mb	11.5	5	1.41	5/8
30	B3H1.4Sa	11.5	3	1.41	5/8
31	B3H1.4Sb	11.5	3	1.41	5/8
32	B3H1.4Ma	11.5	3	1.41	5/8
33	B3H1.4Mb	11.5	3	1.41	5/8
34	B3H1.4La	11.5	3	1.41	5/8
35	B3H1.4Lb	11.5	3	1.41	5/8
36	B3L1.4XLa	5.4	3	1.41	5/8
37	B3L1.4XLb	5.4	3	1.41	5/8
38	B3L1XLa	5.4	3	1.06	5/8
39	B3L1XLb	5.4	3	1.06	5/8

3.4 INSTALLATION

3.4.1 Preparation of Specimens

The concrete surfaces, anchor holes, specimen corners and mid-span notch were prepared before installation of CFRP U-wraps, CFRP strips and CFRP anchors. The concrete surface was cleaned and laitance was ground off for better bond between the concrete surface and the CFRP (Figure 3-12 (a)). Two holes were drilled to the desired depth on both ends of the beam tension face for anchor installation (Figure 3-12 (b)). The anchor hole was rounded to avoid premature CFRP anchor failure (Figure 3-12 (c)). Compressed air or a vacuum cleaner was used to blow or vacuum dust out of anchor holes (Figure 3-12 (d)). For good bond between CFRP and concrete material, all dust or oil on the surface was removed.



(a) Grinding concrete surface

Figure 3-12 Preparations before CFRP installation



(b) Drilling holes



(c) Rounding edge off



(d) Cleaning holes with compressed air or vacuum cleaner

Figure 3-12 Preparations before CFRP installation

As shown in Figure 3-13, the corners were rounded so that U-wrapped CFRP strips would not fail at sharp corners. Finally, a 1 in. deep notch was cut at mid-span to control the location of concrete flexural cracking.

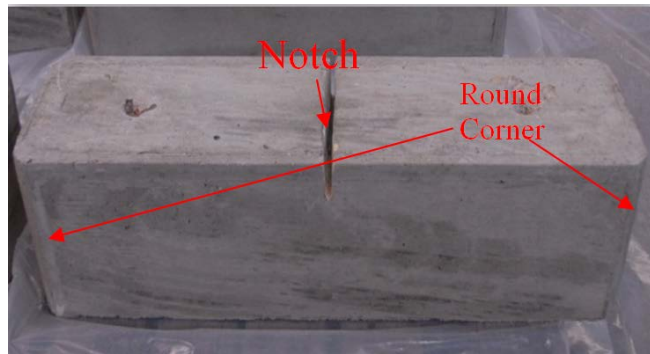


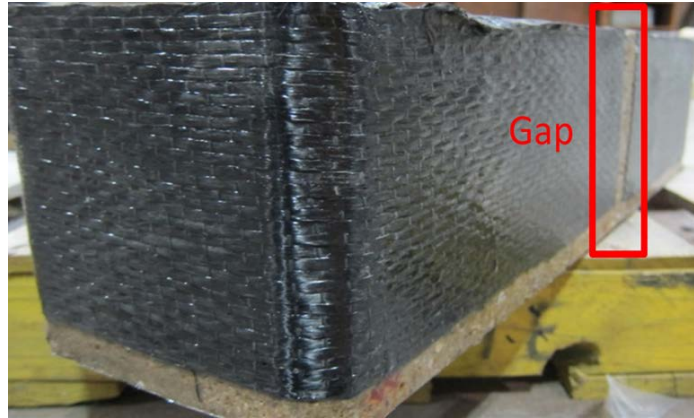
Figure 3-13 Prepared specimens

As shown in Figure 3-14, one serious disadvantage of this beam is its vulnerability to shear failure due to lack of transverse reinforcement (Huaco, 2010). Various options were considered to avoid a premature shear failure in the concrete. Considering the ease of installation of the CFRP material, CFRP strips were used to U-wrap concrete specimens to reduce the possibility of shear failure originating at the anchor hole. A gap was deliberately left at mid-span between two CFRP U-wrapping strips to prevent increasing flexural capacity as shown in Figure 3-14.



a) Shear concrete failure (Huaco, 2010)

Figure 3-14 U-wrapping specimens with CFRP strips



(b) U-wrapping

Figure 3-14 U-wrapping specimens with CFRP strips

3.4.2 Installation of CFRP strips and anchors

CFRP anchors and CFRP strips were prepared as shown in Figure 3-5. Another surface cleaning was recommended immediately before installation of CFRP to remove any remaining dust on concrete surface.

Epoxy was prepared following the supplier's instructions of FYFE Co., LLC regarding volume of components A and components B. The components were mixed for 5 minutes (Figure 3-15).



(a) Mixing components



(b) Epoxy after preparation

Figure 3-15 Preparing epoxy (Huaco, 2010)

The surfaces of the beam where CFRP strips were to be installed were saturated with epoxy (Figure 3-16). CFRP strips were then saturated with epoxy and both sides of specimens were wrapped as shown in Figure 3-16 and Figure 3-17. Putty knives and rollers were used to remove air bubbles and excess epoxy.



Figure 3-16 Saturating epoxy on concrete (left) and CFRP strip (right)



Figure 3-17 U-wrapping CFRP strip

The same procedure was used to install the CFRP strip on the tension face of the beam. Anchor holes, tension surface (Figure 3-18) and CFRP strips were saturated. Saturated CFRP strips were then applied to the concrete surface (Figure 3-19). The CFRP strips were carefully aligned and smoothed to keep them in the desired position. Putty knives and rollers were used to eliminate air bubbles and excess epoxy.

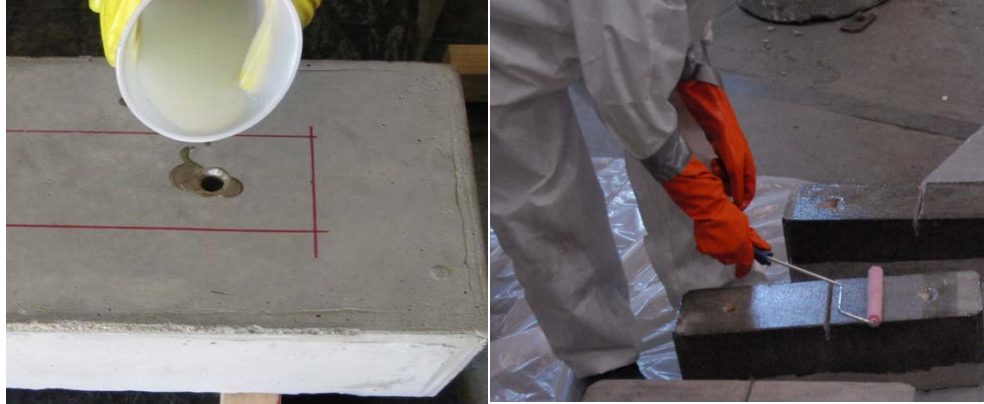


Figure 3-18 Saturating holes (left) and flexural surface (right) (Hauco, 2010)



Figure 3-19 Applying CFRP strips

Two patches of CFRP were applied over the center of each anchor for better load transfer from the strip to the anchor. The fiber direction of the first patch was parallel with the CFRP strip and was applied before the anchor was inserted (Figure 3-20). Holes were carefully made through the first patch and CFRP strip by moving the CFRP fibers with an awl. A saturated CFRP anchor was then inserted into the hole (Figure 3-21). After the anchor was installed in the hole, the anchor material had to be fanned out (Figure 3-22) to engage the width of the CFRP strips to provide force transfer from the entire width of the strip to the anchor (Niemitz, 2008). A second patch with fiber direction perpendicular to the fiber direction of the CFRP strip was placed over the CFRP anchors (Figure 3-23). A completed installation is shown Figure 3-24.



Figure 3-20 Applying the first patch



Figure 3-21 Inserting CFRP anchor



Figure 3-22 Fanning the anchor



Figure 3-23 Applying the second patch

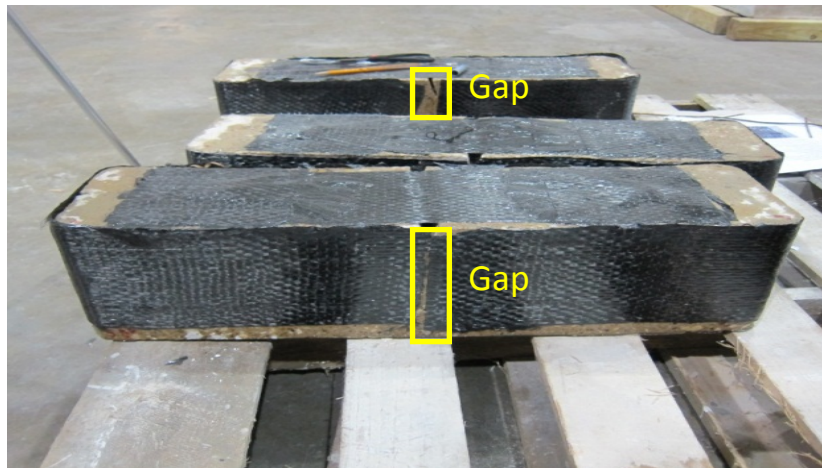


Figure 3-24 Specimens with CFRP installed

Generally, two people are needed to install the CFRP since the pot life (working life) of epoxy is normally less than three hours especially during Texas summer when the temperature exceed 90° F. One more hour may be gained if the epoxy bucket is placed in ice water. This duration may increase up to two hours or more as ambient temperature lower than 60° F. The epoxy was allowed to cure for at least one week before testing. Two weeks or more are suggested if temperature is lower than 60° F.

3.5 TEST APPARATUS AND LOADING PROTOCOL

The concrete beam was loaded at the middle span and supported by rockers and threaded rods as shown in Figure 3-25 and Figure 2-28.

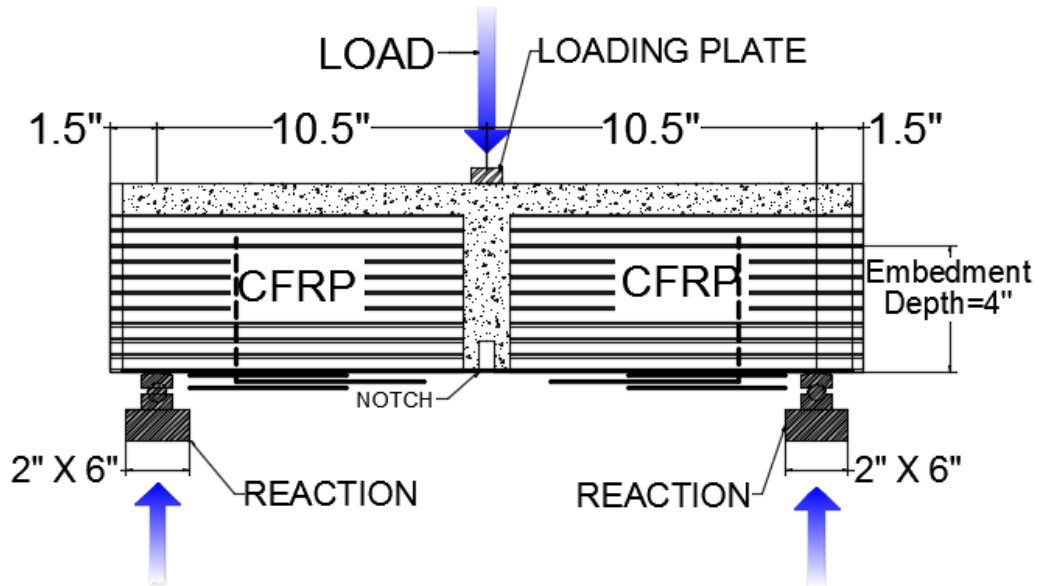


Figure 3-25 Load setup I

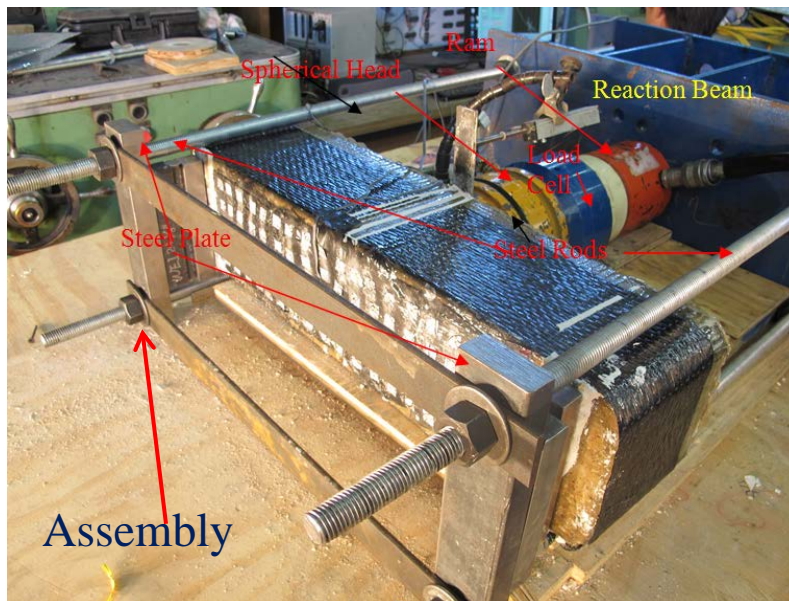


Figure 3-26 Load setup II

In order to visualize and record the behavior of the CFRP strips and CFRP anchors during testing, beams were loaded horizontally with the tension face exposed to the vision system discussed in section 3.5.3.

As shown in Figure 3-26, the loading setup contains one spherical head, one ram and one reaction beam. Four steel rods were used to connect the roller mechanism (Figure 3-27) to the test beam through two steel plates. The rods were flexible and prevented the development of axial force into the beam as beam deformation increased. This setup was placed on a table so that the height matched that of the cameras used in the vision system.

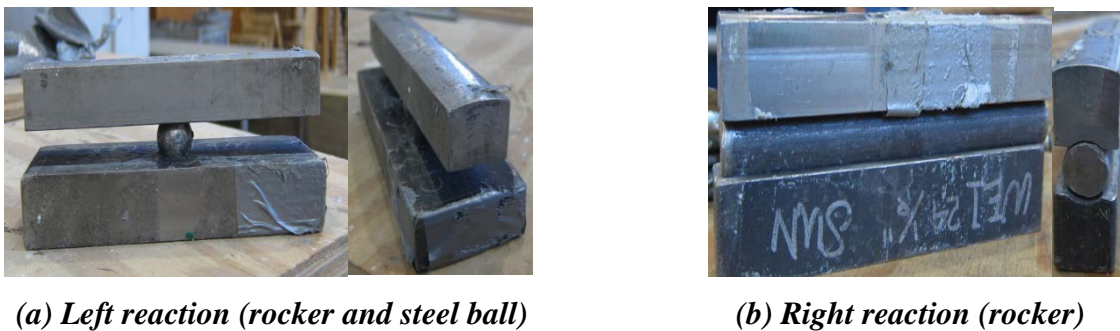


Figure 3-27 Rocker assemble

3.6 INSTRUMENTATION

3.6.1 Load and Deformation Measurement

A load cell with 25k capacity and 5 in. diameter loading area was placed between a spherical head and the loading ram to record the applied load (Figure 3-28). Care was taken to align the steel plate, spherical head, load cell and loading ram to produce a point load on the specimens. The rocker and steel ball as shown in Figure 3-27 (a) prevented torsion from being introduced to the beam.



Figure 3-28 Measurements for load and displacement

Two linear variable differential transformers (LVDT) were used to record relative deformation at mid-span during the test. One LVDT was placed at the reaction end of beams to account for rod elongation. The actual mid-span deformation of the beam is the difference in deflection between the two LVDTs.

Figure 3-29 shows the load versus deformation plots of two typical tests. Both tests had concrete strength of 11 ksi and a 5 in. CFRP strip. The material ratio of CFRP anchor to CFRP strip was 1.41 for both tests. The anchor fan length is 4 in. long in a) and 7.5 in. in b).

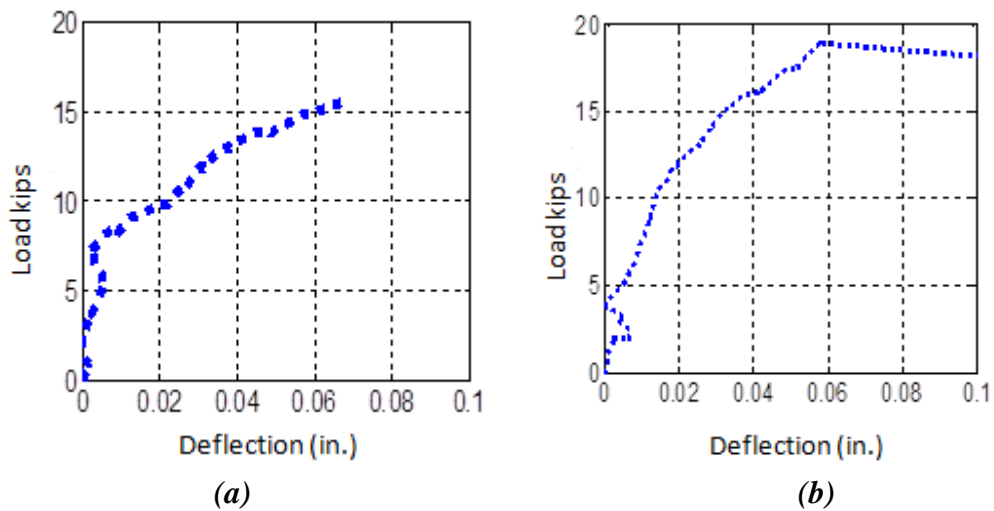


Figure 3-29 Load versus deformation plots with data collected by load cell and LVDT

3.6.2 Strain Gauges

Two strain gauges were affixed at the mid-span of the beams as shown in Figure 3-30. Figure 3-31 shows the strain versus time frame number using data collected by strain gauges on specimen B5L1Mc. The Frame number represents data and pictures recorded at a particular stage. In this test, 721 stages were recorded during the test.

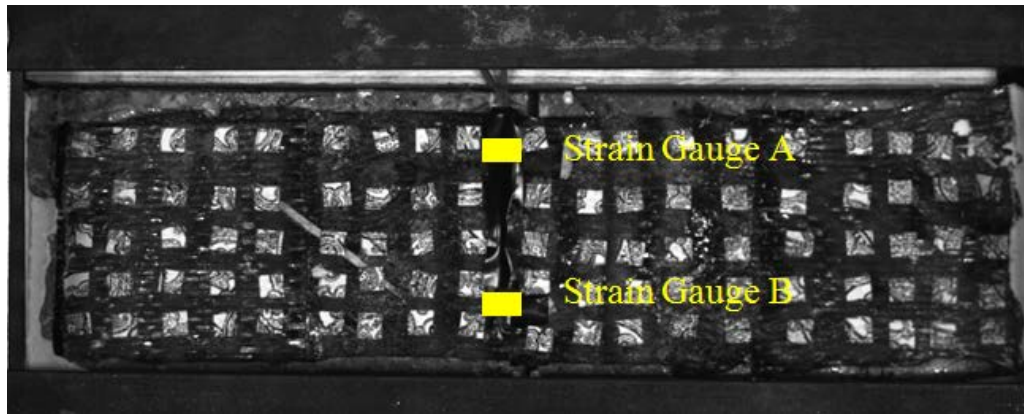


Figure 3-30 Strain gauges on CFRP strip

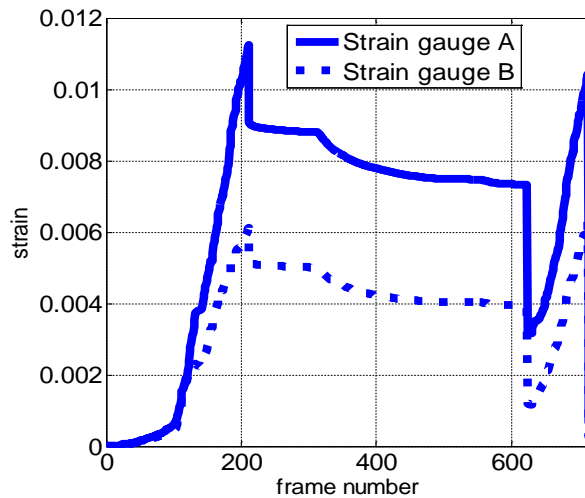


Figure 3-31 Strain versus frame number plot with data collected by strain gauges

3.6.3 UT Vision System

3.6.3.1 Overview of System

In order to determine the characteristics of the load transfer mechanism from CFRP strips to CFRP anchors, strains need to be measured along the strip between anchors. While strain gauges affixed on the surface of CFRP can produce reliable strain measurements, they are impractical to use for obtaining a complete surface-strain profile due to cost, and installation time considerations. Recently, Digital Image Correlation (DIC) systems have been introduced in structural engineering to measure surface deformations (Choi et al., 2011; Helfrick et al., 2011; Jurjo et al., 2010; Lee et al., 2006; Olaszek, 1999; Stephen et al., 1993; Wahbeh et al., 2006). In some cases, speckled paint patterns are applied to a specimen surface to facilitate tracking of movements by DIC systems. In others, targets that offer high contrast patterns are affixed on the surface of a specimen. Digital cameras are used to capture successive images during testing, from which movement of selected areas of a specimen or targets are extracted.

The UT Vision System (UTVS), a high-resolution DIC system developed at the Ferguson Structural Engineering Laboratory, was used in this study to record the 3-D movements of targets affixed on the tension surface of beam specimens as shown in Figure 3-32. The DIC system allows tracking of the movements of as many targets as can be fit on a specimen. The system can therefore monitor the progression of the complete surface-strain profile of a specimen throughout a test. In this study, the UTVS was used to monitor the movement of up to 252 targets.



Figure 3-32 Targets affixed on tension surface of a beam specimen

The UTVS was developed to allow surface-strain measurement of full-scale structural systems and members. The system is able to resolve surface strains on the order of 10^{-4} over a field of view of 8 ft and a gauge length of 2.5 in. (63 mm). Similar strain resolutions were achieved in this study but for a much smaller gauge length of approximately 0.75 in.

3.6.3.2 UTVS Hardware and Software

The UTVS hardware consists of two high-resolution cameras (Proscilica GE4900, 16 Megabits) connected to two computers. The computers are networked through a router. Key properties of the high resolution cameras used in the UTVS (Figure 3-33) are presented in Table 3-3. Two cameras are needed to measure three-dimensional (3D) movements. Each camera is connected to a computer that triggers frame-grabbing and records images during a test (Figure 3-34). Whenever a camera is ready to grab an image, its computer issues a ready signal to the master-computer synchronization software. Once all cameras are ready, the master-computer software issues a command to all cameras to capture the subsequent images simultaneously. The system can trigger several pairs of cameras simultaneously in cases where deformations of several locations are needed. The network router can be connected to a Data Acquisition system (DAQ) such that frame numbers can be sent to the DAQ. This feature allows the UTVS data to be synchronized with DAQ data in post-processing.

Table 3-3 Camera properties

Sensing Area, H x V (mm)	36.1 x 24.0
Pixels (H x V)	4872 x 3248
Frame Rate (fps)	3
Pixel Size, H x V (μm)	7.4 x 7.4
Image Type	Grayscale, 8 bit, raw format

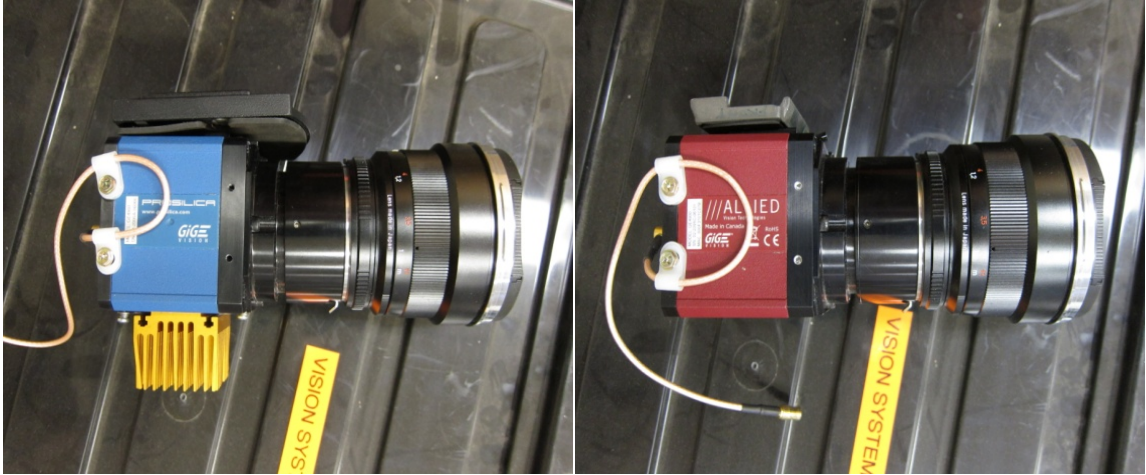


Figure 3-33 Cameras used by the UTVS



Figure 3-34 UTVS computers

The UTVS software consists of LabVIEW (National Instruments) scripts used for frame grabbing and synchronization as well as target location, and Matlab (Mathworks) scripts used for calibration and post-processing of target data.

3.6.3.3 Typical Test

DIC measurements are sensitive to variations in light intensity and distribution during testing. Care was taken to ensure a uniform light intensity across the surface of specimens throughout the tests. High-intensity artificial lighting was used to achieve uniform light intensity over the field of view of interest, and to mitigate the effects of varying ambient light conditions during testing. A typical test setup of the UTVS is shown in Figure 3-35.

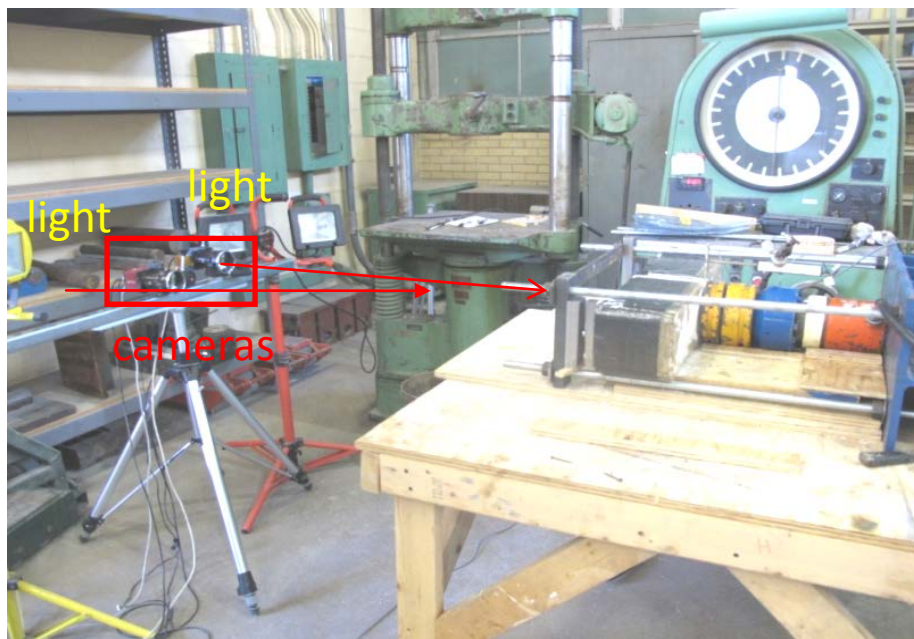


Figure 3-35 Setup of vision system

Once cameras are positioned in the desired locations and oriented in the desired directions, several calibration snapshots are taken of a grid as shown in Figure 3-36. In order to provide accurate displacement for each target, the intrinsic parameters including focal length of camera, skew coefficients, principal point and distortions as well as extrinsic parameters which was used to define the 3D position of camera relative to the test specimen are required to correct

the raw data. The calibration images are used in post-processing to determine camera intrinsic and extrinsic parameters, from which the 3D triangulation of target locations and compensation for lens distortion are performed.



Figure 3-36 Calibration

Following the acquisition of calibration images, the test can be conducted with the UTVS grabbing images at approximately 0.75 Hz and the DAQ acquiring frame numbers from UTVS as well as LVDT, load-cell, and strain gauge data at approximately 1 Hz. Thus, UTVS grabbing images was 1.33 times faster than DAQ acquired data. The UTVS LabView scripts are able to track locations and plot strains between select targets throughout an experiment. Following an experiment, a user can select all the targets that need to be tracked in the first camera frames and have the software go through all subsequent saved images from both cameras and locate the targets in image-pixel coordinates. An advantage of this system is that it allows users to select different or additional targets to track in post-processing.

The Matlab calibration scripts are then run to evaluate camera intrinsic and extrinsic parameters and triangulate in 3D target locations based on image-pixel data extracted by the LabView script. The calibration script also compensates for lens distortion in evaluating the 3D location of targets.

3.6.3.4 Data Processing

Once the 3D (or X, Y, Z) coordinates of targets are known for each frame number, deformation measures (such as specimen deformation) and strain measures can be calculated. For example, the X-component strain ϵ_x in a given frame number (i) is calculated as the change in X-direction distance (Δl_x^i) between two targets divided by the original X-direction distance (Δl) between those two targets:

$$\epsilon_x = \frac{\Delta l_x^i}{\Delta l} \quad \text{Equation 3-1}$$

In addition, the targets can be used as nodes to mesh a grid of quad planar elements. The X and Y direction in-plane strains of the elements can be calculated by the coordinate changes of four targets assuming linear strain profiles. Deformations can be calculated by the relative movement in the desired direction between targets at the location the measurement is needed (mid-span in this study) and the targets at the reactions.

3.6.3.5 Data Verification

Deformation measurements obtained by the UTVS were compared with strains measured by externally applied strain gauges and deformations measured using LTVDs. Excellent agreement was observed between UTVS strain measurements using Equation 3-1 and those recorded using strain gauges, as shown in Figure 3-37. It is important to note that strains do not match exactly between UTVS and strain gauges as they were not measuring strains at the same exact location.

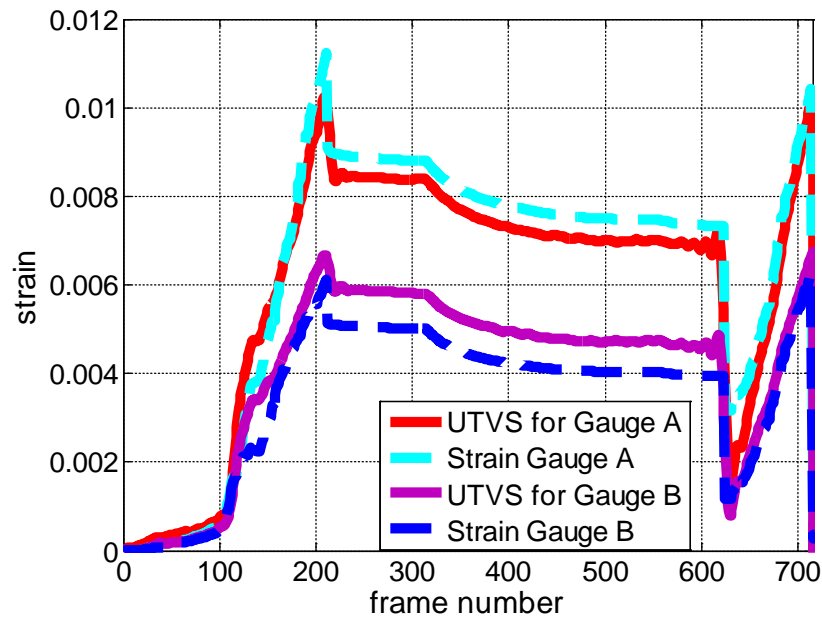


Figure 3-37 Comparisons between UTVS strains and the strain gauges in Figure 3-30

Similarly, good correlation between deformations recorded by LVDTs and the UTVS were observed. Figure 3-38 presents UTVS-LVDT comparisons for mid-span deformations for two tests. Discrepancies in measurements can be attributed to the UTVS and LVDTs not measuring at exactly the same locations.

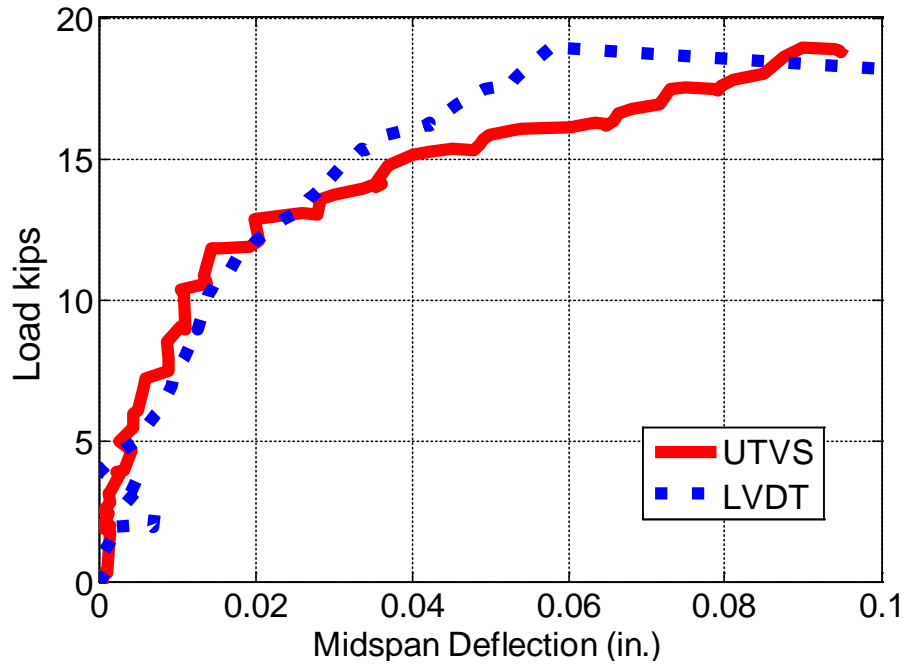
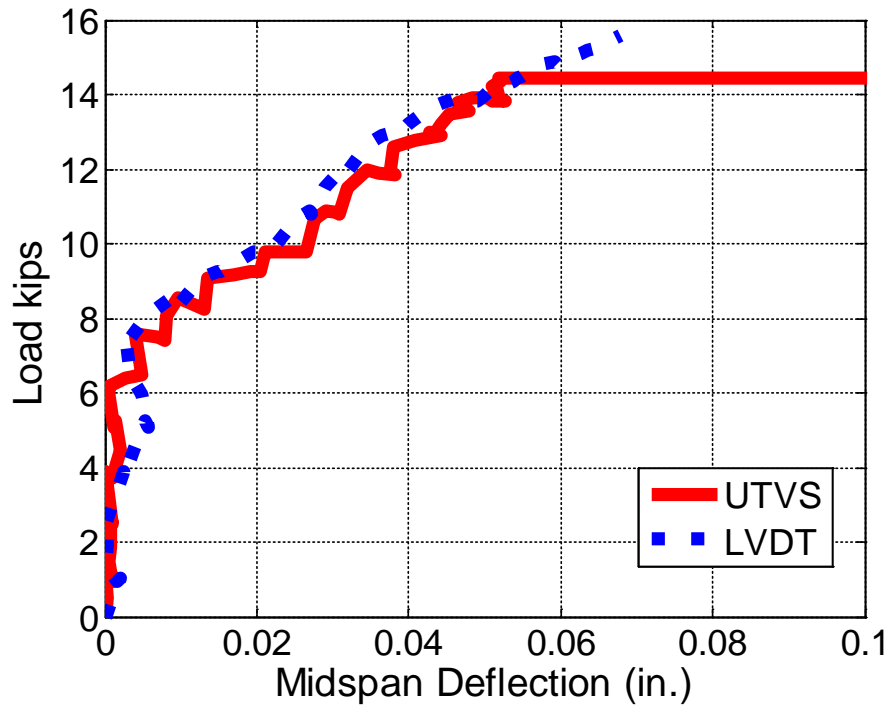


Figure 3-38 Mid-span deflection comparison for two tests between LVDT and UTVS

3.6.3.6 Noise Reduction

In any DIC measuring system, target locations are extracted with a certain level of noise. The lower the noise level, the smaller the strains and deformations resolved by a DIC system. The UTVS was developed to minimize noise levels to the extent possible. Cameras with large, low-noise digital sensors were selected and lighting carefully distributed. However, some noise is inevitable in measurements and smoothing functions were used to reduce noise levels.

Three smoothing functions were investigated: a zero-phase digital filter, moving mean filter, and a moving median filter. The zero-phase digital filter uses frequency domain analyses to trim signals beyond a specified frequency range. This method is unable to smooth data in which targets are missing. Since loss-of target was not uncommon, especially at large damage states, either a moving mean or a moving median smoothing function was used to reduce the noise within the data.

Figure 3-39 shows a comparison between raw and smoothed deformation data. Figure 3-40 shows a comparison between raw and smoothed strain data. Note that test nomenclature and description is presented in Section 3.3. Those two plots indicate that the smoothing functions produce curves that capture the trends and magnitudes of the raw data. In subsequent plots throughout the dissertation, smoothed data are presented.

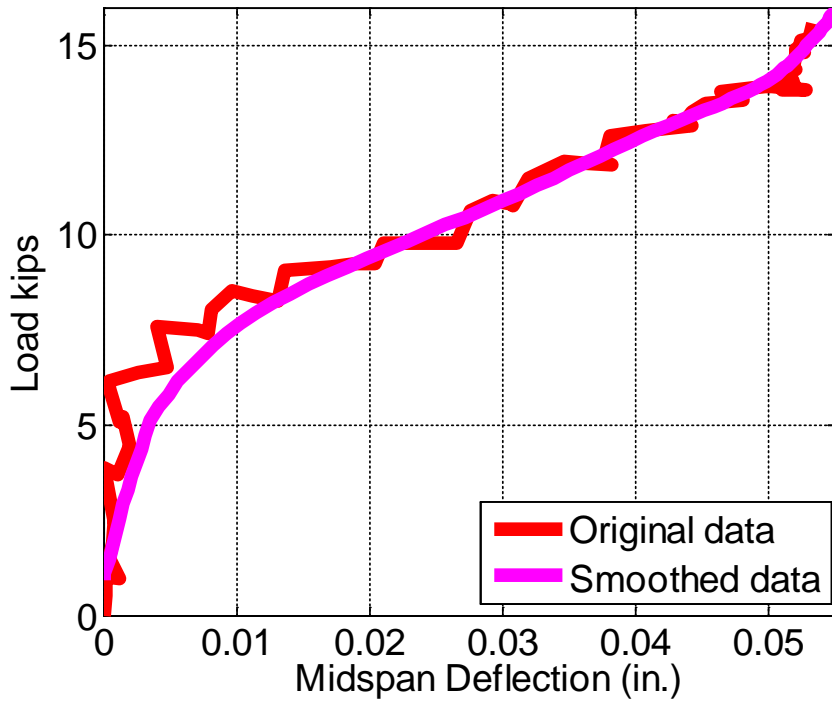


Figure 3-39 Comparison between raw and smoothed deflection data for test B5H1.4S2

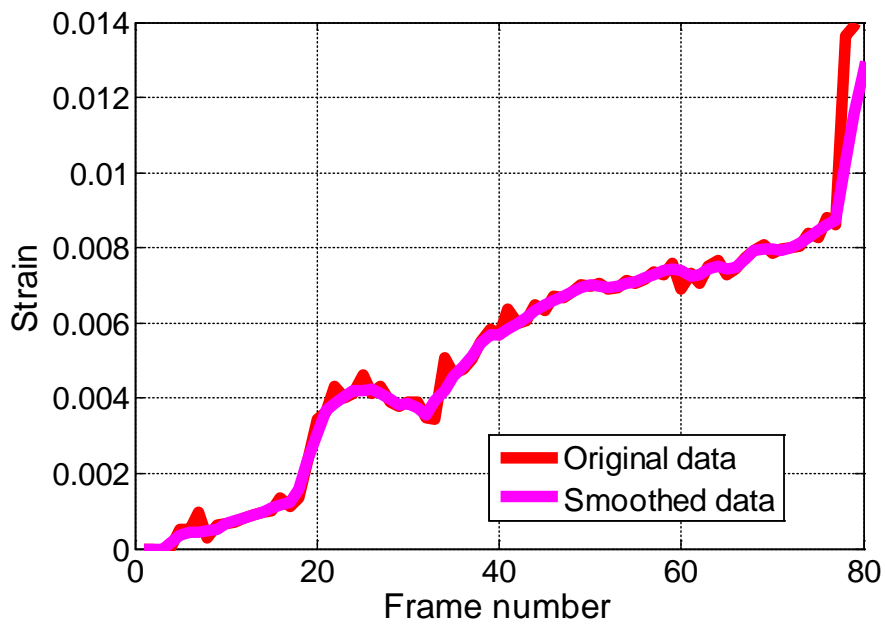
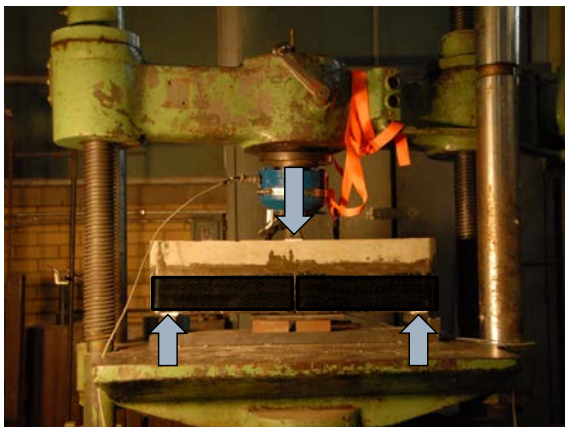


Figure 3-40 Comparison between raw and smoothed strain data for test B5H1.4S2

3.7 MATERIAL PROPERTIES OF CFRP

Tyfo® SCH 11-UP CFRP material was used to make anchors and strips in this study. Tyfo® S Epoxy was selected as the adhesive to install CFRP material on specimens.

Material tests were conducted by Changhyuk Kim at the beginning of this research project to determine the properties of CFRP material. In order to develop tensile force on CFRP strip, 2.5 in. wide anchored strips were attached on the tensile surface of 6 in. by 6 in. by 24 in. concrete beams as shown in Figure 3-41. The rupture strain was measured by the mid-span strain gauge. The rupture stress was calculated by equilibrium at the ultimate load. The elastic modulus was calculated by stress-strain response in which strain was measured by the mid-span strain gauge and stress was determined using the applied load on the beam.



(a) Test setup



(b) Strip fracture

Figure 3-41 Tests for the CFRP material properties (courtesy of Changhyuk Kim)

The comparisons made in Table 3-4 indicated the measured CFRP material properties were very close to manufacturer specified values. It is importance to note that the measured CFRP material properties came from the average value of three bending tests. The manufacturer specified values from direct tensile tests ASTM D-3039 (2007) seem more conservative and will be used in this study.

Table 3-4 Comparisons of CFRP material properties between material tests and manufacturer specified values

	Material tests by Changhyuk Kim	Manufacturer specified typical test values
Elastic modulus	15600 ksi	15300 ksi
Rupture strain	0.0096	0.0093
Rupture stress	150 ksi	143 ksi

3.7 CONCRETE

Specimens were casted by ready mixed concrete. Typical proportions of the concrete mixture are presented in Table 3-5.

Table 3-5 Typical concrete mixture proportions

Material	Quantity
Type I Portland Cement	300 lb/cy
Flys Ash	79 lb/cy
CA: ¾ in. River Rock	1846 lb/cy
Water	22 gallons/cy
FA: Sand	1554 lb/cy
Water/Cement Ratio	0.62
Set Retardant Admixture	5.6 oz/cy
HRWR Admixture	30 oz/cy
Slump	6 ± 2 in.

CHAPTER 4

Test Results

4.1 OVERVIEW

Experimental results for all 39 beam tests designed in Chapter 3 are summarized and discussed in this chapter. The effects of the following parameters concrete strength, the anchor-fan length/angle, the width of CFRP strips, the ratio of CFRP anchor material to CFRP strip material, and the bond between CFRP and concrete on strip and anchor strengths are discussed in this chapter.

4.2 SUMMARY OF TEST RESULTS

4.2.1 Typical Test and Results

In this section, tests results of specimen B5H1.4Sb are discussed in detail to illustrate typical results obtained in tests. The evaluation procedures used to analyze test data are presented.

4.2.1.1 Failure Mode

The failure mode of specimen B5H1.4Sb was anchor rupture as shown in Figure 4-1. In this test, the CFRP anchor was weaker than the CFRP strip and failed at the top of the embedded anchor.

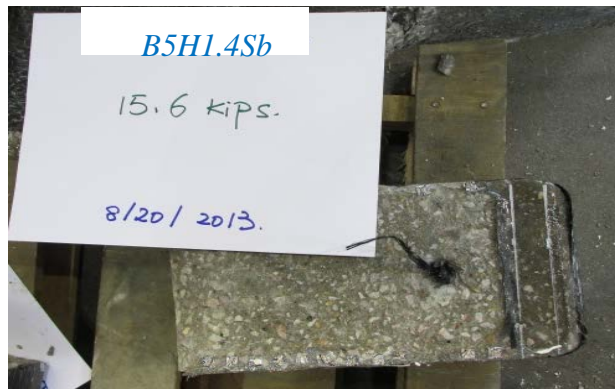


Figure 4-1 Anchor rupture of beam B5H1.4Sb

4.2.1.2 Forces and Deflections

In beam specimens, CFRP strips carried the tensile loads generated by flexural demands. Estimates of the tensile forces developed in the CFRP strips were determined using the applied loads and sectional analysis. A concrete stress of $0.85f'_c$ was assumed uniformly distributed over an equivalent compression block bounded by the edges of the cross section and a straight line located parallel to the neutral axis at a distance $a = \beta_1 c$ (Figure 4-2); where c is the depth to the neutral axis measured from the extreme compression fiber and β_1 is the equivalent rectangle stress block factor defined in ACI 318-11. The value of β_1 is 0.85 for a concrete compressive strength of 4 ksi and is 0.05 less for each 1 ksi in excess of 4 ksi. A lower limit of 0.65 applies to β_1 , thus the value of β_1 is 0.65 for specimen B5H1.4Sb. From equilibrium, the distance c can be calculated as $c = A_{CFRP} f_{CFRP} / (0.85f'_c b \beta_1)$ and was calculated as 0.67 in. for this specimen. The force in the CFRP strip (F_{strip}) can be determined from equilibrium as shown in Figure 4-3, based on the applied load P and the neutral axis depth c (Equation. 4-1).

$$F_{strip} = (P/2 \times 10.5 \text{ in.}) / (6 - a/2) \quad \text{Equation 4- 1}$$

in which

A_{CFRP} = area of CFRP anchor, in.²

f_{CFRP} = manufacturer specified tensile strength of CFRP strip, ksi

b = width of beam specimen, in.

h = height of beam specimen, in.

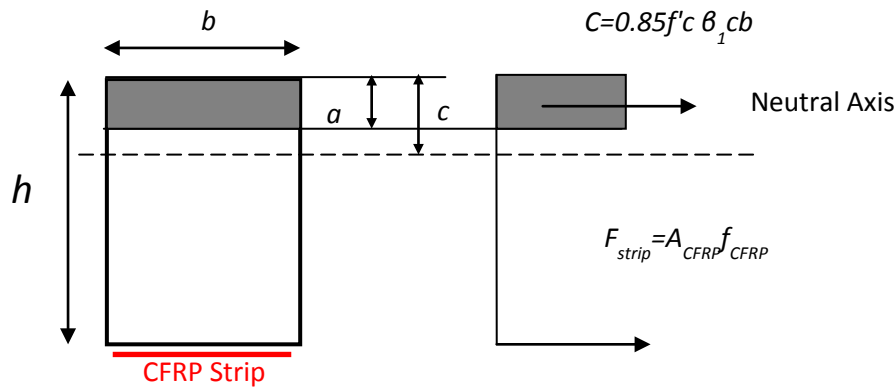


Figure 4-2 Beam-section equilibrium illustration

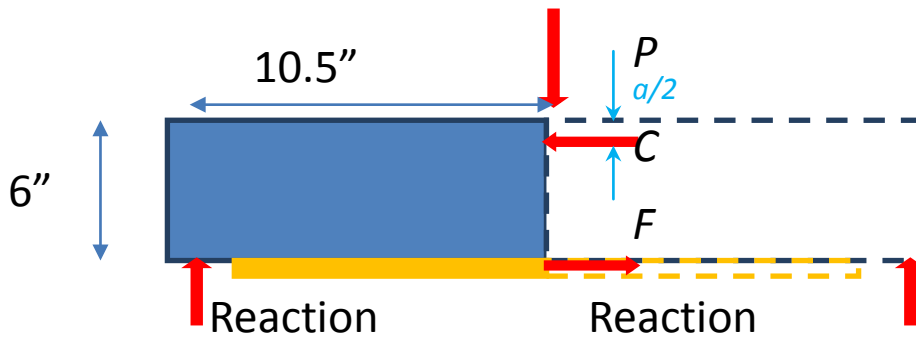


Figure 4-3 Beam equilibrium

The expected load at failure of a specimen assuming a CFRP strip rupture mode of failure can be calculated using equation 4-1 with F_{strip} taken as the expected tensile strength of the CFRP strip as provided by the manufacturer. Thus, the expected load at failure of specimens with a 5 in. strip width and high strength concrete considering CFRP strip fracture was evaluated as 16 kips. The expected CFRP strip tensile strength for CFRP strip used in this study was 143 ksi. This value was used to calculate the expected load at failure for all specimens. As shown in Figure 4-4, the ultimate load developed in test B5H1.4Sb was 15.6 kips, which corresponds to 98% of its expected load at failure.

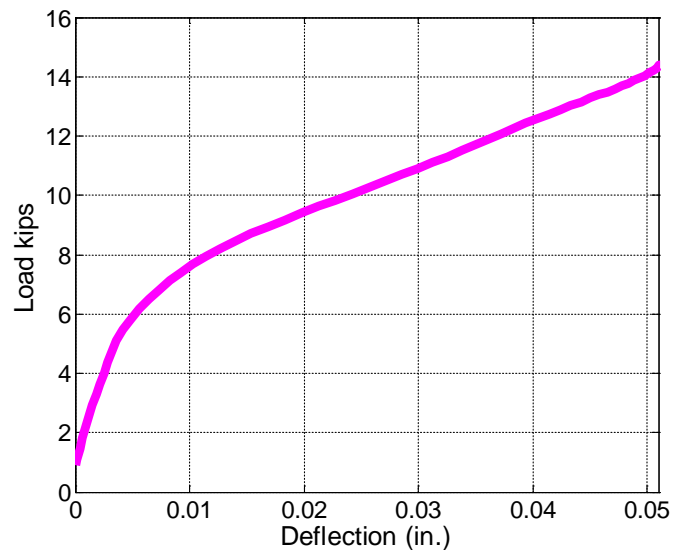


Figure 4-4 Load vs deflection at mid-span for B5H1.4Sb

In all tests, eight targets highlighted in Figure 4-5 were selected to calculate the deflection of beam specimens. Rigid-body movement of test beams due to the elongation of the reaction rods was subtracted from target movement data. Beam deflection was calculated as the relative displacement in the Z-direction (perpendicular to beam surface) between the targets at mid-span and those at the ends. For example, the deflection of the left side was the relative Z-displacement between targets numbered 2 and 4 and the deflection of right side was the relative Z-displacement between targets 6 and 8. The deflections of left side and right side were averaged to obtain the deflection at the beam top edge. The deflection at the beam bottom edge was calculated in the same way. Finally, the deflection of a specimen was calculated by averaging the top and bottom edge deflections.

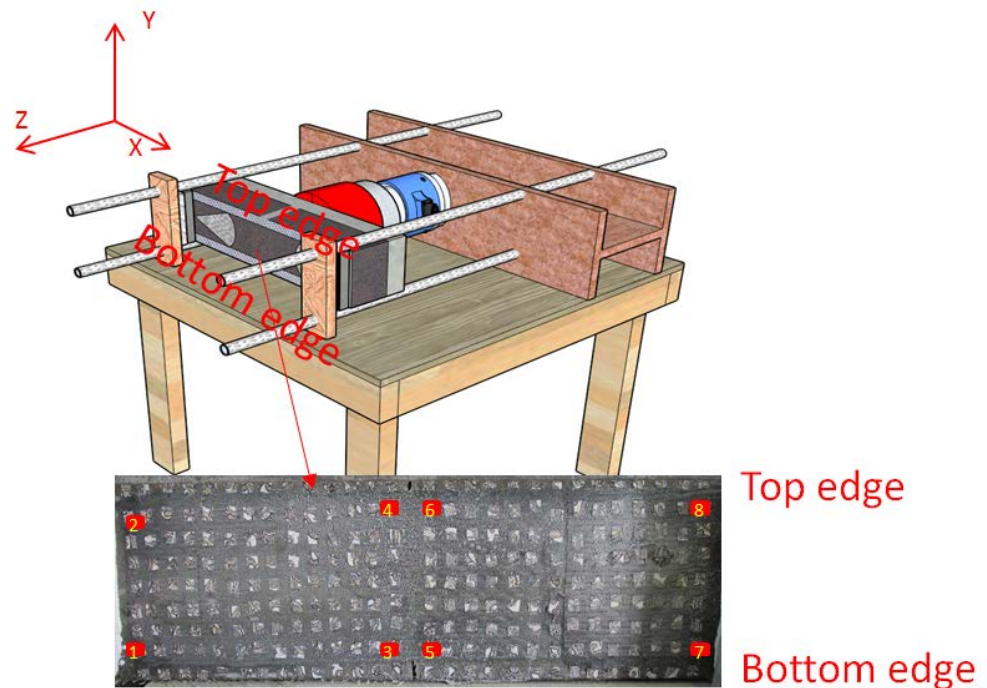


Figure 4-5 Beam targets on the tensile surface of beam used for deflection measurement

4.2.1.3 Maximum Strains and Strain Distributions

Strains were also used to evaluate the performance of the CFRP strips and anchors. CFRP surface-strain measurements from the UTVS were plotted as contours to locate regions of strain concentrations. Surface-strain profiles were also plotted across various sections to better assess strain distributions and associated load paths.

Strain distributions of the CFRP strip of test B5H1.4Sb is shown in Figure 4-6 at four loading stages. Small, nearly uniform strains were observed across the CFRP strip at 25% of ultimate load. In the plots, the white solid lines outline the anchor fans. The CFRP patches start from the end of CFRP strip and extend to the purple dashed lines. At 50% of ultimate load, significant strains developed near mid-span and then propagated towards both ends. The contour plot at 50% of ultimate load indicates that the CFRP strains near mid-span are larger than 0.004, which corresponds to an upper-bound debonding strain as defined by ACI 440, 2008. At 75% of ultimate load, strains were relatively uniform across the CFRP surface between the two anchors. UTVS strain measurements therefore indicated that strip debonding started at mid-span just after flexural cracking of the concrete beam and progressed toward the anchors. CFRP strips were almost completely debonded from the concrete substrate between the two anchor fans at 75% of ultimate load. At that load level, strain measurements indicated that CFRP anchors were carrying the bulk of the force in the CFRP strip. Large strains were observed adjacent to the edge of the right anchor at 98% ultimate load. Failure of test B5H1.4Sb occurred when the right anchor ruptured. The locations of selected critical sections are shown in Figure 4-7. From the contour plot at 98% ultimate load, the critical sections of highest strains were near the anchor fans rather than at mid-span, as illustrated in Figure 4-6. The maximum recorded strains near anchor fans were larger than 0.0093 in B5H1.4Sb, as shown in Figure 4-6. High strains around anchor fans indicate strain concentrations in those regions. Plots of strains at critical sections are discussed next to aid in the interpretation of observations.

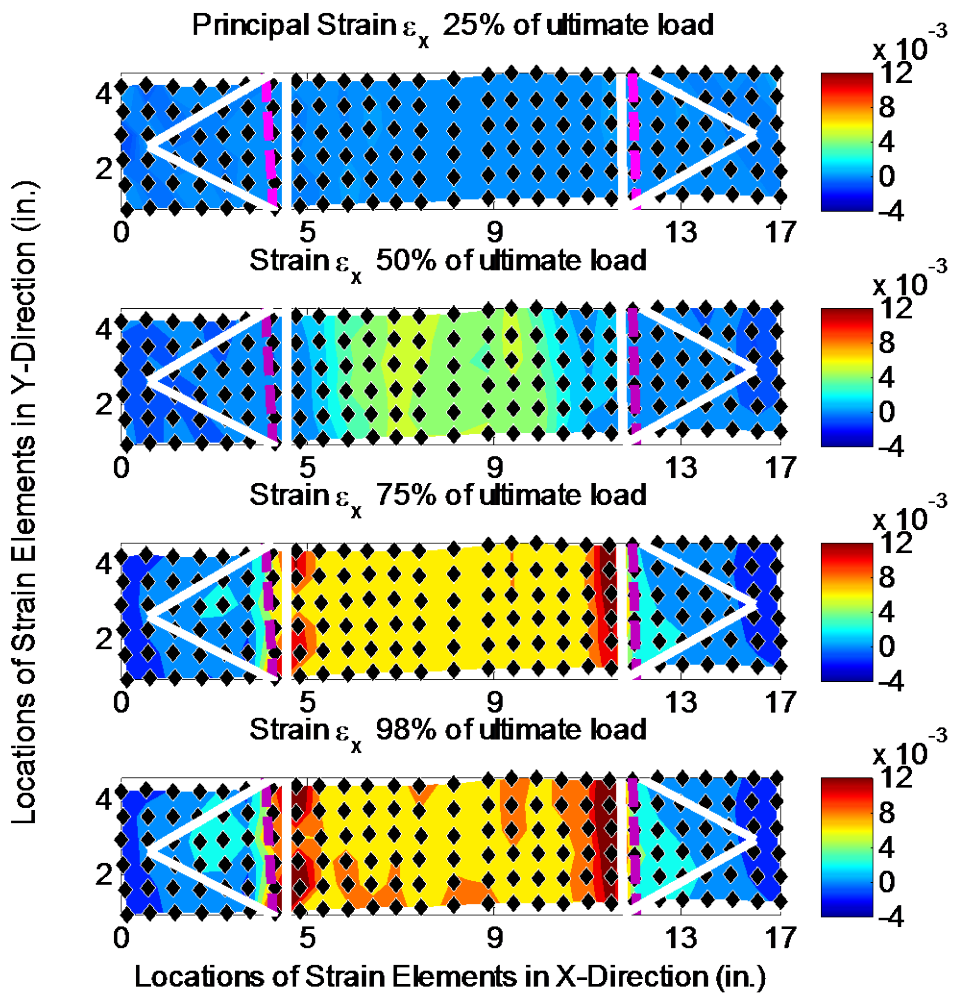


Figure 4-6 Contour plot of ϵ_x for B5H1.4Sb

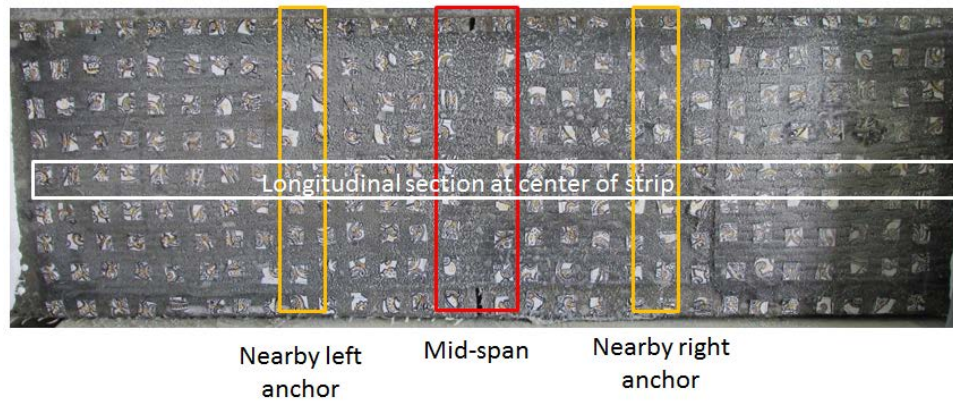


Figure 4-7 Critical sections on CFRP strip

Figure 4-8 highlights the distribution of X-direction strains at mid-span across the width of the CFRP strip, for test B5H1.4Sb. Strains in the X-direction are those measured in the direction of the CFRP-strip fibers and beam length. Insignificant strains evenly distributed between two anchor fans as shown in Figure 4-8 and Figure 4-9. A nearly uniform strain distribution with an average value of 0.0057 at mid-span was observed at 50% of the ultimate load. The CFRP strips were likely debonded from the concrete substrate at mid-span at that load level. At the same load level, however, strains in the CFRP strip near both anchors were below 0.002, as shown in Figure 4-9. The CFRP strip was therefore likely still bonded to the concrete substrate near the anchors at 50% of the ultimate load. At 75% of the ultimate load, the strains between the two anchor fans were larger than 0.005 indicating that the strip had likely totally debonded from the concrete substrate and the CFRP anchors were carrying most of the tensile force in the CFRP strip.

At 98% ultimate load, as shown in Figure 4-8, the maximum strain at the mid-span section was 0.011 at one beam edge, while the strain was lower at the other edge (0.008). The average strain at mid-span was 0.01, which is larger than the expected fracture value of 0.0093 given by the manufacturer. At 98% ultimate load, the largest X-direction strain readings were observed near the right anchor fan with an average value around 0.013 as shown in Figure 4-9. The strains at mid-span had an average value around 0.01 and the average strain near the left anchor fan was around 0.006.

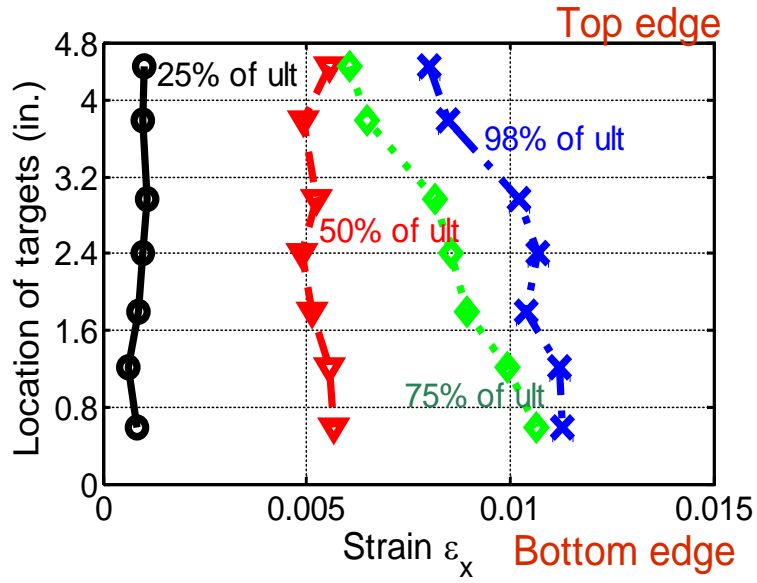


Figure 4-8 X-direction CFRP strip strain distribution across the mid-span section for test B5H1.4Sb

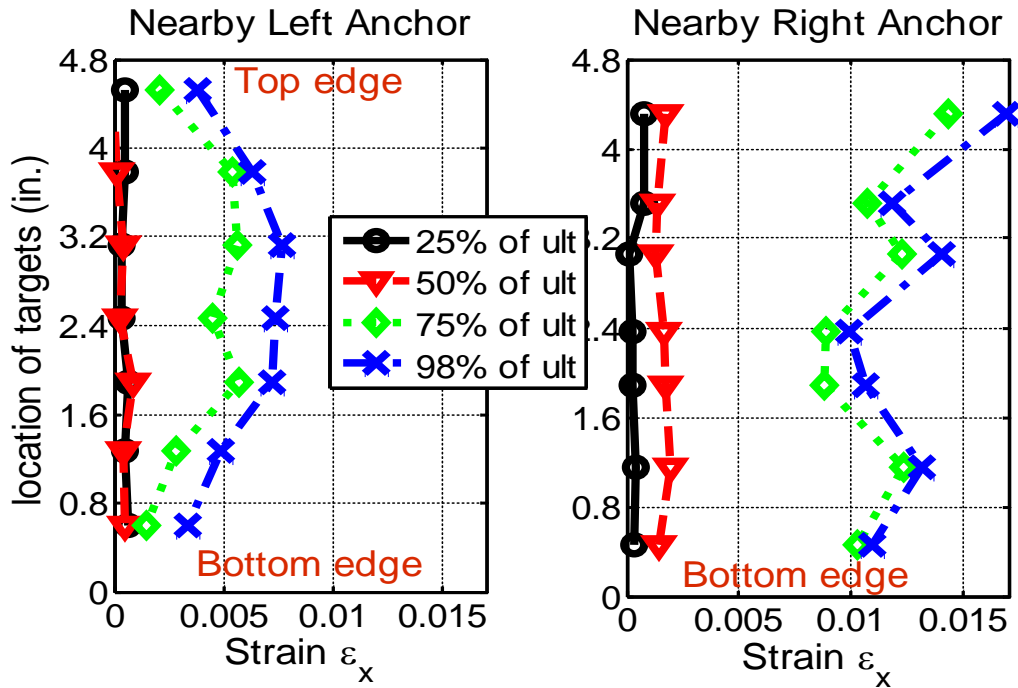


Figure 4-9 X-direction CFRP strip strain distribution nearby CFRP anchors for test B5H1.4Sb

In Figure 4-10, strains in the X-direction along the centerline (see Figure 4-7) of the CFRP strip are plotted for test B5H1.4Sb. Peak strains were observed at the sections near both anchor fans at the centerline of the CFRP strip.

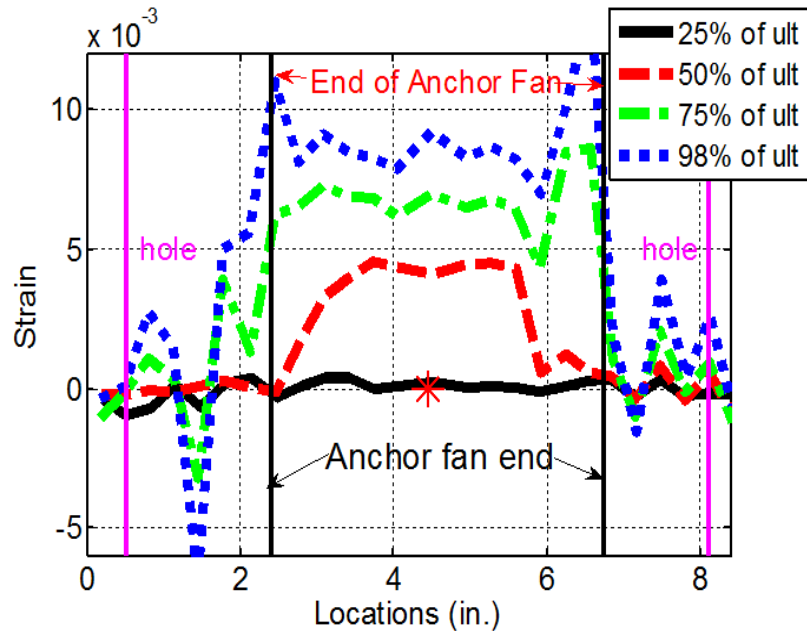


Figure 4-10 Centerline strains in the longitudinal direction for test B5H1.4Sb

4.2.1.3 Debonding Mechanism

In order to investigate the influence of bonding on the performance of CFRP anchorages, a relation between bond stress and slip was extracted from the test data. The extraction process is presented in this section and the resulting bond vs slip relation for test B5H1.4Sb is shown. Bond stress versus slip relations are used to propose a computational model in Chapter 5 to numerically study the load transfer mechanism from the CFRP strips to the CFRP anchors.

The change in tensile force along a CFRP strip ΔF_i is assumed to be generated through bond forces at the interface between the strip and the concrete substrate (Figure 4-11). The bond

stress developed between CFRP and concrete can be determined from strain measurements as follows:

$$\Delta F_{i,i+3} = \tau_{i,i+3} \times \Delta X_{i,i+3} \times b_t \quad \text{Equation 4-2}$$

the change in strip tensile force can also be written as:

$$\Delta F_{i,i+3} = (\varepsilon_{i+2,i+3} - \varepsilon_{i,i+1}) \times E_f \times t_f \times b_t \quad \text{Equation 4-3}$$

where

$\Delta X_{i,i+3}$ is the distance between two adjacent pairs of targets starting at target i and ending at target $i+3$

$\tau_{i,i+3}$ is the average bond stress over the shaded area bounded by the centroid of two adjacent pairs of targets

$\varepsilon_{i,i+1}$ is the strain measured between the two left targets

$\varepsilon_{i+2,i+3}$ is the strain measured between the two right targets

E_f is the specified modulus of elasticity of the CFRP strip

t_f is the specified thickness of the CFRP strip

b_t is the center-to-center distance between target rows = 0.5 in.

$\Delta F_{i,i+3}$ is the change in tensile force in the CFRP strip over distance $\Delta X_{i,i+3}$ within width b_t

Thus, solving for $\tau_{i,i+3}$

$$\tau_{i,i+3} = \frac{\varepsilon_{i+2,i+3} - \varepsilon_{i,i+1}}{\Delta X_{i,i+3}} E_f t_f \quad \text{Equation 4-4}$$

The slip between a CFRP strip and the concrete substrate is evaluated as the cumulative X-direction elongation between the locations of targets at the edge of the anchorage region where no slip occurs, and the target locations where slip is evaluated:

$$\mathit{slip}_{i,i+1} = \frac{\Delta_i + \Delta_{i+1}}{2} - \Delta_0 \quad \text{Equation 4-5}$$

where:

Δ_i is the X-direction displacement of i th target

Δ_{i+1} is the X-direction displacement of $i+1$ th target

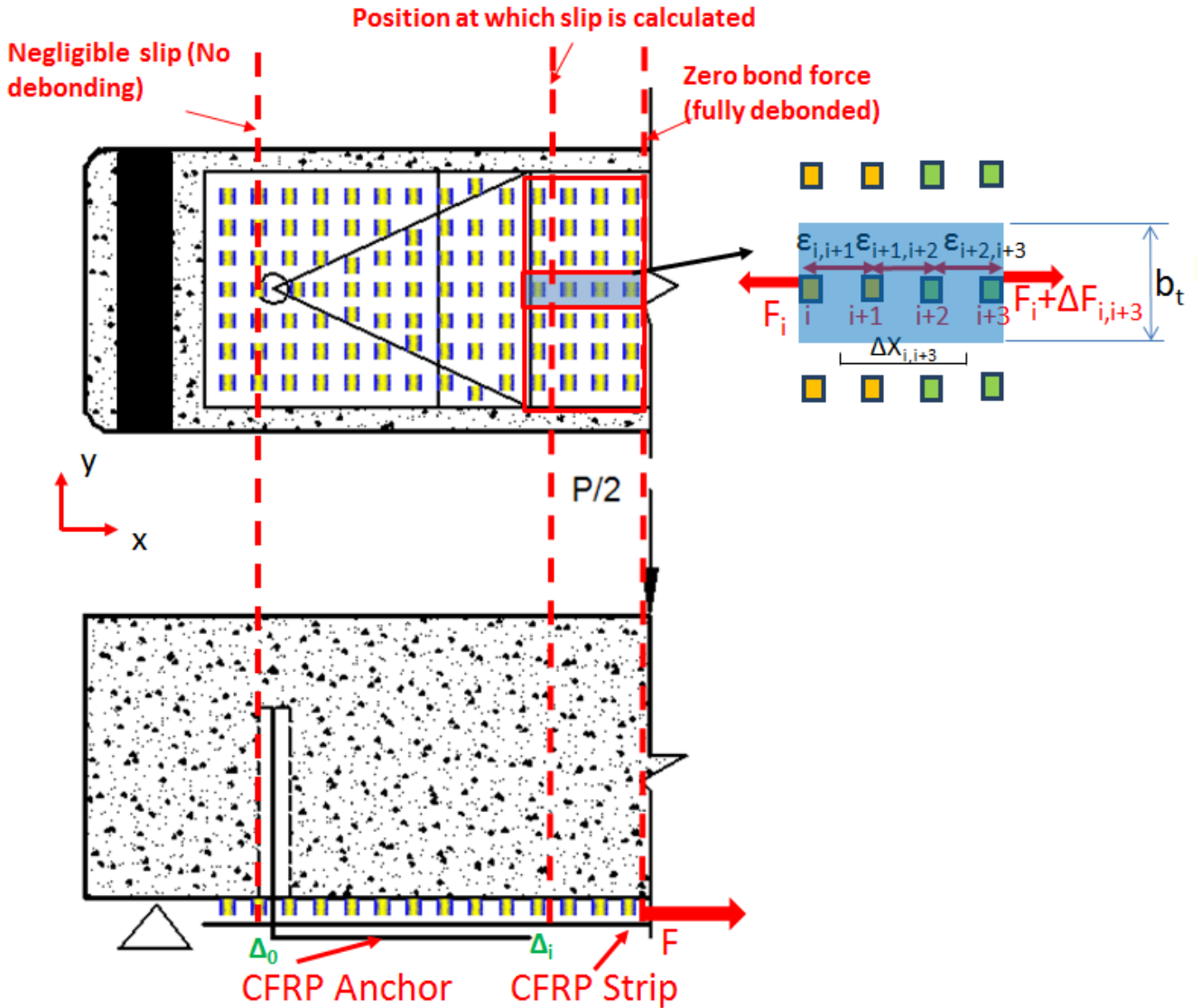


Figure 4-11 Tensile force transfer from CFRP strip to concrete substrate

Equations 4-4 and 4-5 provide the bond stress and slip values for one group of targets. The reported bond stress and slip in this study come from the average value of seven groups of targets across the strip width.

Bond stress and slip evaluated across strip width between strip target pairs bonded by anchor fan edges were averaged. The resulting bond stress versus slip plot for B5H1.4Sb is shown in Figure 4-12. Bond stress increased up to 0.51 ksi at a slip of 0.003 in. After that, bond stress decreased to zero when slip reached 0.01 in.

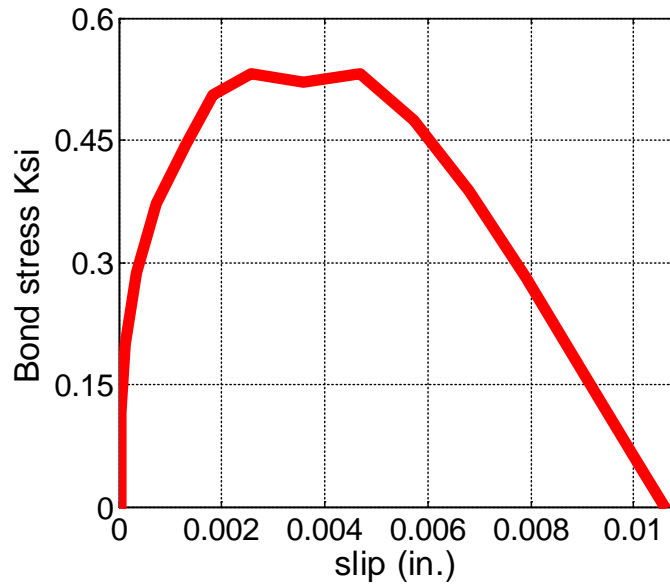


Figure 4-12 Bond stress vs slip reaction for test B5H1.4Sb

4.2.2 Failure Modes and Strength Evaluation

The failure mode of each specimen is presented and discussed in this section. The only failure mode observed for non-anchored specimens was that of debonding (Figure 4-13); that is the CFRP strip debonded from the concrete substrate. Four other failure modes were observed for anchored specimens: CFRP strip fracture (Figure 4-14), CFRP anchor rupture (Figure 4-15), concrete beam shear (Figure 4-16), and delamination (Figure 4-17) between the CFRP strip and the CFRP anchor fans.



Figure 4-13 Debonding failure



Figure 4-14 CFRP strip fracture



Figure 4-15 CFRP anchor rupture



Figure 4-16 Concrete beam shear failure (Huaco, 2010)

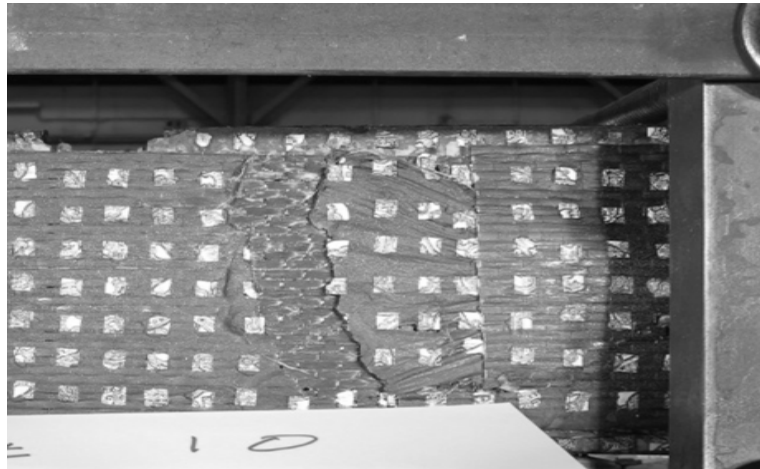


Figure 4-17 Delamination between CFRP strip and anchor

A primary objective of this research was to determine characteristics of CFRP anchors that allow them to fully develop the tensile strength of CFRP strips. A qualified CFRP anchorage system is expected to result in the fracture of the CFRP strip. Therefore, the failure mode was used to evaluate the performance of anchorage systems.

The ultimate load applied on a beam specimen at failure was also used to evaluate the performance of CFRP anchorage systems. A qualified anchorage system is expected to provide capacities equal to or greater than the expected load at failure derived from the expected CFRP strip strength at failure.

4.2.3 Summary of test results

In Table 4-1, the experimental results of the 39 tests computed are summarized. The experimental results were used to evaluate the influence of parameters on strip strength and anchor strength.

In Table 4-1:

P_{ult} = The ultimate applied load at failure.

P_{des} = The design beam strength which is calculated by equilibrium using the manufacturer specified design stress for the CFRP strip ($\sigma_{des} = 121$ ksi).

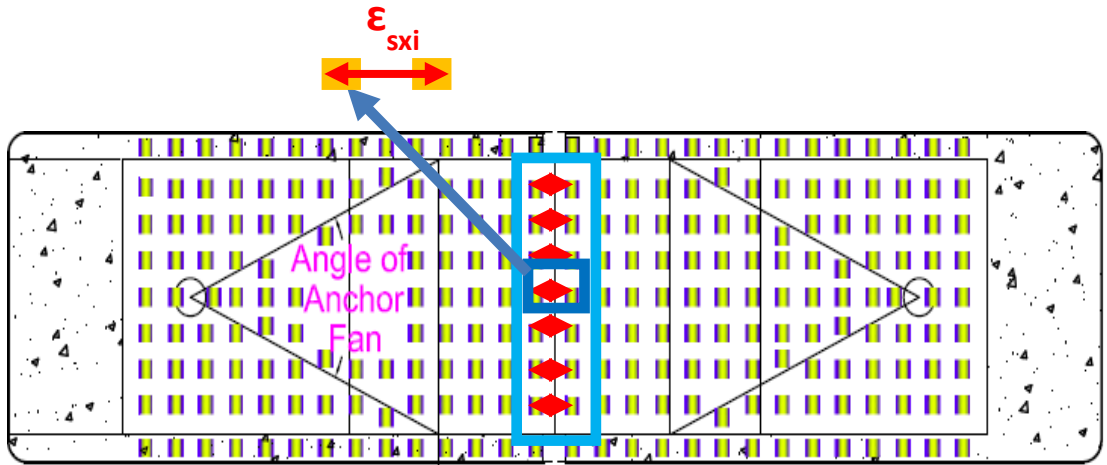
P_{exp} = The expected beam load at failure which is calculated by equilibrium using the expected rupture stress for the CFRP strip provided by manufacturer ($\sigma_{exp} = 143$ ksi).

$F_{f\ mid}$ = The strip force at mid-span which is calculated by equilibrium at ultimate load (P_{ult}).

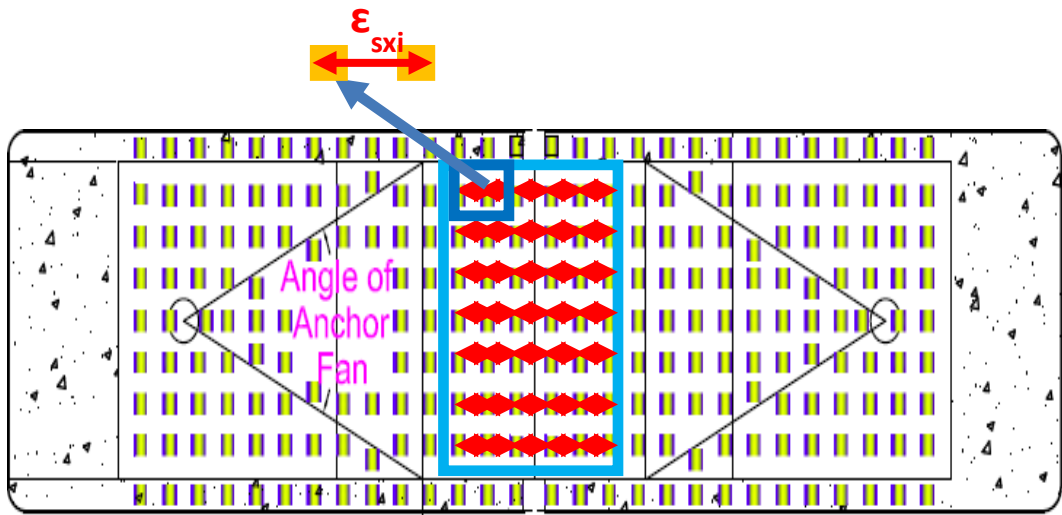
$\sigma_{fx\ mid\ ult}$ = The strip stress at mid-span which is evaluated at ultimate load = $F_{f\ mid} / A_{CFRP}$ in which A_{CFRP} is the cross-sectional area of the CFRP strip.

$\epsilon_{sx\ mid\ 98\%\ ult}$ = The mid-span strip strain in the strip fiber direction (X-direction) which is measured at 98% P_{ult} .

The selected strip measurement targets and area for $\epsilon_{sx\ mid\ 98\%\ ult}$ are shown in Figure 4-18. Based on the evaluation, design guidelines are provided in Chapter 6.



(a) Selected area and targets used to measure the mid-span strip strain $\epsilon_{sx \text{ mid } 98\% \text{ ult}}$



(b) Selected area and targets used to measure the mid-span strip strain $\epsilon_{sx \text{ 98\% ult}}$

Figure 4-18 Area and targets selected for strain measurements

Table 4-1 Summary of experimental results

A	B	C	D	E	F	G	H	I	G	K	L
Tests	Failure Mode	P_{ult} kips	P_{des} kips	P_{ult}/P_{des}	P_{exp} kips	P_{ult}/P_{exp}	F_f mid kips	$\sigma_{fx\ mid}$ ult ksi	Mean $\epsilon_{sx\ mid\ 98\%}$ ult	Mean $\epsilon_{sx\ 98\%}$ ult	Max $\epsilon_{sx\ 98\%}$ ult
B5H2Ma	Strip Fracture	18.2	13.6	1.34	16	1.14	16.3	163	0.0112	0.0099	0.0158
B5H2Mb	Strip Fracture	18.6	13.6	1.37	16	1.16	16.6	166	0.0109	0.0106	0.0135
B5H1.4Ma	Strip Fracture	15.8	13.6	1.16	16	0.99	14.1	141	0.0101	0.0089	0.0163
B5H1.4Mb	Strip Fracture	16	13.6	1.18	16	1.00	14.3	143	0.0099	0.0106	0.0160
B5H1.4Mc	Delamination	16.1	13.6	1.18	16	1.01	14.4	144	0.0097	0.0092	0.0119
B5H1.4Md	Strip Fracture	16	13.6	1.18	16	1.00	14.3	143	0.0117	0.0101	0.0147
B5H1.4Sa	Concrete Shear	13.4	13.6	0.99	16	0.84	12.0	120	0.0081	0.0079	0.0108
B5H1.4Sb	Anchor Rupture	15.6	13.6	1.15	16	0.98	13.9	139	0.0101	0.0095	0.0151
B5H1.4La	Strip Fracture	18.9	13.6	1.39	16	1.18	16.9	169	0.0113	0.0113	0.0132
B5H1.4Lb	Anchor Rupture	15.6	13.6	1.15	16	0.98	13.9	139	0.0117	0.0117	0.0138
B5L1.4Ma	Strip Fracture	15.8	13.4	1.18	15.6	1.01	14.5	145	0.0097	0.0092	0.0164
B5L1.4Mb	Strip Fracture	14.7	13.4	1.10	15.6	0.94	13.4	134	0.0112	0.0093	0.0134
B5L1.4Mc	Anchor Rupture	17.2	13.4	1.28	15.6	1.10	15.7	157	0.0093	0.0089	0.0111
B5L1.4Md	Delamination	10	13.4	0.75	15.6	0.64	9.1	91	0.0105	0.0089	0.0119
B5H1Ma	Anchor Rupture	15	13.6	1.10	16	0.94	13.4	134	0.0087	0.0087	0.0136
B5H1Mb	Anchor Rupture	15.8	13.6	1.16	16	0.99	14.1	141	0.0102	0.0083	0.0130
B5H1Mc	Anchor Rupture	16.1	13.6	1.18	16	1.01	14.4	144	0.0095	0.0087	0.0126
B5H1Md	Delamination	17	13.6	1.25	16	1.06	15.2	152	0.0118	0.0100	0.0146
B5L1Ma	Anchor Rupture	15.5	13.4	1.16	15.6	0.99	14.2	142	**	**	**
B5L1Mb	Anchor Rupture	11.4	13.4	0.85	15.6	0.73	10.4	104	**	**	**
B5L1Mc	Anchor Rupture	13.7	13.4	1.02	15.6	0.88	12.5	125	0.0089	0.0090	0.0114
B5L1Md	Anchor Rupture	14.8	13.4	1.11	15.6	0.95	13.5	135	0.0087	0.0085	0.0119
B5L1Me	Anchor Rupture	15.4	13.4	1.15	15.6	0.99	14.1	141	0.0105	0.0088	0.0134
B5L1Mf	Concrete Shear	16.9	13.4	1.26	15.6	1.08	15.4	154	0.0103	0.0089	0.0130
B5L1Mg	Concrete Shear	11.1	13.4	0.83	15.6	0.71	10.2	102	0.0088	0.0090	0.0126
B5L1Mh	Anchor Rupture	11.2	13.4	0.84	15.6	0.72	10.2	102	0.0084	0.0085	0.0115
U5H2Ma	Concrete Shear	14.9	13.6	1.10	16	0.93	13.3	133	0.0088	0.0076	0.0126
U5H1.4Ma	Anchor Rupture	14.0	13.6	1.03	16	0.87	12.2	122	0.0082	0.0081	0.0134
U5H1.4Mb	Anchor Rupture	14.8	13.6	1.09	16	0.93	13.2	132	0.0091	0.0087	0.0135
B3H1.4Sa	Strip Fracture	10.4	8.2	1.27	9.7	1.07	9.2	154	0.0090	0.0083	0.0107
B3H1.4Sb	Strip Fracture	11.8	8.2	1.44	9.7	1.22	10.5	174	0.0114	0.0099	0.0128
B3H1.4Ma	Strip Fracture	12.4	8.2	1.51	9.7	1.28	11.0	183	0.0100	0.0106	0.0140
B3H1.4Mb	Strip Fracture	10.4	8.2	1.27	9.7	1.07	9.2	154	0.0099	0.0096	0.0141
B3H1.4La	Strip Fracture	12.6	8.2	1.54	9.7	1.30	11.2	186	0.0096	0.0097	0.0139
B3H1.4Lb	Strip Fracture	10	8.2	1.22	9.7	1.03	8.9	148	0.0103	0.0097	0.0125
B3L1.4XLa	Strip Fracture	10.2	8.1	1.26	9.6	1.06	9.0	151	0.0070	0.0092	0.0148
B3L1.4XLb	Strip Fracture	11	8.1	1.36	9.6	1.15	9.7	162	0.0085	0.0098	0.0123
B3L1XLa	Strip Fracture	10.3	8.1	1.27	9.6	1.07	9.1	152	0.0073	0.0095	0.0145
B3L1XLb	Strip Fracture	11.6	8.1	1.43	9.6	1.21	10.3	171	0.0105	0.0102	0.0155

** Strain data is not available.

As shown in Figure 4-19, strip fracture was observed in 18 tests only two beams that failed by strip fracture at a load lower than the expected load, one at 99% and the other at 94% of P_{exp} . Anchor rupture was observed in 14 tests from which only two tests reached the expected load at failure P_{exp} . Delamination between anchors and strips only occurred in three tests. The remaining four tests failed due to concrete shear failure. The delamination failures and the two tests with strip fractures that failed to reach the expected load highlight the importance and necessity of developing a standard test methodology for quality control.

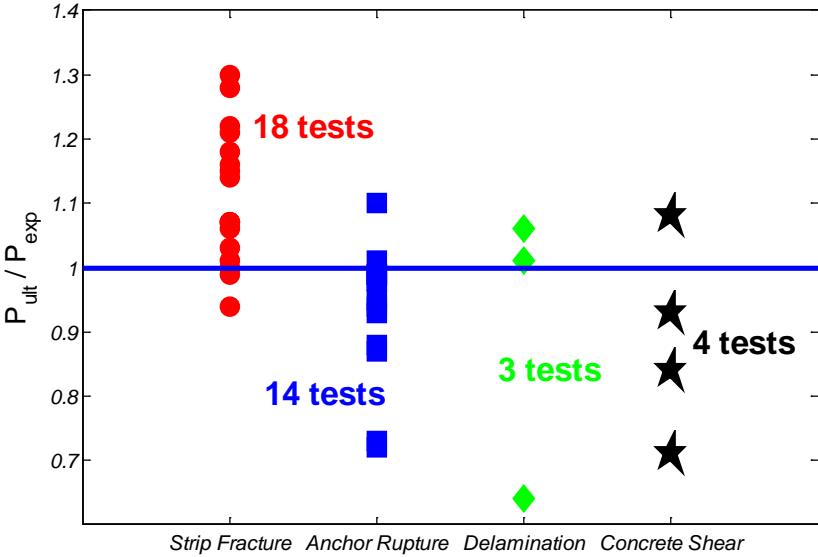


Figure 4-19 P_{ult} / P_{exp} vs failure modes

In Figure 4-20, the values of $\epsilon_{sx\ 98\% \text{ ult}} / \epsilon_{sx \text{ mid } 98\% \text{ ult}}$ vs. test number for all 39 tests are plotted. The figure indicated that the values of $\epsilon_{sx\ 98\% \text{ ult}} / \epsilon_{sx \text{ mid } 98\% \text{ ult}}$ ratio for most tests were within + or – one standard deviation. The sample standard deviation for the strain ratio is equal to 0.11. It revealed the mean strain measured at mid-span agreed well with the mean strain measured between two anchor fan ends at 98% expected load at failure.

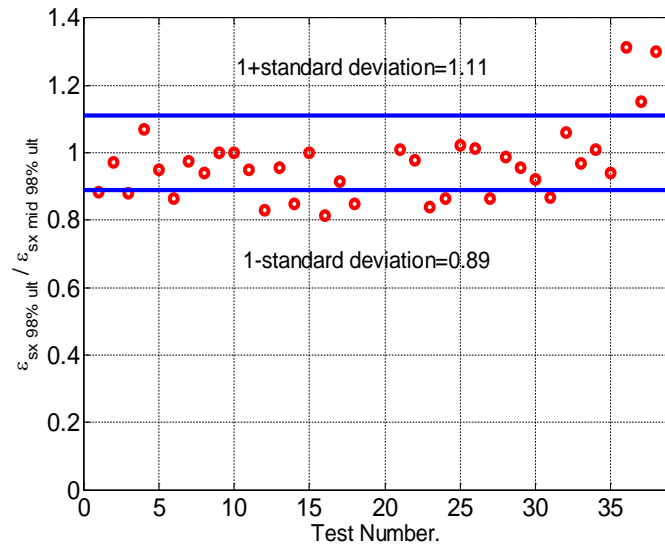


Figure 4-20 The distribution on the values of the strain ratio $\epsilon_{sx\ 98\% \text{ ult}} / \epsilon_{sx\ \text{mid}\ 98\% \text{ ult}}$ among tests

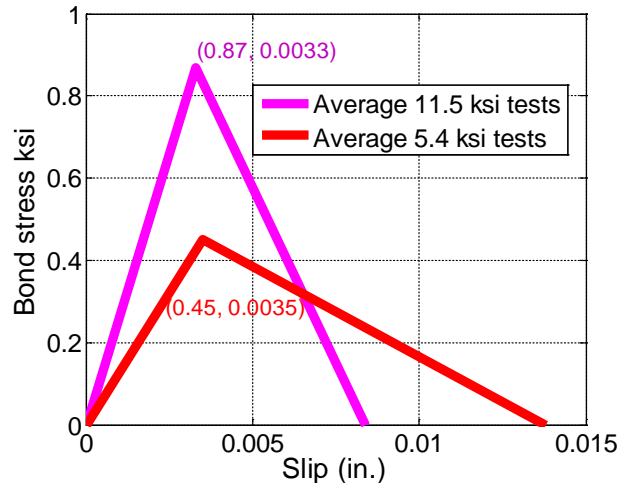
4.3 EFFECT OF CONCRETE STRENGTH

This series was designed to evaluate the impact of concrete strength on bond strength and anchor performance.

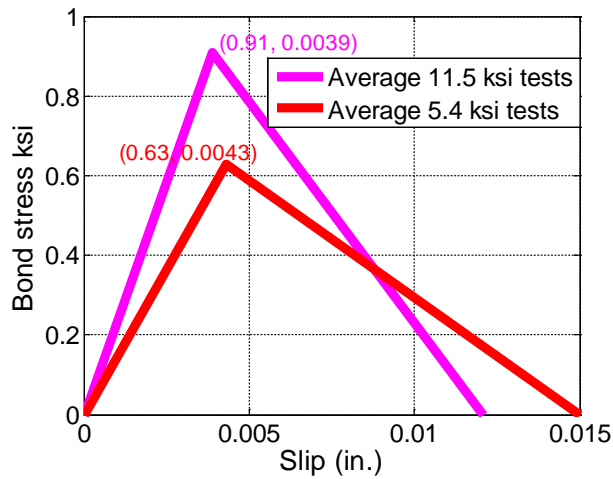
4.3.1 Bond Strength

Bond versus slip relations were extracted for tests with 5 in. and 3 in. strips separately. In Figure 4-21, simplified bond versus slip relations between CFRP strips and concrete in test beams are presented, derived from strain data as discussed in Section 4.2.1.3. The simplified bond versus slip relations are comprised of a linear bond stress versus slip behavior to the peak bond stress. Then, a linear degrading behavior is used until the ultimate slip at which the CFRP strip completely debonded from the concrete substrate and bond stress is zero. The peak bond stress and its corresponding slip, as well as the ultimate slip are listed in Table 4-2 and Table 4-3 for tests where reliable data was extracted. Average values of the parameters are also presented in the tables. Excluded from these tables are tests that failed by delamination or concrete shear. In addition, tests B5H1.4La and B5H1.4Lb were also excluded because the clear length between anchor fans was less than 2 in. and was too short to provide reliable results. As can be seen in the

Figure 4-21, the higher strength concrete generates a higher peak bond stress but lower slip at peak stress than the lower strength concrete. The higher peak bond stress and lower slip at peak stress make the ascending slope of the bond vs. slip relation stiffer for higher strength concrete. For the degrading branch, a steeper slope was also observed for specimens with high-strength concrete compared with that of specimens with normal-strength concrete.



(a) 5 in. strips



(b) 3 in. strips

Figure 4-21 Concrete-CFRP bond stress versus slip relations extracted from UTVS strain data

Table 4-2 Peak bond stress, slip at peak bond stress, and ultimate slip for tests with 5 in. strips

Tests	Failure modes	Peak bond stress (ksi)	Slip at peak bond stress in.	Ultimate slip in.
B5H2Ma	Strip Fracture	1	0.004	0.008
B5H2Mb	Strip Fracture	0.95	0.0027	0.01
B5H1.4Ma	Strip Fracture	0.8	0.003	0.006
B5H1.4Mb	Strip Fracture	0.9	0.004	0.007
B5H1.4Md	Strip Fracture	1	0.0035	0.008
B5H1.4Sb	Anchor Rupture	0.51	0.003	0.011
B5H1Ma	Anchor Rupture	0.65	0.0045	0.01
B5H1Mb	Anchor Rupture	0.9	0.004	0.0075
B5H1Mc	Anchor Rupture	0.83	0.003	0.01
Average	-	0.87	0.0033	0.0086
B5L1.4Ma	Strip Fracture	0.42	0.0045	*
B5L1.4Mb	Strip Fracture	0.45	0.0035	0.01
B5L1.4Mc	Anchor Rupture	0.3	0.0025	0.008
B5L1Mc	Anchor Rupture	0.5	0.0032	0.02
B5L1Md	Anchor Rupture	0.41	0.003	0.017
B5L1Me	Anchor Rupture	0.63	0.0042	*
Average	-	0.45	0.0035	0.0138

**The ultimate slip could not be determined since the bond stress during the entire test was non-zero*

Table 4-3 Peak bond stress, slip at peak bond stress, and ultimate slip for tests with 3 in. strips

Tests	Failure modes	Peak bond stress (ksi)	Slip at peak bond stress in.	Ultimate slip in.
B3H1.4Sa	Strip Fracture	0.56	0.0027	0.008
B3H1.4Sb	Strip Fracture	0.9	0.0044	0.02
B3H1.4Ma	Strip Fracture	1.1	0.0027	0.012
B3H1.4Mb	Strip Fracture	0.94	0.0022	0.015
B3H1.4La	Strip Fracture	1.3	0.004	0.01
B3H1.4Lb	Strip Fracture	0.79	0.0035	0.007
Average	N.A.	0.9	0.0039	0.012
B3L1.4XLa	Strip Fracture	0.8	0.004	0.008
B3L1.4XLb	Strip Fracture	0.85	0.008	0.015
B3L1XLa	Strip Fracture	0.48	0.0022	0.017
B3L1XLb	Strip Fracture	0.37	0.0028	0.02
Average	N.A.	0.63	0.0043	0.0143

In Figure 4-22, pictures of the CFRP and concrete surfaces after debonding failures are shown. A debonding failure occurs when the CFRP strip detaches the beams. The detachment may occur in the epoxy layer or in the concrete substrate in which case some concrete remains

bonded to the CFRP strip. This observation suggests that bond strength between concrete and CFRP is primarily governed by concrete strength instead of the tensile strength of the interfacial material (resin epoxy). The peak bond stresses of tests with high-strength concrete were 0.87 ksi and 0.91 ksi, for 5 in. and 3 in. strips respectively. Those values are close to the tensile strength of the high-strength concrete (11.5ksi) which can be estimated as 0.80 ksi. Similarly, the peak bond stress of tests with normal strength concrete (5.4 ksi) were 0.45 ksi and 0.63 ksi, for 5 in. and 3 in. strips respectively, which were close to the tensile strength of the normal concrete (0.55 ksi).



(a) High strength concrete (b) Normal strength concrete
Figure 4-22 Concrete and CFRP surfaces after debonding

4.3.2 Strip Fracture

Five comparable tests were evaluated to study the impact of concrete strength on CFRP strip strength. Every parameter except the concrete strength was kept constant in this comparison. An anchor material ratio of 1.41 was used. CFRP strips were 5 in. wide, and anchor fan lengths were 6 in. in all the tests. All specimens failed by fracture of the CFRP strip. A summary of experimental results for those five tests is presented in Table 4-4.

As shown in Table 4-4, the average ultimate strip stress at mid-span evaluated from beam equilibrium (Average $\sigma_{fx \text{ mid ult}}$) was 142 ksi for specimens with high strength concrete and 140

ksi for specimens with normal strength concrete. The concrete strength did not have a significant effect on ultimate strip stress at failure ($\sigma_{fx\ mid\ ult}$).

Table 4-4 Experimental results for effect of concrete strength on strip fracture

Specimens	f'_c	$\sigma_{fx\ mid\ ult}$ (ksi)	Average $\sigma_{fx\ mid\ ult}$ (ksi)
B5H1.4Ma	11.5 ksi	141	142
B5H1.4Mb		143	
B5H1.4Md		143	
B5L1.4Ma	5.4 ksi	145	140
B5L1.4Mb		134	

As shown in Figure 4-23, the only difference was on the cracking load. The cracking load for specimens with 11.5 ksi concrete was around 7 kips. For specimens with a concrete strength of 5.4 ksi, the cracking load was around 5.8 kips. After cracking, all tests except for test B5L1.4Mb had showed similar load-deflection responses. The causes of the significantly larger deflections for the same load after cracking for B5L1.4Mb could not be determined.

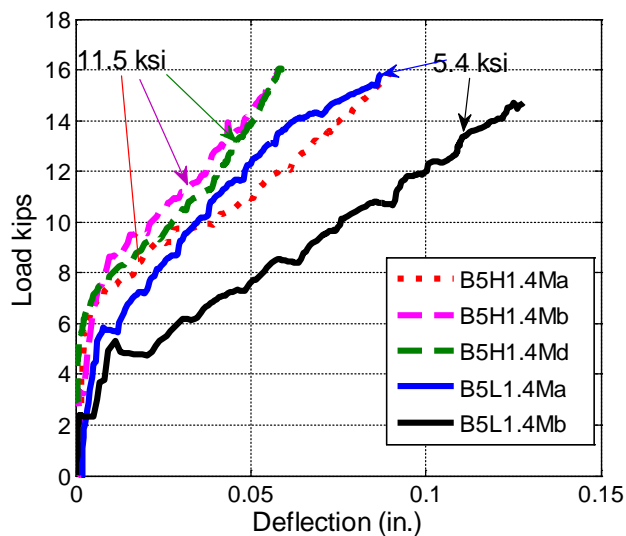


Figure 4-23 Load vs deflection for effect of concrete strength on strip fracture

4.3.3 Anchor Rupture

Seven comparable specimens were evaluated to study the impact of concrete strength on anchor strength. All parameters except the concrete strength were constant. An anchor material ratio of 1.06 was used, CFRP strips were 5 in. wide, and anchor fan lengths were 6 in. in all tests. All specimens failed by anchor rupture. As shown in Table 4-5, the average ultimate strip stress at mid-span evaluated from beam equilibrium (Average $\sigma_{fx\ mid\ ult}$) was 140 ksi for specimens with high strength concrete and 127 ksi for specimens with normal strength concrete. The high strength concrete resulted in an increase of about 10% in in the ultimate strip stress at anchor failure.

Table 4-5 Experimental results for effect of concrete strength on anchor rupture

Specimens	f'_c	$\sigma_{fx\ mid\ ult}$ (ksi)	Average $\sigma_{fx\ mid\ ult}$ (ksi)	$\sigma_{ax\ mid\ ult}$ (ksi)	Average $\sigma_{ax\ mid\ ult}$ (ksi)
B5H1Ma	11.5 ksi	134	140	126	132
B5H1Mb		141		133	
B5H1Mc		144		136	
B5L1Ma	5.4 ksi	142	127	134	120
B5L1Mb		104		98	
B5L1Mc		125		118	
B5L1Md		135		127	

However, as illustrated in Figure 4-24, the tensile force in the CFRP strips can be carried by CFRP anchors and interfacial bond between the CFRP strips and the concrete beams. Possibly, in areas where CFRP strips remain bonded on high strength concrete prior to anchor failure, the higher bond strength between the CFRP strips and concrete may have increased the apparent strength at anchor fracture. Considering the average peak bond stress were 0.87 ksi for high strength concrete and 0.45 ksi for normal strength concrete (section 4.5.1), a 13 ksi

difference in the average value of ultimate strip stress listed in Table 4-5 may suggest that CFRP strip area around the anchor of about a 3 in^2 ($=13 \text{ ksi} \cdot 0.02 \text{ in.} \cdot 5 \text{ in.} / (0.87 \text{ ksi} - 0.45 \text{ ksi})$) remains bonded until anchor rupture. Due to the speed at which anchor fracture occurs, it is difficult to ascertain experimentally how large a bonded CFRP area is contributing to anchor strength. Another possibility could be that the stiffer higher-strength concrete may help distribute anchor stresses more evenly at the anchor bend. More studies are needed to investigate this effect further.

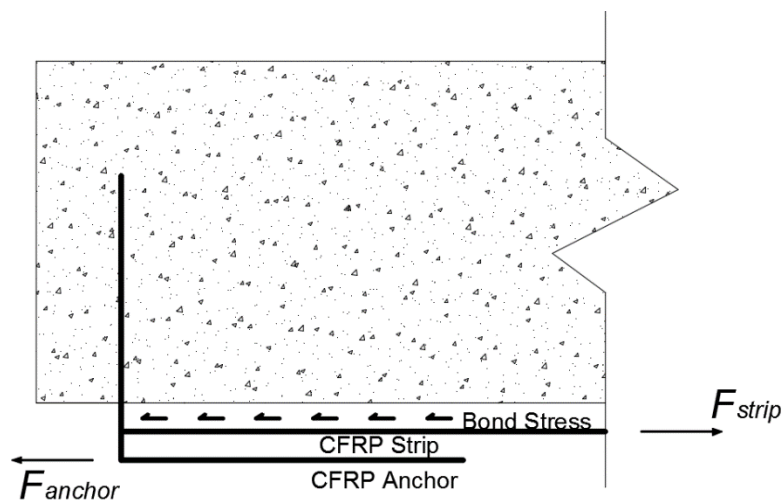


Figure 4-24 Load transferring from CFRP strip to CFRP anchor

As shown in Figure 4-25, the cracking load for specimens with 11.5 ksi concrete was around 7 kips. For specimens with concrete strength of 5.4 ksi, the cracking load was around 5.2 kips. After cracking, all tests exhibited similar load-deflection behaviors. No reliable deflection measurement for test B5H1Mb after a load of 10.4 kips was reached.

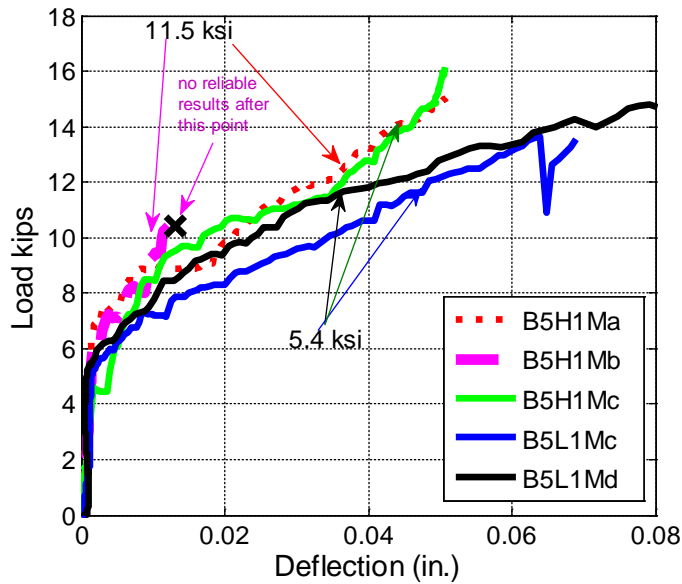


Figure 4-25 Load vs deflection for effect of concrete strength on anchor rupture

4.3.4 Summary

Concrete strength was not found to have a major impact on ultimate CFRP-strip or beam strength. Increasing concrete strength increased the bond strength between CFRP strips and the concrete substrate. Thus, debonding of the CFRP strip occurred at a higher load for higher strength concrete. A higher concrete strength was found to increase slightly (10%) the apparent strength of CFRP anchors embedded in it.

4.4 EFFECT OF ANCHOR FAN LENGTH/ANCHOR FAN ANGLE

This section was designed to evaluate the effects of anchor fan length/anchor fan angle on the strength of CFRP strips. In this section, the applicability of the maximum recommended fan angle of 60° (Kim, 2011) is verified.

4.4.1 Strip Fracture

Six comparable tests were evaluated to study the impact of anchor fan length/ angle on strip strength. Every parameter except the anchor fan length/angle was kept constant in each group. To effectively develop the strength of CFRP strips, CFRP anchors should be fanned out across the width of CFRP strips. Since strip width was kept the same in each group, the length of the anchor fan determines the anchor-fan angle. All tests had 3 in. wide CFRP strips and high-strength concrete. An anchor material ratio of 1.41 and high-strength concrete were used. A summary of experimental results is presented in Table 4-6.

Table 4-6 Experimental results for effect of fan geometry on strip fracture

Specimens	Fan length/ Angle	$\sigma_{fx\ mid\ ult}$ (ksi)	Average $\sigma_{fx\ mid\ ult}$ (ksi)
B3H1.4Sa	2.4 in.	154	164
B3H1.4Sb	64°	174	
B3H1.4Ma	3.6 in.	183	169
B3H1.4Mb	45°	154	
B3H1.4La	4.5 in.	186	167
B3H1.4Lb	37°	148	

As shown in Table 4-6, all strips fractured at an ultimate strip stress larger than the expected tensile strength provided by the manufacturer (143 ksi). Both the lowest (148 ksi) and highest (186 ksi) ultimate strip stresses were from tests with the large anchor fan length (4.5 in. and 37°). Overall, increasing the fan angle from 37° to 64° did not produce a significant change in the ultimate strip stress at strip fracture.

As shown in Figure 4-26, the cracking load for all tests was around 3 kips where CFRP strips start debonding from the concrete substrate. There was considerable variability that can be attributed to the variations in the CFRP area where the anchor fan are located, bond variations

and the amount of patch material. Changing the fan angle from 37° to 64° did not change the failure mode or the strength at strip fracture.

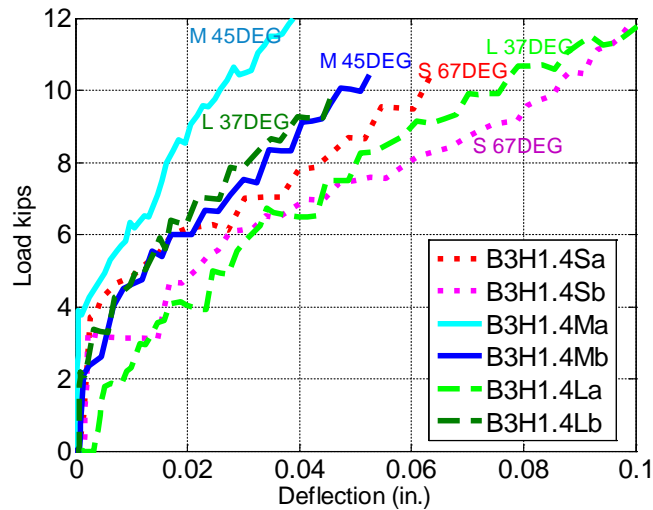


Figure 4-26 Load vs deflection for effect of fan geometry on strip fracture

4.4.2 Anchor Rupture

No conclusion could be made concerning the effects of anchor fan geometry on anchor strength due to insufficient data from tests sustaining anchor failures and having a range of fan geometries.

4.4.3 Summary

Anchor fan angles as low as 37° were able to develop the strength of CFRP strips. Little difference was observed in the response of beams reinforced with strips anchored using fan angles between 37° and 64°.

4.5 EFFECT OF WIDTH OF CFRP STRIP

4.5.1 Strip Fracture

4.5.1.1 Directly Comparable Tests

Five directly comparable tests were conducted to investigate the impact of strip width. All parameters except the width of the CFRP strip were kept constant in this comparison. An anchor material ratio of 1.41, high strength concrete and medium anchor-fan lengths were used in all five tests. All tests failed due to strip fracture.

In Table 4-7, the results of the five tests are given. In tests with 5 in. wide CFRP strips, the ultimate strip stress at fracture was near the same and ranged from 141 ksi to 143 ksi. The average ultimate strip stress at fracture was 142 ksi for the 5 in. strips. In tests with 3 in. wide CFRP strips, the average ultimate strip stresses averaged 169 ksi. The average ultimate strip stress was therefore found to be 19% larger in the narrower strips than the wider ones.. All tests reached the expected CFRP strip stress at failure (143 ksi), except test B5H1.4Ma which failed at 99% of the expected strip stress.

Table 4-7 Experimental results for effect of strip width on strip fracture

Specimens	Strip Width	$\sigma_{fx \text{ mid ult}}$ (ksi)	Average $\sigma_{fx \text{ mid ult}}$ (ksi)
B5H1.4Ma	5 in.	141	142
B5H1.4Mb		143	
B5H1.4Md		143	
B3H1.4Ma	3 in.	183	169
B3H1.4Mb		154	

In Figure 4-27, CFRP strains calculated from applied loads and measured by the UTVS are compared for the five tests considered. The strip strain at the ultimate load $\epsilon_{fx \text{ mid ult}}$ is the ultimate strip strain at mid-span reported in Table 4-1 and evaluated from beam equilibrium:

$$\epsilon_{fx \text{ mid ult}} = \sigma_{fx \text{ mid ult}} / E_f$$

Equation 4-6

$$\sigma_{fx \text{ mid ult}} = F_{CFRP} / A_{CFRP}$$

Equation 4-7

where

F_{CFRP} is obtained from equilibrium as discussed in section 4.2.1.2

E_f is the manufacturer specified elastic modulus.

The mean strip strain $\epsilon_{sx \text{ 98\% ult}}$ is the surface longitudinal strain measured between two adjacent targets on the CFRP strip between the anchor fan ends at 98% of specimen ultimate load. The mean and maximum values are reported in Table 4-1. As can be seen in Figure 4-27, the UTVS mean strip strains ($\epsilon_{sx \text{ 98\% ult}}$) agreed well with strain ($\epsilon_{fx \text{ mid ult}}$) estimates derived from equilibrium. The maximum and mean of the differences between strains obtained from the two methods are 3%, 14%, and 8%, respectively. These observed differences may be partly the result of converting strip forces in the equilibrium method, to strip strains using an estimated laminate thickness of 0.02 in. and an estimated modulus of elasticity, E_f .

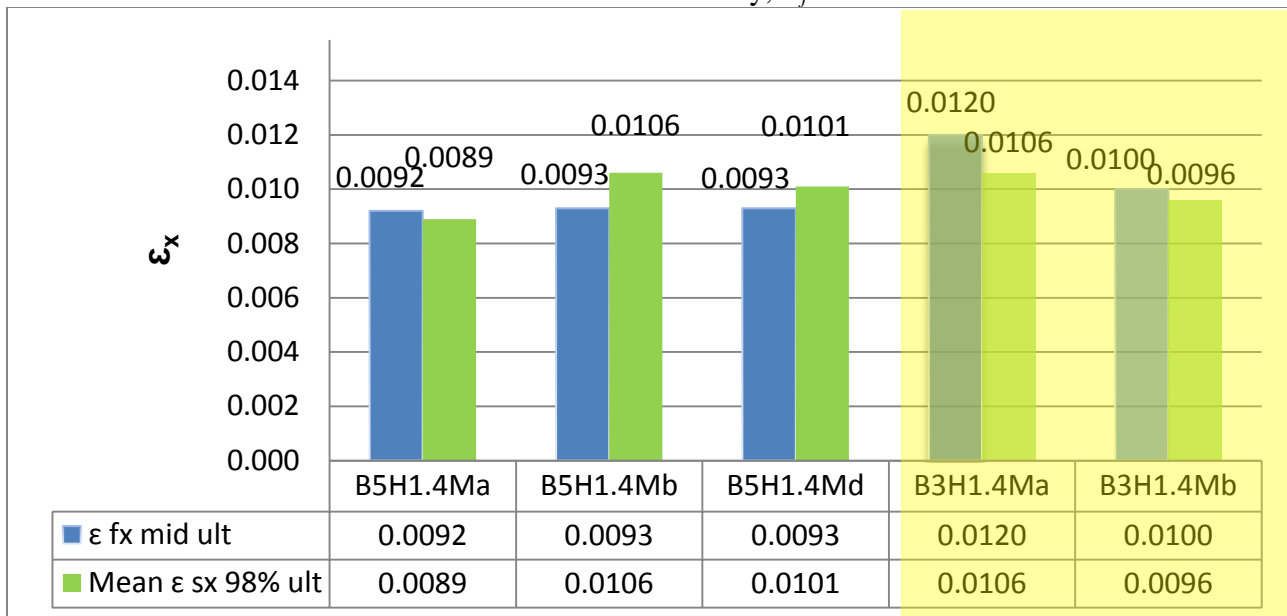


Figure 4-27 Strain comparison between $\epsilon_{fx \text{ mid ult}}$ and the mean of $\epsilon_{sx \text{ mid 98\% ult}}$ for different strip widths

In Figure 4-28, the mean and maximum values of ϵ_{sx} 98% ult for the five directly comparable tests are compared. The maximum longitudinal strip strains just prior to strip fracture ranged from 0.0147 to 0.0163 for 5 in. strips. Differences between the maximum and mean strip strains at 98% of the ultimate load ranged from 0.0046 to 0.0074 for 5 in. strips. For 3 in. strips, the maximum strip strains were lower than those for 5 in. strips, and ranged from 0.0140 and 0.0141. Differences between the maximum and mean strip strains in 3 in. strips were significantly lower than those for 5 in. strips, and ranged from 0.0036 to 0.0045. Thus, the wider strips were observed to experience both higher localized maximum strip strains and higher differences between maximum and mean strip strains. These findings indicate that as CFRP strip get wider, strain distributions across their area become less uniform and exhibit higher localized strain concentrations. Since CFRP is a brittle material, higher localized strain concentrations in wider strips may be the cause of their observed weaker strength compared with narrower strips.

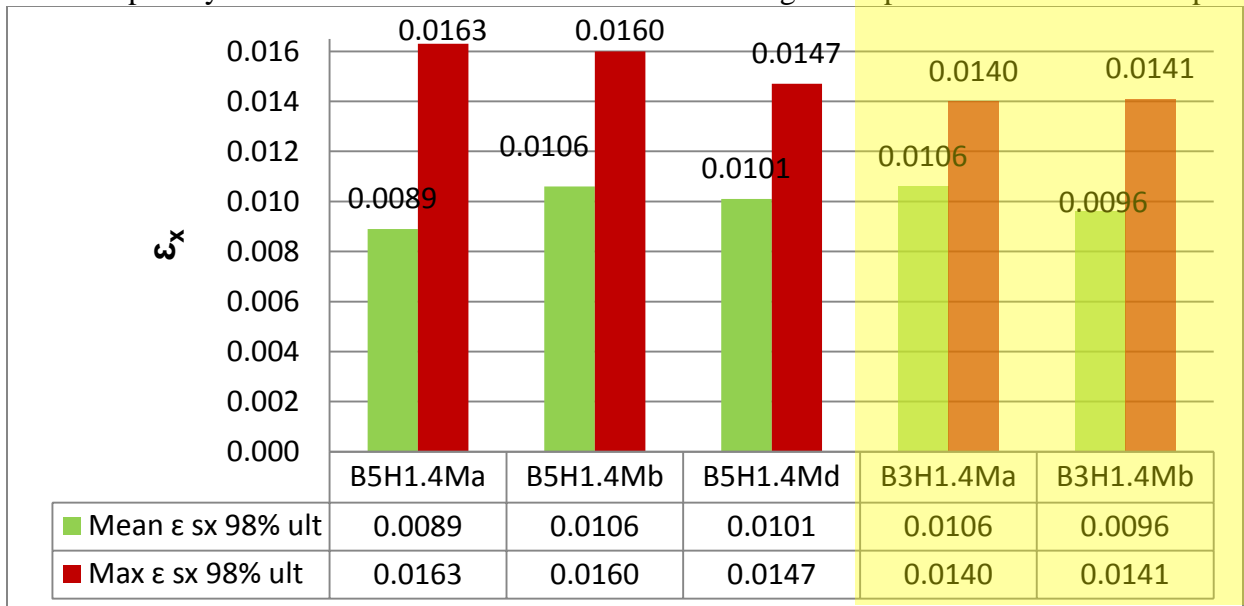


Figure 4-28 Comparison of mean and maximum values of ϵ_{sx} 98% ult for different strip widths

In this study, all CFRP strips were developed by a single anchor at each end. Thus, in this study, the effective width of CFRP strip developed by each anchor increased from 3 in. to 5 in. for the 3- and 5-in. wide strips. Possibly, adding anchors to wider strips to reduce the effective

width of CFRP strip developed by each anchor may counter the weaker strength observed in wider strips. Additional tests wide with FRP strips developed by multiple anchors are needed to confirm this postulation.

As shown in Figure 4-29, the slope of the beam load versus deflection response is observed to be similar for all five comparable specimens until the cracking load. After flexural cracking, a similar behavior was observed for two specimens with 5 in. strips. For specimens with 3 in. strips, the load-deflection slope of test B3H1.4Mb was softer than that of test B3H1.4Ma. The weaker bond conditions between the concrete and CFRP strip reported in Table 4-3 for B3H1.4Mb compared to B3H1.4Ma may partially explain the deference in softer load-deflection response. Eventually, all tests reached or exceeded the expected load at failure.

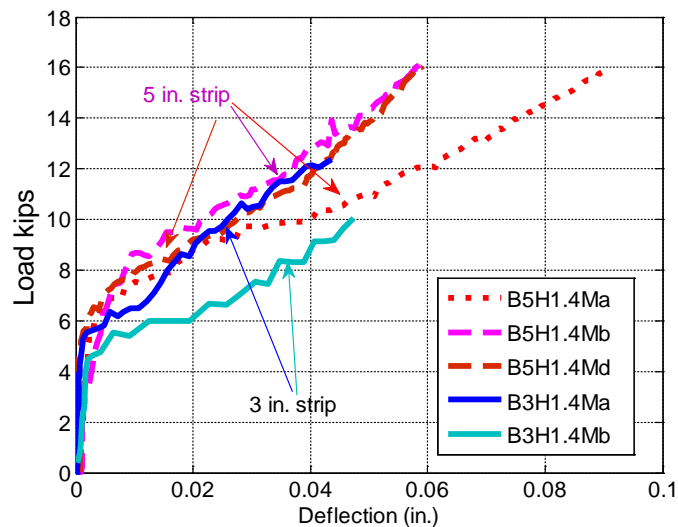


Figure 4-29 Load vs deflection for effect of strip width on strip fracture

4.5.1.2 Strip Fracture

Table 4-8 contains of all tests that failed by strip fracture with an anchor material ratio of 1.41. The table contains results for tests with varying concrete strength and fan size, as these parameters were found to have limited influence on strip strength (Sections 4.3 and 4.4). As

indicated in Table 4-8, the average strip stress at strip fracture for six tests with 5 in. strips is 145 ksi; which is 14% lower than that obtained for eight tests with 3 in. CFRP strips (164 ksi).

Table 4-8 Results for tests sustained strip fracture and with an anchor material ratio of 1.41 for different strip widths

Specimens	Strip Width	$\sigma_{fx \text{ mid ult}}$ (ksi)	Average $\sigma_{fx \text{ mid ult}}$ (ksi)
B5H1.4Ma	5 in.	141	145
B5H1.4Mb		143	
B5H1.4Md		143	
B5H1.4La		169	
B5L1.4Ma		145	
B5L1.4Mb		134	
B3H1.4Sa	3 in.	154	164
B3H1.4Sb		174	
B3H1.4Ma		183	
B3H1.4Mb		154	
B3H1.4La		186	
B3H1.4Lb		148	
B3L1.4XLa		151	
B3L1.4XLb		162	

In Figure 4-30 the mean and maximum strip strains measured using the UTVS for the six tests with 5 in. strips and eight tests with 3 in. strips are shown. Figure 4-30 corroborates findings observed in Figure 4-28 plotting the same strains for five directly comparable tests. In Figure 4-30, the wider strips are observed to experience both higher localized maximum strip strains and higher differences between maximum and mean strip strains. The higher localized strip strains may be the cause of the observed lower strip strength in beams with wider CFRP strips.

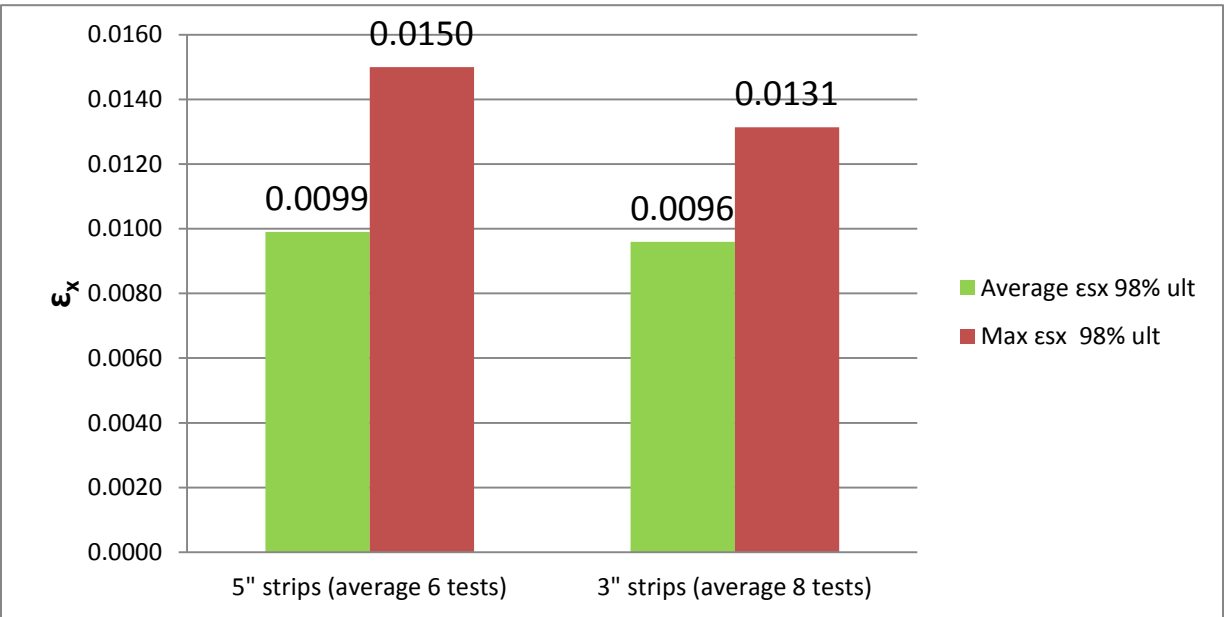


Figure 4-30 Strain comparison between mean and maximum ϵ_{sx} 98% ult for different strip widths tests sustaining strip fracture and with an anchor material ratio of 1.41

4.5.2 Anchor Rupture

More research is needed to determine the influence of strip on anchor strength.

4.5.3 Summary

The failure mode for all tests was strip fracture. The ultimate strip stress of all tests using 5 in. strips was very close to the expected tensile strength provided by the manufacturer of 143 ksi. For tests using 3 in. strips, the ultimate strip stresses at fracture were on average about 15% larger than the expected tensile strength provided by the manufacturer. Strain distributions across the area of a CFRP strip were found to be less uniform and exhibit higher localized strain concentrations. The higher localized strain concentrations in wider strips may have caused their observed weaker strength compared with narrower strips. Similar trends were observed when additional tests with 3 in. and 5 in. strip were investigated.

Test results therefore indicate that strength increase of test specimens was less than proportional to the increase in the amount of CFRP material used in the wider strips. Increasing the width of CFRP strips tended to decrease the efficiency of CFRP anchors at developing strip forces. Anchors developing wider strips do not appear to distribute forces as evenly across strips as narrower strips.

4.6 EFFECT OF MATERIAL RATIO OF CFRP ANCHOR TO CFRP STRIP

In this series, anchors with anchor-to-strip material ratios of 1.06, 1.41 and 2.0 were studied to determine the effects of anchor-material ratio on strip and anchor strengths. Twenty-four tests were conducted on 5 in. strips with anchor material ratios of 1.06, 1.41 and 2.0. Another ten tests were conducted on beams with 3 in. strips using anchors with material ratios of .06 or 1.41.

For beams with 5 in. strips, those with an anchor material ratio of 2.0 failed at around 115% of the expected load at strip fracture (Figure 4-31). Beams with an anchor material ratio of 1.41 sustained strip fractures were observed in six cases, anchor ruptures were found in three cases, concrete shear failure was in one case, and remaining two cases were delamination. As for beams with an anchor material ratio of 1.06, none failed due to strip fracture and 75% of the beams were unable to reach the expected load at failure. Test results therefore indicate that an anchor material ratio of 2.0 is needed to reliably fracture 5-in. wide CFRP strips.

For tests with 3 in. strips, the CFRP strip fractured in all ten tests, as shown in Figure 4-32. Eight of these tests had an anchor material ratio of 1.41 and two tests had a ratio of 1.06. All ten tests exceeded the expected load at failure based on a CFRP strip fracture mode of failure. Considering that only two tests had a 1.06 anchor material ratio, it is not possible to estimate the variations that might occur if a larger number of tests had been conducted. However, it is likely some would not have reached the expected load. Therefore, it is reasonable to suggest that an anchor ratio of 1.41 should be used to reach fracture of 3 in. strips. It is interesting to note that no tests in which a 5 in. strip fractured exceeded 120% of the expected load at failure; even when

using an anchor material ratio of 2.0. Four tests that fractured a 3 in. strip failed at a greater load than 120% of the expected load at failure. One of them had a 1.06 anchor material ratio, while the remaining three had a ratio of 1.41. It appears that the efficiency of a CFRP anchor at developing the strength of a CFRP strip decreases as the width of the strip increases.

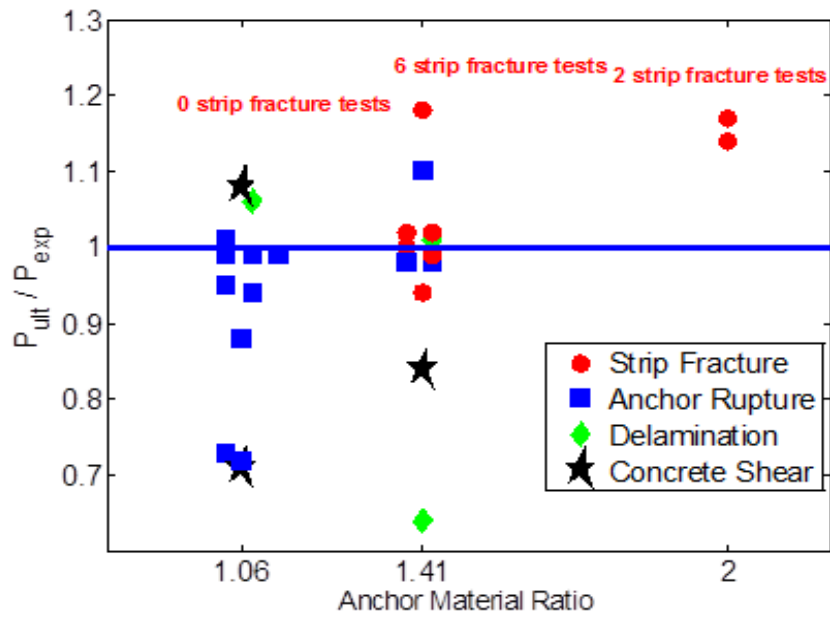


Figure 4-31 Failure modes for tests with 5 in. strips

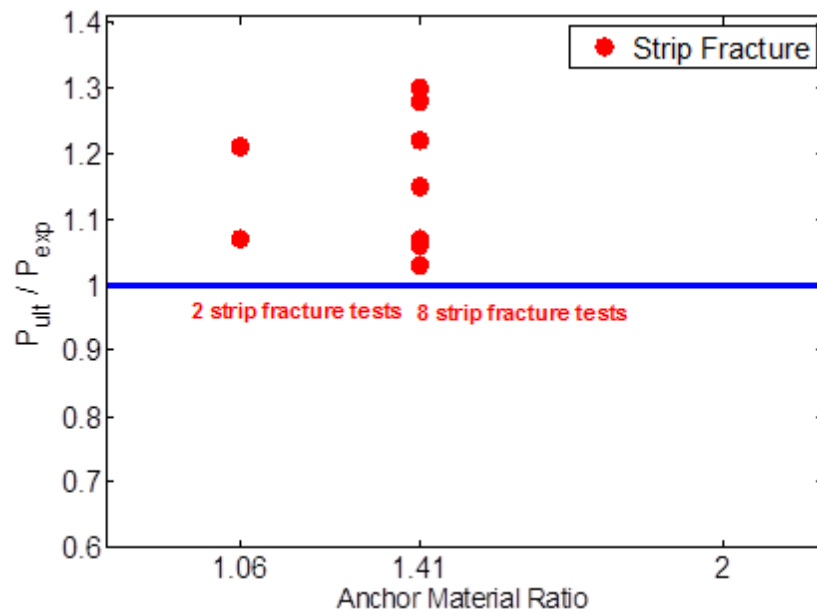


Figure 4-32 Failure modes for tests with 3 in. strips

4.6.1 Strip Fracture

Five directly comparable tests were conducted on specimens with 5 in. strips and using anchor material ratios of 1.41 or 2.0. All tests had high-strength concrete, medium anchor fan length, and failed by strip fracture. For tests with 3 in. strips, four directly comparable tests were conducted using anchor material ratios of 1.06 or 1.41. The four tests had normal strength concrete, extra-large anchor fans lengths and failed by strip fracture.

4.6.1.1 Tests with 5 in. Strips

Table 4-9 lists the ultimate strip stress at fracture for the directly comparable tests with 5 in. strips. Results presented in the Table 4-9 indicate that strips with anchors having a material ratio of 1.41 fractured around their manufacturer-provided expected tensile strength of 143 ksi. When anchors having a material ratio of 2.0 are used however, higher strips stresses were observed at fracture by about 14% from those obtained for strips anchored with anchors having a material ratio of 1.41.

Table 4-9 Experimental results for effect of anchor-material ratio on strip fracture

Specimens	Anchor material ratio	P_{ult} (kips)	$\sigma_{fx\ mid\ ult}$ (ksi)	Average $\sigma_{fx\ mid\ ult}$ (ksi)
B5H1.4Ma	1.41	15.8	141	142
B5H1.4Mb		16	143	
B5H1.4Md		16	143	
B5H2Ma	2.0	18.2	163	165
B5H2Mb		18.6	166	

Increasing the anchor material ratio, however, did not significantly reduce the maximum strip strain just prior to strip fracture, nor did it reduce significantly the difference between maximum and mean strip strains, as shown in Figure 4-33. The maximum strip strain recorded for tests with a 2.0 anchor material ratio was 0.0158 and 0.163 for tests with a 1.41 anchor

material ratio. The second largest variation between maximum and mean strip strains was 0.0059 and was recorded in test B5H2Ma with material ratio of 2.0.

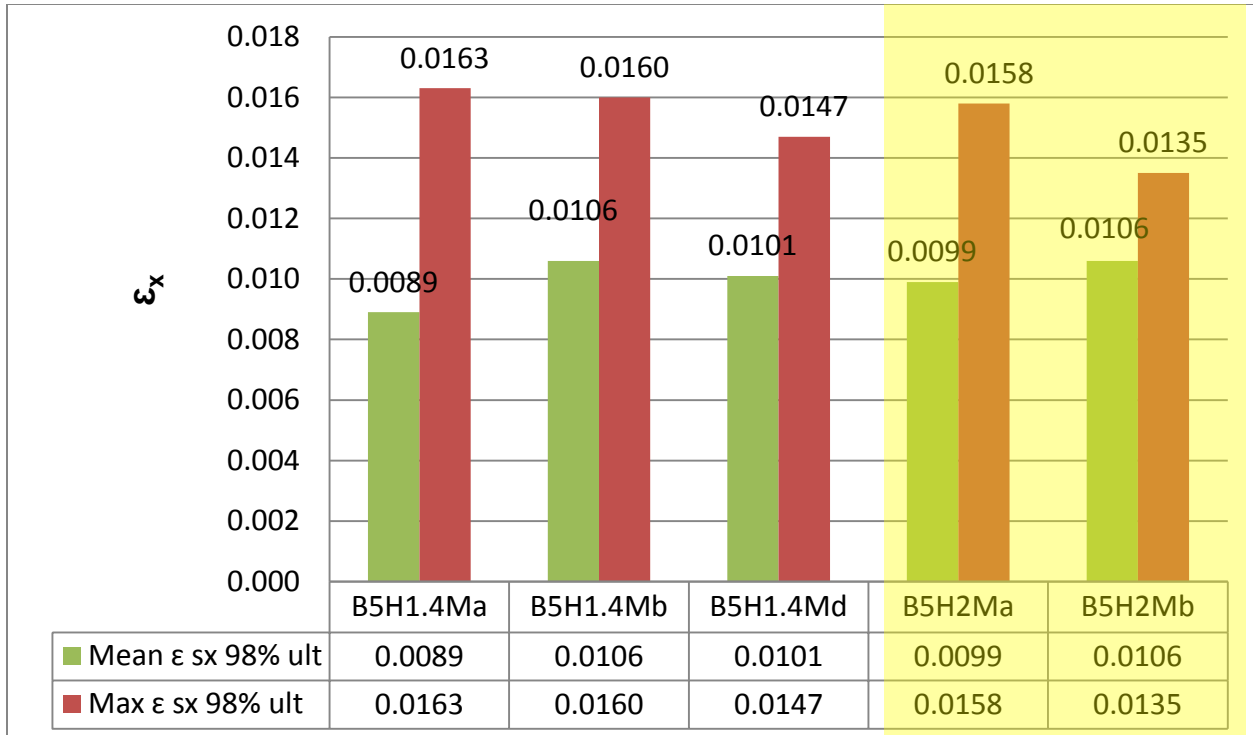


Figure 4-33 Strain comparison between Mean and Maximum ϵ_{sx} 98% ult for directly comparable tests with 5 in. strips and different anchor-material ratio

It should be noted, however, that the ultimate load of the tests with an anchor material ratio of 2.0 were around 14% larger than the tests with anchor material ratio of 1.41 as presented in Table 4-9. Figure 4-35 compares mean and maximum strip strains in the directly comparable specimens at the given load of 95% of the expected beam strength. As can be seen in the Figure 4-34, at the same applied load, anchors with a material ratio of 2.0 had significantly reduced maximum strip strains and differences between maximum and mean strip strains, compared with anchors having a material ratio of 1.41. Therefore, anchors with a larger cross section are observed to achieve, at a given load, more even strain distributions and lower maximum strains than smaller anchors. Such favorable strain distributions resulted in an increase in the ultimate strip stress at fracture when larger anchors were used.

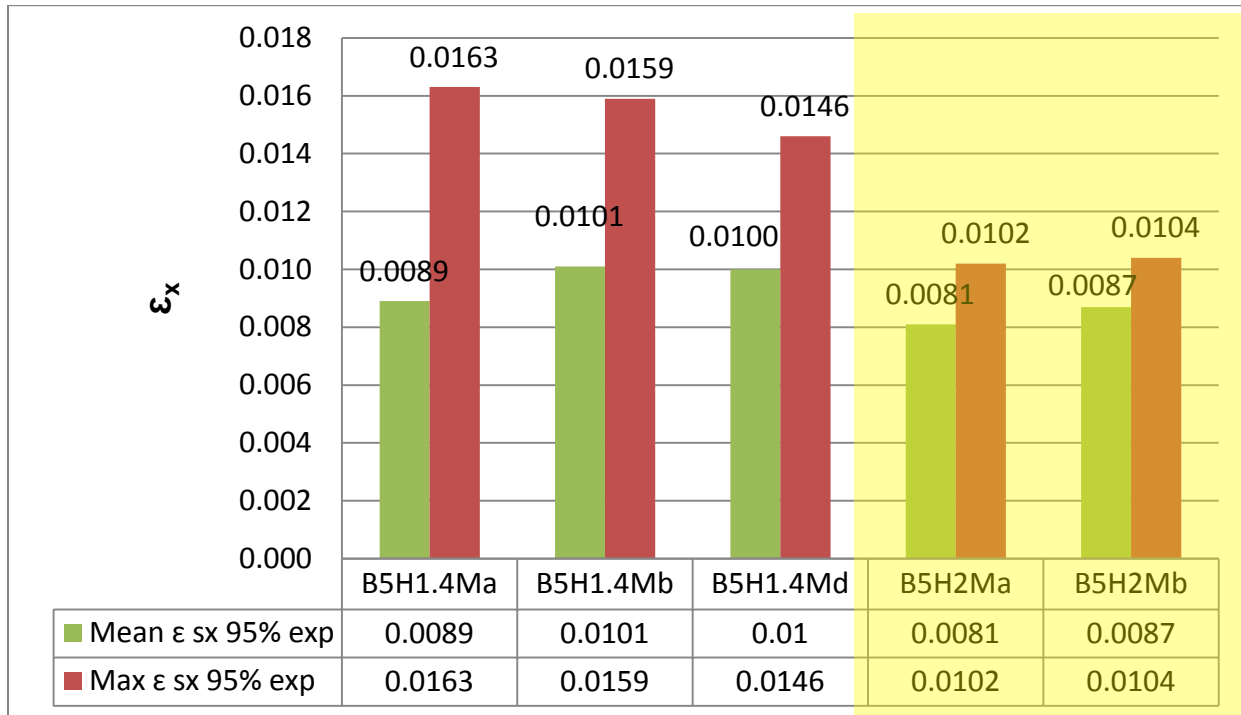


Figure 4-34 Strain comparison between Mean and Maximum ϵ_{sx} 95% exp for directly comparable tests with 5 in. strips and different anchor-material ratio

As shown in Figure 4-35, the slope of load versus deflection was similar for all five specimens before cracking of the beam. After cracking, the load-deflection relations diverge more markedly without a discernable trend.

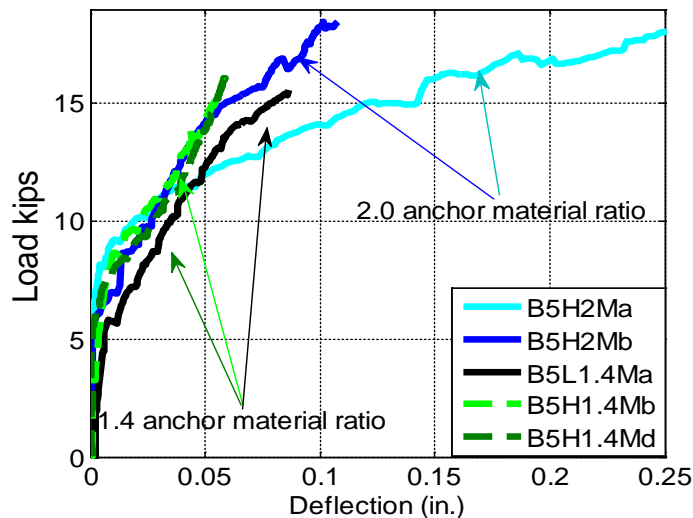


Figure 4-35 Load vs deflection for effect of anchor-material ratio on strip fracture

Specimens with different concrete strengths and anchor-fan lengths are added the five directly comparable tests to expand the dataset. As discussed previously, concrete strength and anchor-fan length did not affect strip strength significantly. In Table 4-10, the stress and strain results for two tests with an anchor material ratio of 2.0 and all six tests with anchor material ratio of 1.41 that sustained strip fracture were listed. Results presented in Table 4-10 corroborate findings from the limited set of five tests described above. Overall, increasing the anchor material ratio from 1.41 to 2.0 increased the ultimate strip stress and reduced both the maximum and mean strip strain at a given load.

Table 4-10 Results for strip fracture tests with 5 in. strips

Specimens	Anchor material ratio	$\sigma_{fx\ mid\ ult}$ (ksi)	Average $\sigma_{fx\ mid\ ult}$ (ksi)	Mean $\epsilon_{sx\ 95\%\ exp}$	Average of Mean $\epsilon_{sx\ 95\%\ exp}$	Max $\epsilon_{sx\ 95\%\ exp}$	Average of Max $\epsilon_{sx\ 95\%\ exp}$
B5H1.4Ma	1.41	141	145	0.0089	0.0097	0.0163	0.015
B5H1.4Mb		143		0.0101		0.0159	
B5H1.4Md		143		0.0100		0.0146	
B5H1.4La		169		0.0110		0.0128	
B5L1.4Ma		145		0.0090		0.0159	
B5L1.4Mb		134		0.0091		0.0130	
B5H2Ma	2.0	163	165	0.0081	0.0084	0.0102	0.0103
B5H2Mb		166		0.0087		0.0104	

4.6.1.2 Tests with 3 in. Strips

In Table 4-11, the ultimate strip stress of tests with 3 in. strips are listed. Increasing anchor material ratio from 1.06 to 1.41 to strength 3 in. strip did not significantly increase the ultimate strip stress. The average ultimate strip stress for tests with anchor material ratio of 1.41

was 157 ksi. It was even 5 ksi less than the average value of tests with anchor material ratio of 1.06.

Table 4-11 Experimental results for directly comparable tests with 3 in. strips of Series III

Specimens	Anchor material ratio	$\sigma_{fx \text{ mid ult}}$ (ksi)	Average $\sigma_{fx \text{ mid ult}}$ (ksi)
B3H1.4XLa	1.41	151	157
B3H1.4XLb		162	
B3H1XLa	1.06	152	162
B3H1XLb		171	

Increasing the anchor material ratio from 1.06 to 1.41 did not significantly reduce the maximum strip strain and the variation between maximum strip strain and mean strip strain as shown Figure 4-36. The maximum strip strains were 0.0148 and 0.0123 for the test with 1.41 material ratio anchors. For the test with 1.06 material ratio anchors, the maximum strip strain was 0.0145 ksi and 0.0155 ksi. The largest and lowest variation between maximum and mean strip strain was 0.0058 and 0.0025 which were found on the tests using 1.41 material ratio anchors. The variation between maximum and mean strip strain of two tests with 1.06 material ratio anchor were 0.0050 and 0.0053, respectively.

As shown in Figure 4-37, the slope of load versus deflection is similar for all specimens until the load reaches around 4.5 kips where CFRP strips started debonding from the concrete substrate. Variability in the bond conditions at the concrete/CFRP interface of individual specimens resulted in the load deflection relations diverging after debonding initiate. All test reached the expected load at failure.

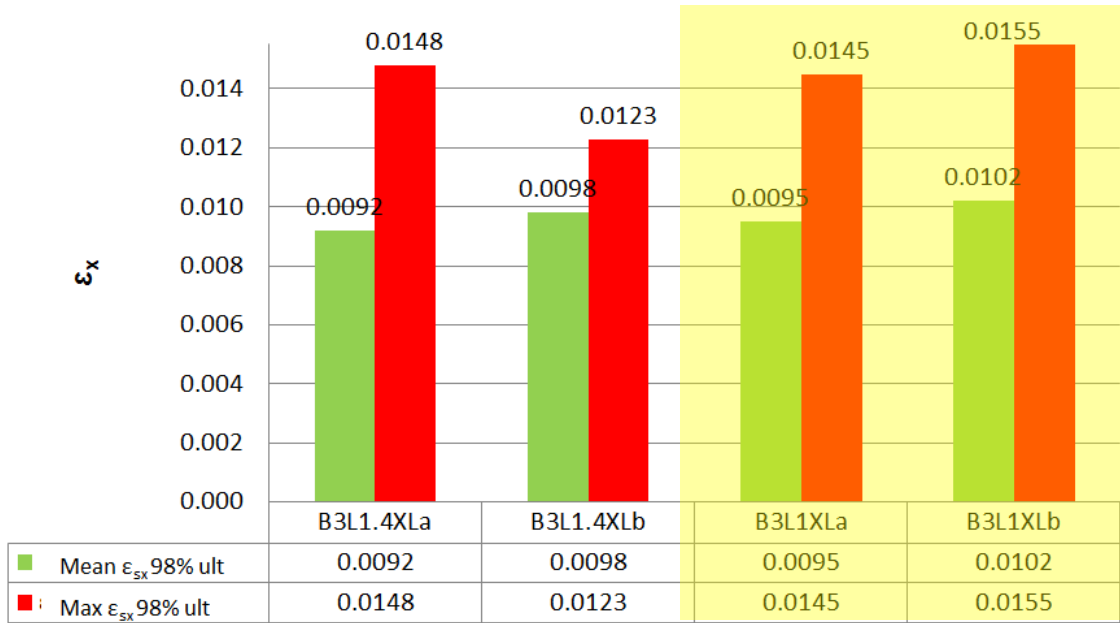


Figure 4-36 Strain comparison between Mean ϵ_{sx} 98% ult and Max ϵ_{sx} 98% ult for directly comparable tests with 3 in. strips and different anchor material ratio

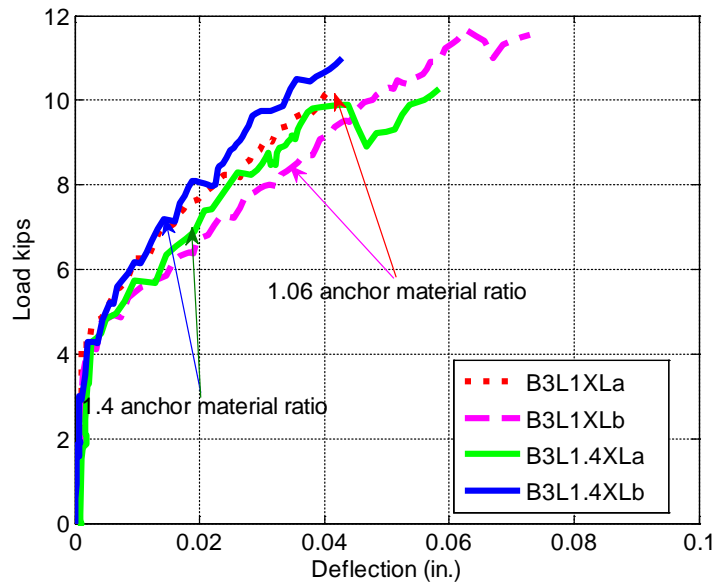


Figure 4-37 Load vs deflection response of tests with varying anchor-material ratios for 3 in. strips

In Table 4-12, the strip ultimate stress for 8 tests with anchor material ratio of 1.41 and 2 tests with anchor material ratio of 1.06 are listed. All tests had 3 in. strip and failed in strip fracture. Overall, higher anchor material ratio slightly increased the average value of ultimate strip stress from 162 ksi to 164 ksi. It should be noted that only 2 tests had anchor material ratio of 1.06 in this section. The strip of one test with an anchor material ratio of 1.06 failed at 171 ksi. Therefore, the application of a higher anchor material ratio than 1.06 did not necessarily result in an increase in strip strength.

Table 4-12 Results for strip fracture tests with 3 in. strips of Series IV

Specimens	Anchor material ratio	$\sigma_{fx \text{ mid ult}}$ (ksi)	Average $\sigma_{fx \text{ mid ult}}$ (ksi)
B3H1.4Sa	1.41	154	164
B3H1.4Sb		174	
B3H1.4Ma		183	
B3H1.4Mb		154	
B3H1.4La		186	
B3H1.4Lb		148	
B3L1.4XLa		151	
B3L1.4XLb		162	
B3L1XLa	1.06	152	162
B3L1XLb		171	

4.6.2 Anchor Rupture

Anchor rupture occurred only in the tests with 5 in. strips. In Table 4-13, the strip ultimate stress and anchor ultimate stress of 6 selected tests in which 3 tests with anchor material ratio of 1.41 and the anchor material ratio for the rest 3 tests was 1.06 are listed. Assuming that

all the tensile force in CFRP strips at failure was carried by CFRP anchors, the ultimate anchor stress ($\sigma_{ax\ mid\ ult}$) could be calculated by $(\sigma_{fx\ mid\ ult} \times A_{CFRP})/ A_{anchor}$.

Table 4-13 Results for anchor rupture tests with 5 in. strips and different anchor-material ratio

Specimens	Anchor material ratio	$\sigma_{fx\ mid\ ult}$ (ksi)	Average $\sigma_{fx\ mid\ ult}$ (ksi)	$\sigma_{ax\ mid\ ult}$ (ksi)	Average $\sigma_{ax\ mid\ ult}$ (ksi)
B5H1.4Sb	1.41	139	145	99	103
B5L1.4Mc		157		111	
B5H1.4Lb		139		99	
B5H1Ma	1.06	134	140	126	132
B5H1Mb		141		133	
B5H1Mc		144		136	

Overall, increasing the anchor material ratio from 1.06 to 1.41 slightly increased the average ultimate strip stress from 140 ksi to 145. It should be noted that the strip stress of one test with anchor material ratio of 1.41 was 157 ksi at failure which is over 109% manufacturer specified tensile strength of CFRP strip. The strip stress of rest two tests with anchor material ratio of 1.41, however, only reached 139 ksi at failure which is less than the average ultimate strip stress of tests with anchor material ratio of 1.06. Therefore, increasing anchor material ratio did not result in a significant increase on anchor strength. The ultimate anchor stress, however, significantly reduced after using anchor material ratio of 1.41. An average 30 ksi increase was observed after using the anchor material ratio of 1.06. Increasing anchor-material ratio therefore did not result in a proportional increase in anchor strength.

4.6.3 Summary

Increasing the anchor material ratio from 1.41 to 2.0 reduced the strain concentration in 5 in. strip which could be observed by the reduction on maximum strip strain as well as the variation between the maximum and mean strip strain. A more evenly strain distribution on the 5 in. strip with 2.0 material ratio anchor eventually fracture the strips at a larger ultimate strip stress.

Increasing the anchor material ratio from 1.06 to 1.41 did not result in a significant increase on 3 in. strip strength. For the tests with 5 in. strips, increasing anchor material ratio from 1.06 to 1.41 did not significantly change the ultimate strip stress. Assuming the tensile force of CFRP anchor was equal to the tensile force of CFRP strip at failure increasing anchor material ratio eventually reduced the ultimate stress developed in CFRP anchor.

4.7 BONDED VERSUS UNBONDED APPLICATIONS

A bonded test designates that epoxy resin was used as interfacial material to attach the CFRP strip to the concrete substrate. Unbonded tests designates that a plastic film was placed between the CFRP strip and the concrete substrate to simulate the behavior of a completely debonded strip.

4.7.1 Strip Strength & Anchor Strength

Seven tests were conducted in two groups of comparable specimens. The only difference in each group was bonding of the CFRP strip to the concrete using epoxy or using a plastic film. The anchor-material ratios were 1.41 or 2.0. All tests in the series had 5 in. wide strips, 6 in. long anchor fans, and high-strength concrete. A summary of experimental results is presented in Table 4-14.

Table 4-14 Experimental results for tests with different bond condition

Anchor-material ratio	Specimens	$\sigma_{fx \text{ mid ult}}$ (ksi)	Average $\sigma_{fx \text{ mid ult}}$ (ksi)	$\sigma_{ax \text{ mid ult}}$ (ksi)	Average $\sigma_{ax \text{ mid ult}}$ (ksi)	Failure Mode	
2.0	U5H2Ma	133	133	67	67	Concrete Shear	
	B5H2Ma	163		82		82	Strip Fracture
	B5H2Mb	166		83			Strip Fracture
1.41	U5H1.4Ma	122	127	87	90	Anchor Rupture	
	U5H1.4Mb	132		94		Anchor Rupture	
	B5H1.4Ma	141	142	100	101	Strip Fracture	
	B5H1.4Mb	143		101		Strip Fracture	

Without bond between the CFRP strip and concrete, anchor rupture occurred. Test U5H2Ma failed in concrete shear. Unbonded specimens failed at ultimate strip stress lower than design strength. As shown in Figure 4-38 and Figure 4-39, unbonded cases failed at ultimate loads lower than the expected load at failure (16 kips) even with a 2.0 material ratio anchor.

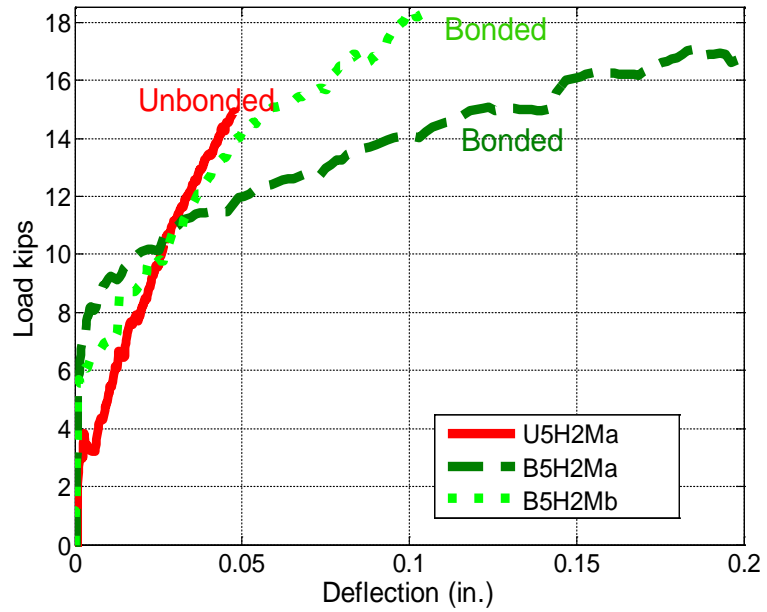


Figure 4-38 Typical load vs deflection responses for tests with different bond condition and a 2.0 anchor-material ratio

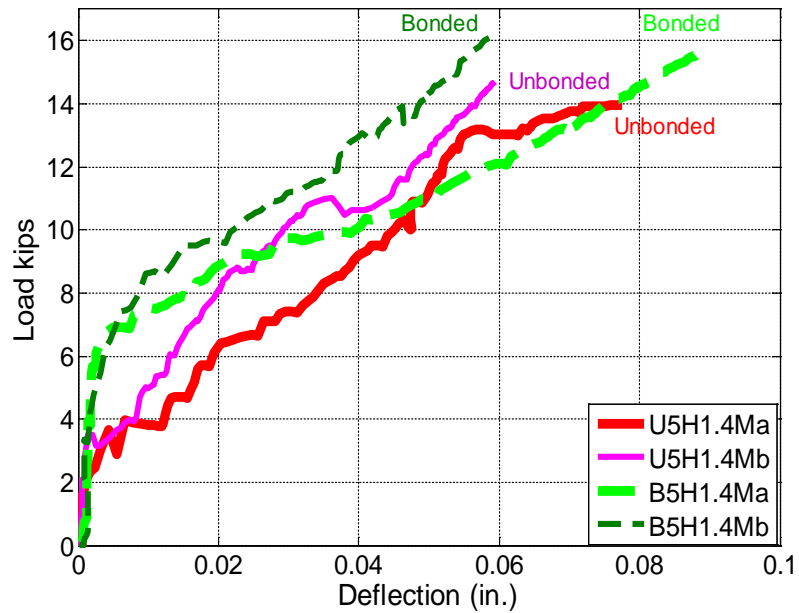


Figure 4-39 Typical load vs deflection responses for tests with different bond condition and a 1.41 anchor-material ratio

4.7.2 Summary

Epoxy helps transfer load from CFRP strips to the concrete substrate. When CFRP strips were unbonded from the concrete, specimens failed at ultimate loads lower than the design strength. When CFRP strip were bonded to the concrete, however, specimens with anchor-material ratios of 1.41 and 2.0 developed ultimate loads greater than their design strength.

In unbonded specimens, premature failures occurred by either concrete shear or anchor rupture before the specified fracture strain was developed in the CFRP strips.

4.8 VARIABILITY STUDY

Since CFRP is a brittle material and attached on beams made of brittle concrete material, small variations in geometry, material properties, and installation quality can lead to significant variations in overall response. In many cases, several tests were conducted on nominally identical specimens to evaluate such variability.

To illustrate this point, the load versus deflection response of a pair of nominally identical specimens is plotted in Figure 4-40. As can be seen in the figure, responses are typically similar for nominally identical specimens up to concrete cracking. After cracking, variations in installation quality and bond quality and uniformity between the CFRP strips and the concrete surface can result in large differences in beam overall response. In Figure 4-41, the average bond stress versus slip response is compared for the nominally identical specimens. Results in Figure 4-41 indicate that there was a more rapid degradation of bond stresses and a lower peak in test B5H1Mc than in test B5H1Md. Variability in bond stress response is discussed in more detail in Chapter 5.

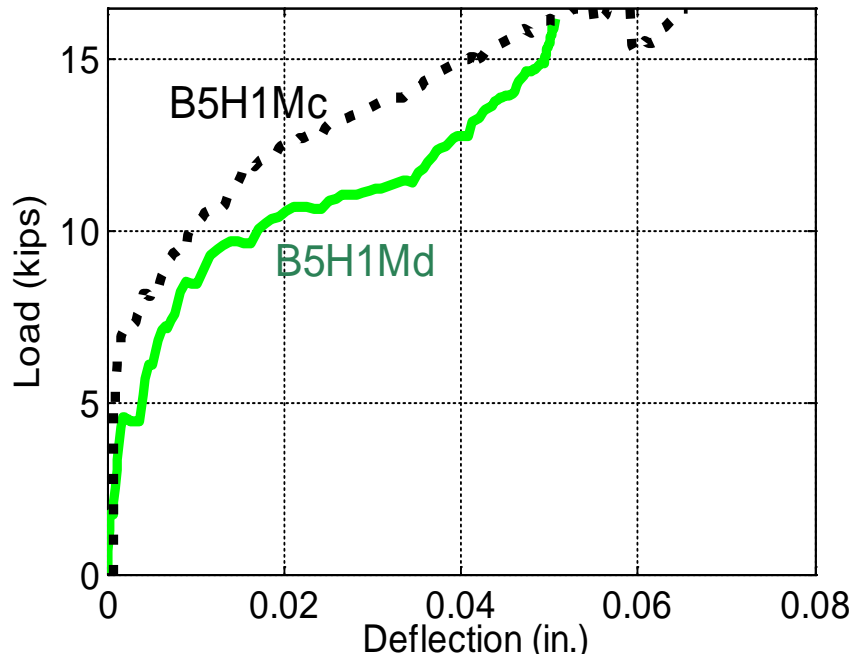


Figure 4-40 Load vs deflection of nominally identical test specimens

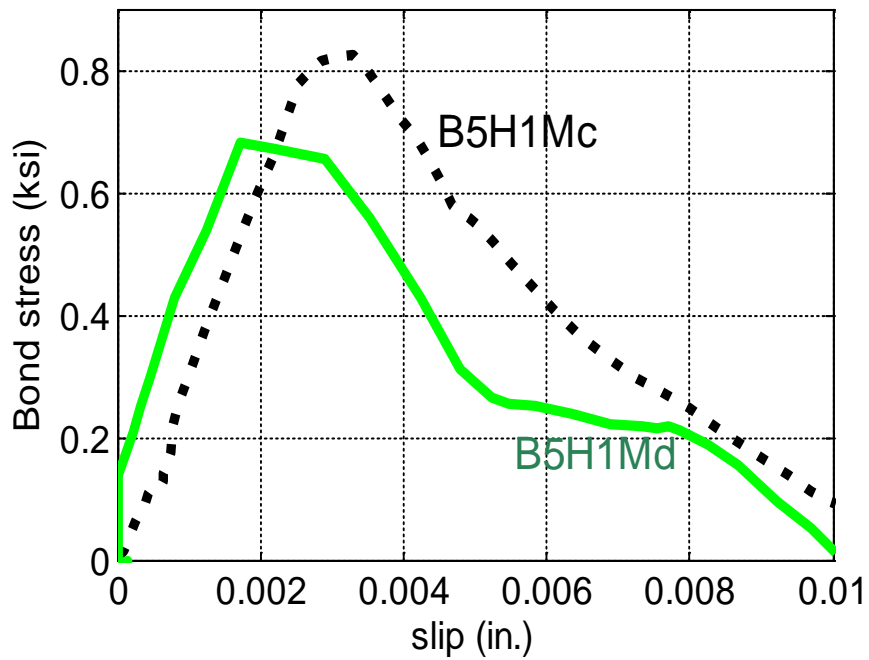


Figure 4-41 Bond stress vs slip of nominally identical test specimens

4.9 SUMMARY

In this chapter, failure modes and ultimate load and strain measurements were used to evaluate the effect of five parameters, 1) concrete strength; 2) length/angle of anchor fan and; 3) width of CFRP strip; 4) anchor-material ratio of CFRP anchor to CFRP strip; 5) bond and unbonded application, on anchor design.

Higher beam concrete strength tends to delay the debonding of CFRP strips from the concrete substrate. A higher concrete strength was found to slightly increase the strength of CFRP anchors embedded in it.

To fully develop tensile strength of a CFRP strip, an anchor-fan angle less than 64° is recommended for anchor design. The application of a smaller anchor-fan angle than 64° (down to 37°), however, had no significant effect on the strength and behavior of the CFRP strengthening system.

Test results show that increasing the width of CFRP strips increased the strain concentration, produced lower ultimate strip stress, and decreased the efficiency of CFRP strips at carrying tensile forces.

Test results also indicate that in order to fracture a 5 in. strip, the anchor material ratio should be no less than 2.0. Increasing the anchor material ratio from 1.41 to 2.0 reduced strain concentrations resulting in higher average ultimate strip stress. An anchor material ratio of 1.41 is recommended for reaching fracture of 3 in. strip.

Adequately bonding the CFRP strips to the concrete substrate helped to transfer tensile forces from CFRP strips to CFRP anchors, and prevented premature anchor rupture due to strain concentrations.

CHAPTER 5

Finite Element Analysis

5.1 INTRODUCTION

The computational work described in this chapter was conducted to identify available computational tools that are best suited for simulating the response of the test beams, and particularly the CFRP strips and anchors. A three-dimensional continuum finite element model representing test beams strengthened using CFRP strips and anchors is presented. The proposed model is intended to be simple. It requires a limited number of input parameters and can be easily built in most structural analysis software. The model utilizes the expected CFRP material properties provided by the manufacturer and a simplified concrete/CFRP bond model. The parameters of the bond model were established from this study's experimental results. The computational model was validated using test results from six beams with varying anchor-material ratios, concrete strengths, length of anchor fan and, bond conditions. Four additional simulations were conducted to evaluate the sensitivity of computational results to the choice of bond and CFRP material parameters. The proposed model was built in the analysis program ANSYS (SAS, 2009) but is intended to be implementable.

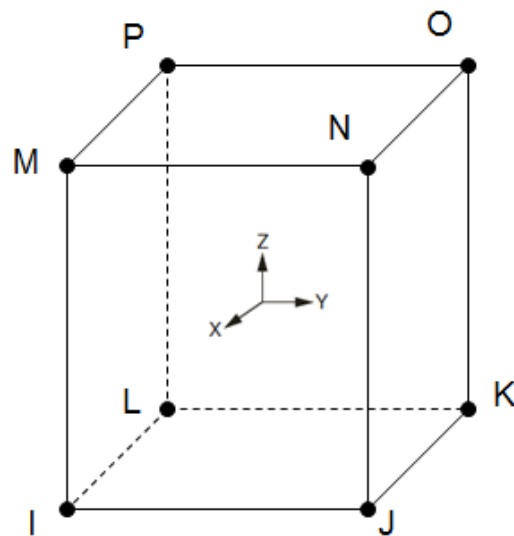
5.2 MATERIAL MODELING

In this section, the elements and material properties used to model the plain concrete beams, the CFRP strips, the CFRP anchors, the CFRP-concrete interface, and the steel loading plates are presented.

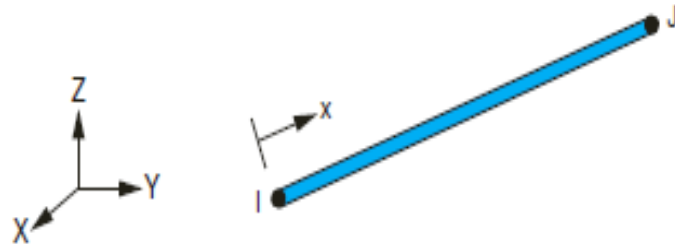
5.2.1 Element Types

Solid elements were selected to model the steel loading plates and concrete beam. The solid elements have eight nodes, each having three translational degrees of freedom in the x, y, z

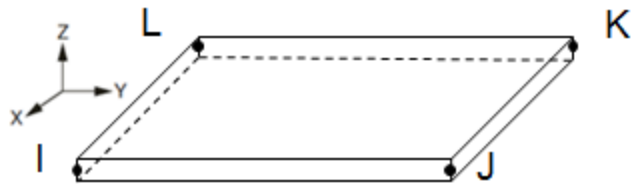
directions and no rotational degrees of freedom, as shown in Figure 5-1 (a). Truss elements were selected to simulate the uniaxial tension behavior of the CFRP fibers in the strip and anchors (Figure 5-1 (b)). The truss elements have two nodes and cannot transfer moments at the ends. For CFRP laminates, the stiffness and strength in the transverse direction is determined mostly by the properties of the epoxy resin matrix. In this simulation, four-node plate elements were selected to model the in-plane load transfer mechanism of the CFRP laminate in the transverse direction (Figure 5-1 (c)). The rotational degrees of freedom at the nodes of the plate elements were released. The plate element therefore only has three translational degrees of freedom in the nodal x , y , and z directions. Bond between concrete and CFRP was simulated using uniaxial nonlinear spring elements illustrated in Figure 5-1 (d). The spring elements are governed by a user-defined non-linear force-deformation relation that represents the bond stress versus slip behavior between CFRP material and the concrete substrate.



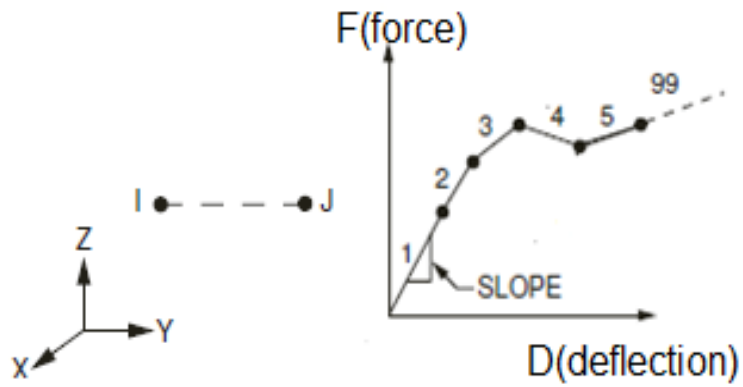
(a) *Solid element*



(b) *Truss element (SAS, 2009)*



(c) *Plate element*



(d) *Nonlinear spring element (SAS, 2009)*

Figure 5-1 Element Types

Table 5-1 lists the names of the elements used in ANSYS for each component of the computational model.

Table 5-1 Element types

Material	ANSYS Element Types
Steel	SOLID 45
Concrete	SOLID 65
CFRP fibers in strip and anchor	LINK 8
Resin epoxy Matrix	SHELL 63
CFRP-Concrete Interface material	COMBIN39

5.2.2 Geometric Model

The symmetry in xy-plane and yz-plane allows one quarter of the specimen to be modeled as shown in Figure 5-2. As shown in Figure 5-3, constraints were applied in both the xy and yz planes of symmetry to prevent movement in the Z-direction and X-direction, respectively. A single line of nodes on the reaction steel plate was constrained not to displace in the vertical direction (Y-direction) to simulate a roller support. No constraints were applied on the concrete nodes of the yz-plane of symmetry for the bottom to 1 inch of the beam depth to simulate the 1in.-deep notch cut in test specimens.

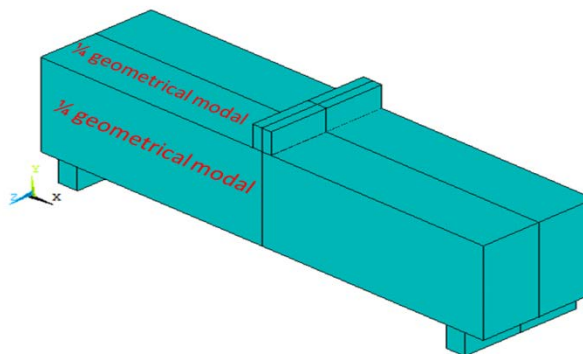


Figure 5-2 Complete beam showing planes of symmetry for the quarter model simulated

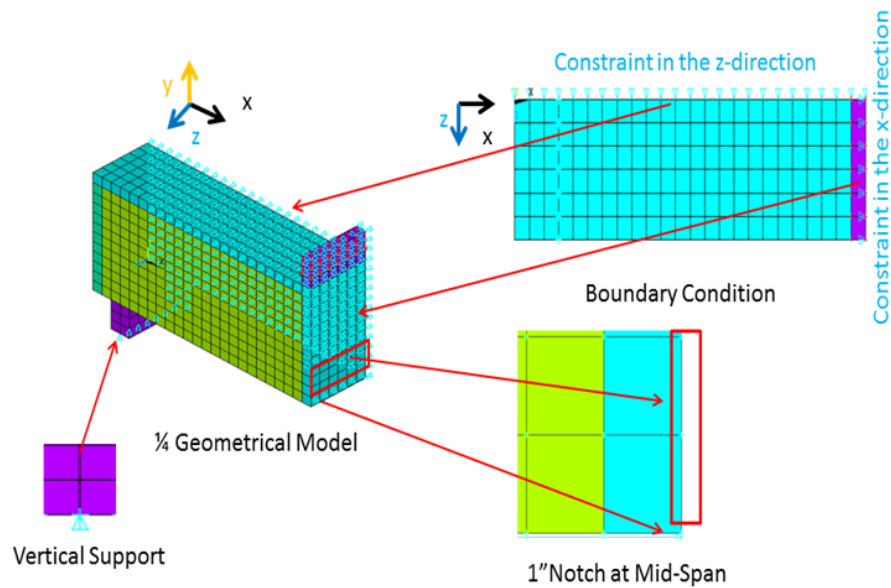


Figure 5-3 1/4 beam model and its boundary conditions

As shown in Figure 5-4, the CFRP strip being tested was simulated using truss line elements placed 0.02 in. away from the concrete surface; a distance equal to the specified thickness of the CFRP laminate. Transverse CFRP patches were simulated using transverse truss elements as well. The truss elements of the transverse CFRP patches share the same nodes with the truss elements of the longitudinal CFRP strips. Plate elements simulating the epoxy resin planar stiffness were introduced on a 1/2 in. grid matching the grid of the concrete elements. CFRP strip and patch line elements were also 1/2 in. long and connected to the plate elements at grid nodes. The mesh size was selected based on targets spacing, and past studies (Brena, 2013; Lu, 2005), in which ranging from 0.4 in. to 1.2 in. were found to provide adequate simulation results

CFRP anchors consisted of line elements fanning at the same level of the CFRP strips and line elements embedded in the concrete beam (Figure 5-4). Embedded line elements share the same nodes as the concrete elements surrounding them.

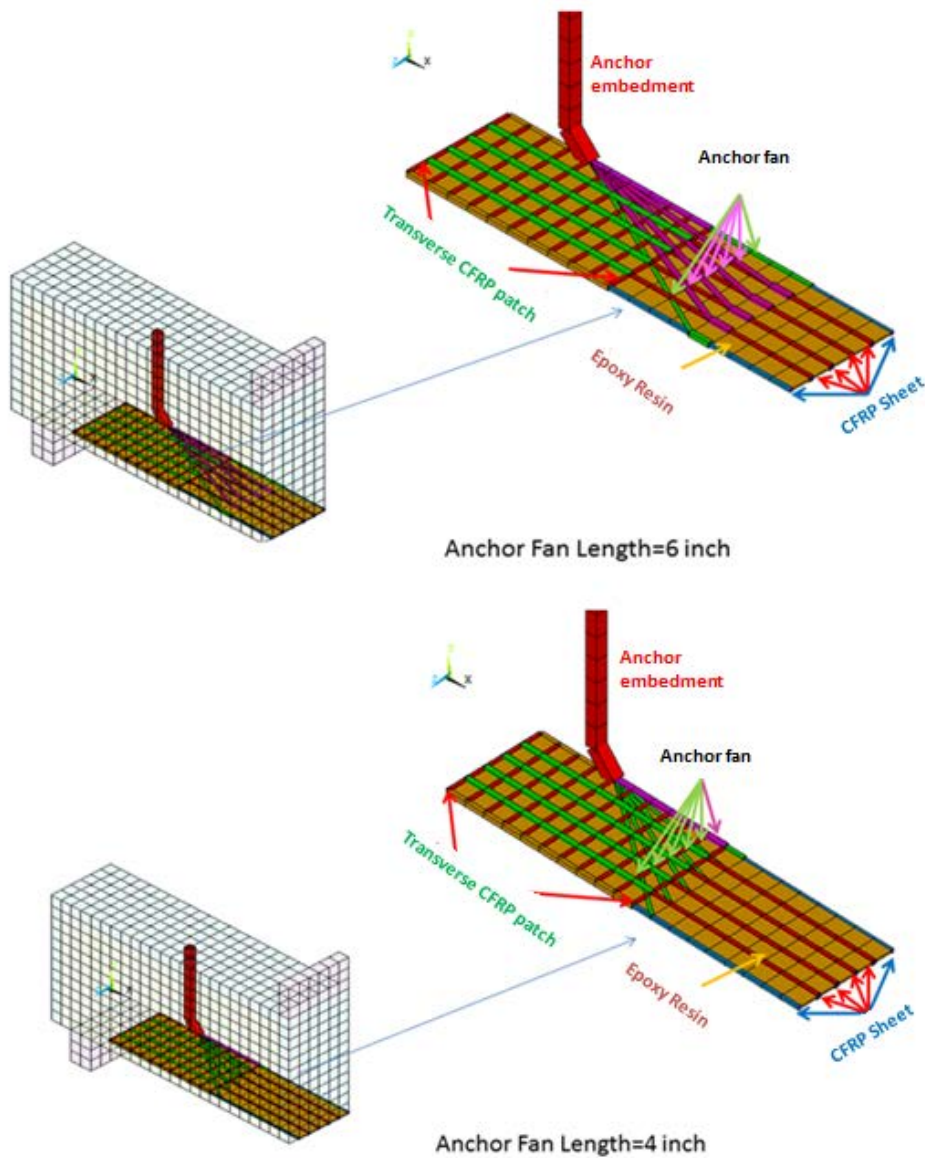
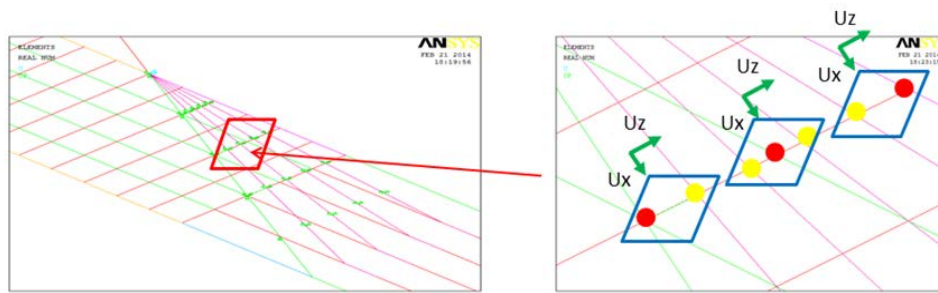


Figure 5-4 CFRP strip and CFRP anchor

The fan portion of the CFRP anchors was simulated using fanning CFRP line elements of representative CFRP material areas (the sum total of which equals the area of the anchor material). The axial elements were connected to the CFRP strip laminate through additional nodes introduced as shown in Figure 5-5. The added nodes were constrained to move as the nearby nodes of the CFRP strip in both x and z direction as shown in Figure 5-5.



- Existing Nodes on CFRP Sheet
- Added Nodes for Connecting CFRP anchor and CFRP Sheet

Figure 5-5 Connections between CFRP strip and CFRP anchor

As illustrated in Figure 5-6, CFRP strip nodes were connected to the adjacent concrete nodes by nonlinear spring elements perpendicular to the surface and having an undeformed length of 0.02 in. The CFRP strip nodes were constrained to move identically to the adjacent concrete nodes in the direction perpendicular to the interface (y -direction). Since the spring elements cannot transfer moments at their ends, bond shear stresses (F_x in Figure 5-6) can only be developed across the interface when the lateral movement of the spring elements increases and spring tensile forces (F in Figure 5-6) develop due to inclination from the normal to the surface. A large deformation formulation was used for the nonlinear spring elements. The advantage of using such an implementation is that it accounts for any loss in bond due to slip in one direction when the slip is reversed or applied in another direction.

To obtain the desired bond stress-slip relation in the direction of F_x , a nonlinear spring material model in the direction of F was input accounting for large geometry equilibrium as presented in Equation 5-1. Thus the response in the direction of F_x starts with zero stiffness at zero slip but quickly picks up stiffness and load to match the desired peak bond stress and

associated slip. Similarly, the elongation of the springs (Δ) can be related to slip in the plane of the interface according to Equation 5-2

$$F = F_x \times \left(\sqrt{s^2 + t_f^2} \right) / s = F \sin \theta \quad \text{Equation 5-1}$$

$$\Delta = \sqrt{s^2 + t_f^2} - t_f \quad \text{Equation 5-2}$$

in which,

t_f = thickness of CFRP laminate as shown in Figure 5-6. The thickness is 0.02 in. in this study

θ = angle of inclination of spring element as shown in Figure 5-6

s = bond slip in the direction of F_x , in. (Figure 5-6)

Δ = elongation of spring in. (Figure 5-6)

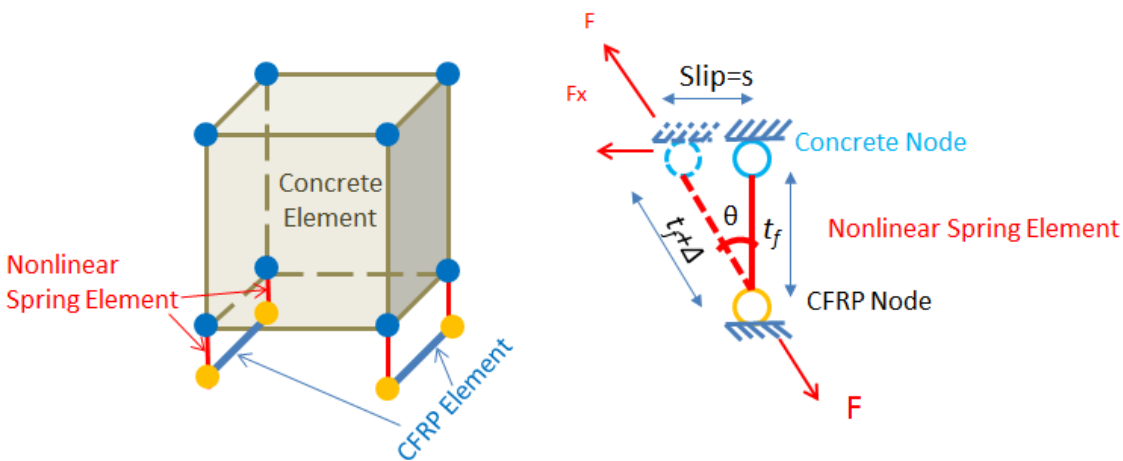


Figure 5-6 CFRP-concrete interface modeling

5.2.3 Material Properties

The steel material for the loading plates was modeled as a bilinear isotropic element with an elastic modulus $E_s=29,000$ ksi, a yield stress $f_y=60$ ksi, and a Poisson's ratio $\mu =0.3$. Loading plates were not expected to be loaded beyond their linear range.

The concrete material model governing the eight-node concrete elements is a multi-linear isotropic material model. The model accounts for multi-axial effects on compression strength according to the failure surface illustrated in Figure 5-7. This particular model was selected as it was readily available in ANSYS. However, the test beams only experienced cracking at mid-span with no other concrete damage. Although the comprehensive ANSYS concrete material model is used in the proposed computational model, the tension strength, Poisson ratio, and modulus of elasticity are the parameters with the greatest impact on simulation results. Simpler concrete models that account for these three critical parameters should result in similar results as those presented herein.

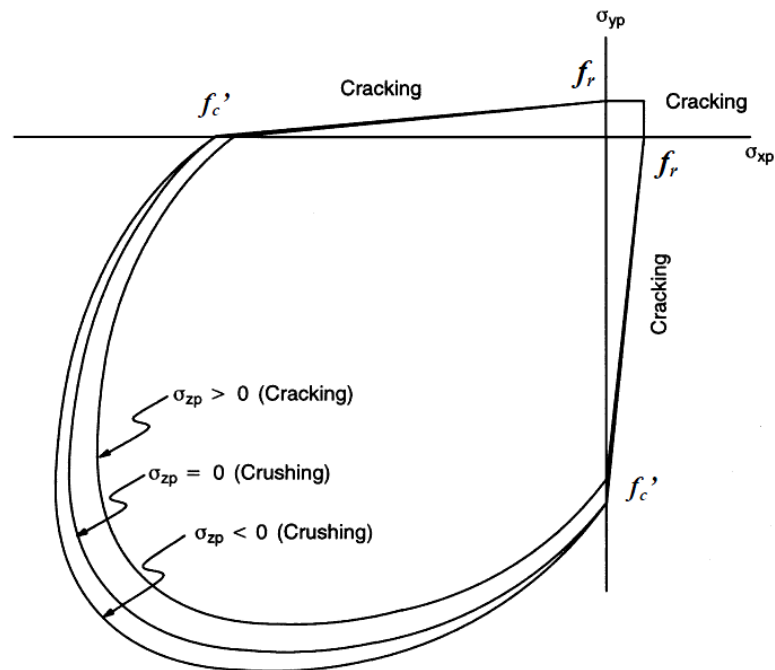


Figure 5-7 Spatial failure surface for concrete (SAS, 2009);

$$f_r = \text{uniaxial tensile strength} \quad f_c' = \text{uniaxial crushing strength}$$

$$\sigma_{xp}, \sigma_{yp}, \sigma_{zp} = \text{principal stresses in principal directions}$$

The concrete material model requires the input of the concrete compressive strength, the residual stress at large compressive strains, the Poisson ratio, shear transfer parameters, and tensile properties. From these parameters, the model builds the multi-directional failure surface

illustrated in Figure 5-7 and defines the uniaxial tension/compression behavior according to the equations shown below (Macgregor, 2001) and illustrated in Figure 5-8. The numbered points shown in Figure 5-8 (a) were used to plot the compressive stress-strain curves shown in Figure 5-8 (b). The input elastic modulus (E_c) was calculated as $E_c = 57000\sqrt{f'_c}$, in which f'_c is the concrete compressive strength (in psi units). The Poisson's ratio was user-defined as 0.3 following the suggestion of (Wolanski, 2004).

$$f = E_c \varepsilon / (1 + (\varepsilon / \varepsilon_0)) \quad \text{Equation 5- 3}$$

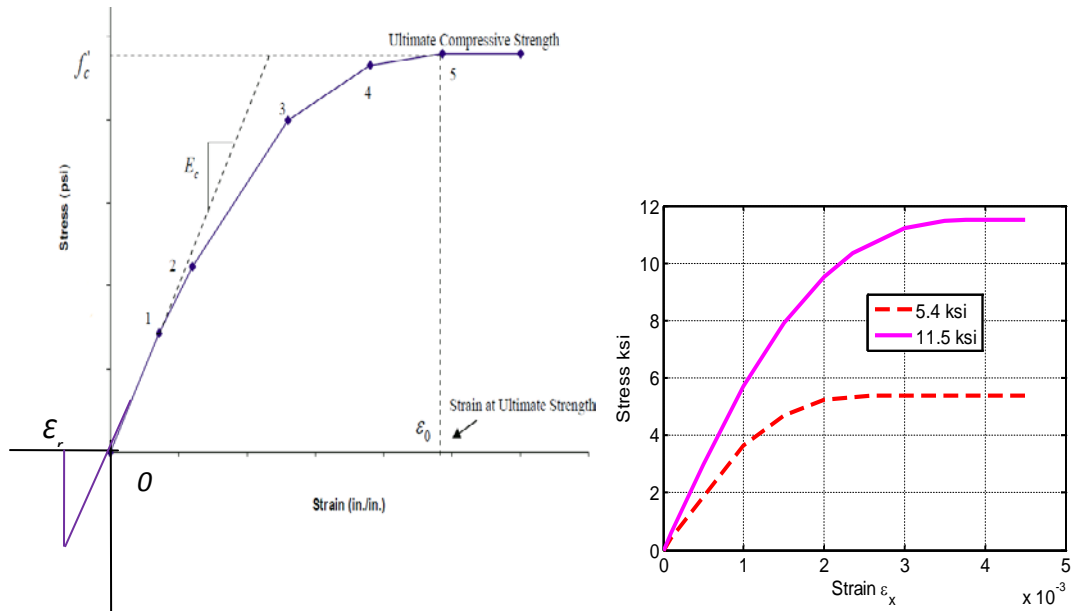
$$\varepsilon_0 = 2f'_c / E_c \quad \text{Equation 5- 4}$$

$$E_c = 57000\sqrt{f'_c} \quad \text{Equation 5- 5}$$

in which,

f is stress at any given strain ε , ε_0 is strain at ultimate compressive strength f'_c , and ε is any given strain between 0 and ε_0 . For numerical stability, a user-defined plastic behavior was introduced at strains larger than ε_0 .

The user-defined concrete cracking stress f_r was calculated as $f_r = 7.5\sqrt{f'_c}$ (in psi units) in accordance with ACI 318-11. ε_r is the strain at f_r and was calculated as E_c / f_r (SAS, 2009). The shear transfer coefficients for open and closed cracks were selected as 0.35 and 1 following the suggestion of (Wolanski, 2004). The tensile strength of concrete was set to zero after cracking.



(a) (Wolanski, 2004) (b) Determined curves for concrete element
Figure 5-8 Compressive stress-strain curve for concrete

Force (F) versus elongation (Δ) relations were input for the nonlinear bond elements accounting for large geometry to achieve the desired bond stress (τ) versus slip (s) relation along the interfacial plane (Figure 5-9). In all simulations, a linear ascending branch was input in the nonlinear spring elements up to the peak force and associated elongation. When conducting parametric-study simulations, the descending branch of the relation was input accounting for large deformations to achieve the same nonlinear degrading shape in the direction of Fx as the bond relation proposed by Lu et al (2005). When conducting sensitivity studies, the descending branch of the force versus elongation relation in the direction of F was taken as bi-linear to investigate the effects of using different shapes and slopes on simulation results.

The target peak bond stress and associated slip were selected based on experimental results. Bond stress-slip relations were extracted from test data as an average over an area bounded by the edges of anchor fans. Averaging the experimental bond relations over the relatively large CFRP strip area was done to generate smoothed relations and reduce the effects of noise in the measurements. However, as the debonding progressed from mid-span to the edges of the anchors in the tests, some areas within the region of measurement were in the ascending

branch of the bond stress-slip relation, while others were in the descending branch of the relation. The result of averaging the response over an area of uneven bond demand was a curbing of the extracted bond stress-slip relations at the peak stress and a less steep degrading branch than determined by the model proposed by (Lu et al, 2005) (Figure 5-9); which was developed for regions of constant bond demands.

For 11.5 ksi specimens, the mean measured bond stress versus slip behavior matched reasonably well the peak stress and associated slip of the model proposed by (Lu et al, 2005) (Figure 5-9). However, the measured relation showed a less steep descending branch than that of the model, which can be attributed to the uneven bond and slip demands over the measurement area. The peak stress and associated slip determined using the relations of Lu et al. (2005), were therefore targeted for specimens with 11.5 ksi concrete.

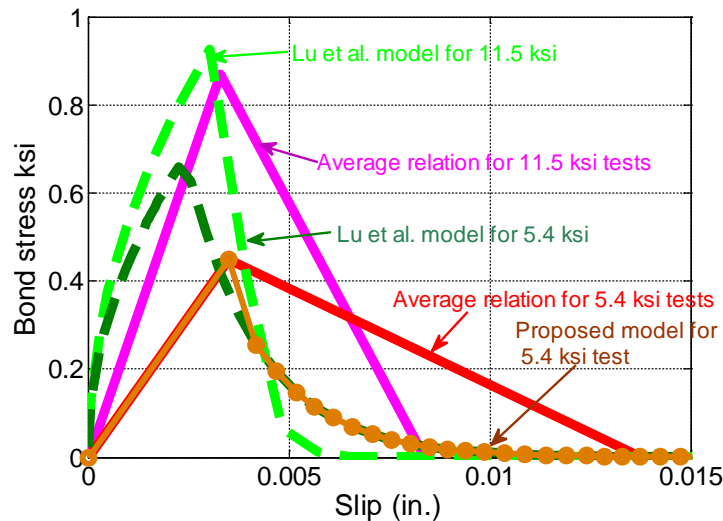


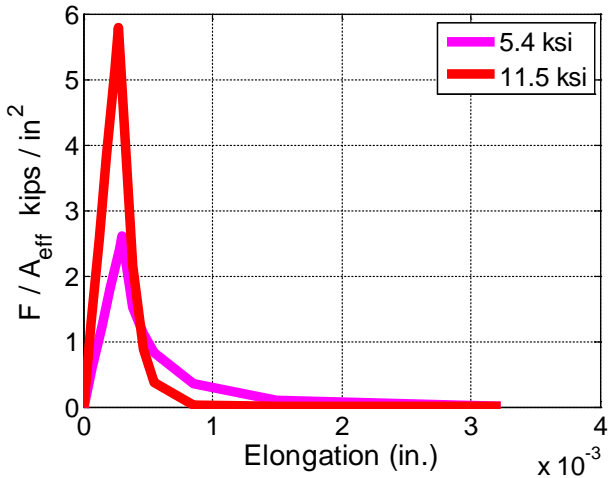
Figure 5-9 Comparison between the selected bond stress-slip relations and the average relations extracted from tests

The peak bond stress extracted from the test data for 5.4 ksi concrete specimens was significantly lower than that estimated using the model by Lu et al. For 5.4 ksi concrete, the peak stress and slip at peak stress were therefore targeted at the mean experimental values.

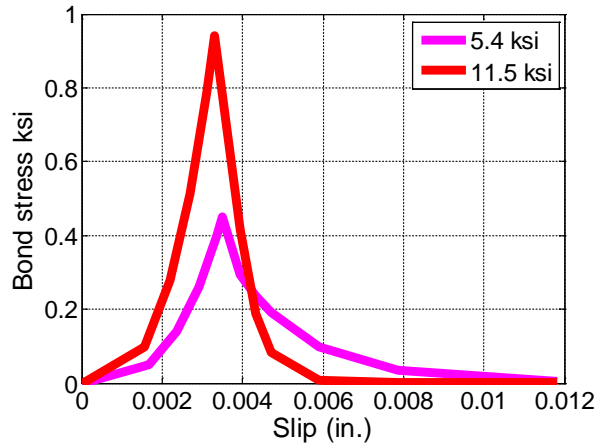
The peak bond stress and slip at peak bond stress (in the F_x direction) resulting from input in the nonlinear spring elements and large deformations are given in Table 5-2. The validity and accuracy of the selected bond stress-slip relations will be examined in the Numerical Results Section. Figure 5-10 illustrates the spring input force versus elongation relations used in the parametric-study simulations and the resulting bond stress-slip relations. As can be seen in the figure the input relation is linear in the ascending branch and nonlinear in the degrading branch. The resulting ascending branch in the direction of F_x is nonlinear with an initial zero slope at zero slip. The resulting descending branch in the direction of F_x matches the functional form of the model proposed by Lu et al. (2005).

Table 5-2 Peak bond stress and slip at peak bond stress from the input in the nonlinear spring elements (F_x direction, Figure 5-10)

Concrete Strength	5.4 ksi	11.5 ksi
Peak Bond Stress	0.45 ksi	0.94 ksi
Slip at Peak Bond Stress	0.0035 in.	0.0033 in.



(a) Input behavior of F/A_{eff} vs. Elongation



(b) Resultant behavior of bond stress vs. slip

Figure 5-10 Input behavior of F/A_{eff} vs. Elongation and resultant behavior of bond stress vs. slip for 5.4 ksi and 11.5 ksi concrete (A_{eff} = the effective surface area represented by a nonlinear spring element)

5.4 NUMERICAL RESULTS

Two series of simulations were conducted. Series 1 consists of six simulations, in which parameters in the computational model were varied to match key experimental variables. Series 2 consists of four simulations, in which CFRP and epoxy material properties were varied to evaluate the sensitivity of the proposed model to the selection of material properties. In all simulations, failure was defined in the simulations as the load at which the CFRP strip on the tension face reached the expected fracture strain provided by the manufacturer of 0.0093.

5.4.1 Series 1 Simulations: Parametric Study Based on Beams Tested in this Study

The first series of simulations focused on achieving accurate simulations of the load transfer mechanisms from CFRP strip to CFRP anchors across the range of experimental variables investigated. The six simulations had varying anchor-material ratios, concrete strengths, anchor fan lengths, and CFRP/concrete bond. Table 5-3 lists the key parameters varied in the simulations of Series 1 and the experimental tests that are directly comparable with the simulations. In all simulations of this series, the input elastic modulus of CFRP and epoxy were taken as the manufacturer specified expected values of 15300 ksi and 461 ksi, respectively.

Table 5-3 Parameters of Series 1 simulations

Name	Bonded/ Unbonded	CFRP Strip Width (inch)	Anchor Material Ratio	Concrete Strength (ksi)	Anchor Fan Length (inch)	Compares with Beam Tests
Simulation 1	Bonded	5	1.41	11.5	6	B5H1.4Ma B5H1.4Mb B5H1.4Md
Simulation 2	Bonded	5	1.06	11.5	6	B5H1Ma B5H1Mb B5H1Mc B5H1Md.
Simulation 3	Bonded	5	2.0	11.5	6	B5H2Ma B5H2Mb
Simulation 4	Bonded	5	1.41	5.4	6	B5L1.4Ma B5L1.4Mc
Simulation 5	Bonded	5	1.41	11.5	4.0	B5H1.4Sa B5H1.4Sb
Simulation 6	Unbonded	5	1.41	11.5	6	U5H1.4Ma U5H1.4Mb

* Note: Test B5H1.4Mc failed by delamination between the CFRP anchors from the CFRP strip and therefore was not used as a comparable test. B5L1.4Md has glare problems and B5L1.4Md failed due to delamination (glare problems come from the reflection of lights on the cured epoxy, which make UTVS fail to track the targets).

5.4.1.1 Verification of Selected Bond-Slip Relations

As mentioned previously, bond stress versus slip relations were extracted experimentally over the CFRP strip area bounded by anchor fans. On the other hand, the bond stress versus slip relations was defined in the computational models for nonlinear springs representing a much smaller interface area. Since the bond demands are uneven across the CFRP strip interface,

verifying the selected computational bond relations can only be done by comparing computational bond results averaged over the same area used to extract bond relations experimentally (Figure 5-11). As expected, the computational bond relations obtained by averaging the behavior of the nonlinear bond springs over the CFRP strip area show a smoothed peak behavior and a less steep descending branch than the relation governing individual bond spring elements. As can be seen in Figure 5-11, the ascending portions of the relations seem to be captured well by the computational model for both concrete strengths. Beyond the peak strain, computational results show closer agreement with experiments for the 11.5 ksi beams than for the 5.4 ksi beams. It is useful to note the relatively large variability in bond response recorded from experiments with similar or even nominally identical parameters. Bond between concrete and CFRP is a brittle mechanism that is highly dependent on concrete tensile strength and quality of installation.

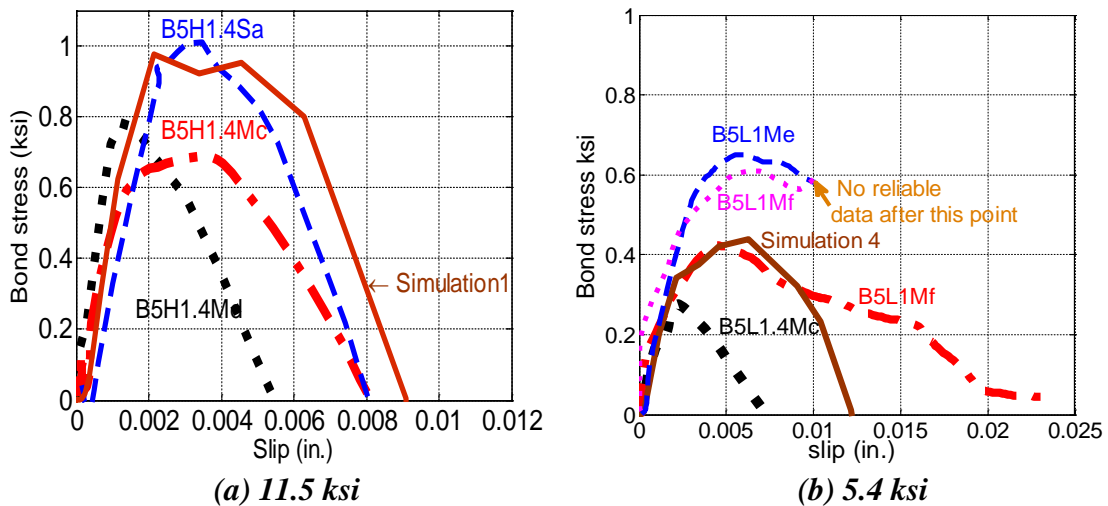


Figure 5-11 Comparison between the computationally derived bond stress versus slip relations and the relations extracted from sample tests

5.4.1.2 Evaluation of Beam Ultimate Loads

The failure load obtained from numerical simulations is defined as the applied load when the maximum CFRP strain at mid-span reaches 0.0093, which is the expected fracture strain provided by the manufacturer. As shown in Table 5-4, the simulations produced ultimate loads that are very close to experimental ones, and even captured the reduced strength observed in experiments when the CFRP strips were debonded from the concrete (Simulation 6). The simulations also captured the general trend of increased strip strength with increasing anchor material ratio.

The largest errors are observed in Simulations 3. It is useful to note that the applied load of test B5H2Mb (which compares directly with Simulation 3) was 16.5 kips when the maximum recorded strain in the CFRP strip at mid-span reached 0.0093. This load compares favorably with the load in Simulation 3 of 16.9 kips at a maximum CFRP strain of 0.0093. It appears that Simulation 3 is not capturing the full extent of the strength gains generated by an anchor material ratio of 2.0 observed in experimental tests.

Table 5-4 Comparison of failure loads of FE simulations and test (kips)

Simulation 1	B5H1.4Ma	B5H1.4Mb	B5H1.4Md	Test Average
16	15.8	16	16	15.9

Simulation 2	B5H1Ma	B5H1Mb	B5H1Mc	B5H1Md	Test Average
15.6	15	15.8	16.1	17	16

Simulation 3	B5H2Ma	B5H2Mb	Test Average
16.9	18.2	18.6	18.3

Simulation 4	B5L1.4Ma	B5L1.4Mc	Test Average
16.1	15.9	17.2	16.5

Simulation 5	B5H2Sb	Test Average
16	15.6	15.6

Simulation 6	U5H1.4Ma	U5H1.4Mb	Test Average
14.8	14.0	14.8	14.4

5.4.1.3 Evaluation of Beam Load-Deflection Responses

In this section, the computational load versus mid-span deformation responses are compared with those derived experimentally.

Figure 5-12 shows that the load-deflection curve of Simulation 1 agrees well with the curve of the directly comparable tests B5H1.4Mb and B5H1.4Md, and less so for test B5H1.4Ma. Simulation 1 shows beam flexural cracking and initiation of CFRP strip debonding at an applied load of 4.5 kips, which compares favorably with the observed cracking load of B5H1.4Ma and B5H1.4Mb. No significant debonding was observed until a load of about 6 kips for test B5H1.4Md, even though the test was nominally identical to tests B5H1.4Ma and b. The bond peak stress (0.94 ksi) used in Simulation 1 matches better the bond behavior in B5H1.4Mb (1 ksi) and B5H1.4Md (0.9 ksi) but is stronger than the bond recorded for B5H1.4Ma (0.8 ksi). The lower peak bond stress measured in B5H1.4Ma may have caused its response to be softer than that of the other two experiments and Simulation 1.

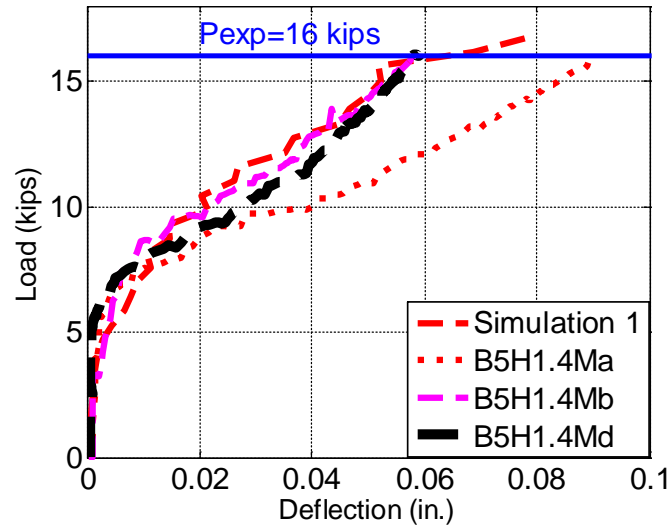


Figure 5-12 Load-deflection comparison for Simulation 1 and comparable tests

Among Simulation 1, Simulation 2, and Simulation 3, all parameters were identical except for the anchor-material ratio, which was 1.41 in Simulation 1, 1.06 in Simulation 2 and 2.0 in Simulation 3. Figure 5-12, Figure 5-13 and Figure 5-14 show that the entire computational load-deflection responses agree well with results from at least one experimental test for each simulation. Inherent variability in the behavior of nominally identical test specimens has led to FE simulations matching some test results with higher accuracy than others. Experimental results for tests comparable with Simulations 1 and 3 indicate that cracking loads of the concrete beam are higher than the computational cracking loads. A selected low peak bond stress for the bond model could be attributed to the discrepancies. Beyond a load of about 10 kips, debonding progressed in all tests to the edge of the anchors, which start carrying most of the load. Beyond that load, closer fit between experimental and computational load-deflection responses are observed, indicating the simulations are reproducing the behavior of the stiffness of the CFRP strip and anchorage system reasonably well.

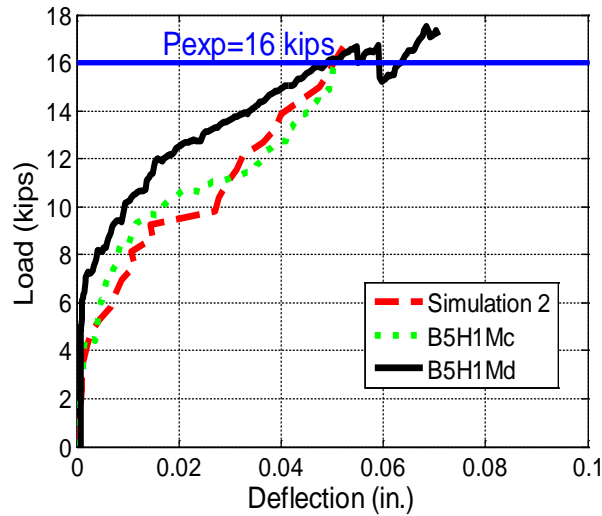


Figure 5-13 Load-deflection comparison for Simulation 2 and comparable tests

Note: B5H1Ma and B5H1Mb failed to provide reliable deflection results because of lighting glare

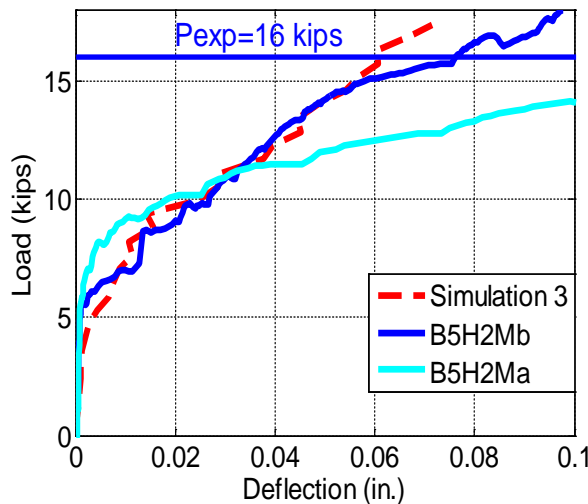


Figure 5-14 Load-deflection comparison for Simulation 3 and comparable tests

Simulation 4 is identical to Simulation 1 except for having a lower concrete strength and an associated weaker bond model. Figure 5-15 shows that the entire nonlinear load-deflection response of Simulation 4 agrees well with the experimental results, which show a softer response than for the higher concrete strength as seen in Figure 5-12.

A smaller anchor fan length of 4 in. was applied in Simulation 5 while keeping other parameters the same as in Simulation 1. Figure 5-16 shows good agreement between the load-deflection response of Simulation 5 and that obtained experimentally.

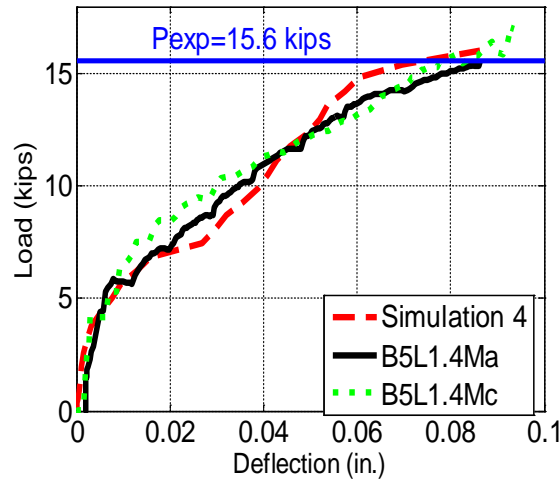


Figure 5-15 Load-deflection comparison for Simulation 4 and comparable tests

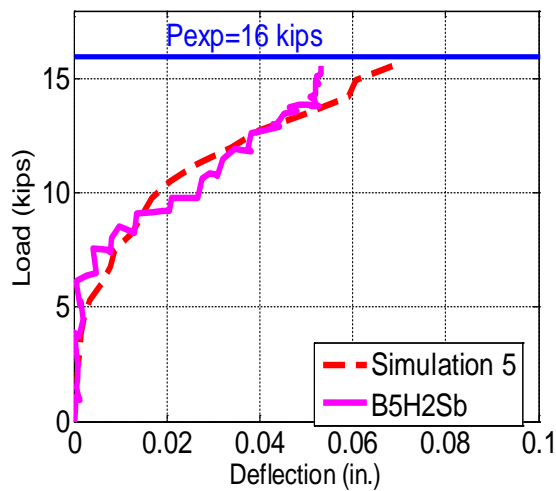


Figure 5-16 Load-deflection comparison for Simulation 5 and comparable tests

Note: B5H2Sa is not shown because it failed in concrete shear

Simulation 6 was built without interfacial bond elements between the CFRP strip and the concrete beam. This model is compared with tests results from an unbonded test in Figure 5-17. As shown in Figure 5-17, the load-deflection response from simulation results and experimental

test are in reasonable agreement. Simulation 6 captures well the initial softening of the response after flexural cracking and the subsequent stiffening arising from the engagement of the CFRP anchors. Simulation 6 was pushed to a load in excess of 16 kips, which corresponds to the CFRP strip reaching the expected fracture strain. In tests U5H1.4Ma and U5H1.4Mb, the anchors fractured at a lower load. The proposed computational model is not intended to capture the anchor failure mode.

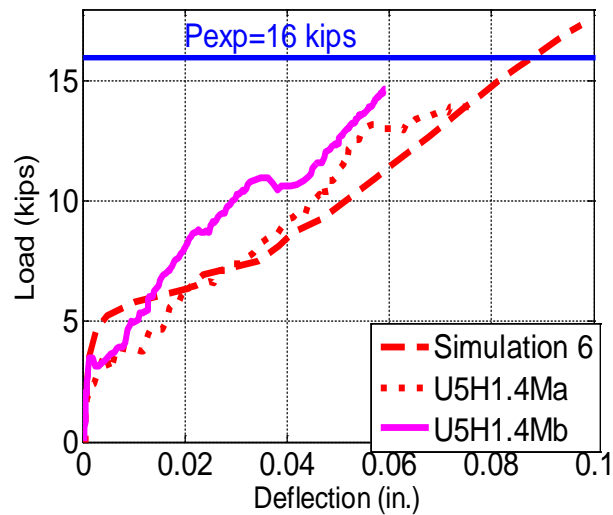


Figure 5-17 Load-deflection comparison for Simulation 6 and comparable tests

5.4.1.4 Evaluation of Section Average Strain Results

In this section, CFRP surface strains from simulations and experimental tests are compared. Section strain data plotted subsequently were obtained by averaging strains in the longitudinal direction (X-direction) across sections located at mid-span, on the strip adjacent to anchor fan end, on the fan at the end of it, and across the mid-span of the CFRP anchor (Figure 5-18). Evaluations of the variations in the strain distributions across the width of CFRP strips will be presented in section 5.4.3.

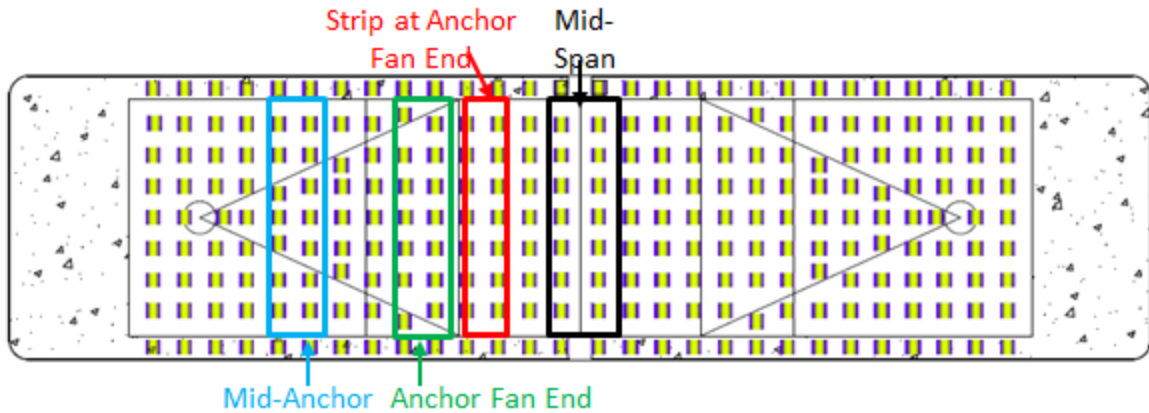


Figure 5-18 Selected sections on specimens used to perform average strain comparisons

5.4.5.4.1 CFRP Strip Section Strains

Figure 5-19 to Figure 5-24 compare CFRP strip strains of experiments and the six simulations of Series 1. The figure plots the applied load versus the average CFRP strip (X-direction) strains along sections at beam mid-span and on the strip adjacent to the anchor fan end.

In all cases, the simulations delivered CFRP strip strains that are in reasonable agreement with experimental results at both sections considered. Overall, the simulations matched experimental strip strains closer at beam mid-span than adjacent to anchor fan ends where a disturbed state of strain occurs.

As shown in Figure 5-19, closer agreement between analysis and B5H1.4Mb can be seen at beam mid-span than at anchor fan end. The UTVS failed to capture the behavior of B5H1.4Md before concrete cracked. It is unclear why B5H1.4Md saw significant CFRP strain increases at loads below the cracking load.

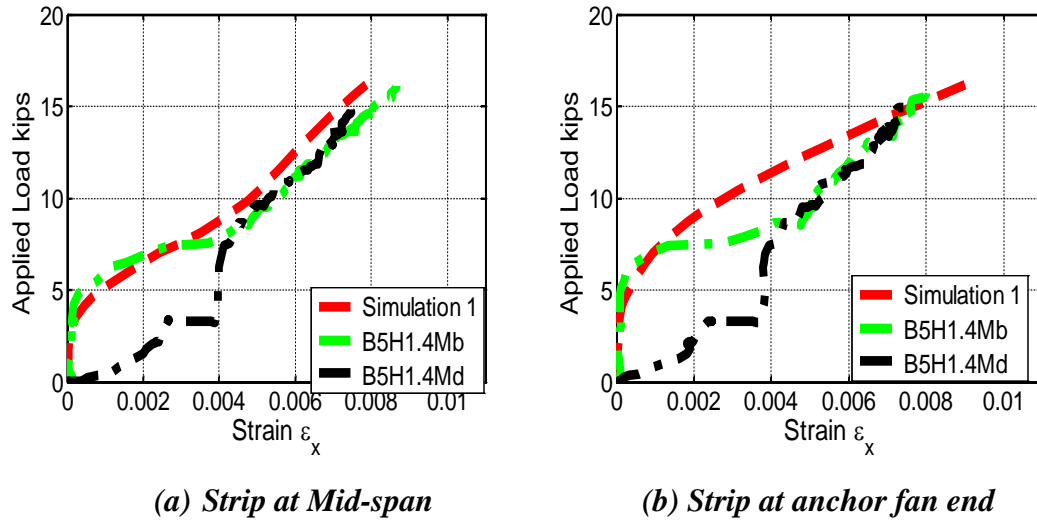


Figure 5-19 Comparison of load-strain response between Simulation 1 and comparable tests

Figure 5-20 shows similar trends as Figure 5-19 for Simulation 2 and comparable tests, with analysis matching the experiment more closely at beam mid-span than on the strip at anchor fan end.

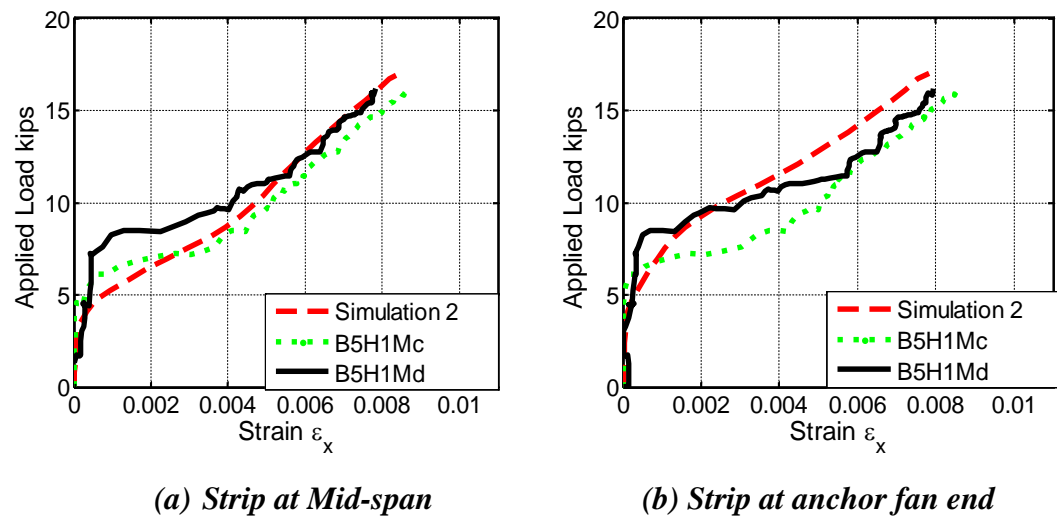
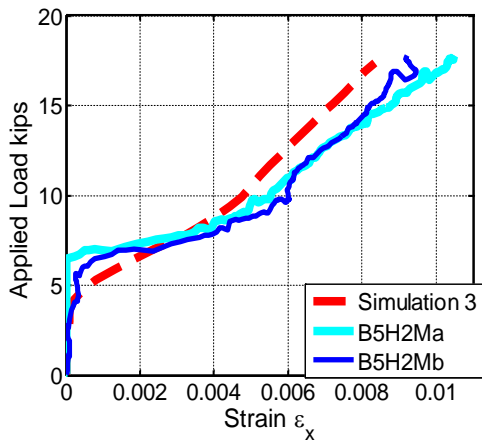


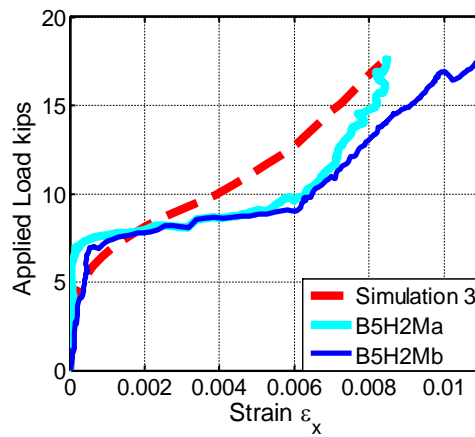
Figure 5-20 Comparison of load-strain response between Simulation 1 and comparable tests

Figure 5-21, Figure 5-22 and Figure 5-23 show similar trends as the previous two figures, with the analysis matching experiment more closely at beam mid-span than on the strip at the

another fan end. Figure 5-22 shows excellent agreement between Simulation 4 and both comparable tests.

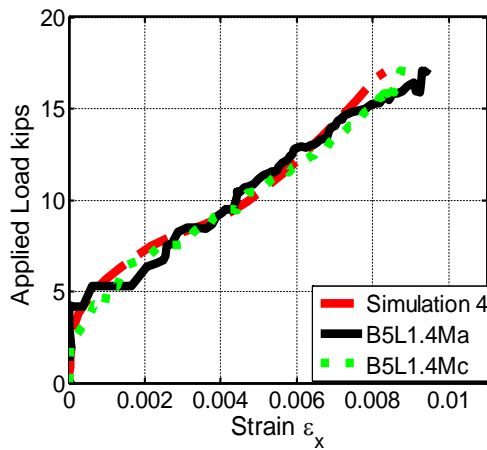


(a) Strip at Mid-span

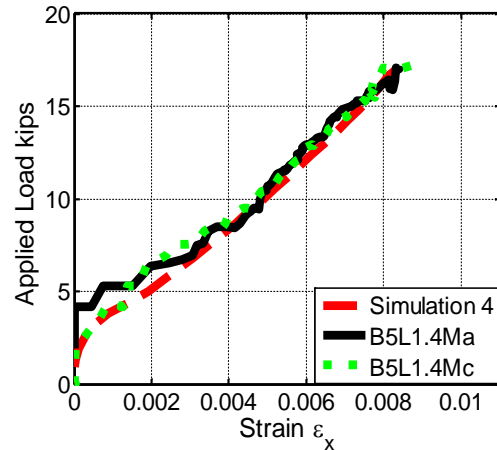


(b) Strip at anchor fan end

Figure 5-21 Comparison of load-strain response between Simulation 3 and comparable tests

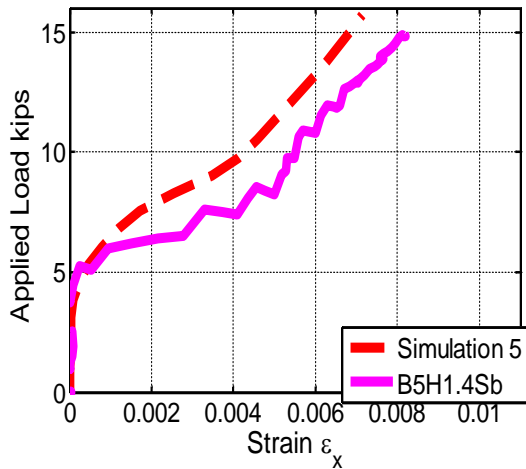


(a) Strip at Mid-span

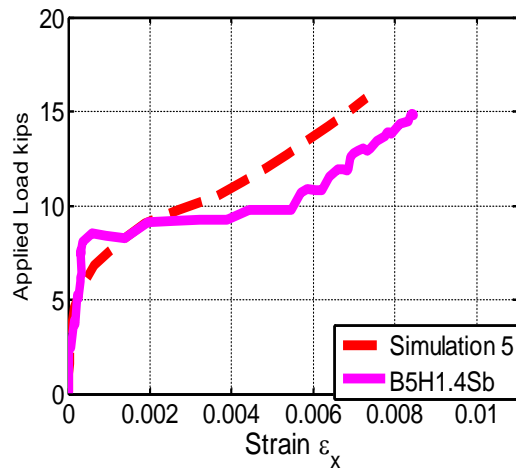


(b) Strip at anchor fan end

Figure 5-22 Comparison of load-strain response between Simulation 4 and comparable tests



(a) Strip at Mid-span



(b) Strip at anchor fan end

Figure 5-23 Comparison of load-strain response between Simulation 5 and comparable test

Figure 5-24 compares the strain results of Simulation 6 and a comparable test where the CFRP strip was completely debonded from the beam. This comparison highlights the ability of the proposed computational model to simulate the behavior of the CFRP strips and anchors. Good agreement between analysis and U5H1.4Mb can be seen at both sections from Figure 5-24. The comparison between analysis and U5H1.4Ma, however, shows that the concrete cracked in flexure at a lower load in the experimental test than in the simulation. After cracking, the CFRP anchors carried the entire tensile load transferred from the CFRP strip and similar load-strain slopes are observed between analysis and experiment. These findings indicate that the CFRP components of the model can capture well the CFRP stiffness and anchor behavior observed in the tests.

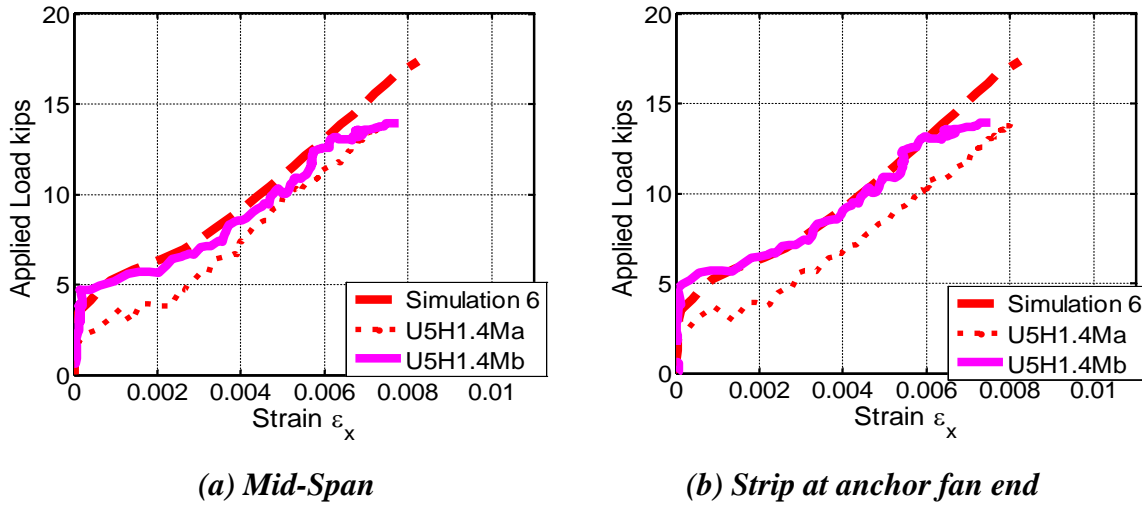
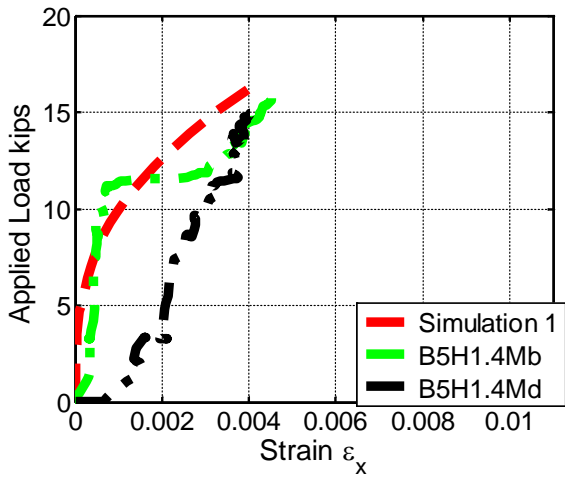


Figure 5-24 Comparison of load-strain response between Simulation 6 and comparable tests

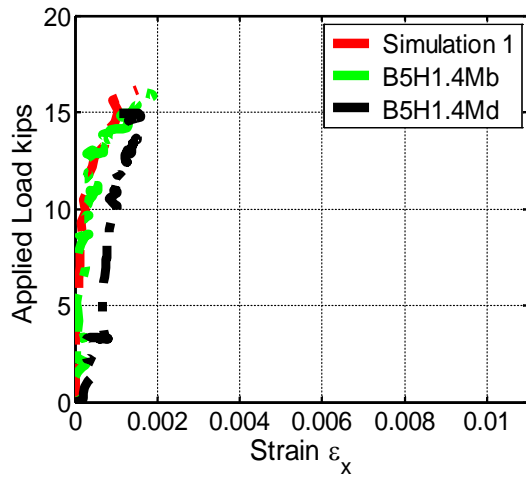
5.4.5.4.2 Surface Strains at CFRP Anchors

This section evaluates CFRP strain data collected at anchor sections located at the fan end and mid-anchor (Figure 5-18). Comparisons are made between simulations and comparable tests in Figure 5-25 to Figure 5-30.

Overall, the computational model appears to match strain response at the section around the middle of the anchors with reasonable accuracy. Figure 5-25 (a) shows a more gradual softening of the strain response at fan end after cracking in Simulation 1 than in test B5H1.4Mb. It is unclear why the experiment shows such a sharp increase in strains at about 11 kips of load. A similar jump in strain can be seen in B5H1Mc from Figure 5-26 (a) and test B5H2Ma from Figure 5-27 (a) but not in other tests shown in Figure 5-25 (a) to Figure 5-30 (a). In Figure 5-27 (a) to Figure 5-30 (a), the simulation matches the strain response at the fan ends reasonably well. In Figure 5-25 (b) to Figure 5-30 (b), the models can be seen to simulate the strain responses at mid-patches with a high degree of accuracy. It indicates that the simulations can reproduce the behavior away from the fan-end discontinuity and around the middle of the anchors much better than around the fan-end discontinuity.

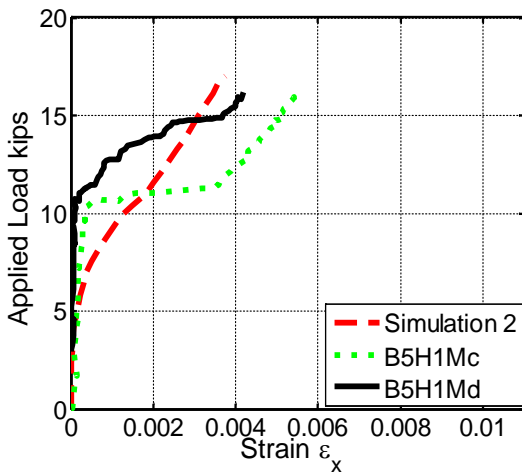


(a) Anchor Fan End

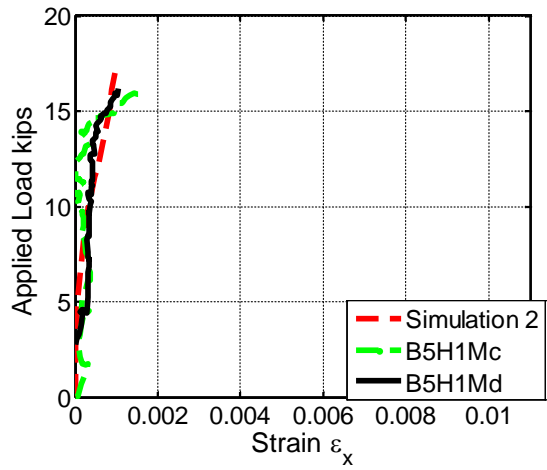


(b) Middle of Anchor

Figure 5-25 Comparison of load-strain response between Simulation 1 and comparable tests

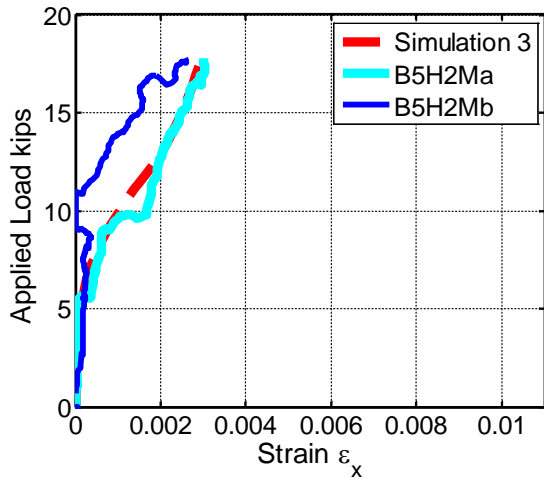


(a) Anchor Fan End

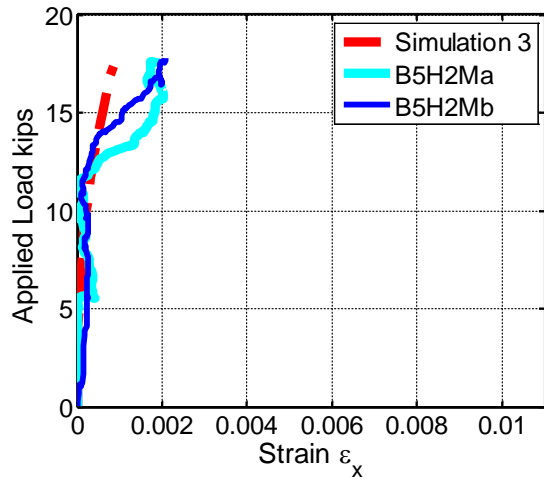


(b) Middle of Anchor

Figure 5-26 Comparison of load-strain response between Simulation 2 and comparable tests

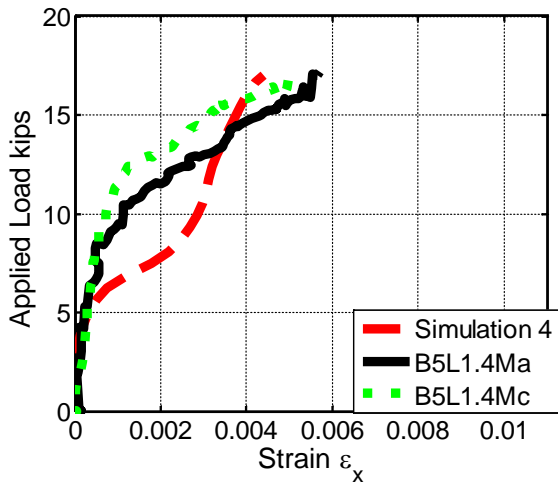


(a) Anchor Fan End

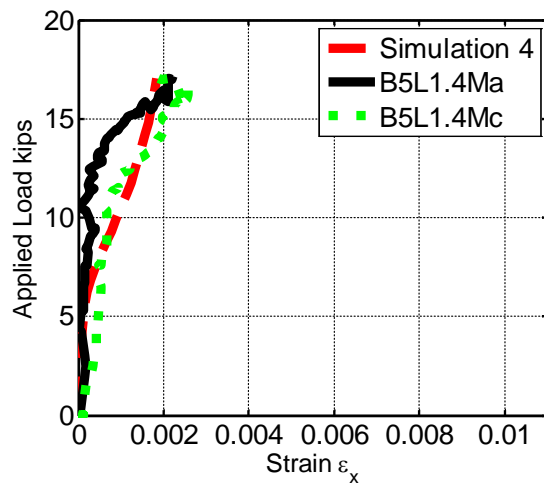


(b) Middle of Anchor

Figure 5-27 Comparison of load-strain response between Simulation 3 and comparable tests

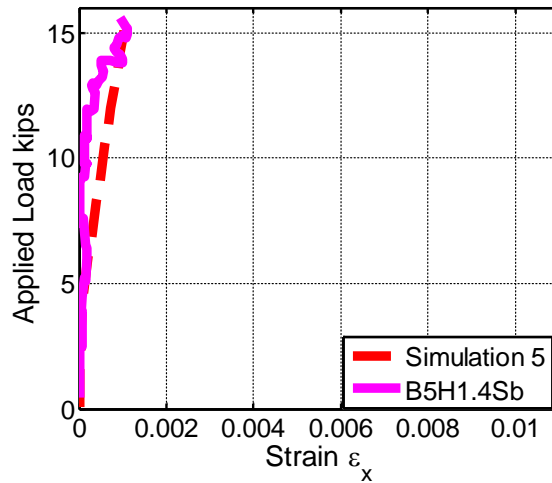


(a) Anchor Fan End



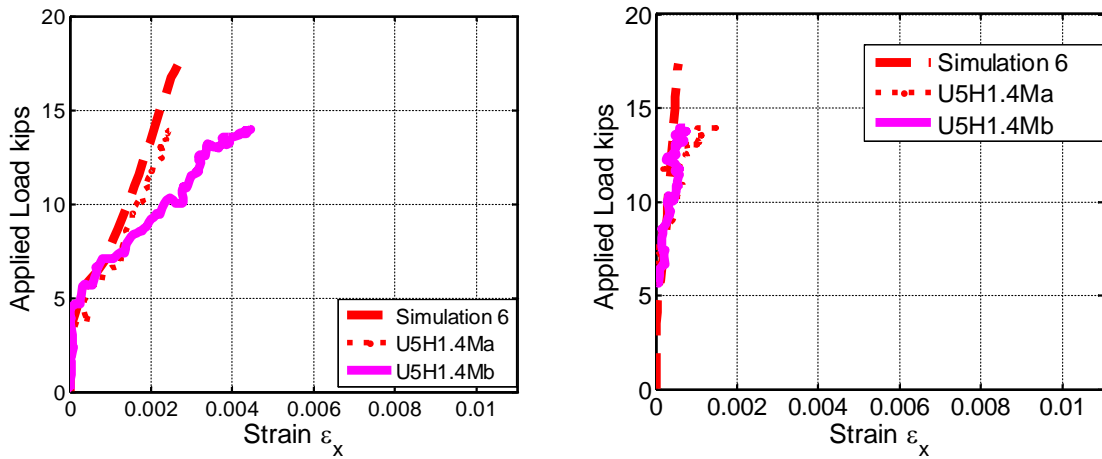
(b) Middle of Anchor

Figure 5-28 Comparison of load-strain response between Simulation 4 and comparable tests



Middle of Anchor

Figure 5-29 Comparison of load-strain response between Simulation 5 and comparable test (anchor fan end is not available due to lack of experimental data in that region in test B5H1.4Sb)



(a) Anchor Fan End

(b) Middle of Anchor

Figure 5-30 Comparison of load-strain response between Simulation 6 and its comparable tests

5.4.5.4.3 Evaluation of Strain Distribution along CFRP Strip Width

The ability of the models to capture variations the X-direction strains across the width of CFRP strips is investigated in this section. Figure 5-31 shows the locations of selected targets

from which an average longitudinal strain was estimated for comparison between simulations and test results. Four colors, red (a), black (b), green (c) and blue (d), were used to represent selected locations given in Figure 5-31.

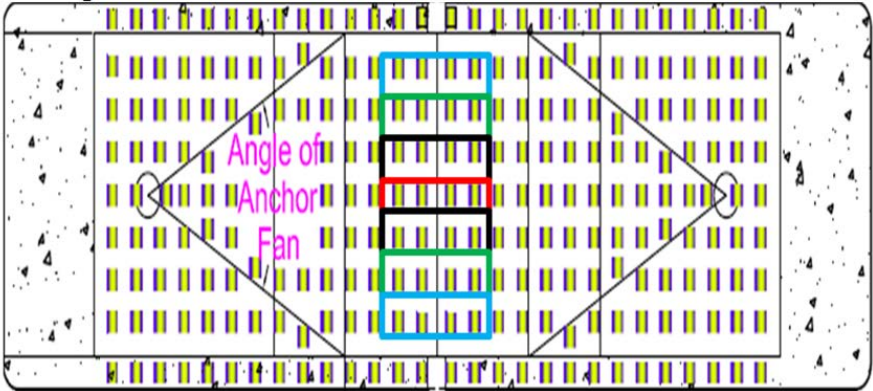
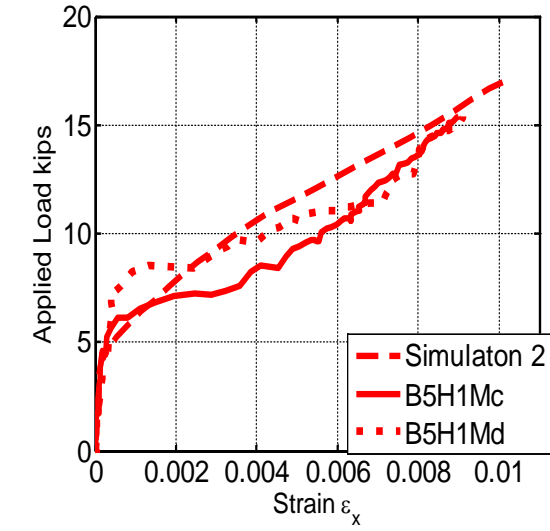
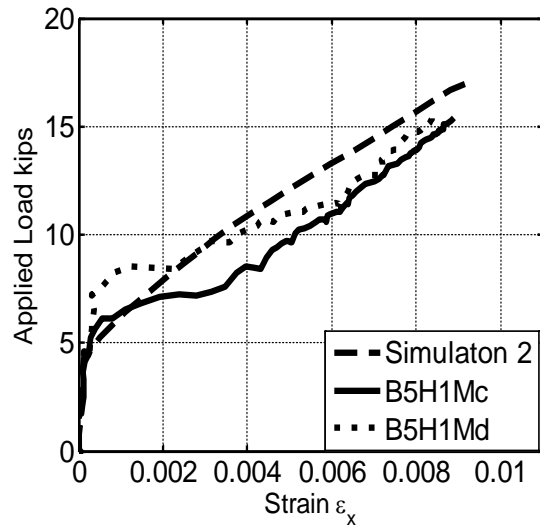


Figure 5-31 Locations of selected targets along width of the CFRP strip

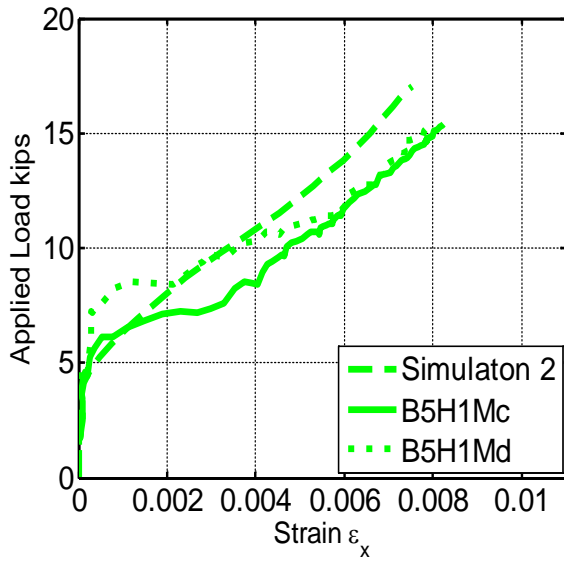
Plots are only shown here for comparisons with Simulation 2 and Simulation 4. In general, good agreement between simulations and comparable tests was seen in all locations before concrete cracked. Bond condition determined the shape of load-strain curves after concrete cracked, which increased the discrepancy between simulations and comparable tests. Closer agreement between simulations and tests is seen around the centerline of the CFRP-strip than at its edges close to the failure load (Figure 5-32 and Figure 5-33). It appears that the anchors in the simulations are not loading the CFRP fibers at the edge of the strip as much as is observed in experiments. Possibly stiffer anchor material properties, or strip and patch laminate properties could improve the distribution of strains to the outer edges of the CFRP strip.



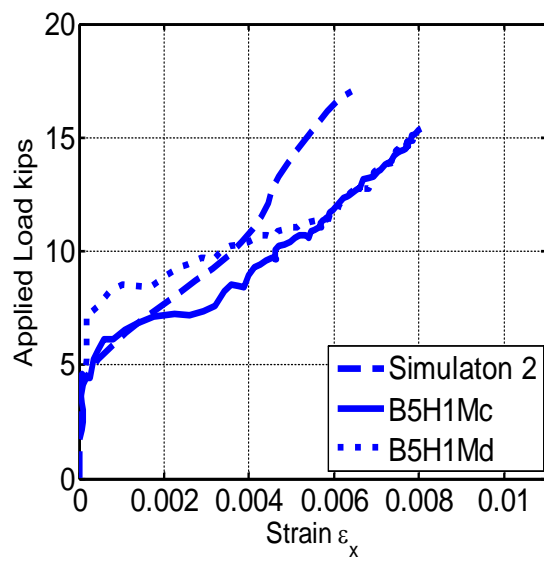
(a)



(b)

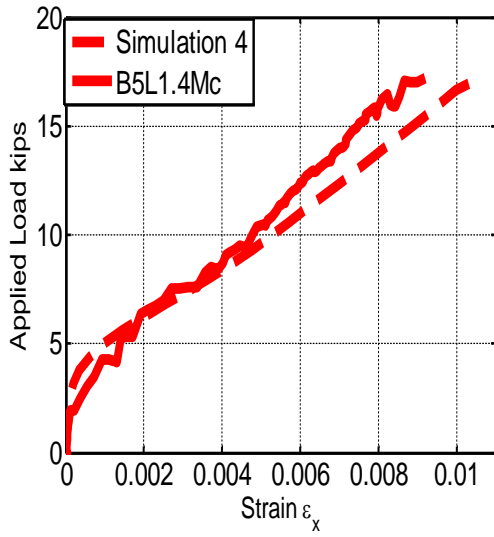


(c)

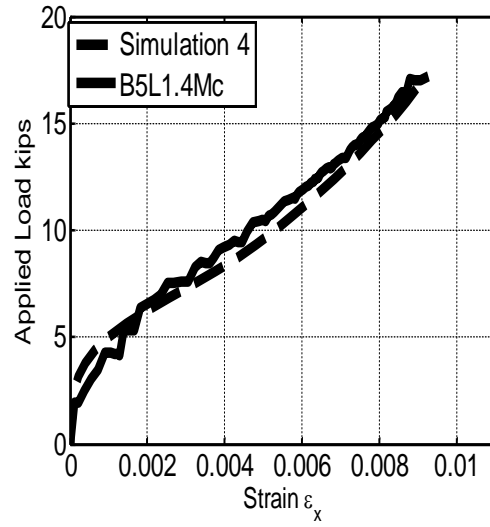


(d)

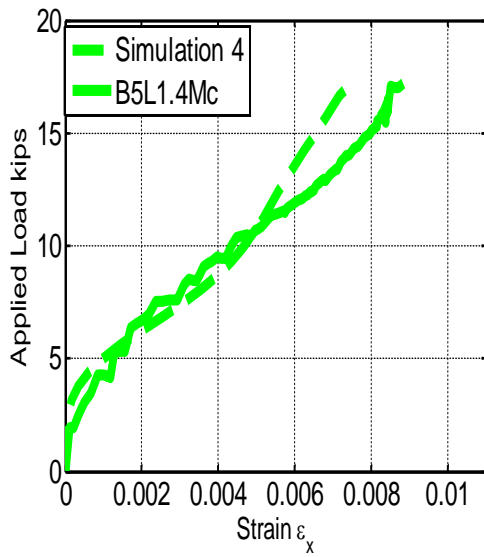
Figure 5-32 Strain comparisons across CFRP strip width between Simulation 2 and B5H1Mc and d



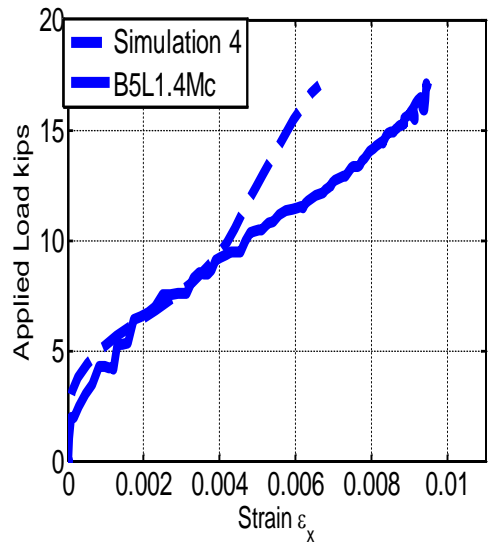
(a)



(b)



(c)



(d)

Figure 5-33 Strain comparisons across CFRP strip width between Simulation 4 and B5L1.4Mc

Note: In test B5H1.4Ma only five rows of targets were placed across strip width and could not provide the same data as for other tests, which had seven rows of targets

5.4.2 Series 2 Simulations: Sensitivity Study

Series 2 simulations were conducted to investigate the sensitivity of simulation results on assumed material properties. In Series 2, the sensitivity of the proposed model on the choices of the modulus of elasticity of the CFRP strip (E_f), the modulus of resin epoxy (E_{epoxy}), and the shape of the bond stress-slip relations are investigated.

Table 5-5 lists the parameters of the four simulations conducted in Series 2 that is different from Simulation 1 from Series 1, which served as the reference simulation.

Table 5-5 Parameters of Series 2 simulations

Name	E_f (ksi)	E_{epoxy} (ksi)	Bond stress-slip model
Simulation 1	15,300	461	Modified Lu 2005
Simulation 7	13,000	461	Modified Lu 2005
Simulation 8	15,300	922	Modified Lu 2005
Simulation 9	15,300	461	Steep descending slope
Simulation 10	15,300	461	Gradual descending slope

The elastic modulus of the epoxy resin matrix was varied from its manufacturer specified value of 461 ksi to twice that at 922 ksi. The CFRP strip modulus of elasticity (E_f) was varied from its manufacturer provided expected values of 15,300 ksi to its manufacturer provided design value of 13,000 ksi. The relation between F / A_{eff} (spring force / effective area of spring) and Δ (spring elongation) with steep and gradual descending slopes were constructed as multi-linear with four points as shown in Figure 5-34. The value of key points are listed in Table 5-6. Relations between spring force (F) and bond stress (τ) and spring elongation (Δ) and slips are given in Equations 5-1 and 5-2. The relations used in Simulation 9 with a steep descending branch constitute a multi-linear simplification on the relations used in Simulation 1. The relations with a shallower descending branch matched those of Simulation 1 at the peak stress but had twice the strain at 10% of the peak stress in the descending branch. The computational results of

the four simulations and Simulation 1 are compared at the global load-deflection level and local strain level to evaluate the sensitivity of the proposed model to assumptions in material properties.

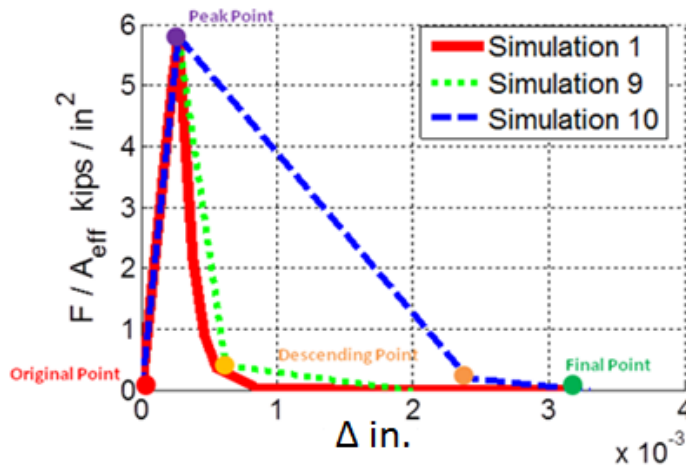


Figure 5-34 Input F/A_{eff} -Elongation relations used in the nonlinear spring bond elements with varying shape

Table 5-6 Spring force (F/A_{eff}) versus elongation (Δ) input and resultant bond stress (τ) versus slip (s) values at key points of Figure 5-34

	s (in.)	τ (ksi)	Δ (in.)	F/A_{eff} (kips/in ²)
Original Point	0	0	0	0
Peak Point	0.0033	0.94	0.00027	5.80
Descending Point (Simulation 9)	0.005	0.094	0.00062	0.40
Descending Point (Simulation 10)	0.01	0.094	0.0024	0.20
Final Point (Simulation 9)	0.0084	0	0.002	0
Final Point (Simulation 10)	0.012	0	0.0033	0

where

τ = bond stress, ksi

s = slip at τ , in.

F = tensile force of nonlinear spring element due to elongation, kips

Δ = elongation of nonlinear spring element, in.

A_{eff} = effective interfacial area represented by each spring

Figure 5-35 shows that the load-deflection curves of the four simulations of Series 2 agree well with the curve of the directly comparable test B5H1.4Ma. Overall, the figure indicates that varying the material properties of CFRP and epoxy in the ranges selected had limited effect on the global load-deflection response. Simulation 1, Simulation 7, and Simulation 10 match the load-deflection response after concrete cracked with higher accuracy. Increasing the epoxy modulus or using a shallower degrading slope is seen to increase the stiffness after concrete cracking. Figure 5-36 therefore indicates that: 1) using the manufacturer specified design value for the elastic modulus of the CFRP laminate (13,000 ksi) instead of expected value (15,300 ksi) has little effect on load-deflection response; 2) the four-point multi-linear bond stress-slip relation performs as well as the relation with a nonlinear degrading branch; and 3) either increasing the elastic modulus of the epoxy or using a more gradual descending slope for the bond stress-slip model tend to produce a stiffer load-deflection curve after concrete cracking.

Larger differences can be observed between Simulation results at the local CFRP strain level (Figure 5-36 and Figure 5-37).

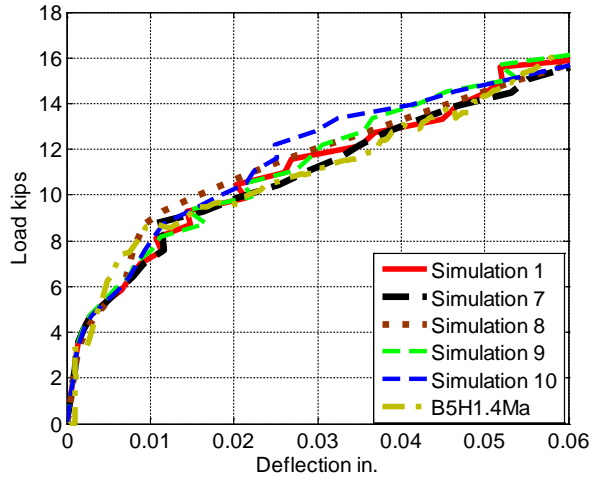


Figure 5-35 Load-deflection comparisons for sensitivity study

Larger differences can be observed between Simulation results at the local CFRP strain level (Figure 5-36 and Figure 5-37).

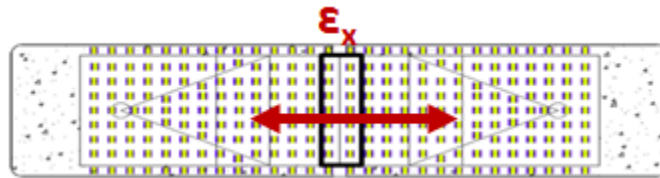
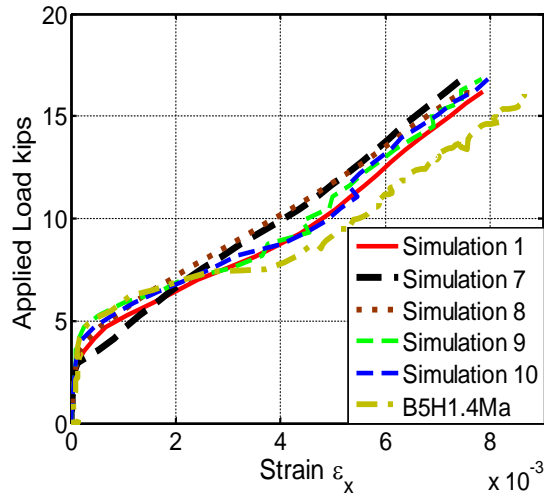
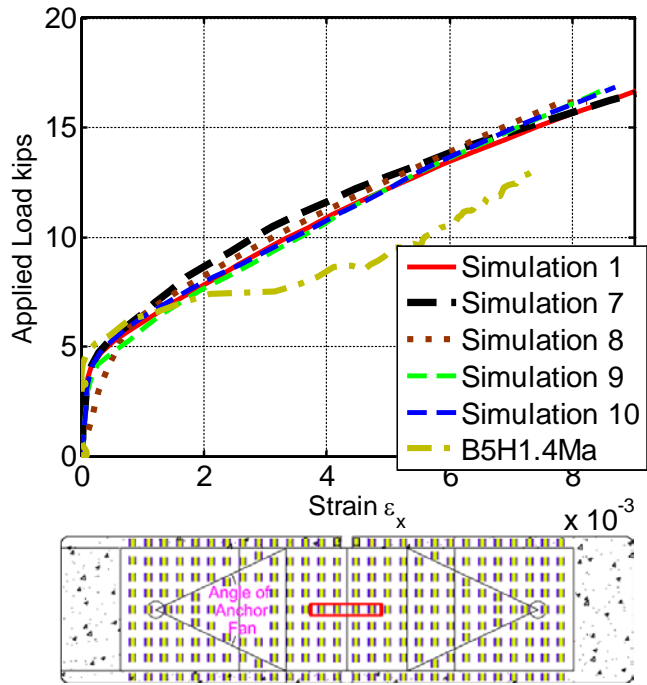
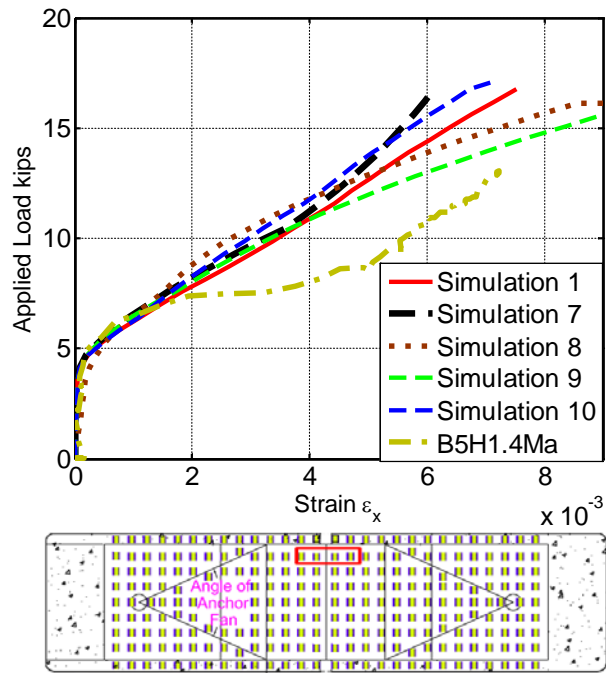


Figure 5-36 Comparison of load-strain response at mid-span for Series 2



(a) At the centerline of strip



(b) At the edge of strip

Figure 5-37 Comparison of load-strain responses across strip width for Series 2 simulations

The largest differences between computational results are seen in the strains at the edges of the CFRP strip (Figure 5-37 (b)). Figure 5-37 shows stiffer load-strain curves in computational results than experimental results at the centerline and edge of the CFRP strip, which suggests stronger input bond stress-slip relations in simulations than the bond conditions in the experimental test. At the centerline of the strip, varying the parameters of E_f , E_{epoxy} , and the shape of bond stress-slip model have limited effects on the load-strain response. At strip edge, either decreasing the modulus of the CFRP strip or using a more gradual descending slope for bond stress-slip consistently raises the stiffness of the load-strain response after concrete cracking. These results indicate that selecting a lower CFRP modulus or a more gradual descending slope on the bond relation is helpful to load the CFRP strip at the edge.

5.5 VALIDATION OF THE PROPOSED MODEL WITH AVAILABLE EXPERIMENTAL RESULTS

The computational studies discussed in this section were conducted to evaluate the performance of the proposed model in predicting experimental tests conducted by other researchers.

In this section, two CFRP anchorage tests (Huaco, 2009) were selected to validate the proposed model. The test specimens are illustrated in Figure 5-38. Test specimens consisted of 6"×8"×24" plain concrete beams strengthened in flexure using an anchored CFRP strip. One test had a 4 in. wide CFRP strip and the other had a 3 in. wide CFRP strip. A 3 in. notch was cut at mid-span to lower the cracking moment. The anchor had a 3 in. fan length and a 4 in. embedment length. The anchors were reinforced with two CFRP patches as in the current study specimens (Figure 5-39). The amount of CFRP material used in anchors was 1.5 times larger than the CFRP material used in strips. The material properties of concrete and CFRP used in the simulations are listed in Table 5-7. The four point F/A_{eff} -*Elongation* relations for bond stress-slip model with steep descending slope was used to simulate the interfacial bond condition between concrete and CFRP strip as shown in Figure 5-40. The value of key points on Figure 5-40 is listed in Table 5-8.

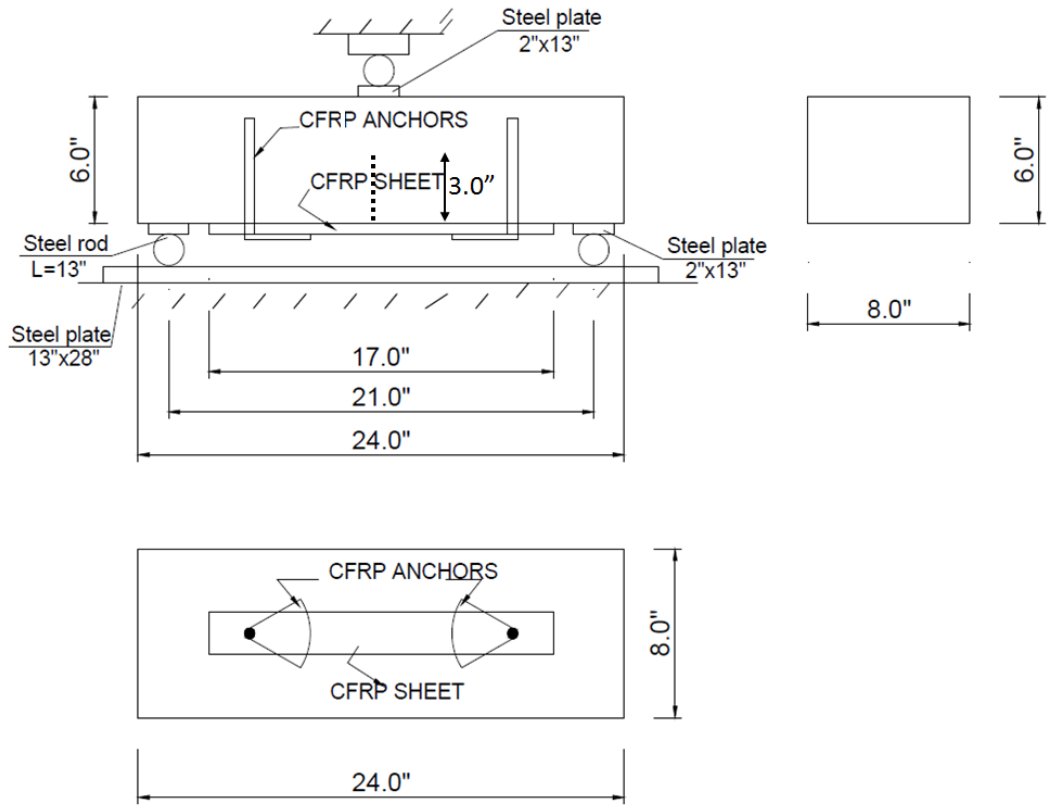


Figure 5-38 The anchorage tests of Huaco (2009)



Figure 5-39 Anchored strip attached on the tensile surface of specimens (Huaco, 2009)

Table 5-7 Properties of concrete and CFRP material used in simulations

	w_f (in.)	f_c' (ksi)	E_f (ksi)	f_{CFRP} (ksi)	t_f (in.)
Huaco 1	4	11.4	13900	143	0.04 in.
Huaco 2	3	11.4	13900	143	0.04 in.

* f_{CFRP} = The expected fracture stress provided by the manufacturer.

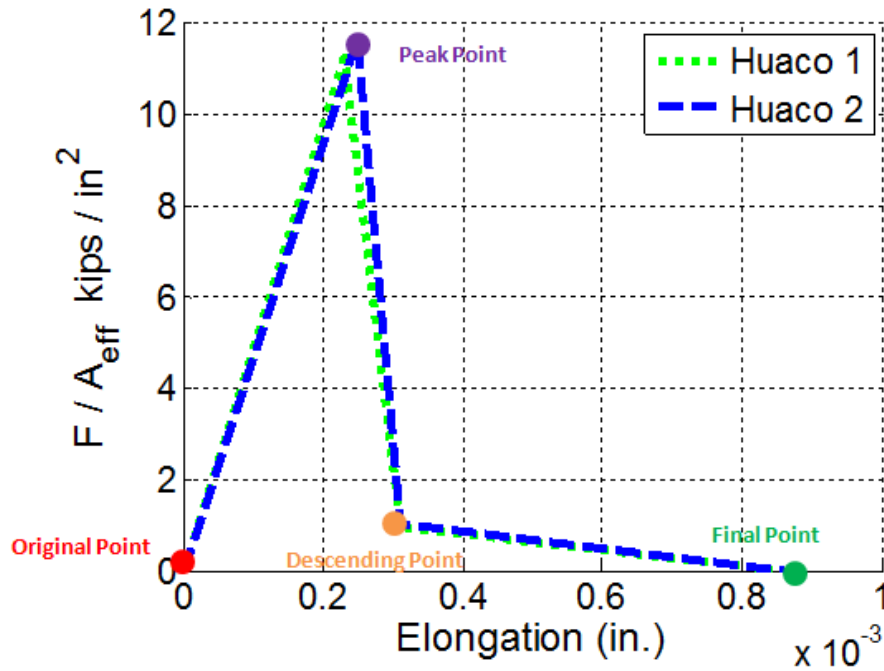


Figure 5-40 Input F/A_{eff} -Elongation relations used to simulate tests with 4 in. strip or 3 in. strip

Table 5-8 Spring force (F/A_{eff}) versus elongation (Δ) input and resultant bond (τ) versus slip (s) values at key points of Figure 5-40

	s (in.)	τ (ksi)	Δ (in.)	F/A_{eff} (kips/in ²)
Original Point	0	0	0	0
Peak Point (Huaco 1)	0.0043	1.2	0.00023	11.22
Peak Point (Huaco 2)	0.0045	1.3	0.00025	11.63
Descending Point (Huaco 1)	0.005	0.12	0.00031	0.98
Descending Point (Huaco 2)	0.005	0.13	0.00031	1.05
Final Point (Huaco 1)	0.0084	0	0.00087	0
Final Point (Huaco 2)	0.0084	0	0.00087	0

As shown in Figure 5-41, a ¼ beam model with symmetry in the xy-plane and yz-plane was built in ANSYS to simulate the anchorage tests. All element and geometric properties were

selected in the model as in the simulations discussed previously. No constraints were applied on the concrete nodes of the yz-plane of symmetry for the bottom to 3 inch of the beam depth to simulate the 3"-deep notch cut in test specimens. The CFRP strip nodes were 0.04 in. away from the adjacent concrete nodes and constrained to move identically to the adjacent concrete nodes in the direction perpendicular to the concrete surface.

Figure 5-42 shows that the load-deflection curves of Simulations Huaco 1 and 2 agree reasonably well with the curves of the directly comparable tests using 4 in. and 3 in. strips. No significant debonding behavior was observed in the test with a 4 in. strip until a load of about 7 kips, which was successfully captured by the simulation. Simulation Huaco 2 shows beam flexural cracking and initiation of CFRP strip debonding at an applied load of 6 kips, which compares favorably with the observed cracking load of tests using 3 in. strip. The ultimate load and the ultimate deflection were also successfully predicted by both simulations with high accuracy.

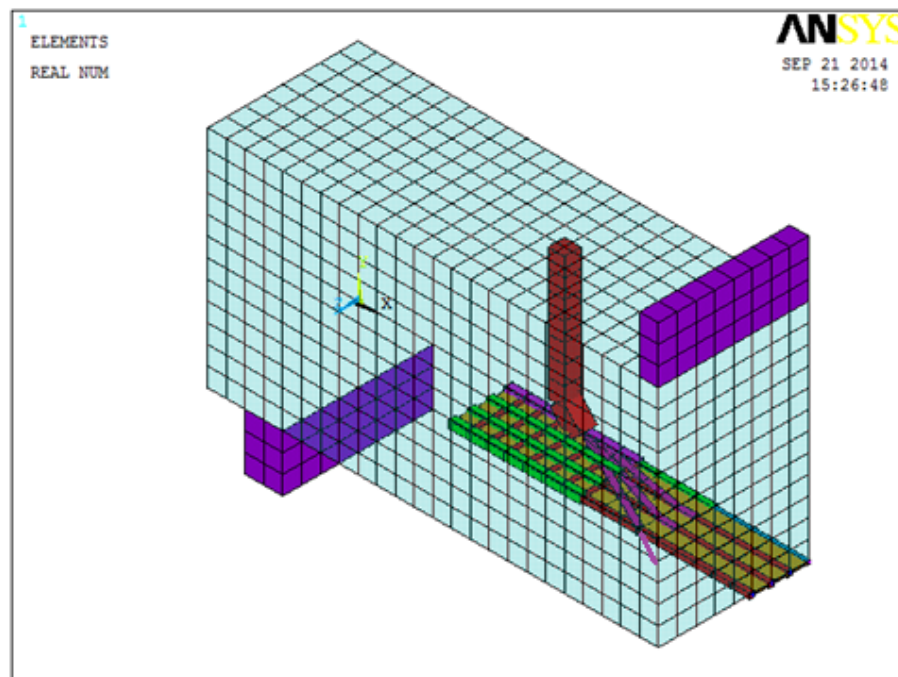
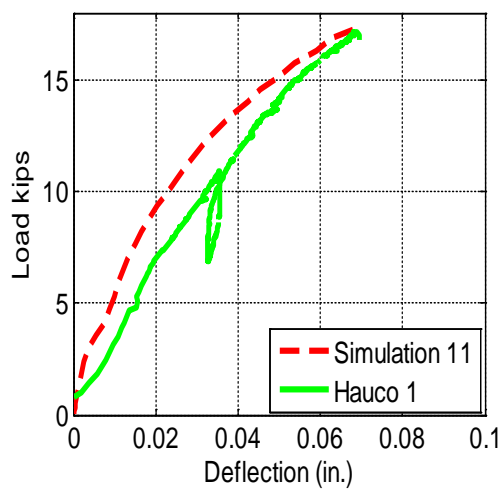
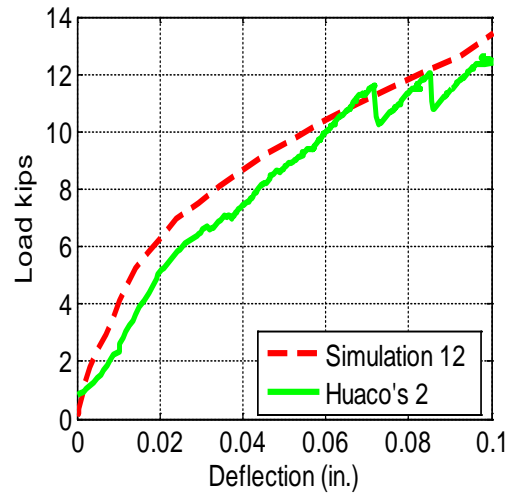


Figure 5-41 1/4 beam models for the simulations of Huaco's tests (2009)



(a) 4 in. strips



(b) 3 in. strips

Figure 5-42 Comparison of load-strain response between simulations and comparable tests of Huaco (2009)

Figure 5-43 compares the strain results of Simulation Huaco 1 and a comparable test where the CFRP strip was 4 in. wide. Close agreement between Simulation Huaco 1 and the applied strain gauge *a* can be seen. The comparison between Simulation Huaco 1 and gauge *b*, however, shows that the bond around gauge *b* was stronger than the bond stress-slip relation used in the simulation. After debonding, the CFRP anchors carried most of the tensile load transferred from the CFRP strip and similar load-strain slopes are observed between Simulation Huaco 1 and strain gauge *a* at loads greater than 14 kips.

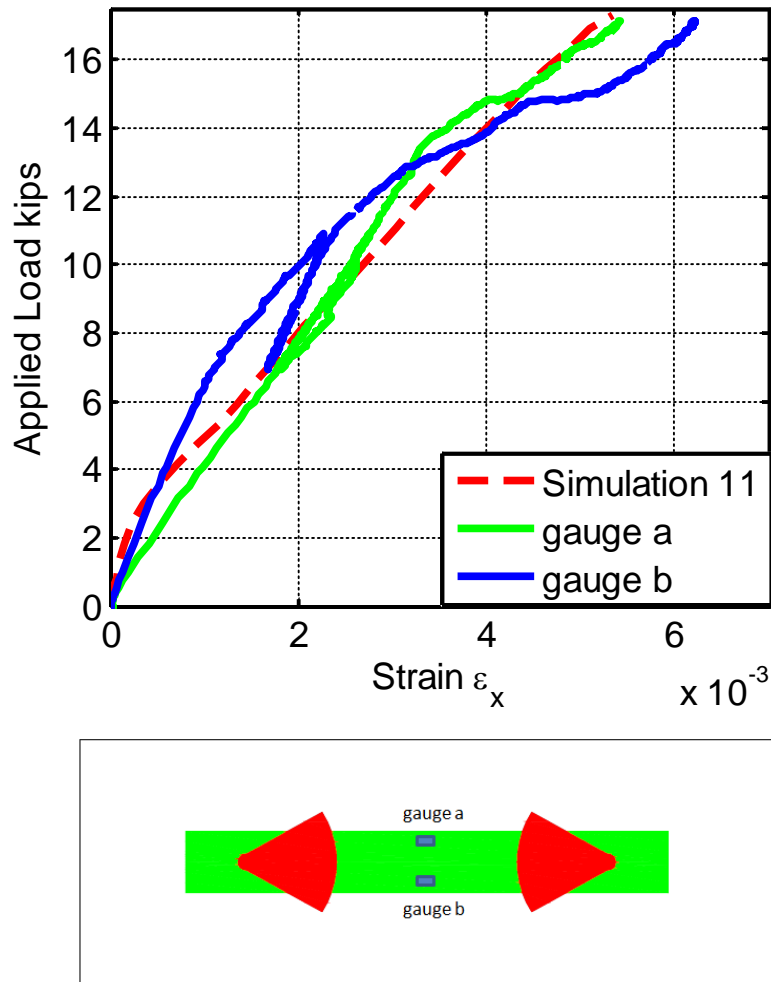


Figure 5-43 Comparison of load-strain response between Simulation 11 and gauges at mid-span from Huaco 1

Similarly, good agreement between Simulation Huaco 2 and gauge *a* can be seen from Figure 5-44 before concrete cracks. After cracking, bond appears weaker in the experimental test than in the simulation.

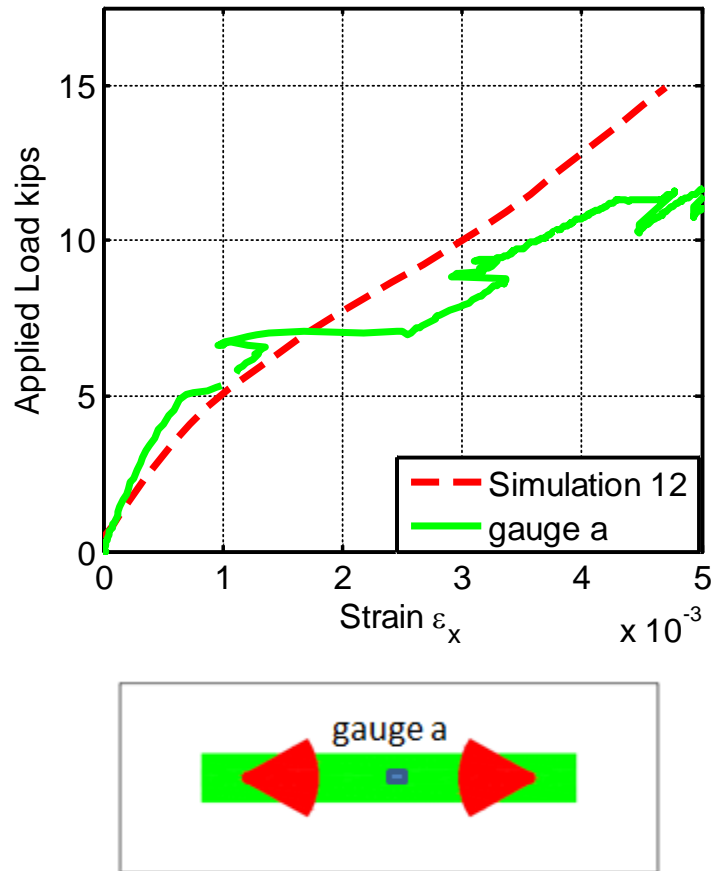


Figure 5-44 Comparison of load-strain response between Simulation 12 and gauge at centerline at mid-span from Huaco 2

5.5 SUMMARY

A computational model was developed to identify available computational tools that are best suited for simulating the response of the test beams, and particularly the CFRP strips and anchors. The proposed model was built in the analysis program ANSYS but is intended to be implementable in most structural analysis software. A three-dimensional continuum finite element model representing test beams strengthened using CFRP strips and anchors are presented. The proposed model is intended to be simple. It requires a limited number of input parameters and can be easily built in most structural analysis software.

In the proposed model, the concrete was modeled using generic cube elements that are able to capture the cracking behavior of concrete. CFRP strips and anchors were modeled using linear elastic truss elements. The epoxy resin matrix was simulated using elastic plate elements that transfer in plane stresses across the CFRP laminates. CFRP strips were connected to the adjacent concrete nodes by nonlinear spring elements perpendicular to the surface and having an undeformed length equal to the thickness of the CRP strip. The spring elements cannot transfer moments at their ends so that bond shear-stresses can only be developed across the interface when the lateral movement of the spring elements increases and tensile forces develop in the springs from the inclination of the springs from the normal to the surface. A large deformation formulation was used for the nonlinear spring elements. The advantage of using such an implementation is that it accounts for any loss in bond due to slip in one direction when the slip is reversed or applied in another direction. The bond stress-slip relations governing the nonlinear spring elements simulating the bond between CFRP laminates and concrete beams were calibrated to experimental results and consisted of a linear ascending branch and either a bilinear or nonlinear descending branch. The nonlinear descending branch was based on the model proposed by (Lu et al, 2005).

Two series of simulations were conducted in the development of the model.

Series 1 focused on achieving accurate simulation of the load transfer mechanisms from CFRP strip to CFRP anchors across the range of experimental variables investigated. Six simulations were conducted using the proposed model in Series 1. The simulations all used the same basic model but had various anchor-material ratios, concrete strengths, anchor fan lengths, and CFRP/concrete bond. Comparisons were made between simulation results and experimental results to evaluate the accuracy of the proposed computational model.

Globally, beam load versus deflection responses compared well between all six simulations and comparable experimental tests. The failure load was determined in simulations as the load at which the CFRP strip reaches the manufacturer provided expected fracture strain. Simulations provided accurate failure load estimates when CFRP strip fracture was the mode of failure, and even captured the reduced strength observed in experiments when the CFRP strips were debonded from the concrete. The simulations also captured the general trend of increased strip strength with increasing anchor material ratio. The proposed computational model is intended to capture a CFRP strip fracture failure mode but not an anchor failure mode.

Locally, load versus CFRP surface strains in the beam longitudinal direction showed similar trends in the simulations as those observed in experiments. The largest CFRP strain errors between simulations and experiments were observed at the edges of the CFRP strip and around the discontinuity in CFRP area at the anchor fan ends. Discrepancies between analysis and experiments can mainly be attributed to differences between the bond-slip relations in the models and those in the tests. Experimentally, however, the bond-slip relation was observed to vary significantly between nominally identical specimens. The bond-slip relations chosen in the models were calibrated to the average of the experimentally obtained bond-slip relations. The models captured with high accuracy the behavior of the CFRP strips and the CFRP anchors as demonstrated by the favorable comparison between results of the model and the experiment with unbonded CFRP strips.

Series 2 simulations were conducted to investigate the sensitivity of simulation results to assumed material properties. In Series 2, the sensitivity of the proposed model to the choices of the modulus of elasticity of the CFRP strip, the modulus of the resin epoxy, and the shape of the bond stress-slip relation was investigated. The sensitivity study indicated that 1) using the manufacturer specified design value for the CFRP strip elastic modulus (13,000 ksi) instead of the expected value (15,300 ksi) has little effect on estimates of global load-deflection response and local load-strain response; 2) the four-point multi-linear bond stress-slip model performs as well as a model with a nonlinear degrading slope; and 3) either increasing the modulus of elasticity of the epoxy or using a more gradual descending slope for bond stress-slip model tend to produce a stiffer load-deflection curve after the concrete cracked. At strip edge, either decreasing the modulus of the CFRP strip or using a more gradual descending slope for bond stress-slip consistently raises the stiffness of the load-strain response after concrete cracking. These results indicate that selecting a lower CFRP modulus or a more gradual descending slope on the bond relation is helpful to load the CFRP strip at the edge.

The proposed model was used in two simulations of small beam tests conducted by Huaco (2009). Good agreement between the tests of Huaco and simulations validated the applicability of proposed model to simulate another set of tests.

Further research is needed to understand the load and strain distributions at the anchor end before anchor failure can be simulated. Additional calibrations for bond-slip models, anchor fan stiffness, and strip in-plane stiffness would be useful in improving proposed model accuracy. Additional sensitivity studies on the peak bond stress would be helpful to evaluate the effects of bond-strength variability in developing the failure load.

CHAPTER 6

Anchor Design and Quality Control Tests

6.1 OVERVIEW

Based on experimental results, recommendations for CFRP anchor design are presented in this section. A proposed test for quality control is also presented.

6.2 ANCHOR DESIGN FOR A GIVEN CFRP STRIP

This research focuses on the application of anchored CFRP strips for shear strengthening of reinforced concrete members. To implement the findings of this study, a previously proposed procedure for designing the CFRP strips is discussed and a procedure for designing associated CFRP anchors is proposed. The capacity of CFRP strips needs to be selected based on the shear force required after the shear capacity of the concrete and transverse steel reinforcement are determined for the section of a member. The CFRP shear contribution needed can be determined by the procedure developed by Kim et al. (2011) as seen in section 2.2.5. In addition, multiple anchors were suggested if the width of the CFRP strip exceeds either 5 in., which is the largest strip used in this research, or $d_f/4$ recommended by Garcia et al. (2014) (with d_f being the distance from anchor to tension chord of beam). In order to fully develop the tensile strength of CFRP strips, CFRP anchors should be designed considering the following parameters: 1) the strength ratio of CFRP anchor to CFRP strip, 2) the CFRP anchor-fan angle, 3) the embedment length, and 4) the anchor bend radius.

6.2.1 Strength ratio of CFRP anchor to CFRP strip

In order to fully develop the tensile strength of CFRP strips by anchorage systems using the same or different CFRP material, the strength of CFRP anchors should be designed to be greater than the fracture strength of the CFRP strip being anchored. Since the same CFRP material was used to make strips and anchors in this research, the anchor-strength ratio was presented as an anchor-material ratio in previous chapters (with both being equal in this experimental study). When anchors are made of a different FRP material than the CFRP strips, an anchor-strength ratio is more appropriate and is defined as the ratio of anchor tensile strength to strip tensile strength. Experimental results presented in Chapter 4 indicate that the anchor-strength ratio must be increased as the width of a CFRP strip increased. In this section, recommendations for selecting an appropriate anchor-strength ratio to ensure strip fracture are presented.

6.2.1.1 Evaluation of Experimental Results

The effectiveness of CFRP anchors was evaluated to determine the minimum anchor-strength ratio for a given strip. An effective CFRP anchor is expected to fully develop the tensile strength of the CFRP strip. The ultimate stress developed in the strip is therefore used to design the anchorage system, which is expected to equal or exceed the tensile strength as provided by the manufacturer. The observation of experimental failure modes can also be used to determine the efficiency of the anchorage system. All specimens failing by strip fracture or at an ultimate stress larger than the design strength provided by the manufacturer are shown in Table 6- 1.

Table 6- 1 Ultimate load and failure mode

Test CFRP strip width	Specimen	Material ratio of anchors to strip	Ultimate stress in strips at failure (ksi)	% of design stress specified by the manufacturer	Failure mode
5 in.	B5H2Ma	2.0	166.8	138%	Strip Fracture
	B5H2Mb	2.0	170.5	141%	Strip Fracture
	B5L1.4&1.8Ma	1.41 & 1.76	153.1	127%	Strip Fracture
	B5H1.4Ma	1.41	144.8	120%	Strip Fracture
	B5H1.4Mb	1.41	146.7	121%	Strip Fracture
	B5H1.4Mc	1.41	147.6	122%	Delamination
	B5H1.4Md	1.41	146.7	121%	Strip Fracture
	B5H1.4Sb	1.41	143.0	118%	Anchor Rupture
	B5H1.4La	1.41	173.3	143%	Strip Fracture
	B5H1.4Lb	1.41	143.0	118%	Anchor Rupture
	B5L1.4Ma	1.41	146.7	121%	Strip Fracture
	B5L1.4Mb	1.41	134.7	111%	Strip Fracture
	B5L1.4Mc	1.41	157.7	130%	Anchor Rupture
	B5H1Ma	1.06	137.5	114%	Anchor Rupture
	B5H1Mb	1.06	144.8	120%	Anchor Rupture
	B5H1Mc	1.06	147.6	122%	Anchor Rupture
	B5H1Md	1.06	155.8	129%	Delamination
	B5L1Ma	1.06	142.1	117%	Anchor Rupture
	B5L1Mb	1.06	104.5	86%	Anchor Rupture
	B5L1Mc	1.06	125.6	104%	Anchor Rupture
B5L1Md	1.06	135.7	112%	Anchor Rupture	
B5L1Me	1.06	141.2	117%	Anchor Rupture	
B5L1Mf	1.06	154.9	128%	Concrete Shear	
B5L1Mh	1.06	102.7	85%	Anchor Rupture	
3 in.	B3H1.8XLa	1.76	165.8	137%	Delamination
	B3H1.4Sa	1.41	158.2	131%	Strip Fracture
	B3H1.4Sb	1.41	179.5	148%	Strip Fracture
	B3H1.4Ma	1.41	188.7	156%	Strip Fracture
	B3H1.4Mb	1.41	158.2	131%	Strip Fracture
	B3H1.4La	1.41	191.7	158%	Strip Fracture
	B3H1.4Lb	1.41	152.2	126%	Strip Fracture
	B3L1.4XLa	1.41	155.2	128%	Strip Fracture
	B3L1.4XLb	1.41	167.3	138%	Strip Fracture
	B3L1XLa	1.06	156.7	129%	Strip Fracture
	B3L1XLb	1.06	161.3	133%	Strip Fracture

Test results summarized in Table 6-2 show that test with an anchor-strength ratio larger than 1.06 resulted in the fracture of 3 in. CFRP strips in all cases. The minimum anchor-strength ratio to fracture 5 in. strips was 1.41. All eleven tests with a 1.41 anchor-strength ratio and 5 in. strips reached the design stress and seven of eleven tests resulted in fracture of the CFRP strips. Only four out of eleven 5 in. strips with a 1.06 anchor-strength ratio reached the design stress, and none failed by fracture of the strip. All tests with an anchor-strength ratio of 2.0 failed due to strip fracture.

Table 6-2 Summary of test results

Strip width	Anchor-strength ratio	Total number of tests	Number of tests failing by strip fracture	% of tests failing by strip fracture	# of test ult. stress \geq design stress	% of test ult. stress \geq design stress
5 in.	2.0	2	2	100%	2	100%
	1.41	11	7	63%	11	100%
	1.06	11	0	0%	4	36%
3 in.	1.76	1	1	100%	1	100%
	1.41	8	8	100%	8	100%
	1.06	2	2	100%	2	100%

6.2.1.2 Proposed Equations for Anchor Design

The area ($w_f \times t_f$) of a CFRP strip can be determined based on the force required to be carried in the CFRP strip as determined from the design requirements for a particular strengthening project as discussed in section 4.2.1.2. The width of a CFRP strip w_f is determined according to the required strip tensile capacity T_f ($T_f = V_f/2$), for an anchored U-wrap providing material on opposite sides of a member.

$$w_f = T_f / (t_f \times f_{fe}) \quad \text{Equation 6-1}$$

Where

V_f = required shear capacity in one CFRP U-wrap, kips (see Equation 2-30)

- T_f = the required strip tensile capacity, kips.
 f_{fe} = effective strength of CFRP composite at specimen shear failure, ksi
 t_f = thickness of CFRP strip, in.

It is assumed that the tensile capacity of the strip will need to be carried by anchors to prevent anchor failure before the strip ruptures. Equation 6-2 can be used to determine the required capacity of a CFRP anchor.

$$T_a = n_a \psi_a \times f_{au} \times A_{anchor} \geq w_f t_f f_{ult} \quad \text{Equation 6-2}$$

- T_a = required capacity of a CFRP anchor, kips
 A_{anchor} = cross sectional area of CFRP material in an anchor, in.²
 f_{au} = tension rupture strength of CFRP anchor at failure, ksi
 ψ_a = anchor efficiency factor (reciprocal of the anchor strength ratio).
 0.7 for a strip with an effective width of 3 in.
 0.5 for a strip with an effective width of 5 in.
 Linear interpolation may be used for widths between 3 and 5 in.
 n_a = the required number of CFRP anchors.
 f_{ult} = tension fracture stress of CFRP strip at failure, ksi.

The anchor efficiency factor is limited because only 5 in. and 3 in. strips were tested. Multiple same size anchors are suggested to strengthen a strip with a width larger than either 5 in. or $d_f/4$. When using a CFRP anchor from a CFRP supplier, the area of the manufactured anchor is provided and the required number for anchors to develop a CFRP strip can be calculated using Equation 6-3.

$$n_a \geq T_a / (\psi_a f_{au} A_{anchor}) \quad \text{Equation 6-3}$$

6.2.2 Other Considerations for Anchor Geometry

In this section, recommendations for anchor geometry are proposed based on work by (Kim, 2011; Niemitz, 2008; and Pham, 2009). Anchor geometry will depend on the following parameters that influence the strength of CFRP anchors: 1) the angle and length of the CFRP

anchor fan; 2) the embedment length; 3) the anchor bend radius, and 4) the diameter of the anchor hole.

6.2.2.1 The Angle and Length of CFRP Anchor Fan

The angle of a CFRP anchor fan and the width of a CFRP strip are used to determine the length of a CFRP anchor. An effective CFRP anchor is expected to be long enough to allow the anchor fan to extend 0.5 in. beyond the width of a CFRP strip (Kim, 2011). Thus, the length of anchor fans can be obtained from a given width of CFRP strip and a given angle of CFRP strip using Equation 6-4.

$$L_{anchor} = \frac{(w_f/2)+0.5}{\tan\left(\frac{\theta_{anchor}}{2}\right)} \quad \text{Equation 6-4}$$

L_{anchor} = Length of CFRP fan anchor, in.

w_f = width of CFRP strip, in.

θ_{anchor} = anchor of CFRP anchor fan, degrees

In general, a smaller angle produces a more gradual transfer of force to the anchor. The angle of the CFRP anchor fan was suggested to be less than 90° (Pham, 2009), while recent research by Kim (2011) recommended a fan angle less than 60° to be more effective in transferring tensile loads from CFRP strips. In addition, the results discussed in Chapter 4 indicate that an anchor-fan angle as low as 37° developed the fracture strain of CFRP strips. Considering that the tensile load transfer from the outer fibers in a strip is less efficient as the angle between the CFRP strip fiber and the anchor-fan fibers increases, a maximum anchor-fan angle of 60° is recommended for anchor design.

6.2.2.2 Embedment Length

A 2 in. embedment length was used by Niemitz (2008) with only one anchor failure observed due to pullout. The conclusion therefore was made that embedment length is not a governing parameter. In reinforced concrete members, however, a 2 in. embedment length is not long enough to reach the core concrete considering a minimum 1.5 in. concrete cover over transverse reinforcement, plus the transverse bar diameter. If an anchor embedment depth of 2 in. is used, anchor failure is likely to occur when concrete cover spalls off due to flexural or axial loads on the member. An anchor depth of 6 in was suggested by Kim (2011) to ensure at least 2 in. embedment into the core concrete to prevent an anchor failure because of the separation of the concrete cover. No anchor pullout, however, was observed in this reported research in which a 4 in. embedment length was used in all 39 tests. A 6 in. embedment length is therefore suggested for most applications. In some cases, the thickness of a member may not permit a 6 in. embedment. A minimum embedment length no less than 4 in. can be used.

6.2.2.3 Bending Radius

To prevent stress concentrations at the edge of an anchor hole, the hole needs to be rounded to provide a gradual transition of forces at the corner. A radius gauge and bend radius shown in Figure 6-1 Radius gauge and bend radius (Pham, 2009) was used by Pham (2009). A bend radius of 0.5 in. as recommended by Pham (2009) for hole chamfer was used in all the tests in this study. All tests with adequate anchor-strength ratio (1.06 for 3 in. strips and 1.41 for 5 in. strips) reached the design stress as shown in Table 6-2. Therefore, an anchor bend radius of 0.5 in. is recommended for anchor design, particularly for the direction in which anchor tension is developed. If larger diameter anchors are used, more tests are needed to determine an acceptable anchor bend radius.

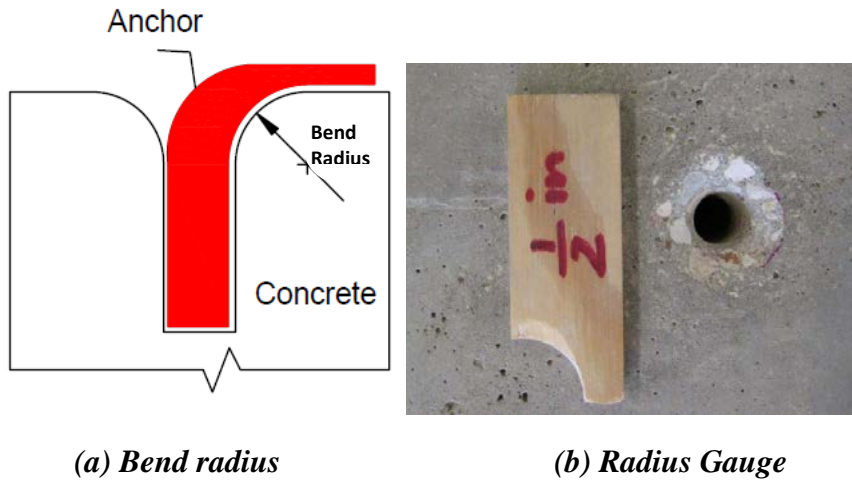


Figure 6-1 Radius gauge and bend radius (Pham, 2009)

6.2.2.4 Diameter of Anchor Hole

An anchor hole at least 1.4 times larger than the area of CFRP anchors was recommended (Pham, 2009). Table 6-3 lists the experimental results of 24 tests from Table 6- 1. All tests had anchorage systems adequate to develop the design strength. All tests with a hole-area ratio from 2.2 to 4.8 reached the design stress at anchor failure. Therefore, a hole diameter is recommended to be at least 2.2 times the cross-sectional area of a CFRP anchor. It is not known if there is a limit on hole size. Holes with areas 4.8 times the anchor area performed well. A hole-area ratio of 2.2 requires less drilling and less epoxy and is therefore recommended for most cases.

Table 6-3 Test results

Strip width	Number of Tests	Fiber area for anchor (A_f) in. ²	Hole diameter	Hole area in. ²	Area ratio	Number of tests that reached design stress
5 in.	2	0.2	3/4 in.	0.442	2.2	2
	12	0.141	5/8 in.	0.307	2.2	12
3 in.	8	0.0846	5/8 in.	0.307	3.6	8
	2	0.0636	5/8 in.	0.307	4.8	2

To determine the diameter of the required anchor hole, Equations 6-5 can be used.

$$d_{hole} = (4 \times 2.2 \times A_{anchor} / \pi)^{0.5} \quad \text{Equation 6-5}$$

where

A_{hole} = the area of anchor hole, in²

d_{hole} = the diameter of anchor hole, in.

6.2.3 Design Example for Single Anchor

To illustrate the design procedure for CFRP anchors, a design example for a required capacity of a CFRP strip $T_f = 6$ kips is presented. In this example, the required CFRP shear capacity (V_f) is 12 kips. A 6 kips capacity is obtained based on $T_f = V_f/2$. Standard anchor diameters of 1/2 in. and 3/4 in. are provided by Fyfe Co. LLC. The manufacturer's reported thickness, elastic modulus, and effective strain of the CFRP strip are 0.02 in., 15,300ksi and 0.004. The tensile strength of the CFRP anchor is 143 ksi.

1. Determine the width of CFRP strips according to Equation 6- 1.

$$w_f = T_f / (t_f \times f_{fe}) \quad \text{in which } f_{fe} = \epsilon_{fe} E_f$$

$$w_f = 6 / (0.02 * 0.004 * 15300) = 4.9 \text{ in.}$$

Therefore a 5 in. strip with one anchor in needed

2. Assuming a 1/2 in. diameter anchor, the area of the CFRP anchor is

$$\pi(1/2)^2/4 = 0.2 \text{ in.}^2$$

3. Determine the required number for CFRP anchors based on Equation 6- 3 in which ψ_a is 0.5 since the width of strip is 5 in. The tensile strength of CFRP is 143 ksi provided by manufacturer.

$$n_a \geq w_f t_f f_{ult} / (\psi_a f_{au} A_{anchor})$$

$$n_a = 5 * 0.02 * 143 / (0.5 * 143 * 0.2) = 1. \text{ One anchor is OK.}$$

4. Determine the length of anchor fan using the recommended 60° fan angle for an effective strip width of 5 in.

$$L_{anchor} = \frac{(5/2)+0.5}{\tan(\frac{60}{2})} = 5.2 \text{ in. Select a fan length of 6 in. (actual fan angle } 53^\circ = <60^\circ, \text{ ok).}$$

5. Embedment length = 6 in.

6. Bending radius = 0.5 in.

7. Determine the diameter of anchor hole based on Equation 6-5.

$$d_{hole} = (4 \times 2.2 \times A_f / \pi)^{0.5}$$

Diameter of hole = $(4 \times 2.2 \times 0.1963 / \pi)^{1/2} = 0.74 \text{ in.}$ use a 3/4 in. diameter hole. The layout of CFRP strip with one CFRP anchor is shown in Figure 6-2.

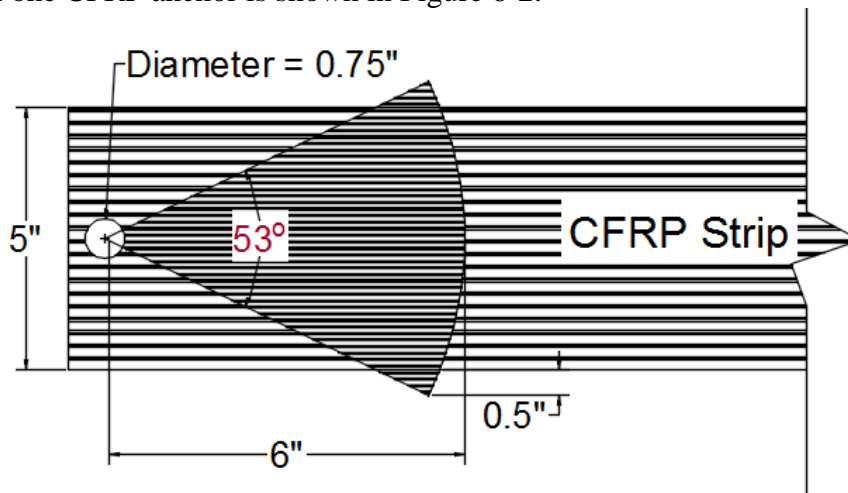


Figure 6-2 Layout of CFRP strip with one CFRP anchor

6.2.4 Design Example for Multiple Anchors

Assuming the required capacity of a CFRP strip is 11 kips. The manufacturer's reported thickness, elastic modulus, and effective strain of the CFRP strip are 0.02 in., 15,300ksi, and 0.004. The tensile strength of CFRP anchor is 143 ksi.

1. Determine the width of CFRP strips according to Equation 6-1

$$w_f = T_f / (t_f \times f_{fe}) \quad \text{in which } f_{fe} = \epsilon_{fe} E_f$$

$$w_f = 11 / (0.02 \times 0.004 \times 15300) = 8.99 \text{ in.}$$

Select a 9 in. strip with two anchors

2. Assuming a 1/2 in. diameter anchor, the area of CFRP anchor is

$$\pi(1/2)^2/4 = 0.2 \text{ in.}^2$$

3. Determine the required number for CFRP anchors based on Equation 6-3 and assuming the effective strip width for each anchor is 4.5 in. (9/2 in. = 4.5 in.). The value of ψ_a can be obtained by linear interpolation with the value of ψ_a on 5 in. and 3 in. strips.

$$\psi_a = 0.5 + (0.7 - 0.5) \times \frac{4.5 - 5}{3 - 5} = 0.55.$$

The tensile strength of CFRP is 143 ksi provided by manufacturer.

$$n_a \geq w_f t_f f_{ult} / (\psi_a f_{au} A_{anchor})$$

$n_a = (4.5 \times 0.02 \times 143) / (0.55 \times 143 \times 0.2) = 0.8 \leq 1$. Use two anchors for an effective strip width of 4.5 in. OK.

4. Determine the length of anchor fan using the recommended 60° fan angle for anchor design considering the effective width for each anchor to cover is 4.5 in.

$$L_{anchor} = \frac{(4.5/2 + 0.5)}{\tan(\frac{60}{2})} = 4.8 \text{ in.} \quad \text{Select a fan length of 5 in. (actual fan angle } 58^\circ = < 60^\circ,$$

OK).

5. Embedment length = 6 in.

6. Bending radius = 0.5 in.

7. Determine the diameter of anchor hole based on Equation 6-6.

$$d_{hole} = (4 \times 2.2 \times A_f / \pi)^{0.5}$$

Diameter of hole = $(4 \times 2.2 \times 0.1963 / \pi)^{1/2} = 0.74 \text{ in.}$ therefore use a 3/4 in. diameter hole.

The layout of CFRP strip with two CFRP anchors is shown in Figure 6-3.

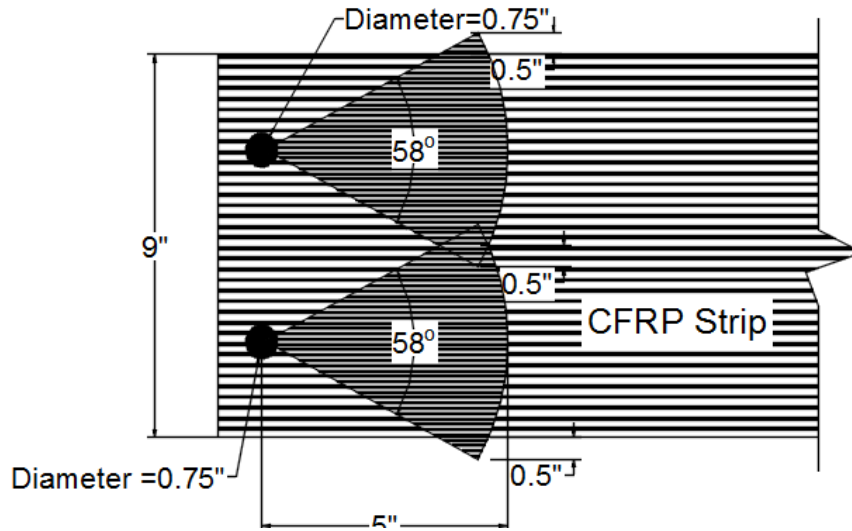


Figure 6-3 Layout of CFRP strip with two CFRP anchors

6.2.5 Limits of Existing Data

Limits on the design procedures resulted from the size of the test specimens. As indicated earlier, the size of the test specimen was chosen to permit easy handling in a materials test laboratory.

First, the 6 in. width of the beam does not permit more than a 5 in. wide CFRP strip or more than a single anchor at each end of the strip. Previous research (Orton et al, 2008), however, indicates a larger number of smaller CFRP anchors are more effective to fully develop tensile strength of CFRP strip than large anchors with the same amount of CFRP material.

Second, the tensile capacity of the concrete beam limits the strength of the layer or layers of CFRP that can be tested. A major problem with the strength of the beam was solved by adding CFRP strips on the side faces of beams. However, stronger (thicker) CFRP strips will increase the likelihood of a shear/tension failure of the beam. The only solution is to use a larger beam but handling of the test beam will be more difficult.

Third, the same CFRP material was used for both strips and anchors. The design recommendations need to address situations where strips and anchors may consist of two different CFRP materials (carbon or glass fibers, for example).

6.2.6 Summary

For a given tensile load, the design of CFRP anchor involves: determining the strength of the CFRP strip required, determining the area of the CFRP anchor and determining the geometry of the anchor fan angle, embedment length, diameter of anchor hole, and bend radius or chamfer of hole.

To optimize anchor design, more tests are required that focus on 1) how to more effectively use CFRP strips more than 5 in. wide; 2) how to anchor CFRP strips with large tensile capacity; and 3) how to design an anchorage system when strips and anchors are made using two different CFRP materials.

6.3 QUALITY CONTROL TEST

In previous research (Huaco, 2010; Pham, 2009), quality control tests are recommended for the purpose of 1) validation of the quality of anchor installation and 2) evaluation of the design parameters for different geometry and material characteristics.

The testing methodology with details of the construction of quality-control beam specimens was presented by Garcia et al. (2014). In that study, the same procedure was used for testing 35 specimens in which the focus was on evaluating one parameter at a time. The parameters studied were 1) width of CFRP strip, 2) strength ratio of CFRP strip to CFRP anchor, 3) concrete strength, 4) length of anchor fan, and 5) bonded/unbonded applications.

6.3.1 Criteria for Quality of Anchor Installation

The quality of an installation or of the work of an installer can be determined by the ability of the installed strengthening system to develop the design load. A qualified test is expected to result in fracture of the CFRP strip. Failures due to anchor rupture or delamination between anchor fan and the strip indicate that either the installation or the anchor design was

inadequate. In the field, the nondestructive testing (NDT) techniques may eventually enable evaluation of CFRP installations.

6.3.2 Criteria for Evaluation of the Anchor Design Geometry

As the use of CFRP increases, the need for expanding the range of parameters used in anchor designs will demand that further testing be done. The 6 in. by 6 in. by 24 in. concrete beams were convenient and sufficient for studying the strips and anchors used in this project. However, when higher capacity strips are needed or when anchor geometry or material (CFRP or concrete) changes, design guidelines will be needed to accommodate the higher capacities. It is likely that larger beams will be needed in many cases. Whatever the size of the beam or the strip capacity needed, the modes of failure that will need to be avoided are:

1. Anchor rupture.
2. Delamination of the strip to anchor connection.
3. Cracking (tension) and shear in the concrete beam near the anchor.

It may be possible to increase the capacity of the concrete beam to avoid a cracking or shear failure by using thicker CFRP U-wraps on the side faces of the concrete beam but that has not been studied in this program.

6.4 SUMMARY

Based on data from the experimental tests conducted in this study, design guidelines are proposed for developing the full strength of CFRP strips using CFRP anchors. Procedures are shown for determining the CFRP strip force needed and for detailing anchors that will develop the design strength of the strip. From the required strip force, the following details are determined: CFRP strip width, thickness, strength ratio of CFRP anchor to CFRP strip, anchor fan length/angle, embedment length, and size and chamfer of the anchor hole.

The concrete beam design used in the experimental portion of the study was shown to work well for qualifying CFRP installations, designs of anchorage systems, and FRP materials.

The beam design is light-weight and convenient for use in a material testing laboratory as it can be manipulated without lifting equipment. It was shown however, that the concrete beam design has limitations that prevented the study of strips with larger capacity and strips with multiple anchors.

CHAPTER 7

Summary and Conclusions

7.1 SUMMARY

Carbon Fiber Reinforced Polymer (CFRP) materials are widely used to strengthen reinforced concrete structures because they are light-weight, have high strength, and are relatively easy to install. In strengthening applications, CFRP strips are typically attached to the concrete surface using epoxy resin with fibers oriented in the direction needing additional tensile strength. However, if CFRP strips rely exclusively on bond strength with concrete, only 40 to 50% of the CFRP tensile strength can be developed before debonding failure occurs. In order to fully develop the tensile strength of CFRP strips, some form of anchorage is needed. CFRP anchors can be applied with relative ease and have recently been shown to provide effective anchorage of CFRP strips to concrete members.

The objectives of this research project were: 1) to provide guidelines for designing CFRP anchorage systems capable of developing the full strength of CFRP strips, 2) investigate “best” practices for simulating the behavior of anchored CFRP strips, and 3) to provide a simple test specimen and methodology for qualifying the installation and materials of FRP anchorage systems. Three main tasks were conducted to achieve the objectives: 1) an extensive experimental testing program was undertaken to explore the influence of key parameters on the performance of anchorage systems, 2) an FE model capable of simulating the behavior of test specimens was selected, calibrated, and validated using experimental data, and 3) design guidelines for CFRP anchorage systems and a test methodology for quality control were developed.

7.1.1 Experimental Program

A test methodology based on the standard test method for flexural strength of concrete using a simple beam with center-point loading was designed to study the behavior of anchored

CFRP strips attached to the tensile surface of a plain concrete member. Failure modes, ultimate load in anchors at failure, and strain distributions on the CFRP strips were used to evaluate test results. An adequate anchorage system is expected to either fracture the CFRP strip or develop an ultimate load larger than the manufacturer specified strength.

The influence of key parameters on the strength of CFRP anchorage systems was investigated through 39 tests performed on 6 in.×6 in.×24 in. concrete beams. Explored parameters were: 1) the width of the CFRP strip, 2) the material ratio of CFRP strip to CFRP anchor, 3) the concrete strength, 4) the length/angle of anchor fan, and 5) bonded/unbonded applications.

Test results demonstrated that the strength of a CFRP anchorage system is mainly determined by the amount of material used in CFRP anchors and the width of CFRP strip being developed.

7.1.2 Simulation of Test Specimen Behavior using FE Model

A three-dimensional continuum finite element model was built to identify simulation tools that are best suited for numerical study of the load transfer mechanisms between CFRP strips and CFRP anchors. Concrete, CFRP, and interfacial materials were modeled by 8-node solid elements, truss elements, and nonlinear spring elements respectively. Those elements are the available in most commercial FE software. Six simulations were conducted using the model to explore the ability of the computational model to simulate the behavior of CRP anchorage systems within the parameter limits tested. Parameters varied in the six FE simulations were: 1) the anchor-material ratio, 2) the concrete strength, 3) the length of anchor fan, and 4) the bond condition between CFRP and concrete. The behavior of each simulation was compared to that of comparable specimen tests. Globally, all simulations performed well and estimated the failure load and the load versus deflection responses with good accuracy. Locally, the load versus CFRP strains responses of the FE simulations showed similar trends as those observed in comparable experimental tests. For some tests however, the FE simulations reproduced CFRP strains with

good accuracy, while for other nominally identical tests the FE simulations did not perform as well. High variability in the experimental response of nominally identical test specimens was the main source of the discrepancy with FE simulation results. The largest errors in strains between simulation estimates and experiments were observed at the edges of the CFRP strips and around the discontinuity in CFRP area at the anchor fan ends.

Sensitivity studies were conducted to evaluate the influence of CFRP modulus of elasticity, resin epoxy modulus, and bond conditions on the proposed computational model. Overall, changing the CFRP modulus (from 13,000 ksi to 15,000 ksi), the modulus of epoxy (from 421 ksi to 922 ksi), and using either a steep or gradual descending slope for the bond stress-slip response produced limited changes on the load-deflection response and load-strain responses at mid-span. Using either a larger epoxy modulus or a more gradual descending slope for bond stress-slip model tends to produce a stiffer load-deflection curve after concrete cracked.

The computational model was used to predict the response of anchorages tested by Huaco (2009). Good agreement between experimental and numerical results for load-deflection and load-strain responses demonstrated the capability of the proposed models for predicting the behavior of anchored CFRP strip systems other than tested in this study.

7.1.3 Design Guidelines and Quality Control

Design guidelines for CFRP anchors were proposed based on test results. Given a required CFRP strip area, the area and number of CFRP anchors required to develop the strip are provided. To fully develop the tensile strength of CFRP strips, recommendations for selecting anchor details such as anchor fan angle, embedment length, diameter of anchor hole, and bending radius or chamfer of hole are provided. The proposed anchor design guidelines take into account the lower efficiency that anchors exhibit when developing wider strips.

The concrete beam design used in the experimental portion of the study was shown to produce a reasonable way to qualify installers, designs of anchorage systems, and FRP materials. The beam design is light-weight and convenient for use in a material testing laboratory as it

could be moved and positioned without lifting equipment. It was shown however that the concrete beam design has limitations that prevented the study of strips with larger capacity and strips with multiple anchors.

7.2 CONCLUSIONS

Conclusions of this research program were drawn from both experimental and numerical results.

7.2.1 Effects of Width of CFRP Strip

Test results show that increasing the width of a CFRP strip decreases the efficiency of the strip and anchorage system at carrying required forces. Consequently, an increase in strip width results in a less than proportional increase in strip strength. A larger strength-ratio of CFRP anchors (or material-ratio for same strip and anchor materials) is also required to strengthen a wider CFRP strip as anchors are not as efficient in resisting loads from wider strips.

7.2.2 Anchor-Material Ratio

Anchor-material ratio is a major factor in determining the ultimate tensile strength developed in a CFRP strip and the failure mode. Higher anchor-material ratios were found to significantly increase the strength of strips at fracture. The maximum stress in the CFRP strips was found to be reduced significantly as the anchor-material ratio is increased. Possibly, anchors with higher anchor-material ratios are able to distribute stresses and strains more evenly across the width of strips than anchors with lower material ratios; the result of which is an increase in the average stress in strips before the critical location of maximum stress initiates strip fracture. However, test results showed that increasing the anchor-material ratio results in a less than proportional increase in anchor strength.

7.2.3 Concrete Strength

Concrete strength is a parameter with limited influence on the bond strength between CFRP strip and concrete substrate. Higher strength concrete produces higher bond strength, which tends to delay the debonding of CFRP strips from the concrete substrate. Higher concrete strength was found to increase moderately but noticeably both CFRP strip and anchor strengths. Possibly, in areas where CFRP strips remain bonded just prior to anchor failure, the higher bond strength between CFRP strip and concrete may help increase the apparent strength of the anchor. Another possibility could be that the stiffer higher-strength concrete may help distribute anchor stresses more evenly at the anchor bend. More studies are needed to investigate this effect further.

7.2.4 Anchor fan length / Anchor fan angle

Anchor fan angles ranging from 37° to 64° were investigated. Within that range of angles, no significant changes in strip or anchor strengths were observed.

7.2.5 Bonded versus Unbonded Applications

Adequate bond helps transfer tensile forces from CFRP strips to CFRP anchors. In this study, unbonded strips failed at loads lower than their design strength. Lower tensile loads were transferred by the anchors to the strips in unbonded cases compared with the bonded cases. Without adequate bond, anchors need to be designed for higher loads than when bond is provided.

7.2.6 Finite Element Analysis

The behavior of the CFRP strips and the CFRP anchors can be captured by the proposed FE model with good accuracy. The model is simple to use and be built in most commercial FE software. A novel approach to simulate interface bond through a nonlinear spring element applied perpendicular to the concrete surface allows the model to simulate bond behavior in the plane of the bond surface. Globally, beam load versus deflection responses compared well

between all six FE simulations and comparable experimental tests. In addition, the models predicted the failure load of tests with good accuracy when strip fracture was the mode of failure. Locally, load versus CFRP surface strains in the beam longitudinal direction had similar trends in the FE simulations as those observed in experiments. The largest CFRP strain errors between models and experiments were observed at the edges of the CFRP strip and around the discontinuity in CFRP area at the anchor fan ends. Discrepancies between analysis and experiments can mainly be attributed to differences between the bond-slip relations in the models and those in the tests. Experimentally, however, the bond-slip relation was observed to vary significantly between nominally identical specimens. The bond-slip relations chosen in the simulations were calibrated to the average of the experimentally obtained bond-slip relations. The simulations captured the behavior of the CFRP strips and the CFRP anchors as demonstrated by the favorable comparison between computational and experiment results for a specimen with unbonded CFRP strips.

The modulus of CFRP and epoxy as well as the descending slope of bond stress-slip model are less sensitive parameters and produce limited changes on load-deflection and load-strain responses. The proposed FE model was used to predict with good accuracy the load-deflection and load-strain responses of tests which are not part of this study.

Further research is needed to understand the load and strain distributions at the anchor end before anchor failure. Additional calibrations for bond-slip models, anchor fan stiffness, and strip in-plane stiffness would be useful in improving proposed model accuracy.

7.2.7 Quality Control Test

The concrete beam design used in the experimental portion of the study was shown to produce a reasonable way to qualify installers, designs of anchorage systems, and FRP materials.

7.3 DESIGN RECOMMENDATIONS

Guidelines for the design of CFRP anchors that develop the full tensile strength of CFRP strips are provided. For a given tensile load, the design of CFRP anchor involves: determining the strength of the CFRP strip required, determining the area of the CFRP anchor and determining the geometry of the anchor fan angle, embedment length, diameter of anchor hole, and bend radius or chamfer of hole. Guidelines for selecting all the aforementioned anchor parameters are given.

7.4 FUTURE WORK

1. Different beam designs are needed to study a wider range of CFRP anchor applications; such as applications with wider strips, strips with multiple anchors, and multi-layered strips necessary for the strengthening of large members.
2. Further research is needed to understand the load and strain distributions at the anchor end before anchor failure. Additional calibrations for bond-slip models, anchor fan stiffness, and strip in-plane stiffness would be useful in improving proposed model accuracy. Additional sensitivity studies on the peak bond stress would be helpful to understand the effect of peak bond stress on failure load.

APPENDIX A

CFRP Material Properties

Table A-1 CFRP strips properties provided by the manufacturer

Property	ASTM Method	Typical Test Value	Design Value
Ultimate tensile strength (ksi)	D-3039	143	121
Elongation at break	D-3039	0.93%	0.79%
Tensile Modulus (ksi)	D-3039	15300	13000

APPENDIX B

Epoxy Resin Material Properties

Table B-1 Epoxy resin Properties provided by the manufacturer

Property	ASTM Method	Typical Test Value
Tensile strength (ksi)	D-638 Type 1	10.5
Tensile Modulus (ksi)	D-638 Type 1	461
Elongation Percent	D-638 Type 1	5.0%

APPENDIX C

Experimental Specimens Details

Construction and installation details of the specimens with 5 in. and 3 in. strips in this reported research are presented in this Appendix.

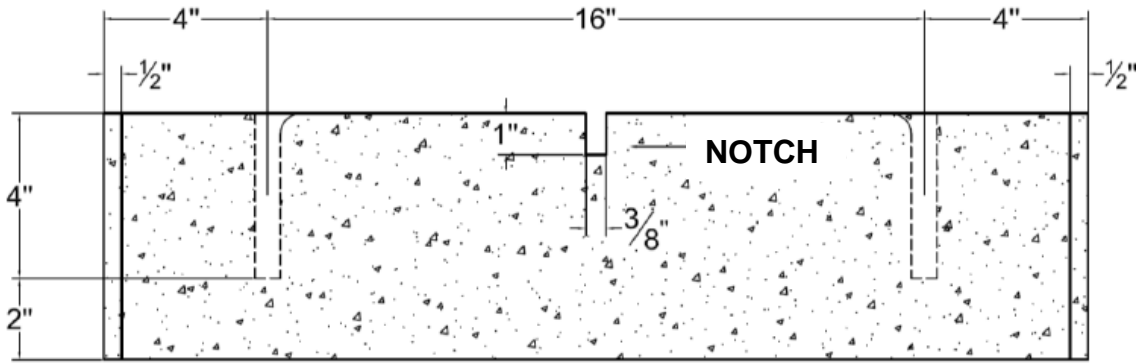


Figure C-1 Side view without CFRP

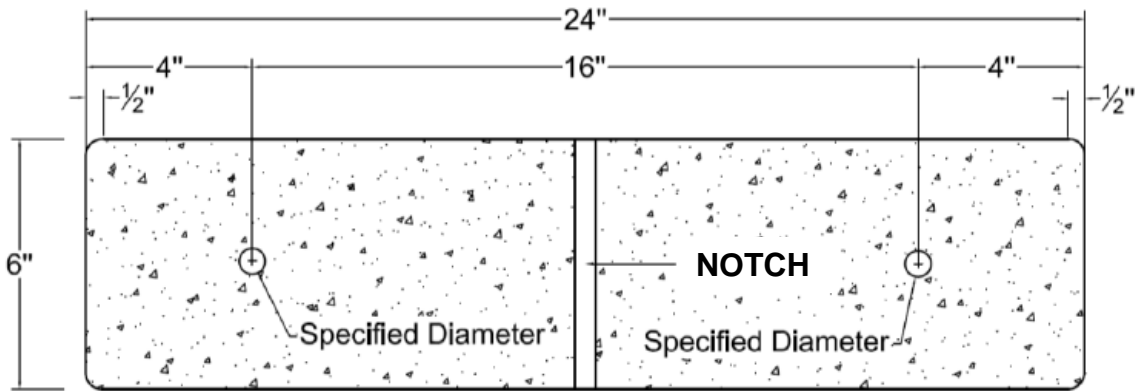


Figure C-2 Bottom view without CFRP

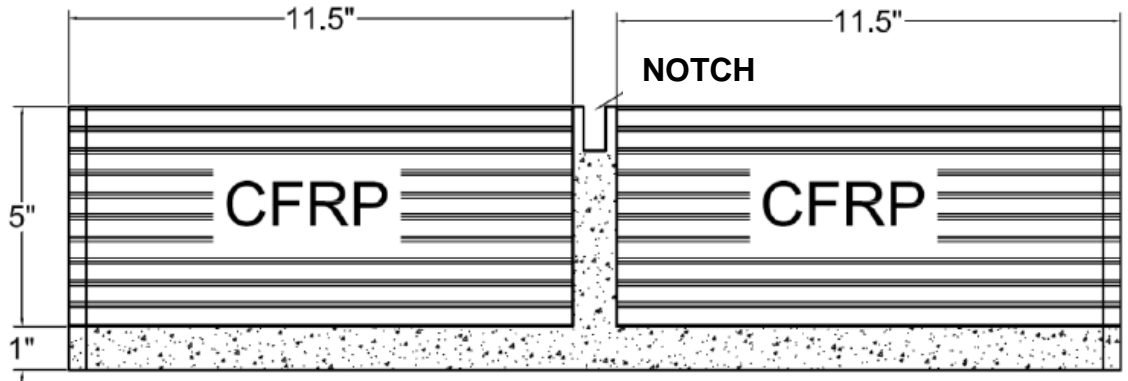


Figure C-3 Side view with CFRP

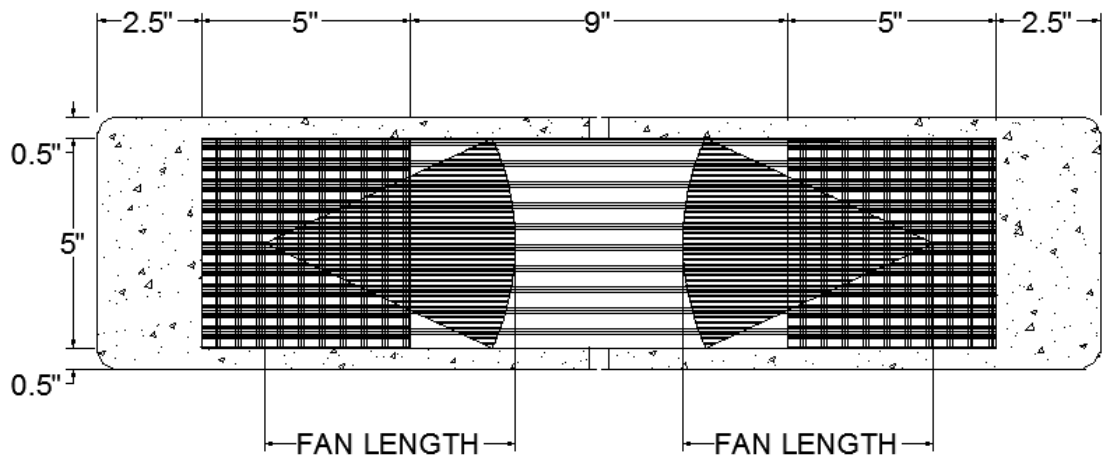


Figure C-4 Bottom view with 5 in. CFRP strip

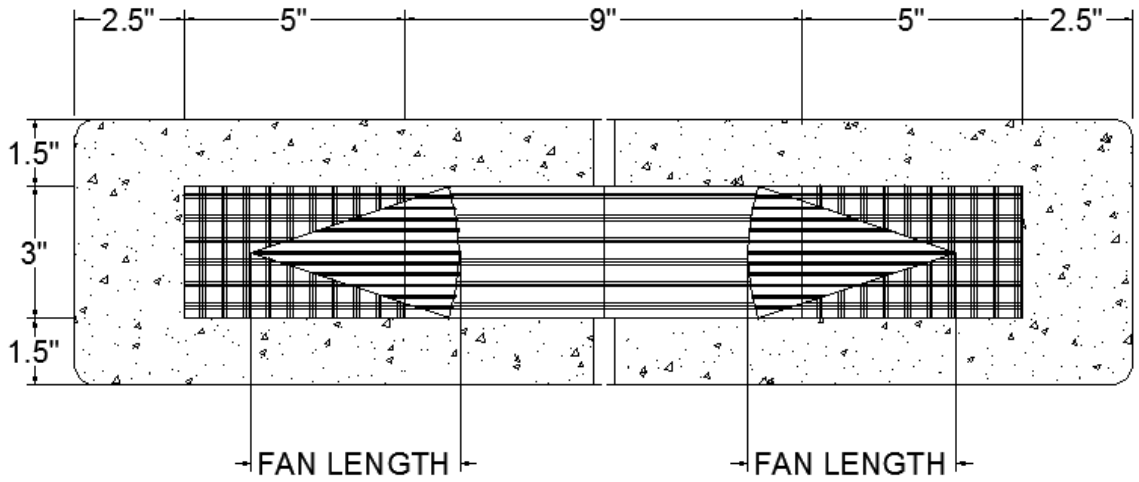


Figure C-5 Bottom view with 3 in. CFRP strip

APPENDIX D

This research is able to provide contour plots for 22 tests in which 21 were shown in this section and another one was shown in section 4.2.1. UTVS was not available for 2 tests. The rest 15 tests failed to show strain developing contours due to local targets lost, local glare issue or local shade issue. Most of targets in those tests, however, performed well to provide reliable results during entire tests. The analysis of those tests was based on those available experimental results,

Contour Plots

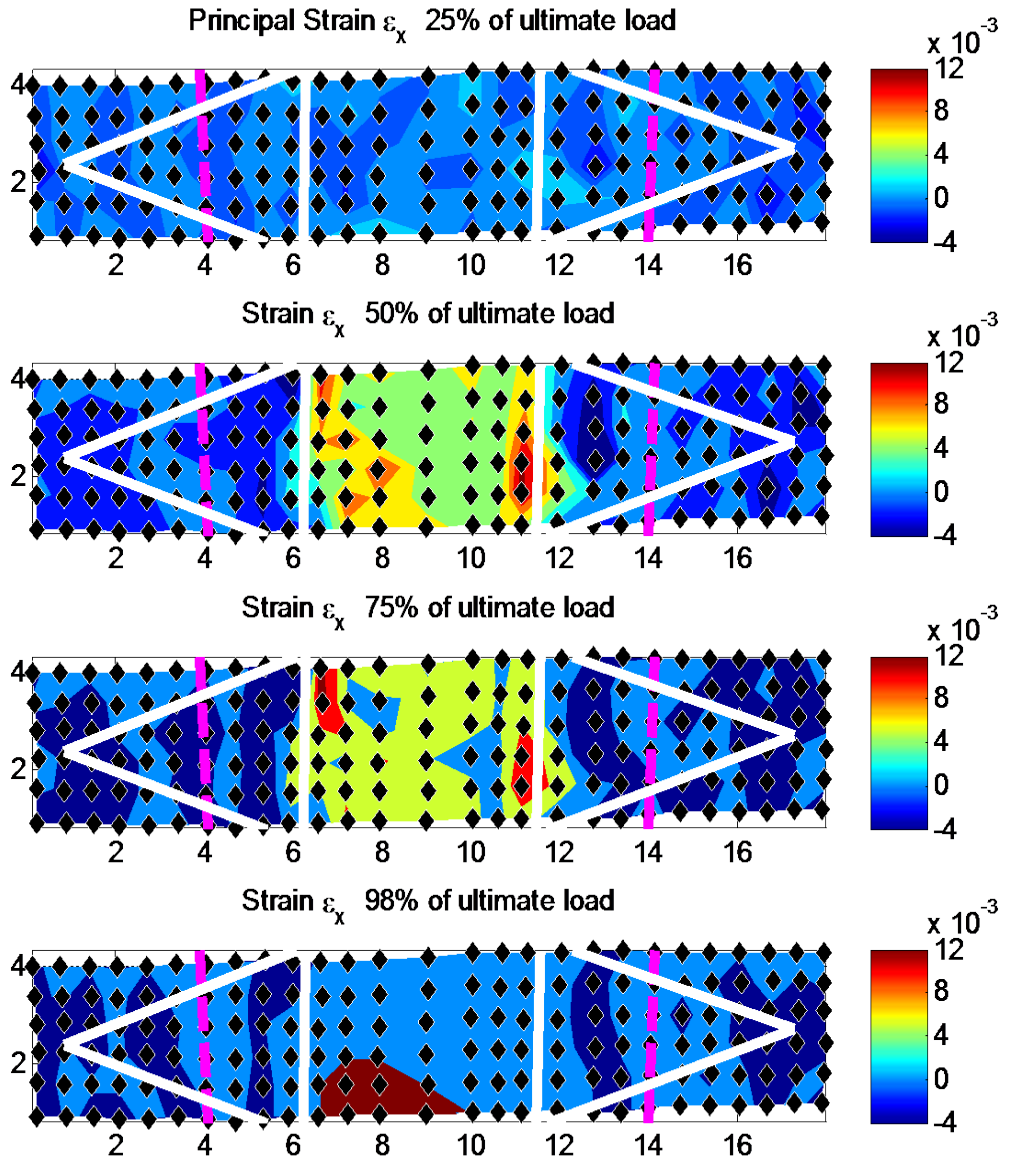


Figure D-1 Contour plots for B5H2Ma

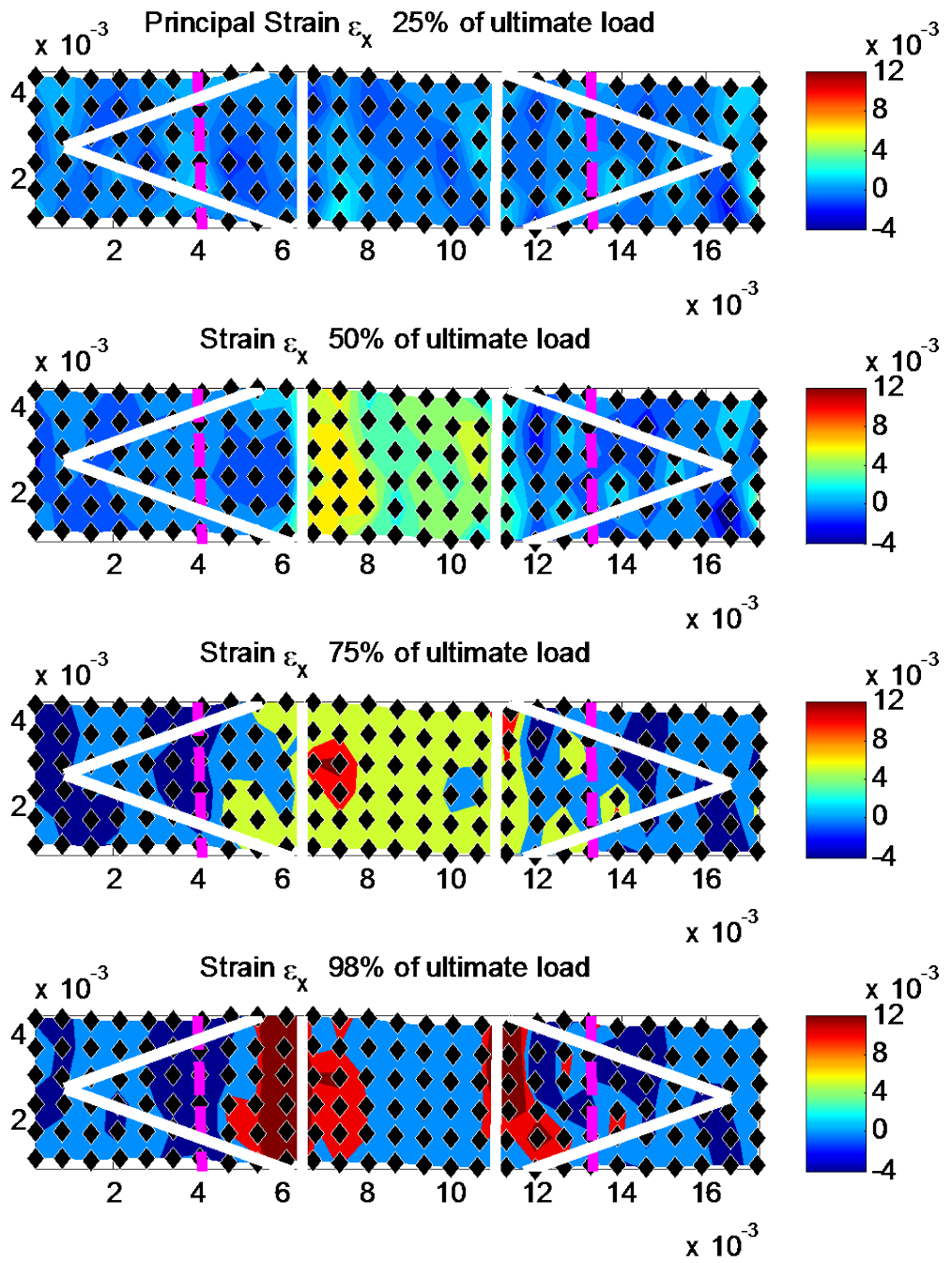


Figure D-2 Contour plots for B5H1.4Mc

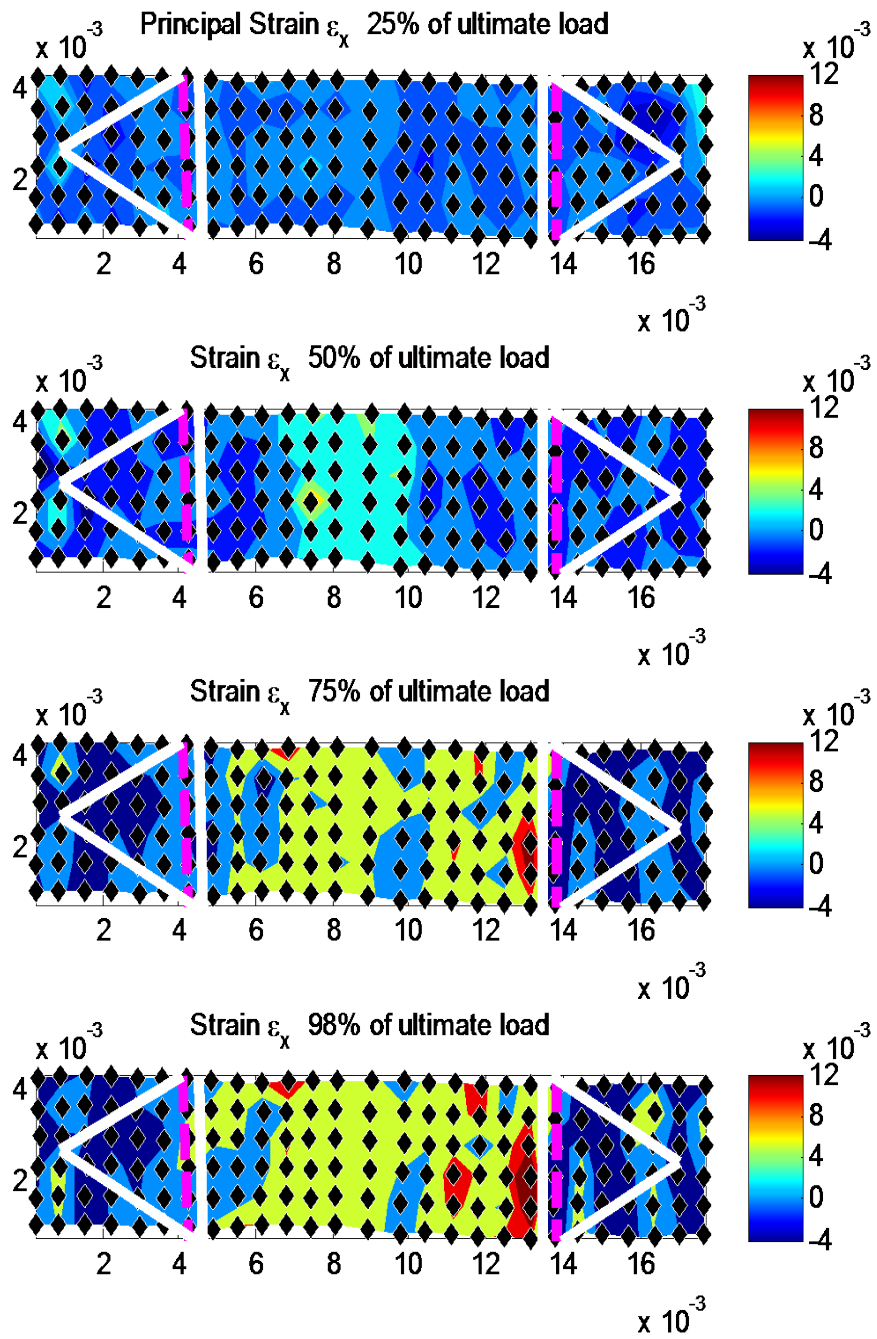


Figure D-3 Contour plots for B5H1.4Sa

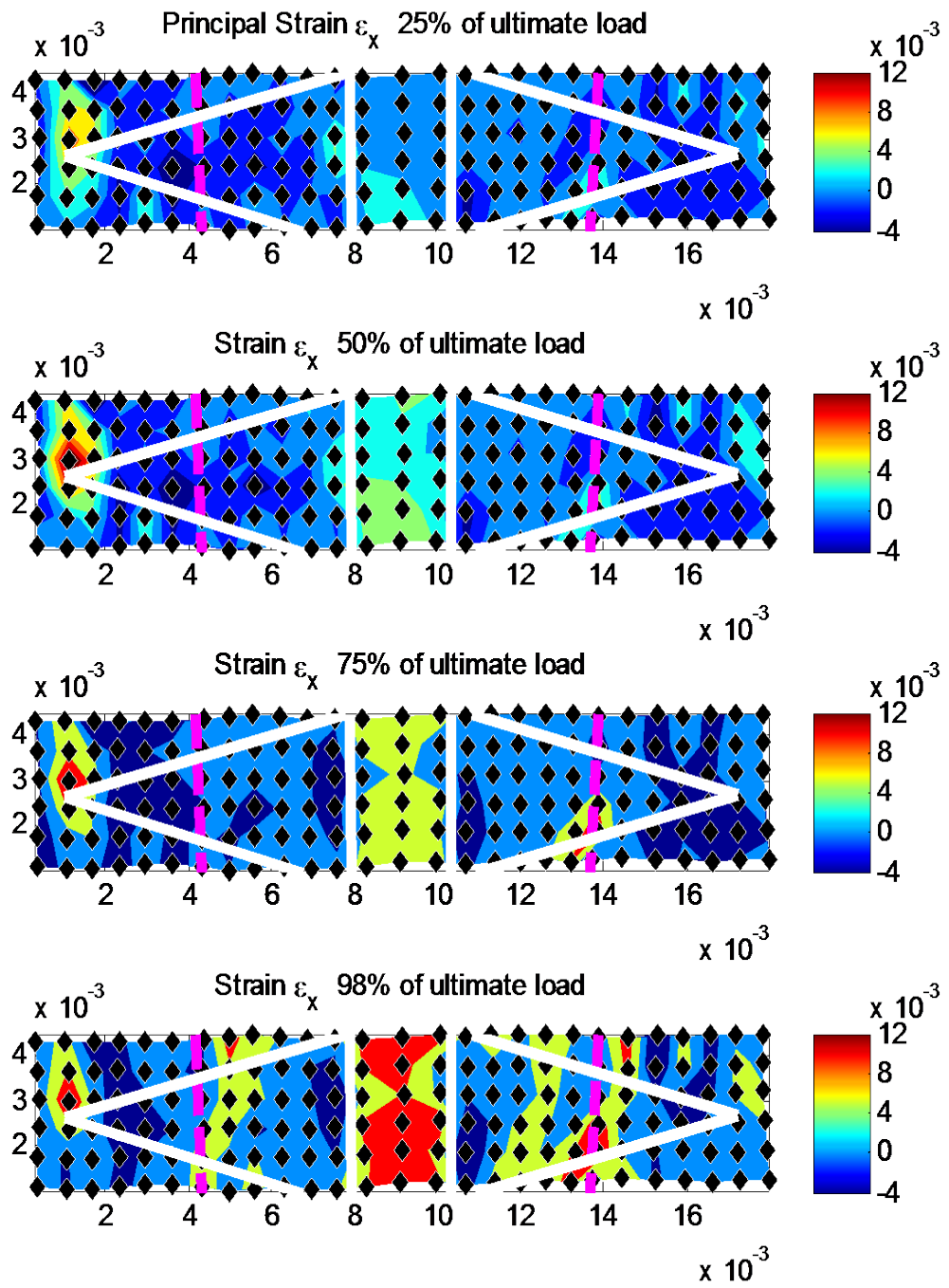


Figure D-4 Contour plots for B5H1.4La

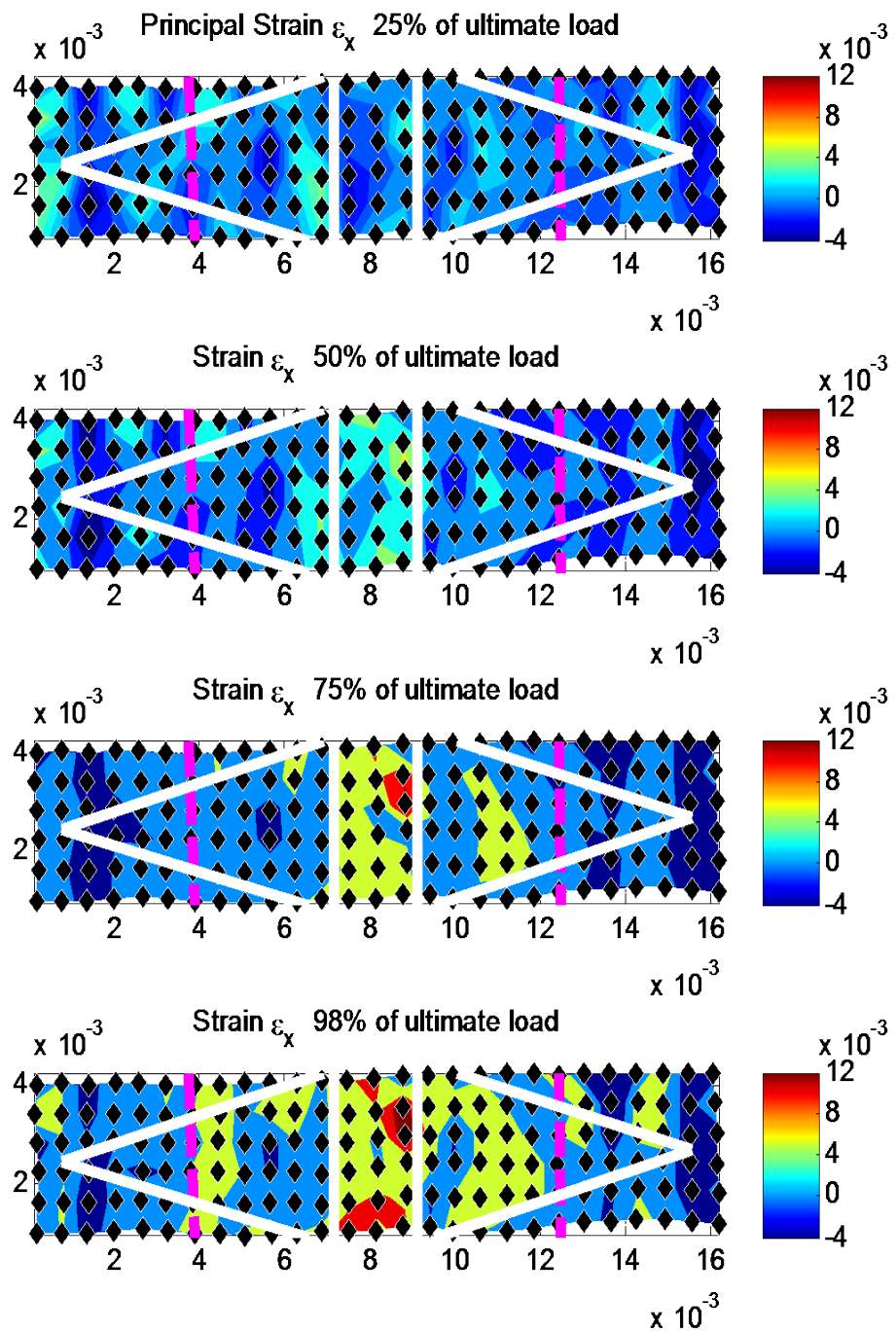


Figure D-5 Contour plots for B5H1.4Lb

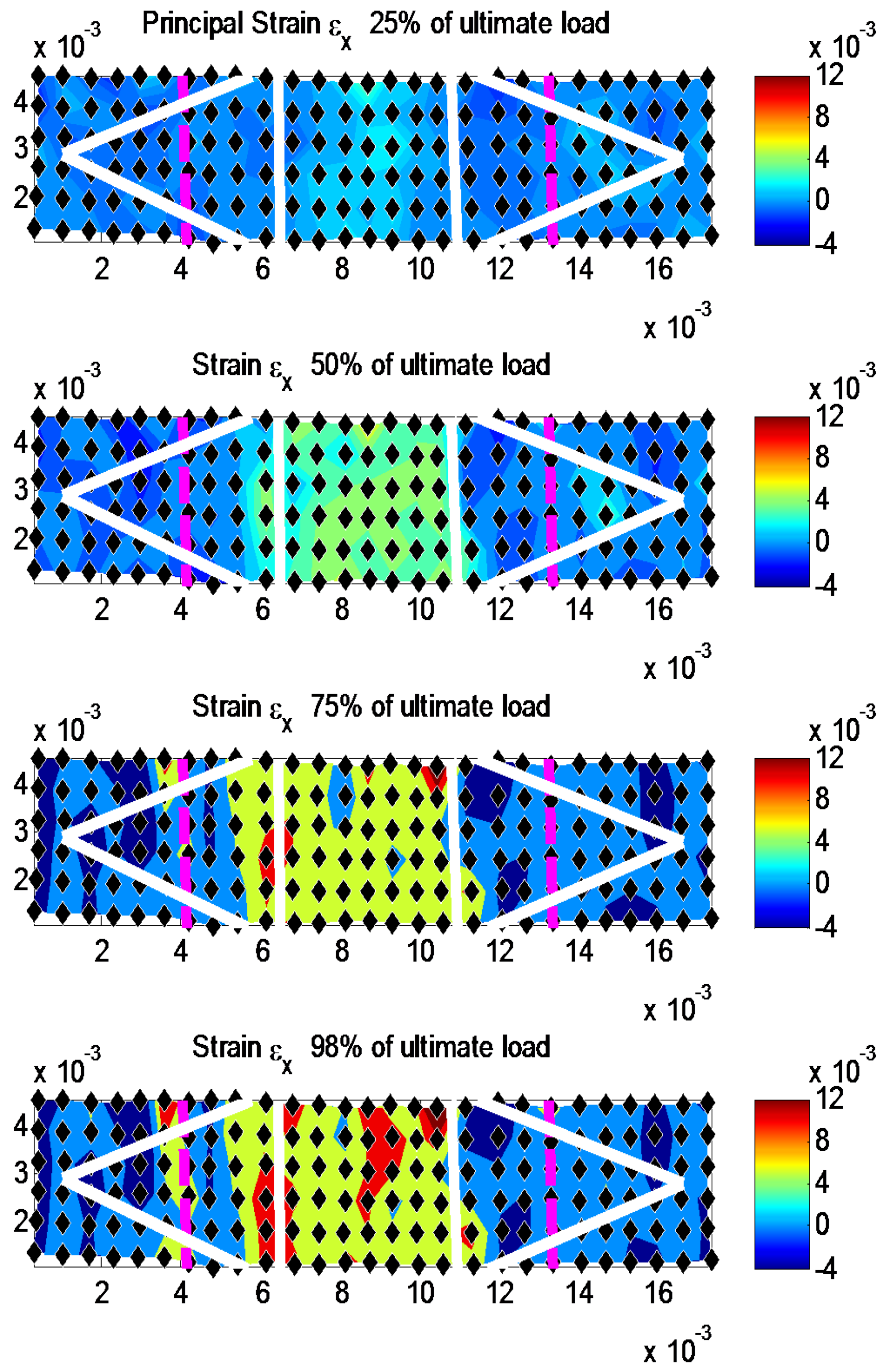


Figure D-6 Contour plots for B5L1.4Mc

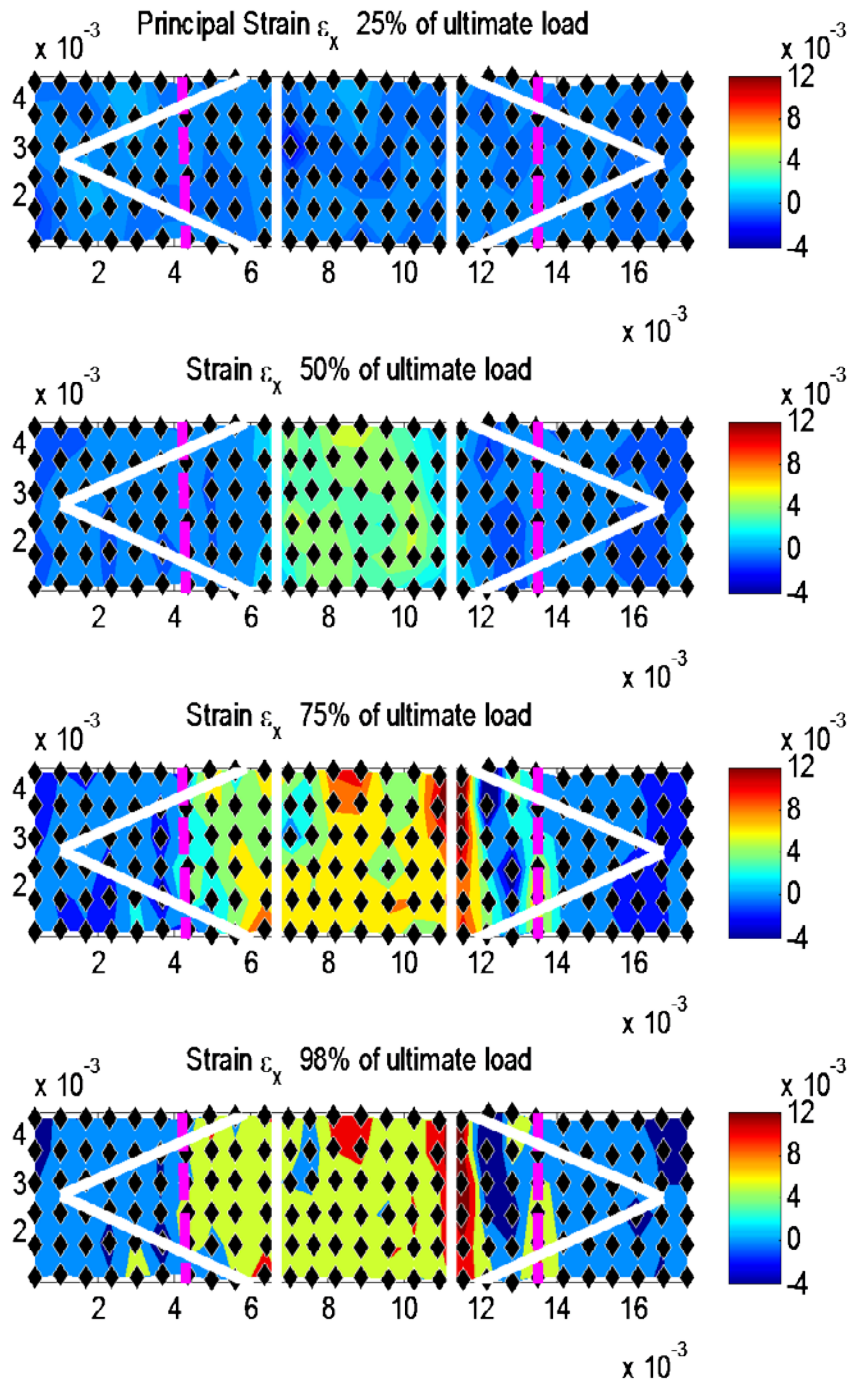


Figure D-8 Contour plots for B5HIMc

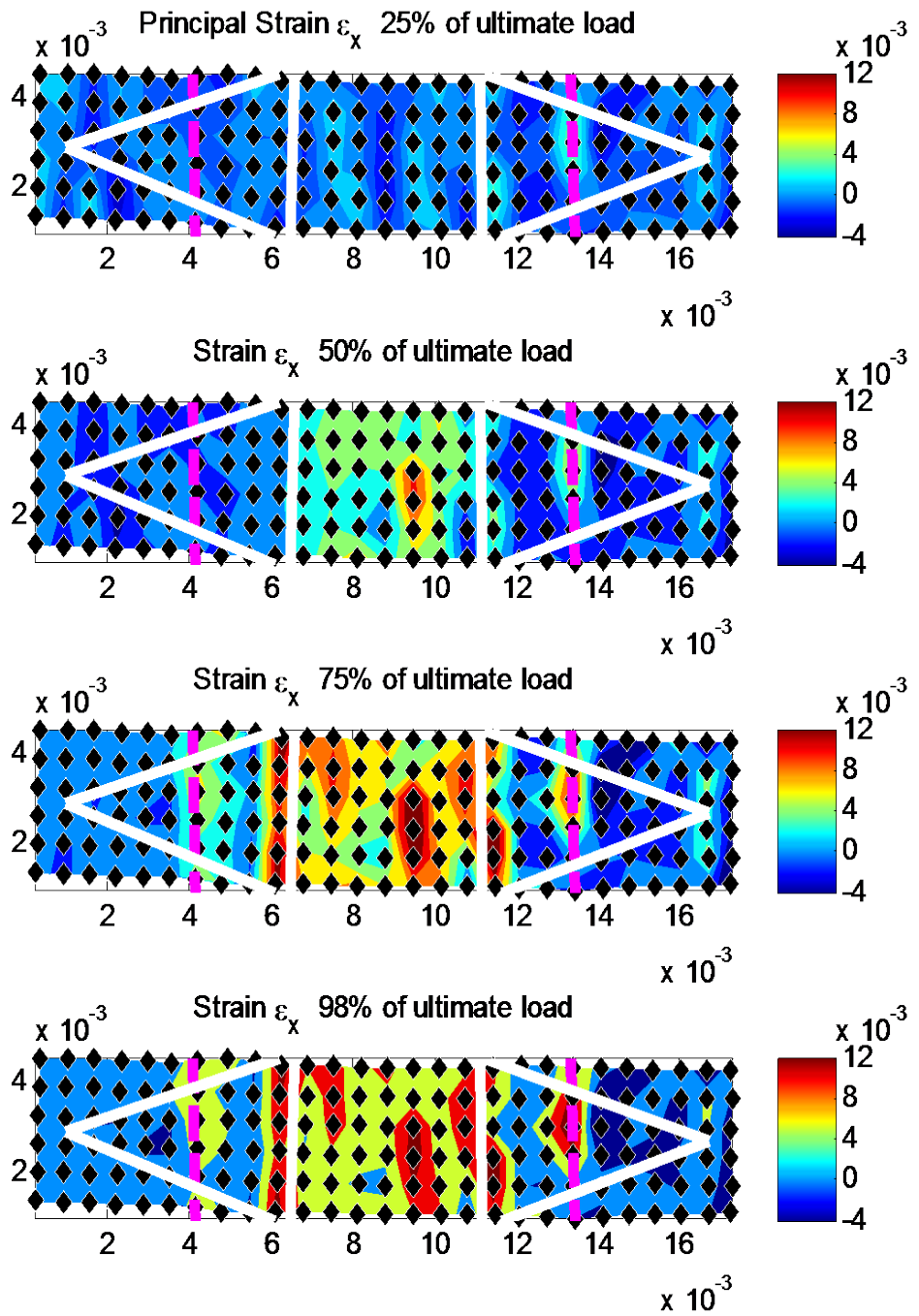


Figure D-9 Contour plots for B5HIMd

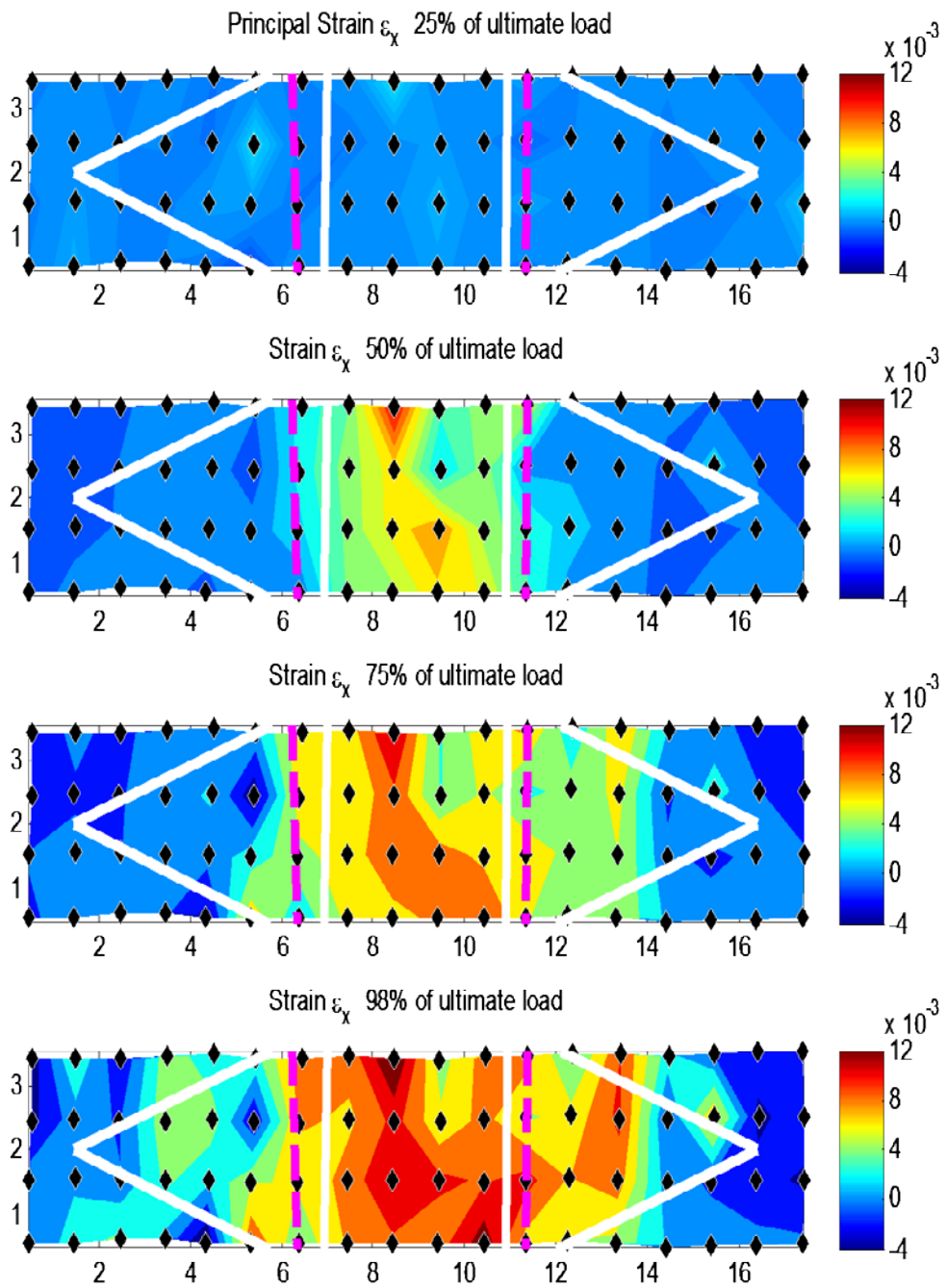


Figure D-10 Contour plots for B5L1Me

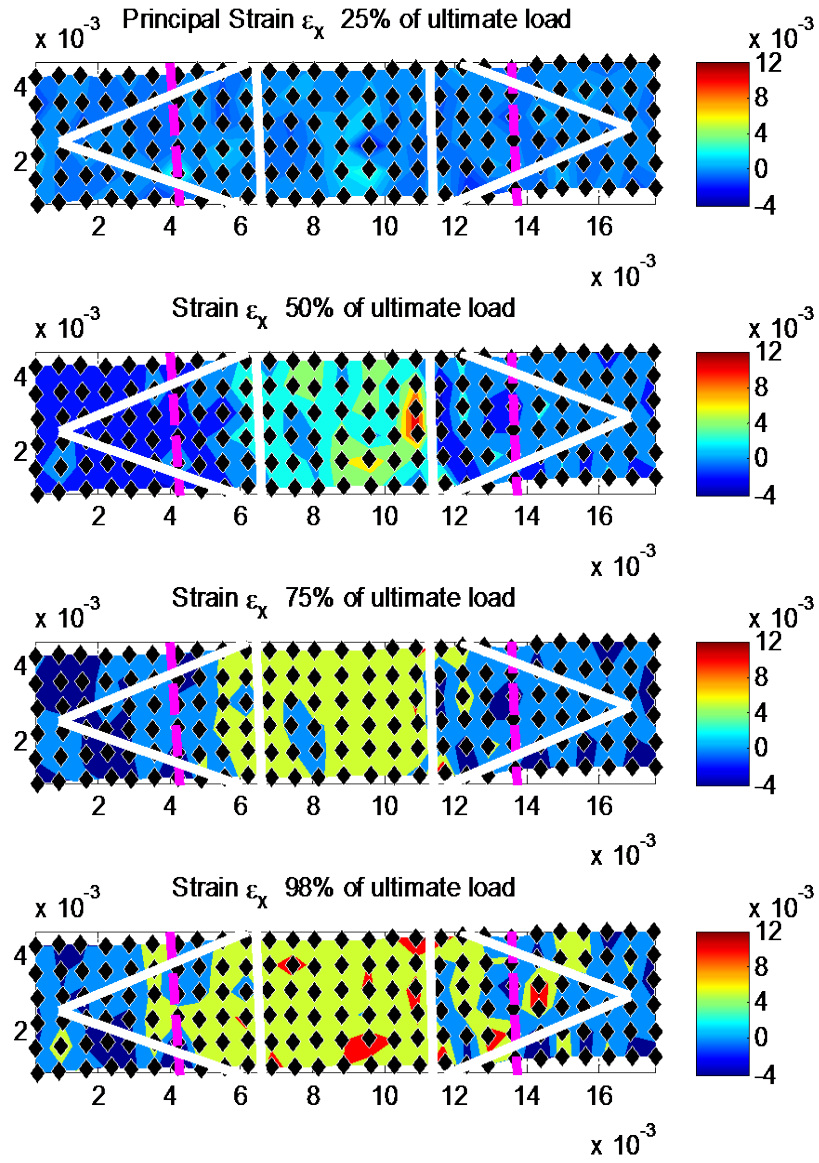


Figure D-11 Contour plots for B5L1Mg

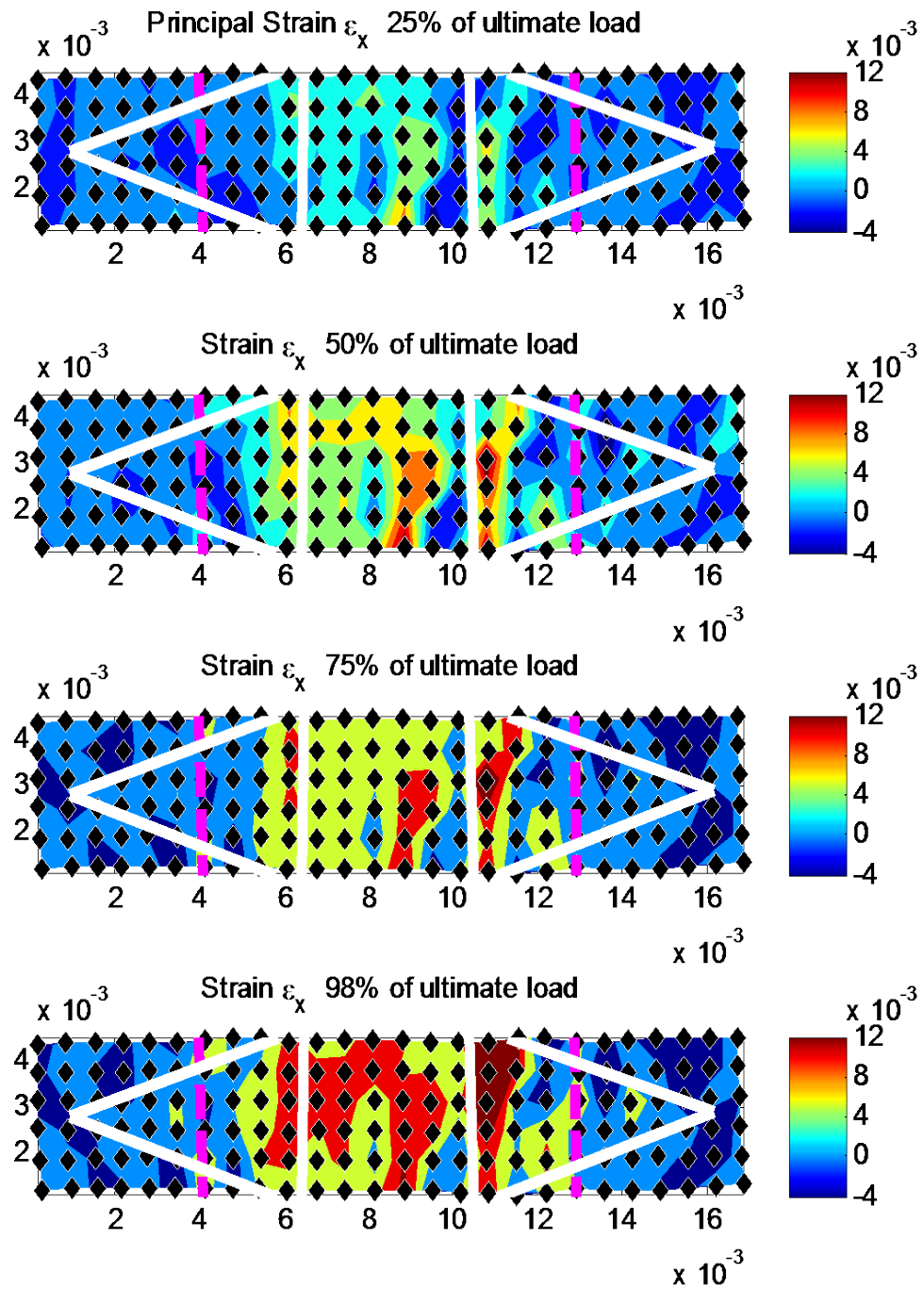


Figure D-12 Contour plots for U5H1.4Mb

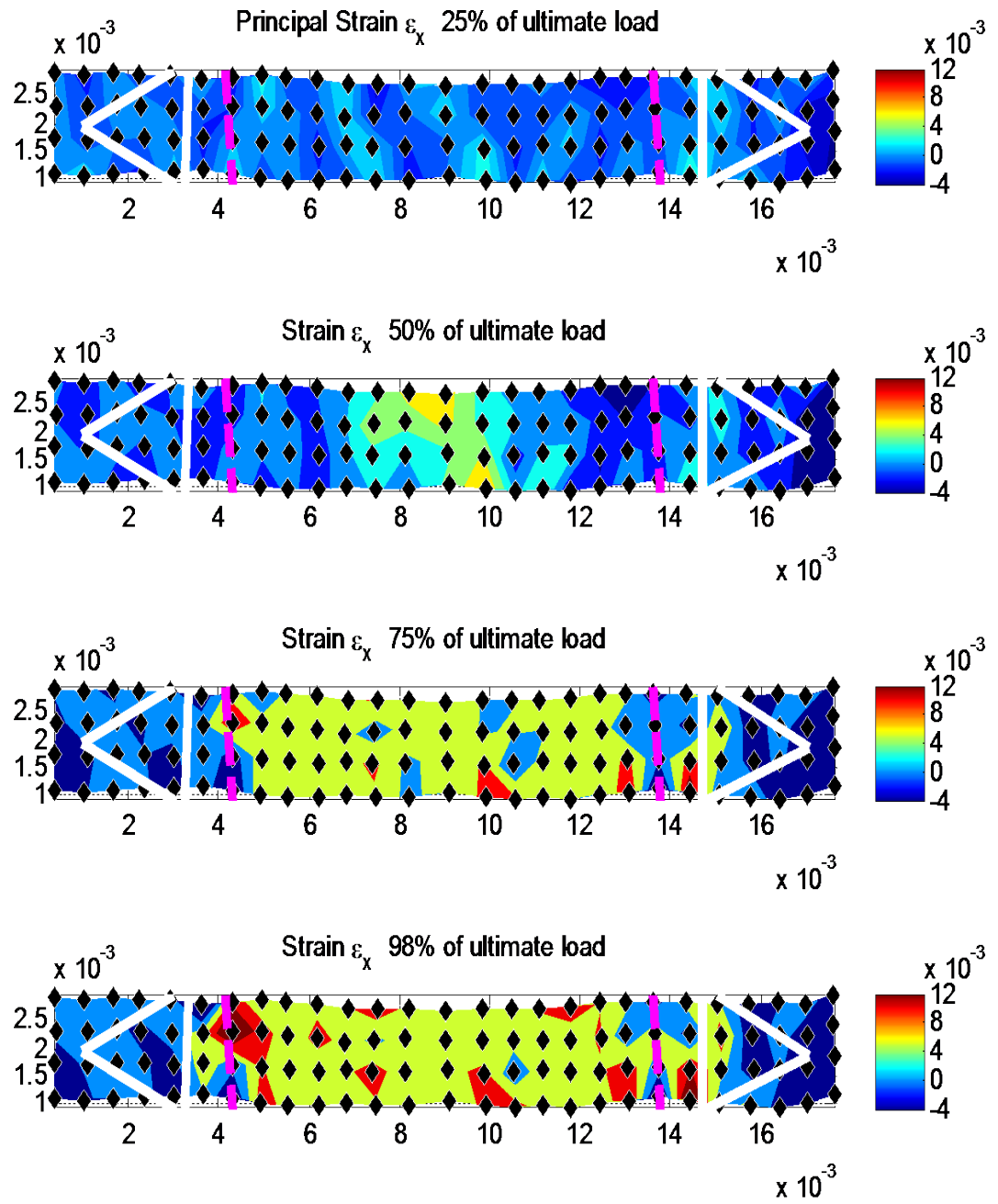


Figure D-13 Contour plots for B3H1.4Sa

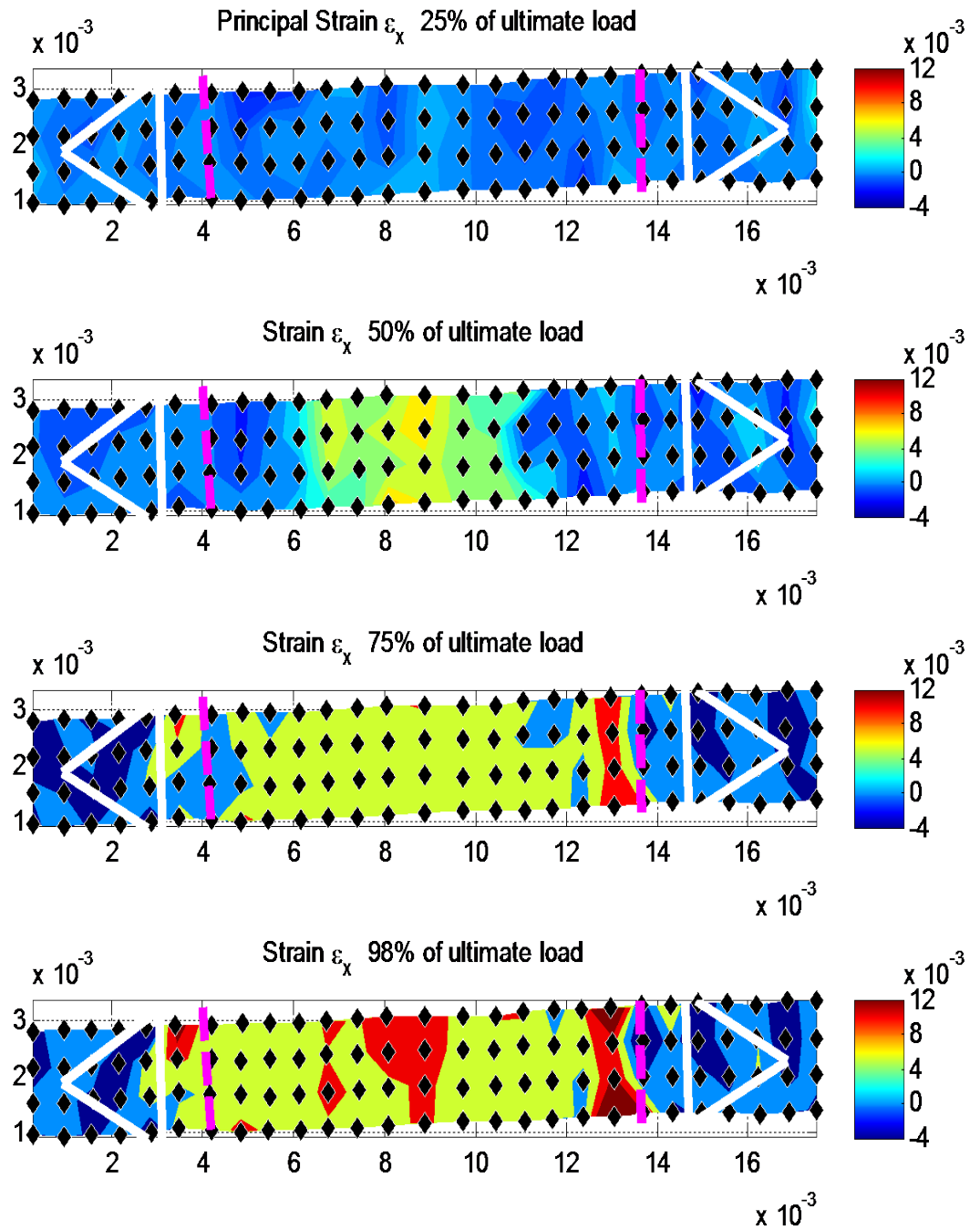


Figure D-14 Contour plots for B3H1.4Sb

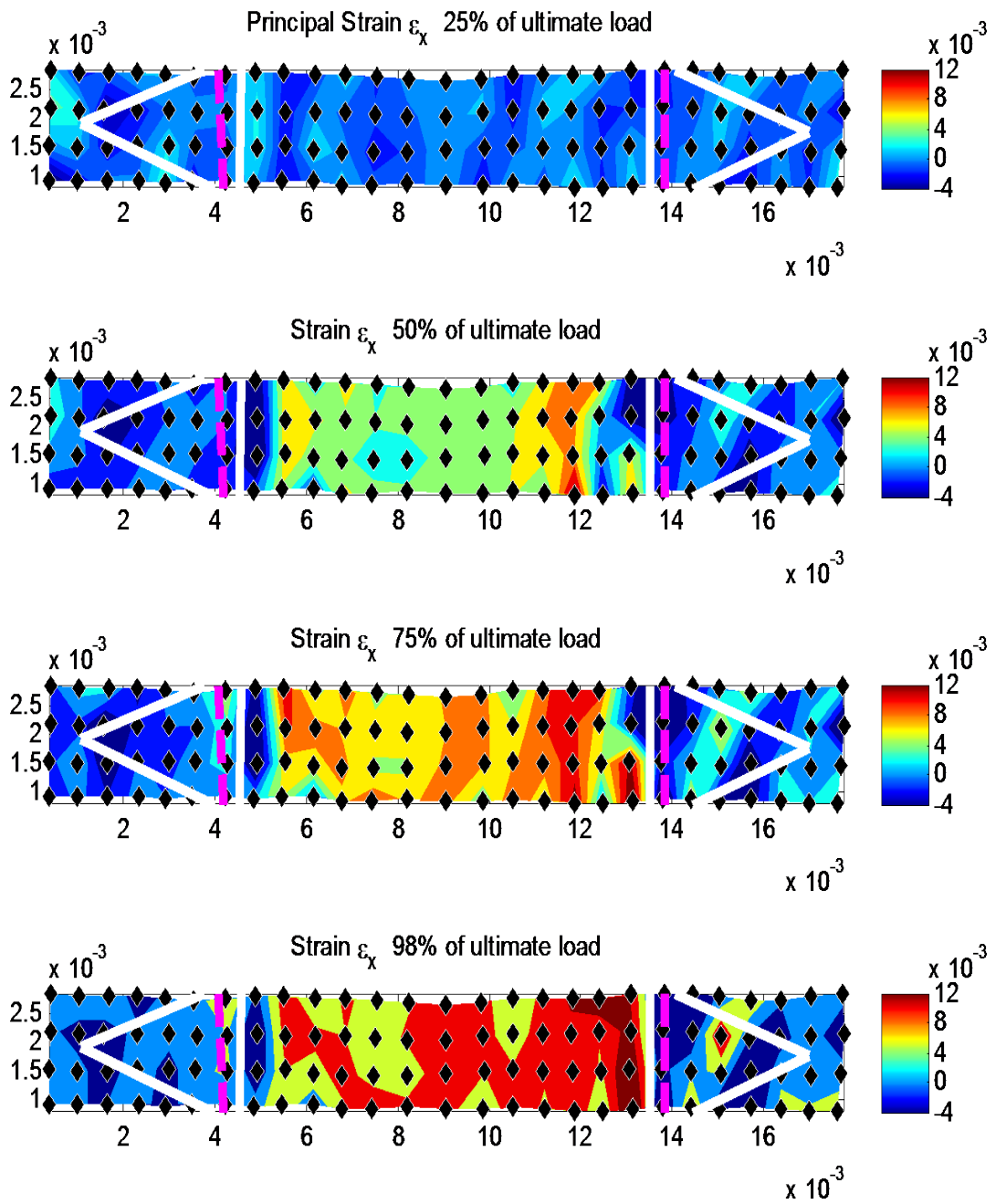


Figure D-15 Contour plots for B3H1.4Ma

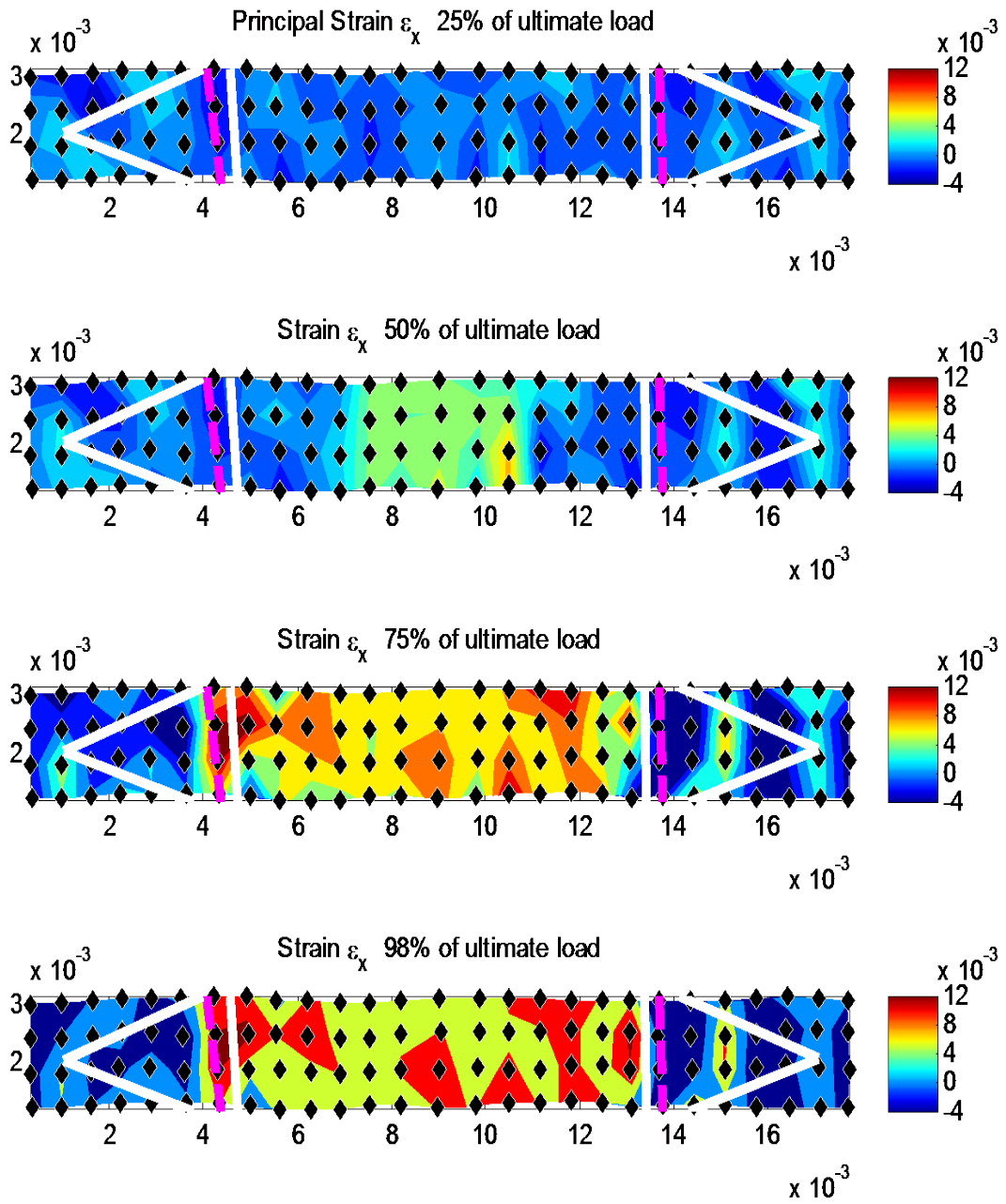


Figure D-16 Contour plots for B3H1.4Mb

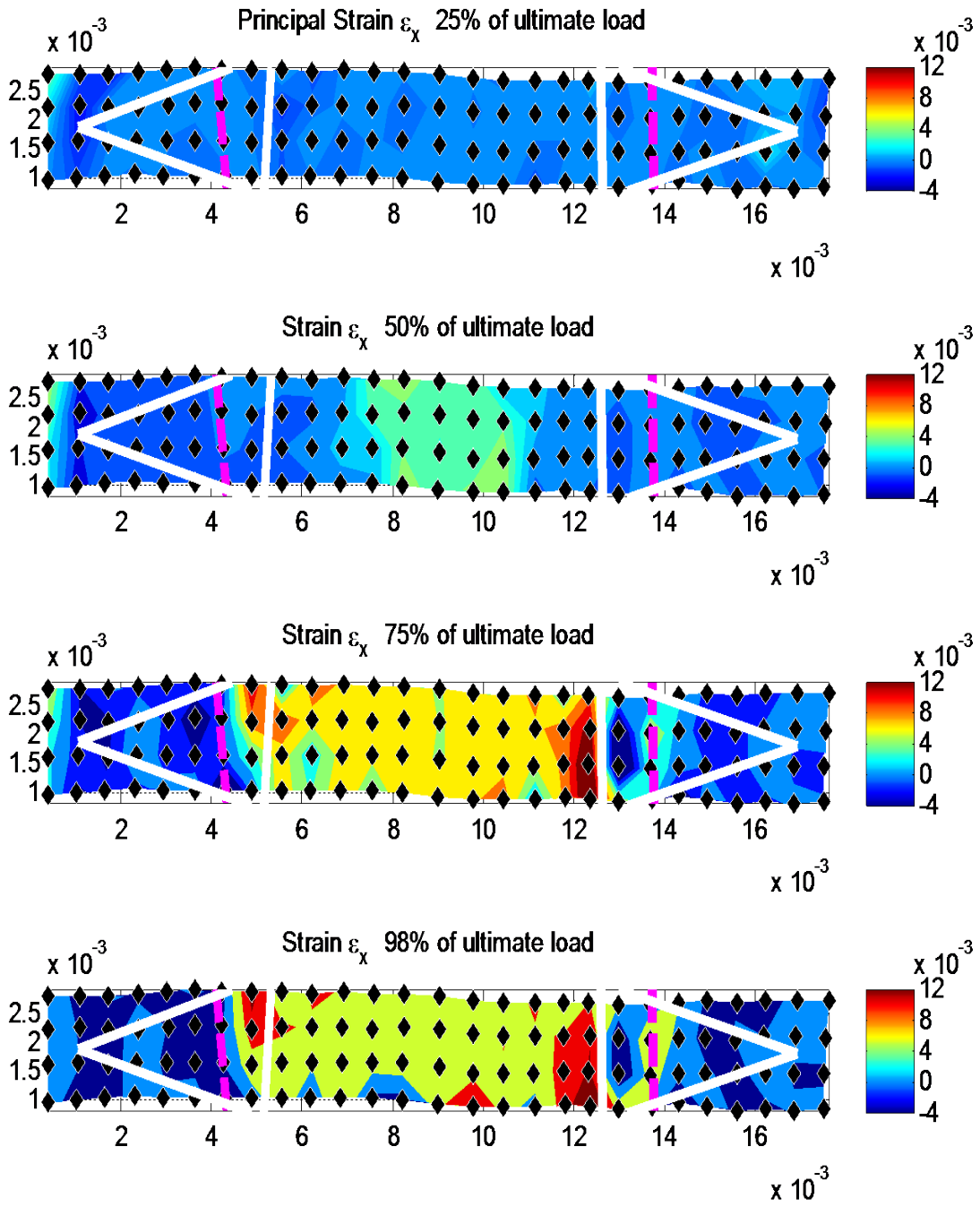


Figure D-17 Contour plots for B3H1.4Lb

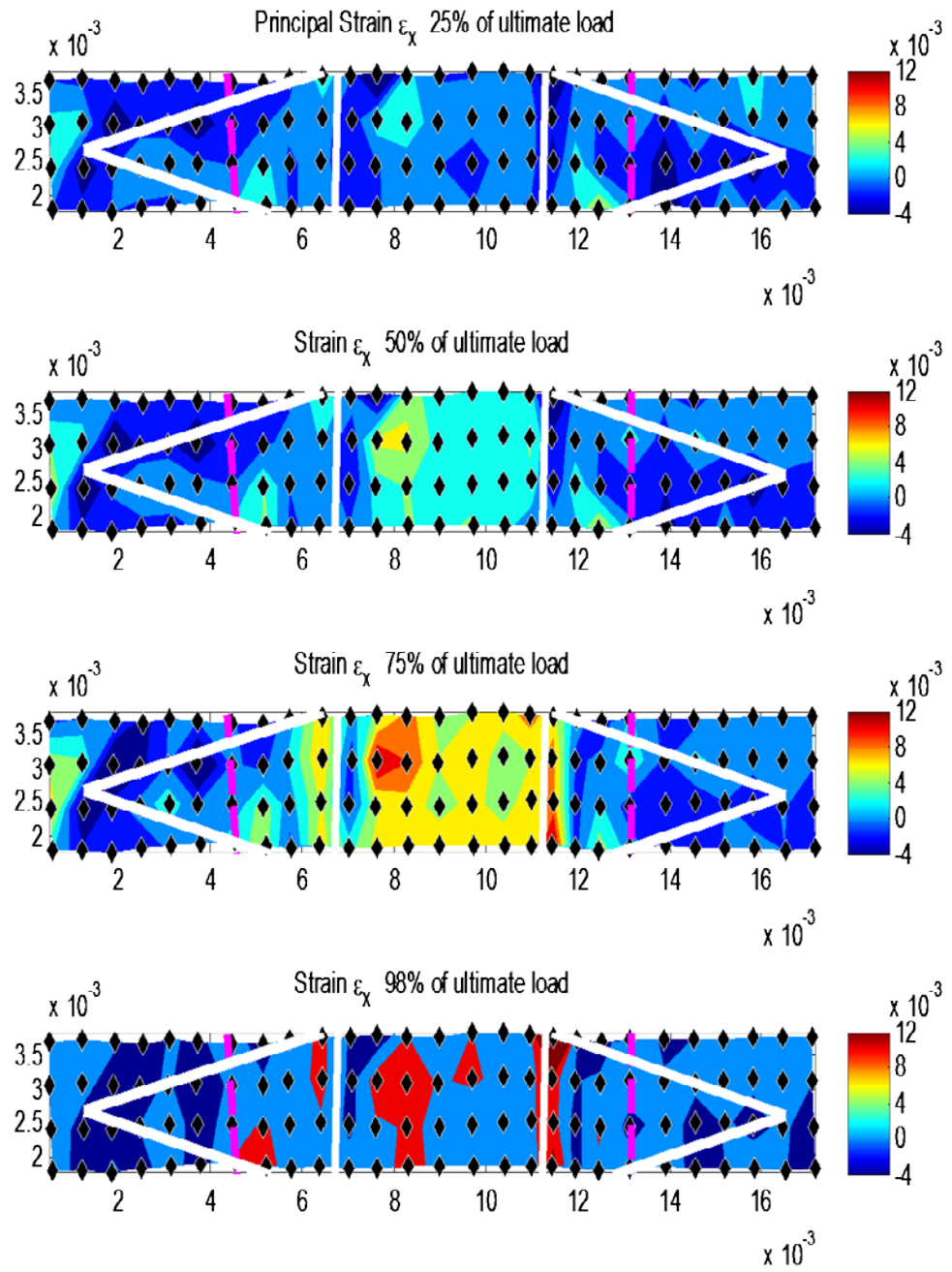


Figure D-18 Contour plots for B3H1.4XLa

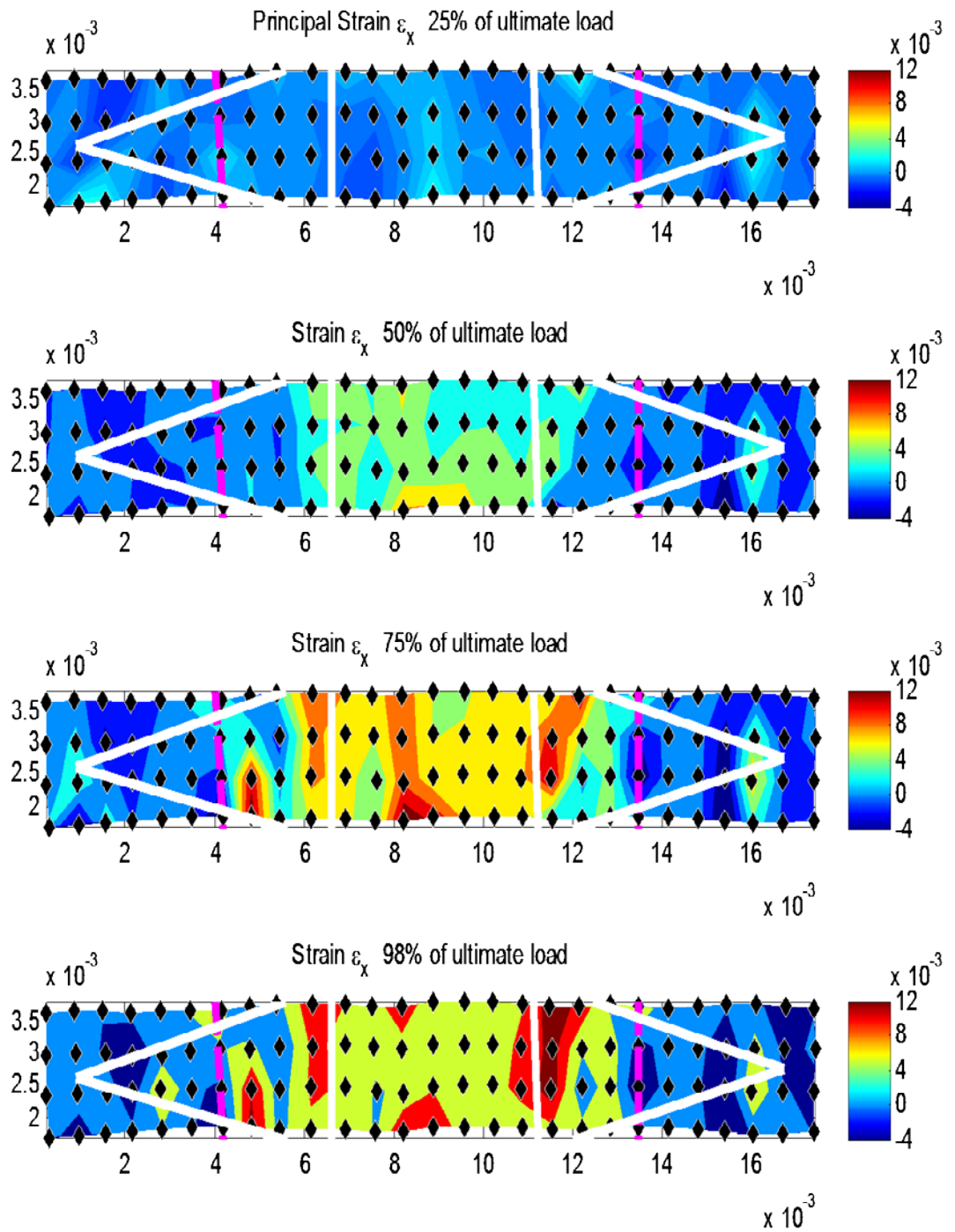


Figure D-19 Contour plots for B3H1.4XLb

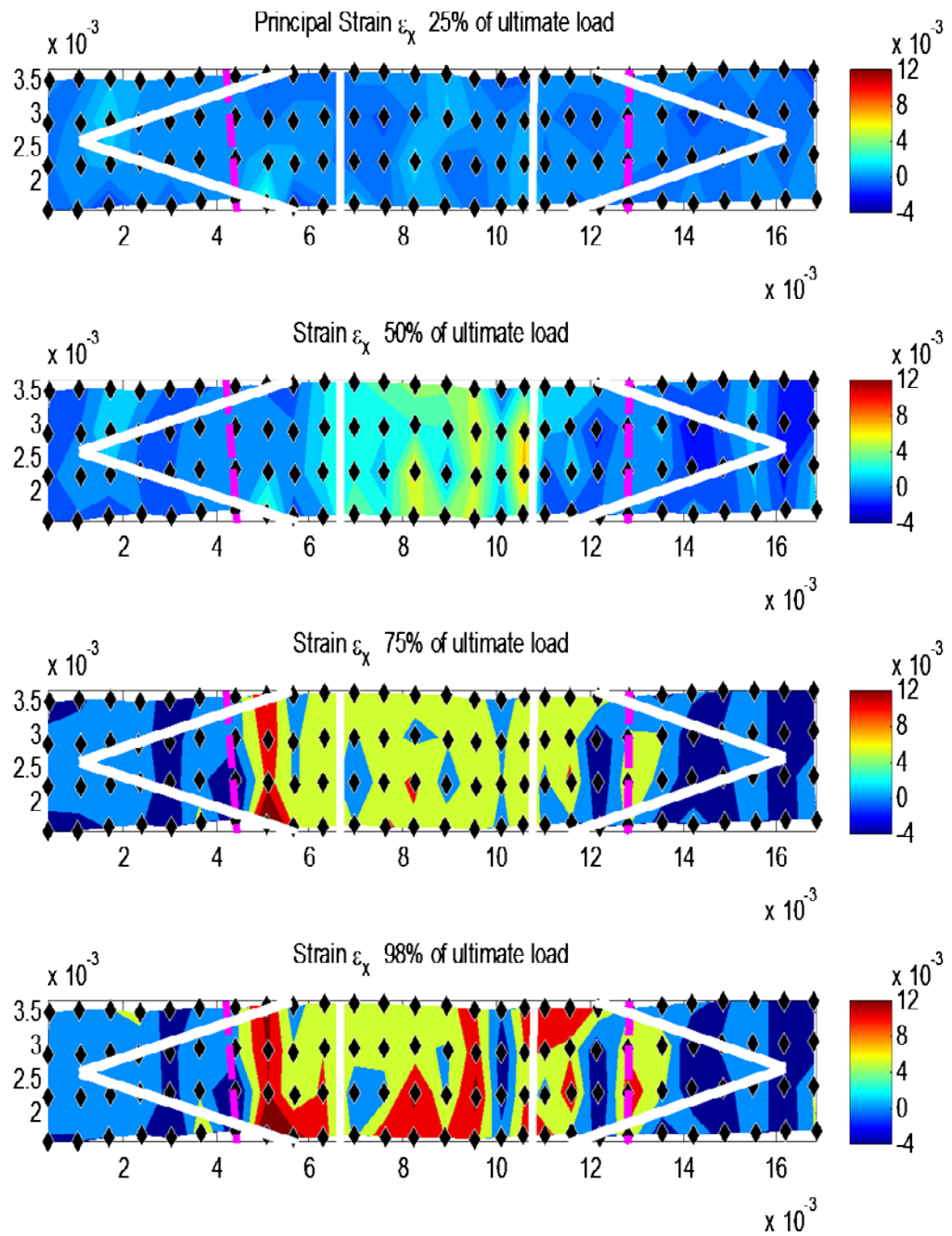


Figure D-20 Contour plots for B311XLa

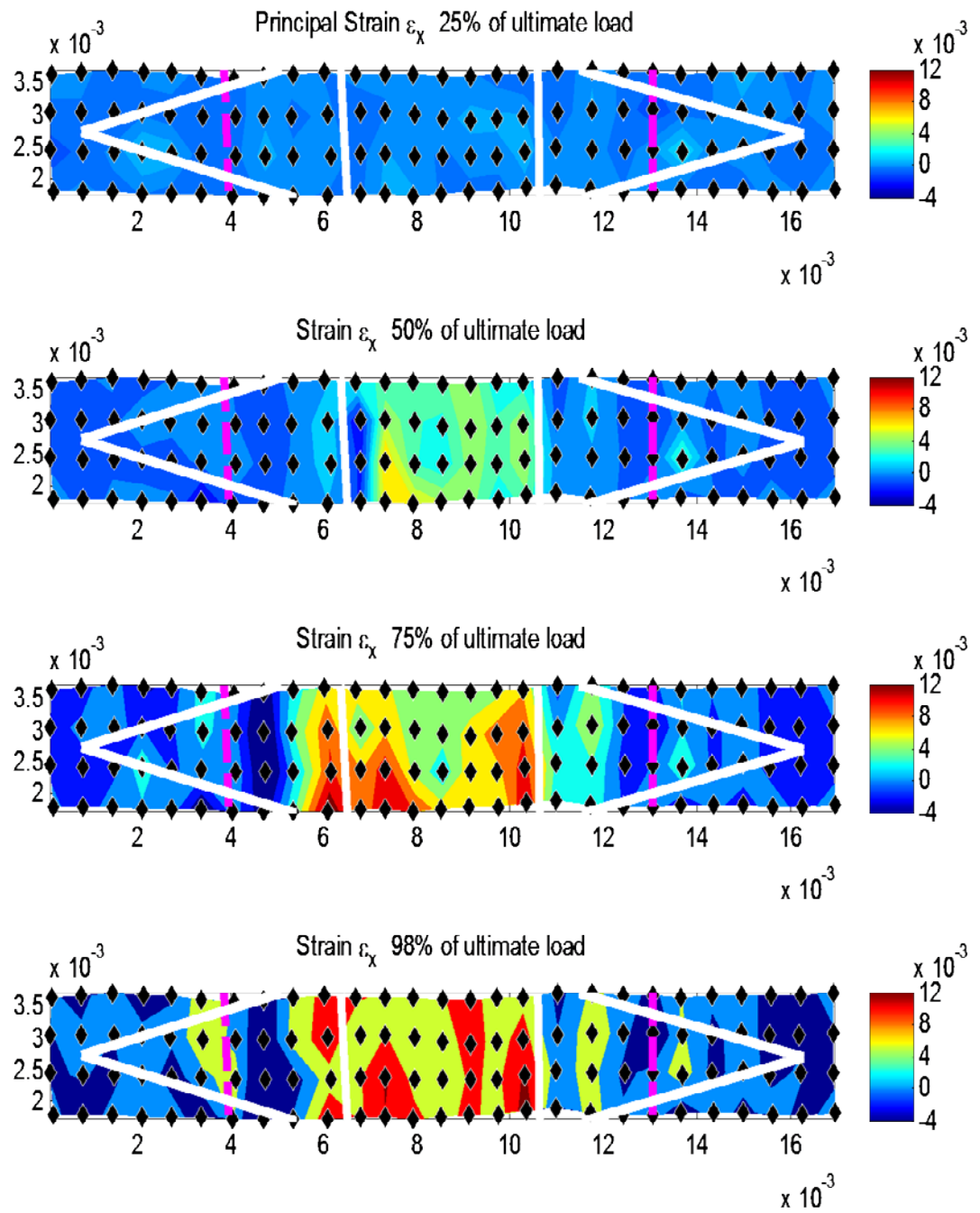


Figure D-21 Contour plots for B311XLb

References

- ACI Committee 318 (2008). Building Code Requirements for Structural Concrete (ACI 318-08), American Concrete Institute, Farmington Hills, Michigan, USA
- ACI Committee 440 (2006). Guide for the Design and Construction of Structural Concrete Reinforced with FRP Bars (ACI 440.1R-06), American Concrete Institute, Farmington Hills, MI, USA.
- ACI Committee 440 (2008). Guide for the Design and Construction of Externally Bonded FRP Systems for Strengthening Concrete Structures (ACI 440.2R-08), American Concrete Institute, Farmington Hills, Michigan, USA
- Al-Mahaidi, R., Lee, K., and Taplin, G. (2001). "Behavior and analysis of RC T-beams partially damaged in shear and repaired with CFRP laminates." *Proc., 2001 Structural Congress and Exposition, ASCE, Washington, DC*
- Artem, L. (2010). Applying Carbon Fiber in Building. Department of Civil and Construction Engineering, Saima University of Applied Sciences, Master Thesis.
- ASTM International, (2007), "Standard Test Method for Flexural Strength of Concrete Using Simple Beam With Center-Point Loading, (C293-07)," ASTM International, West Conshohocken, PA, USA, 3 pp.
- Bonacci, J. F. and Maalej, M. (2001). "Behavioral Trends of RC Beams Strengthened with Externally Bonded FRP," *Journal of Composites for Construction*, Vol. 5, No. 2, pp. 102-113.
- Brena, S.F, et al. (2013). "Advances on the Behavior Characterization of FRP-Anchored Carbon Fiber-Reinforced Polymer (CFRP) Sheets Used to Strengthen Concrete Elements", *International Journal of Concrete Structures and Materials*, Vol.7, No.1, pp. 3-16
- Camata, G., Spacone, Roko Zarnic (2006), "Experimental and nonlinear finite element studies of RC beams strengthened with FRP plates," *Composites Part B: Engineering*, V. 38, No. 2, pp. 277-88.
- Chansawat, K, et al. (2005). "FE Modeling and Experimental Verification of an FRP Strengthened Bridge". Department of Civil, Construction ,and Environmental Engineering, Oregon State University,

- Chen, J. F. and Teng, J. G. (2001). "Anchorage Strength Models for FRP and Steel Plates Bonded to Concrete," *Journal of Structural Engineering*, Vol. 127, No. 7, pp. 784-791.
- Choi, H.S, et al. (2011). "Structural Dynamic Displacement Vision System using Digital Image Processing," *NDT & E International*, Vol. 44, No. 7, pp. 597–608.
- Garcia, J., and Sun, W., et al. (2014). Procedures for the Installation and Quality Control of Anchored CFRP Sheets for Shear Strengthening of Concrete Bridge Girders (Report of TXDOT/5-6306-01-1)
- Helfrick, M. N., et al. (2011). "3D Digital Image Correlation Methods for Full-Field Vibration Measurement," *Mechanical Systems and Signal Processing*, Vol. 25, No. 3, pp. 917–927.
- Huaco.G. (2009). Quality Control Test for Carbon Fiber Reinforced Polymer (CFRP) Anchors for Rehabilitation. Department of Civil, Environmental and Architectural Engineering. Austin, Texas, The University of Texas at Austin. Master Thesis.
- Ibrahim, A. M. (2009). "Finite Element Modeling of reinforced Concrete Beams Strengthened with FRP Laminates," *European Journal of Scientific Research*, Vol. 30, No. 4, pp. 526–541.
- Juenger, M. (2011). "Novel Structural Materials." Department of Civil, Environmental and Architectural Engineering. Austin, Texas, The University of Texas at Austin. CE 393N.
- Jurjo.D, et al. (2010). "Experimental Methodology for the Dynamic Analysis of Slender Structures Based on Digital Image Processing Techniques," *Mechanical Systems and Signal Processing*, Vol. 24, No. 5, pp. 1369–1382.
- Kobayashi,K., Fuji S., Yabe Y., Tsukagoshi H., and Sugiyama T. (2001). " Advanced wrapping system with CF anchor –Stress Transfer Mechanism of CF Anchor." *5th International Symposium on Fiber-Reinforced Polymer (FRP) Reinforcement for Concrete Structures*, Cambridge, UK, 379- 388.
- Kachlakev, D. (2001). "Finite Element Modeling of Reinforced Concrete Structures Strengthened with FRP Laminates." Civil and Environmental Engineerign Department, California Polytechnic State University. Final Report.
- Kalfat, R. et al, "Anchorage Devices Used to Improve the Performance of Reinforced Concrete Beams Retrofitted with FRP Composites State-of-the-Art Review," *Composites for Construction*, Vol, 17, No. 1
- Kim, Insung (2008). Use of CFRP to Provide Continuity in Existing Reinforced Concrete Members Subjected to Extreme Loads. Department of Civil, Environmental and

- Architectural Engineering. Austin, Texas, The University of Texas at Austin. Ph.D Dissertation.
- Kim, S. J., & Smith, S. T. (2009.). "Strengthening of RC Slabs with Large Penetrations Using Anchored FRP Composites," *Proceedings of the 2nd Asia Pacific Conference on FRP in Structures, APFIS 2009*, Seoul, Korea. pp. 111–116.
- Kim, Y. G. (2011). "Shear Behavior of Reinforced Concrete T-Beams Strengthened with Carbon Fiber Reinforced Polymer (CFRP) Sheets and CFRP Anchors. Department of Civil, Environmental and Architectural Engineering." Austin, Texas, The University of Texas at Austin. Ph.D Dissertation.
- Kim, Y. G., et al (2012)., "Shear Strengthening of Large Reinforced and Prestressed Concrete Elements Using Carbon Fiber Reinforced Polymer (CFRP) Sheets and CFRP Anchors," 0-6306-1, Center for Transportation Research (CTR), pp. 296, February 2012.
- Kim, Y. G., et al (2014)., "Strengthening of Reinforced Concrete T-Beams Using Anchored CFRP Materials," *ACI Structural Journal*, V. 111, No. 5, pp. 1027-36.
- Kotynia, R. et al (2008). " Flexural Strengthening of RC Beams with Externally Bonded CFRP Systems: Test Results and 3D Nonlinear FE Analysis." *Journal of Composite for construction*, Vol.12, pp. 190-201.
- Lamanna, A.J. (2002). "Flexural Strengthening of Reinforced Concrete Beams with Mechanically Fastened Fiber Reinforced Polymer Strips." Civil and Environmental Engineering Department, University of Wisconsin. Ph.D Dissertation.
- Lu, X. Z & Teng, et al. (2005a). "Bond–slip models for FRP sheets/plates bonded to concrete." *Engineering Structures*," Vol. 27, No. 6, pp.920–937.
- Lu, X. Z, & Chen, J. F., et al. (2005b). "Theoretical Analysis of Stress Distributions in FRP Side-Bonded to RC Beams for Shear Strengthening," *Proceedings of the International Symposium BBFS 2005*, pp. 363-370
- Lu, X. Z, & Ye, et al (2005c). "Meso-scale finite element model for FRP sheets/plates bonded to concrete," *Engineering Structures*, Vol. 27, No. 4, pp.564-575.
- Lu, X. Z., Teng, J. G., Ye, L. P., & Jiang, J. J. (2007). "Intermediate Crack Debonding in FRP-Strengthened RC Beams : FE Analysis and Strength Model," *Journal of Composites for Construction*, Vol. 11, No. 2, pp.161-174.
- Macgregor, J. G. (2006). Reinforced Concrete Mechanics and Design." *Prentice Hall* ", 4th edition

- Mahjoub, R. et al. (2010). "Finite Element Analysis of RC Beams Strengthened with FRP Sheets under Bending," *Australian Journal of Basic & Applied Sciences*, Vol. 4 No 5, pp. 773–778.
- Marecos J, et al. (1969). "Field observation of Tagus River Suspension Bridge," *Journal of the Structural Division*, Vol. 95, pp.555–583.
- Mccormick, N., & Cantab, M. A. (2014). "Optical imaging for low-cost structural measurements," *Proceedings of the ICE - Bridge Engineering*, Vol 167, No 1, pp. 33–42.
- Mikhail, E. M. (2001). "Introduction to modern photogrammetry." New York ; Chichester : Wiley, c2001.
- Nakaba, K., et al. (2002). "Bond Behavior between Fiber-Reinforced Polymer Laminates and Concrete," *ACI Structural Journal*, Vol 98, pp. 359–367.
- Neale, K.W. et al (2005). "Modelling of Debonding Phenomena in FRP-Strengthened Concrete Beams and Slabs," *Proceedings of the International Symposium on Bond Behaviour of FRP in Structures*, Vol. 203, pp.461-480.
- Niemitz, C. (2008). Anchorage of Carbon Fiber Reinforced Polymers to Reinforced Concrete in Shear Applications. University of Massachusetts Amherst, (February). Master Thesis.
- Olaszek, P. (1999). "Investigation of the Dynamic Characteristic of Bridge Structures using a Computer Vision Method. Measurement," *Road and Bridge Research Institute*, Vol. 25 No.3, pp. 227–236.
- Orton, S. L. (2007). "Development of a CFRP System to Provide Continuity in Existing Reinforced Concrete Structures Vulnerable to Progressive Collapse. Department of Civil, Environmental and Architectural Engineering." Austin, Texas, The University of Texas at Austin. Ph.D Dissertation.
- Orton, Sarah L., and Jirsa, James O. et al. (2008). "Design Considerations of Carbon Fiber Anchors," *Journal of Composites for Construction*, Vol. 12, No. 6, pp. 608-616.
- Ozdemir, G., and Akyuz, U. (2005). "Tensile Capacities of CFRP Anchors", *7th International Symposium on Fiber-Reinforced Polymer (FRP) Reinforcement for Concrete Structures*, Kansas City, MO.
- Pham, H. B., et al (2006), "Modelling of CFRP–concrete bond using smeared and discrete cracks," *Composite Structures*, V. 75, No. 1–4, pp. 145-50, 2006.

- Pham, L. T. (2009). "Development of a Quality Control Test for Carbon Fiber Reinforced Polymer Anchors". Department of Civil, Environmental and Architectural Engineering. Austin, Texas, The University of Texas at Austin. Master Thesis.
- Santhakumar, R. (2004). "Analysis of Retrofitted Reinforced Concrete Shear Beams using Carbon Fiber Composites," *Electronic Journal of Structural Engineering*, Vol. 4, pp. 66-74
- SAS (2009) *ANSYS 12.1 Finite Element Analysis System*, SAS IP, Inc
- Sato, Y., and Vecchio, F. J. (2003). "Tension stiffening and crack formation in reinforced concrete members with fiber-reinforced polymer sheets." *Journal of Structural Engineering*, 129(6), 717–724.
- Smith, S. T. (2009). "FRP Anchors : Recent Advances in Research and Understanding,". *Asia-Pacific Conference on FRP in Structures*, pp. 35–44.
- Smith, S. T. et al. (2007). "Modeling Debonding Failure in FRP Flexurally Strengthened RC Members Using a Local Deformation Model," *American Society of Civil Engineers*, Vol. 11, No.2, pp. 184–192.
- Smith, S. T. et al. (2011). "FRP-strengthened RC slabs anchored with FRP anchors," *Engineering Structures*, Vol. 33, No.4, pp. 1075-1087.
- Smith, S. T. et al. (2013). "Influence of FRP Anchors on the Strength and Ductility of FRP-Strengthened RC Slabs," *Construction and Building Materials*, Vol. 49, pp. 998-1021.
- Stephen, G.A. et al. (1993). "Measurements of Static and Dynamic Displacement from Visual Monitoring of the Humber Bridge," *Engineering Structures*, Vol. 15, No. 3, pp. 197–208.
- Teng, J.G. et al (2003). "Intermediate Crack Induced Debonding in RC Beams and Slabs," *Construction and Building Materials*, V. 17, No. 6-7, pp 447-462
- Thamrin, R., & Kaku, T. (2007). "Bond Behavior of CFRP Bars in Simply Supported Reinforced Concrete Beam with Hanging Region," *Journal of Composites for Construction*, Vol. 11, No. 2, pp. 129–138.
- Vecchio, F.J. et al (1999) "Analysis of Repaired Reinforced Concrete Structures," *Journal of Structural Engineer*, Vol. 125 No.6, pp.644-652.
- Wahbeh, A. M., Caffrey, J. P., & Masri, S. F. (2006). "A Vision-Based Approach for the Direct Measurement of Displacements in," *NDT&E International*, Vol. 785, No.39, pp. 425–431.

- Wong, S.Y. et al. (2003). "Towards Modeling of Reinforced Concrete Members with Externally Bonded Fiber-Reinforced Polymer Composites." *ACI Structural Journal*, Vol. 100, pp. 47-55
- Wolanski, A. J. (2004). Flexural Behavior of Reinforced and Prestressed Concrete Beams Using Finite Element Analysis. Marquette University. Master Thesis.
- Yang, D. Y. (2003). "Rapid Bridge Replacement Techniques," *AASHTO Region 4 Research Advisory Committee Meeting*, August 5, 2003, San Antonio.
- Yao, J. et al (2005). "Experimental Study on FRP-to-Concrete Bonded Joints," *Composites: Part B*, Vol 36, pp. 99-113
- You, Y., Ayoub, A., Belarbi, A. (2011). "Three-Dimensional Nonlinear Finite-Element Analysis of Prestressed Concrete Beams Strengthened in Shear with FRP Composites," *Journal of Composites for Construction*, V. 15, No. 6, pp. 896-907,
- Zhang, H.W. et al. (2012a). "Influence of FRP Anchor Fan Configuration and Dowel Angle on Anchoring FRP Plates," *Composite: Part B*, Vol. 43, pp.3516-3527.
- Zhang, H.W. et al. (2012b). "Optimisation of carbon and glass FRP anchor design," *Construction and Building Materials*, Vol, 32, pp. 1-12

Vita

Wei Sun was born in Dalian, China in 1982, the son of Jiheng Sun and Minghua Chi. He graduated from Dalian No.3 high school in 2001. Afterward, He attended Shenyang Jianzhu University where he received his Bachelors of Science in Civil Engineering in 2005 and Master of Science in Structural Engineering in 2008. Since then, he worked for China Construction Eighth Engineering Bureau as an assistant engineer. In the fall of 2009, Wei began his studies at the University of Texas at Austin.

Name: Wei Sun

E-mail address: soonway18@gmail.com

Address: 10100 Burnet Rd Bldge 177, Austin, TX 78758

Telephone: 512-501-0246

This dissertation was typed by the author.